The University of Manchester

Suspension Dewatering with Aggregate Densification

A thesis submitted to The University of Manchester for the degree of Doctor of Philosophy (PhD) in the Faculty of Engineering and Physical Sciences

2014

Yi Zhang

SCHOOL OF CHEMICAL ENGINEERING AND ANALYTICAL SCIENCE

Contents

Final word count: 56696

List of Figures

List of Tables

The University of Manchester

Abstract of thesis submitted by Yi Zhang for the degree of Doctor of Philosophy and entitled **Suspension Dewatering with Aggregate Densification**. Date: 30 August 2014

This thesis concerns design of two pieces of suspension dewatering equipment (i.e. transient batch settlers and steady state continuous gravity thickeners). In a transient batch settler, very slow densification of aggregates within the suspension is considered whilst the drag on the solids in the suspension is assumed to be negligible. The interface of the suspension is then determined by a balance between gravity and the gradient of the compressive yield stress of the gelled suspension. The compressive yield stress functional form in general could be either a weakly gelled formula, or a strongly gelled formula. These formulae differ in the way they behave for solids concentrations in the neighbourhood of the suspension gel point. The effects of the above two gel formulae, the evolution of the compressive yield stress functional form over time during aggregate densification, different initial suspension heights, and different initial feed solids volume fractions upon the predictions of consolidated bed structures and solids volume fractions obtained at the bottom of a batch settler, and upon the evolution of the heights of the suspension and the consolidated bed have been explored. A sufficiently tall initial suspension height might lead to insignificant increases in the solids volume fractions obtained at the bottom of batch settlers after time-dependent aggregate densification. The interfaces of the suspension and the consolidation zone coincide after aggregate densification if the gel point, which increases with time, is larger than the initial feed solids volume fractions.

Moreover, the maximum permitted underflow solids fluxes predicted from steady state thickeners have been investigated and compared. Pre-shearing of aggregates which densifies aggregates to have smaller diameters upon entering the thickener is necessary if large underflow solids fluxes and small underflow solids volume fractions are specified. The solids volume fraction at the top of the consolidated bed which is the densified gel point is influenced by the extent of pre-shearing of aggregates. An algorithm for determining this densified gel point has also been developed. In reality, thickeners contain not just a consolidating bed, but also a hindered settling region above it. When the hindered settling region is considered in a thickener, the effects of the extent of aggregate densification that has occurred in the hindered settling region and how that impacts upon thickener performance and sludge rheological properties have been explored in this thesis. A new algorithm for predicting the densified gel point obtained at the top of the consolidated bed has been developed when the hindered settling region is present. The effects of underflow solids volume fractions, aggregate densification rate parameters and pre-shearing of aggregates upon the predictions of maximum permitted underflow solids fluxes, sludge rheological properties, and thickener performance have been explored. The predictions of thickener performance using both the weakly and strongly gelled formulae have also been achieved.

In cases where it is possible to neglect the hindered settling region, substantial increases in the maximum permitted underflow solids fluxes, and substantial decreases in the consolidated bed heights and the total solids residence times have been achieved after aggregate densification for a comparatively small underflow solids volume fraction. The benefits arising from aggregate densification are more modest if the underflow solids volume fraction is larger. On the other hand, when the hindered settling region is included, more densification of aggregates occurring in the hindered settling region might lead to taller consolidated bed heights for a specified suspension flux and a specified aggregate densification rate parameter due to higher underflow solids volume fractions.

Declaration

University of Manchester
PhD by published work Candidate Declaration

Candidate Name: Yi Zhang

Faculty: Engineering and Physical Sciences

Thesis Title: Suspension Dewatering with Aggregate Densification

Declaration to be completed by the candidate:

I declare that no portion of the work referred to in the thesis has been submitted in support of an application for another degree or qualification of this or any other university or other institute of learning.

Signed:

Date: 30 August 2014

Copyright Statement

i. The author of this thesis (including any appendices and/or schedules to this thesis) owns certain copyright or related rights in it (the "Copyright")[1] and s/he has given The University of Manchester certain rights to use such Copyright, including for administrative purposes.

ii. Copies of this thesis, either in full or in extracts and whether in hard or electronic copy, may be made **only** in accordance with the Copyright, Designs and Patents Act 1988 (as amended) and regulations issued under it or, where appropriate, in accordance with licensing agreements which the University has from time to time. This page must form part of any such copies made.

iii. The ownership of certain Copyright, patents, designs, trade marks and other intellectual property (the "Intellectual property") and any reproductions of copyright works in the thesis, for example graphs and tables ("Reproductions"), which may be described in this thesis, may not be owned by the author and may be owned by third parties. Such Intellectual Property and Reproductions cannot and must not be made available for use without the prior written permission of the owner(s) of the relevant Intellectual Property and/or Reproductions.

iv. Further information on the conditions under which disclosure, publication and commercialisation of this thesis, the Copyright and any Intellectual Property and/or Reproductions described in it may take place is available in the University IP Policy (see http://www.campus.manchester.ac.uk/medialibrary/polices/intellectual-property.pdf), in any relevant Thesis restriction declarations deposited in the University Library, The University Library's regulations (see http://www.manchester.ac.uk/library/aboutus/regulations) and in The University's policy on presentation of Theses.

[1]This excludes material already printed in academic journals, for which the copyright belongs to said journal and publisher. Pages for which the author does not own the copyright are numbered differently from the rest of the thesis.

Acknowledgements

I would like to thank my supervisors Dr Paul Grassia and Dr Alastair Martin for providing this research project. I am also grateful to Paul and Alastair for their assistance in preparing this thesis and the manuscripts. I would also like to thank Paul and Alastair for their assistance in solving many mathematical issues, especially in solving numerical issues. I am also grateful to Dr Shane Usher who is from The University of Melbourne, Australia for interesting discussion on batch sedimentation.

I would like to thank all friends and colleagues in the office B9 (formerly C19). I am grateful to Denny for her assistance in using LaTeX. I would also like to thank school technicians for supporting this research project. In addition, I would like to thank all my friends who encouraged and helped me in the last 3 years.

I would like to thank my parents who always encourage and support me during my whole PhD study. Without your encouragement and support, I cannot complete this research project and this thesis.

Nomenclature

A	aggregate densification rate parameter (s^{-1})
a_0 (a_1)	curve fitting parameter for the undensified (densified) compressive yield stress functional form (Pa)
b, b_1	curve fitting parameters for the weakly gelled and strongly gelled compressive yield stress functional forms, respectively
B	cross-sectional area (m^2)
c_0 (C_0)	curve fitting parameter for the strongly (weakly) gelled undensified compressive yield stress functional form (Pa)
c_1 (C_1)	curve fitting parameter for the strongly (weakly) gelled densified compressive yield stress functional form (Pa)
c_∞ (C_∞)	curve fitting parameter for the strongly (weakly) gelled fully densified compressive yield stress functional form (Pa)
D_{agg}	aggregate diameter ratio
$D_{agg,\infty}$	final steady state aggregate diameter ratio
$D(\phi)$	diffusivity ($\mathrm{m}^2\,\mathrm{s}^{-1}$)
f_0, f_s, f_e	feed volumetric rate, suspension volumetric flow rate, and volumetric overflow rate, respectively ($\mathrm{m\,s}^{-1}$)
g	gravity acceleration ($\mathrm{m\,s}^{-2}$)

H_0	initial suspension height (m)
H	suspension height (m)
H^{unden}	suspension height determined in the undensified equilibrium state batch settler (m)
$H^{full\ den}$	suspension height determined in the fully densified equilibrium state batch settler (m)
$H^{proposed}$	proposed initial suspension height (m)
H^{lower}	lower limiting value for the initial suspension height (m)
H^{upper}	upper limiting value for the initial suspension height (m)
k_0, k_1, k_2	curve fitting parameters for the weakly gelled undensified, densified, and fully densified compressive yield stress functional form, respectively
k_3, k_4, k_5	curve fitting parameters for the strongly gelled undensified, densified, and fully densified compressive yield stress functional form, respectively
L_0	dimensionless initial suspension height
L	dimensionless suspension height for any instant
L^{unden}	dimensionless suspension height determined in the undensified equilibrium state batch settler
$L^{full\ den}$	dimensionless suspension height determined in the fully densified equilibrium state batch settler
m	curve fitting parameter for the compressive yield stress functional form
n_0 (n_1)	curve fitting parameter for the undensified (densified) compressive yield stress functional form
n_∞	curve fitting parameter for the fully densified compressive yield stress functional form

$P_{y,0}$	undensified compressive yield stress (Pa)
P_y ($P_{y,1}$)	densified compressive yield stress (Pa)
$P_{y,\infty}$	fully densified compressive yield stress (Pa)
$P_{wy,0}$	weakly gelled undensified compressive yield stress (Pa)
$P_{wy,1}$	weakly gelled densified compressive yield stress (Pa)
$P_{wy,\infty}$	weakly gelled fully densified compressive yield stress (Pa)
$P_{sy,0}$	strongly gelled undensified compressive yield stress (Pa)
$P_{sy,1}$	strongly gelled densified compressive yield stress (Pa)
$P_{sy,\infty}$	strongly gelled fully densified compressive yield stress (Pa)
P_s	particle stress (Pa)
p_y	dimensionless compressive yield stress
q_b	solids flux determined in an initially networked batch settler ($\mathrm{m\,s^{-1}}$)
$q_{b,top}$	solids flux determined at the top of the consolidation zone in an initially networked batch settler ($\mathrm{m\,s^{-1}}$)
q_{fs}	free settling solids flux determined in an initially unnetworked batch setter ($\mathrm{m\,s^{-1}}$)
q_u, q_s	underflow solids flux and suspension flux determined in a steady state thickener, respectively ($\mathrm{m\,s^{-1}}$)
q_0, q_e	feed velocity, and overflow velocity, respectively ($\mathrm{m\,s^{-1}}$)
Q_{fs}	dimensionless free settling solids flux
Q_u, Q_0	dimensionless underflow solids flux and dimensionless feed velocity in a steady state thickener, respectively
$Q_{0,max}$	dimensionless maximum feed velocity

Q_{max}	dimensionless maximum permitted underflow solids flux in a thickener
$Q_{u,max}$	dimensionless maximum underflow solids flux permitted in a steady state thickener
$Q_{s,max}$	dimensionless maximum permitted suspension flux in a steady state thickener
$Q_{u,max}^{unden}$	dimensionless maximum permitted underflow solids flux evaluated at the undensified state
$Q_{u,max}^{full\ den}$	dimensionless maximum permitted underflow solids flux evaluated at the fully densified state
Q_{mu}	dimensionless maximum underflow solids flux assuming the undensified gel point at the top of the bed
Q_s	dimensionless suspension flux
r_n, r_g	curve fitting parameters for the undensified hindered settling functional form
r_{agg}	aggregate hindered settling factor
R_0, R, R_∞	undensified, densified, and fully densified hindered settling functions, respectively ($\mathrm{Pa\,s\,m^{-2}}$)
$R_{Stokes,0}$	undensified hindered settling function of an isolated aggregate ($\mathrm{Pa\,s\,m^{-2}}$)
$R_{s,0}$, R_s	dimensionless undensified, and densified hindered settling functions, respectively
$R_{s,\infty}$	dimensionless fully densified hindered settling function
$\tilde{R}_s$	dimensionless approximated densified hindered settling function
t, t_{res}, t_{res}^{pre}	densification time, solids residence time, and solids residence time required for pre-shearing, respectively (s)
t_{res}^{total}	total solids residence time (s)

t_{res}^{upper}, t_{res}^{lower} solids residence times spent in the upper part and lower part of the consolidation zone, respectively (s)

T, T_{res} dimensionless densification time, and dimensionless solids residence time, respectively

T_{res}^{total} dimensionless total solids residence time

T_{corres} dimensionless corresponding solids residence time spent in the hindered settling region

$T_{res,b}$ dimensionless solids residence time spent in the consolidation region

$t_{g,c}, t_{be,c}$ time evaluated at the intersection of interfaces of the suspension and the consolidated bed, and time evaluated at the solids volume fraction obtained at the bottom of the batch settler starting to increase, respectively (s)

$T_{g,c}$, $T_{be,c}$ dimensionless scales of $t_{g,c}$ and $t_{be,c}$, respectively

u_{sb} suspension velocity determined at the bottom of the thickener ($\mathrm{m\,s^{-1}}$)

$u_{Stokes,0}$ Stokes settling velocity ($\mathrm{m\,s^{-1}}$)

z, z_c height, and bed height, respectively (m)

$z_{c,0}$, $z_{c,\infty}$ bed heights evaluated at the undensified and fully densified equilibrium states, respectively (m)

z_b^{upper}, z_b^{lower} heights of the upper part and the lower part of the consolidated bed, respectively (m)

z_b^{total} total height in the bed (m)

Z_h, Z_b, Z_c dimensionless heights of the hindered settling region and the consolidated bed, and dimensionless bed height, respectively

Z, Z^{total} dimensionless height, and dimensionless total thickener height, respectively

$Z_{c,0}$, $Z_{c,\infty}$ dimensionless bed heights evaluated at the undensified and fully densified equilibrium states, respectively

α	dimensionless aggregate densification rate parameter
$\Delta\rho$	density difference between the solids and liquid ($\mathrm{kg\,m^{-3}}$)
ϕ	local solids volume fraction
$\phi_{g,0}$, ϕ_g	undensified gel point, and densified gel point, respectively
$\phi_{g,c}$, $\phi_{g,\infty}$	critical densified gel point, and fully densified gel point, respectively
$\phi_{agg,0}$, ϕ_{agg}	solids volume fractions within the undensified, and densified aggregates, respectively
$\phi_{agg,\infty}$	solids volume fraction within the fully densified aggregates
ϕ_{cp}, ϕ_u	close packing solids volume fraction, and underflow solids volume fraction, respectively
$\phi_{u,max}$	maximum underflow solids volume fraction achieved at the limiting operating conditions in a thickener
ϕ_f, ϕ_{top}	initial feed solids volume fraction, and solids volume fraction evaluated at the top of the bed, respectively
ϕ_e	overflow solids volume fraction
$\phi_{be,0}$, $\phi_{be,\infty}$	solids volume fractions evaluated at the bottom of the undensified and fully densified equilibrium state batch settlers, respectively
ϕ_{be}	solids volume fraction evaluated at the bottom of the batch settler for any instant
ϕ_{corres}	corresponding solids volume fraction delivering the limiting solid flux in a thickener
ϕ_{corres}^{unden}	corresponding solids volume fraction evaluated at the undensified state
$\phi_{corres}^{full\ den}$	corresponding solids volume fraction evaluated at the fully densified state
ϕ_{corres}^{crit}	critical corresponding solids volume fraction

Chapter 1

Introduction

Chemical, physical, and biological processes operated in different industries (e.g. wastewater treatment plants, minerals industries, ceramic industries, and food industries) often produce sludges and slurries which contain a large proportion of the water content and have low solids concentrations (Northcott et al., 2005; Flatt and Bowen, 2006; Stickland et al., 2008; Boger, 2009; Jones and Boger, 2012; Diehl, 2012; Mahmoud et al., 2013). All those sludges and slurries need to be dewatered in order to increase the solids concentrations and hence decrease the volumes of sludges and slurries before further disposal and reuse (Vesilind, 1979; Tchobanoglous and Burton, 1991; Northcott et al., 2005; Stickland et al., 2008; Boger, 2009; Jones and Boger, 2012; Mahmoud et al., 2013). Economic benefits for dewatering of sludges in wastewater treatment plants are to decrease the capital costs and the transport costs, due to the decrease in the volumes of sludges (Vesilind, 1979; Tchobanoglous and Burton, 1991; Northcott et al., 2005; Stickland et al., 2008; Mahmoud et al., 2013). Efficiency of water recovery is improved in the minerals industries after dewatering of slurries (Svarovsky, 2000; Northcott et al., 2005; Jones and Boger, 2012).

A general wastewater treatment plant flow sheet is given in Fig. 1.1 which is reproduced from Svarovsky (2000). As shown in Fig. 1.1, both clarifiers and thickeners are used for sludge dewatering during the process of wastewater treatment. The main aim of clarifiers used in the wastewater treatment plant is to clarify the effluent and minimise the solids concentration in the effluent, owing to comparatively low solids concentrations contained in wastewater entering clarifiers (Bürger and Wendland, 2001a; Diehl, 2001,

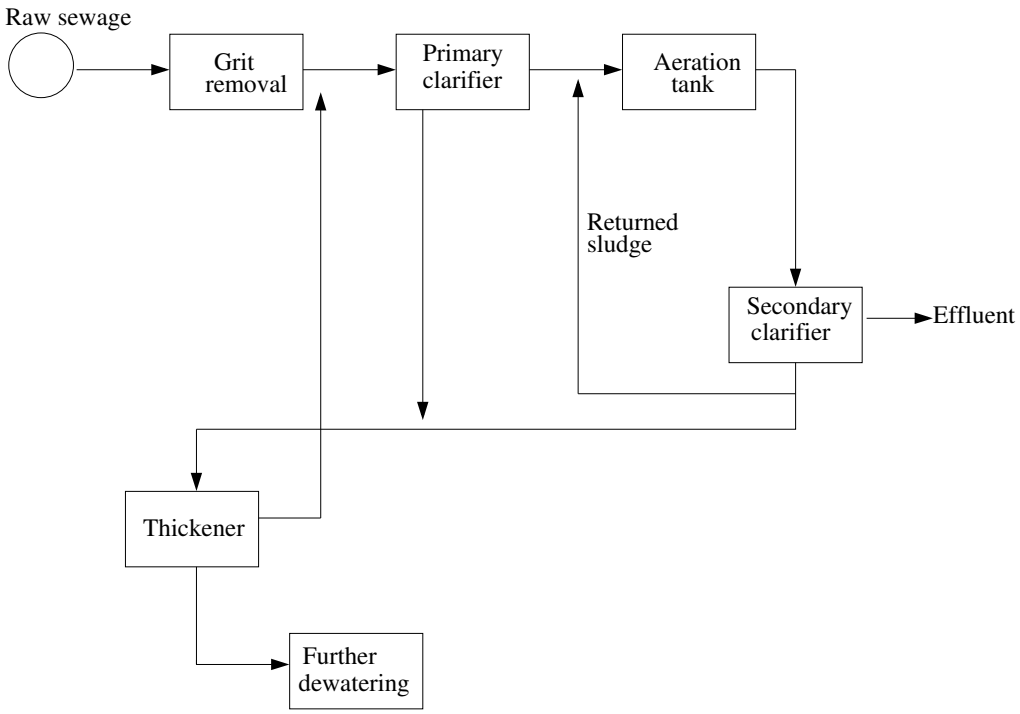

Figure 1.1: Flow sheet of the wastewater treatment plant – this figure is reproduced from Svarovsky (2000)

2006, 2007, 2012). Thickeners aim to increase the solids concentrations for the purposes of further dewatering and/or disposal of sludges (e.g. anaerobic digestion, aerobic digestion, composting, and landfill) (Tchobanoglous and Burton, 1991; Stickland et al., 2008; Diehl, 2006, 2007, 2012). The operation called 'Further dewatering' in Fig. 1.1 may refer to filters and/or centrifuges which can increase the solids concentration to become a much larger value (Wakeman, 2007; Stickland et al., 2008).

Shirato et al. (1970) considered a so called hydraulic excess pressure leading to the liquid to move through the sediment and a so called solid compressive pressure in their mathematical model for slurries dewatering. In addition, two commonly used sedimentation theories developed by Buscall and White (1987) and Bürger et al. (2005), respectively have been applied in the simulation and modelling of the performance of dewatering equipment (e.g. batch settlers, clarifiers, thickeners, filters, and centrifuges) (Landman et al., 1988; Howells et al., 1990; Landman et al., 1991; Landman and White, 1994; Landman et al., 1995; Bürger et al., 2001b; Martin, 2004,a; Usher and Scales, 2005; Berres et al., 2005a,b; Bürger et al., 2005; Bürger and Narváez, 2007; Bürger et al., 2013). Although the notations used in the above two theories are different, both the above two

theories use the so called sludge rheological properties characterising the performance of dewatering equipment. In this thesis, the notations employed by Buscall and White (1987) are used.

When considering the sludge rheological properties, an important parameter is the so-called gel point which is denoted as ϕ_g and is defined by the critical solids concentration determined as the solids contact each other (Buscall and White, 1987; de Kretser et al., 2003; Bürger et al., 2005; van Deventer, 2012; Zhang et al., 2013b). If the solids concentration is larger than the gel point, a compressible space-filling solids network, which is albeit loosely bound, is formed and this solids network can bear weight (Buscall and White, 1987; Landman and White, 1994; de Kretser et al., 2003; Stickland, 2005). The settling processes can be distinguished by several zones depending upon the relationships between the initial feed solids concentration and the gel point. The settling processes in both steady state thickeners and transient batch settlers in general include three zones if the initial feed solids concentration is less than the gel point: the clear liquor zone, the free settling zone (or the hindered settling zone) where solids or aggregates settle 'freely' but the inter-particle hydrodynamic forces may cause particles to influence each other, and the consolidation zone where the loosely bound and compressible space-filling solids network is formed (Bürger and Wendland, 2001a; Usher et al., 2006; Bürger and Narváez, 2007). When the initial feed solids concentration is less than the gel point, the free settling zone may contain two sub-zones: one sub-zone containing a uniform solids concentration and the other sub-zone where the solids concentration may vary with position (Kynch, 1952; Rushton et al., 1996; Lester et al., 2005; Diehl, 2007; Grassia et al., 2008, 2011; van Deventer et al., 2011). Note that the latter sub-zone may not be present in batch settlers, depending upon the proposed initial feed solids concentrations (Kynch, 1952; Lester et al., 2005; Diehl, 2007; Grassia et al., 2008). In addition, the latter sub-zone is not present in a steady state thickener (at least provided the suspension is not subjected to any external shear stresses), since then the solids concentration is known to jump from a uniform concentration sub-zone directly to the gelled zone (Bürger and Narváez, 2007). However, the sub-zone in which the solids concentrations vary with position must be present if the suspension within a thickener is subjected to the shear stress (e.g. via rak-

ing) (Grassia et al., 2014; Zhang et al., 2014). When the initial feed solids concentration is larger than the gel point, sedimentation also includes three zones: the clear liquor zone, the uniform settling zone where the solids concentration is uniformly equal to the initial feed solids concentration, and the consolidation zone (Buscall and White, 1987; Howells et al., 1990; Bürger and Narváez, 2007).

Sludges and slurries need to be pretreated before entering the sedimentation tanks (e.g. clarifiers and thickeners) and dewatering equipment (e.g. filters and centrifuges), in order to increase the dewaterability of sludges and slurries (Rushton et al., 1996; Svarovsky, 2000; Northcott et al., 2005; Wakeman, 2007; Tarleton and Wakeman, 2007). In this chapter, a brief description of sludge pretreatment is introduced and the effects of the pretreatment of sludges upon sludge rheology are also reviewed. Different techniques used to determine the sludge rheological properties are briefly introduced. In addition, the effects of the action of rakes and the shear stress they produce upon the behaviours of aggregates/flocs are briefly introduced in this chapter.

1.1 Sludge pretreatment

Sludges and slurries often have poor dewatering characteristics (e.g. slow settling velocities, long residence times, and the poor compressibility and permeability), due to the presence of fine solids within sludges and slurries (Rushton et al., 1996; Svarovsky, 2000; Northcott et al., 2005; Wakeman, 2007; Tarleton and Wakeman, 2007; Mahmoud et al., 2013). There are many approaches treating sludges and slurries before sedimentation and/or dewatering (e.g. coagulation and flocculation, sludge heating, and freezing) (Tarleton and Wakeman, 2007; Mahmoud et al., 2013). The most commonly used approach in wastewater treatment plants and minerals industries is to add coagulants and/or flocculants producing aggregates/flocs, in order to increase the particle size and the solids settling velocity, and in addition improve the compressibility and permeability (Rushton et al., 1996; Svarovsky, 2000; Northcott et al., 2005; Wakeman, 2007; Tarleton and Wakeman, 2007; Verrelli, 2008; Verrelli et al., 2009; Usher et al., 2009; van Deventer, 2012).

Knowledge of the theories of coagulation and flocculation is useful to design and optimise the coagulation and flocculation processes (Dobiáš, 1993; Rushton et al., 1996;

Svarovsky, 2000; Hogg, 2000; Tarleton and Wakeman, 2007; van Deventer, 2012). For the coagulation process in wastewater treatment plants, inorganic metal ions are often used (e.g. aluminium sulphate and ferric chloride) (Northcott et al., 2005; Tarleton and Wakeman, 2007; Verrelli et al., 2010). For the flocculation process in minerals industries, high molecular weight polymers are often used (Usher et al., 2009; van Deventer, 2012). The coagulation and flocculation processes are affected by many parameters (e.g. suspension pH, temperature, dosages, solids concentrations, and the shear stress) (Tarleton and Wakeman, 2007; Verrelli, 2008; Verrelli et al., 2009, 2010; Franks and Zhou, 2010). The principles for choosing coagulants and flocculants have been summarised in Tarleton and Wakeman (2007). The processes of coagulation and flocculation are beyond the scope of this thesis. In this chapter, only the effects of coagulation and flocculation upon the sludge rheological properties are reviewed and introduced.

1.2 Sludge rheology

Sludge rheological properties which are used in the sedimentation and dewatering theories (Buscall and White, 1987; Bürger et al., 2005) generally include the compressive yield stress, $P_y(\phi)$, the hindered settling function, $R(\phi)$, and the diffusivity, $D(\phi)$ (which can be derived in terms of $P_y(\phi)$ and $R(\phi)$). All those properties are independent of dewatering equipment, but are dependent upon the particle size, the particle shape, the liquid viscosity, the solids concentration, coagulation and flocculation conditions, and different types of coagulants and flocculants (Buscall and White, 1987; Green et al., 1996; Green and Boger, 1997; de Kretser et al., 2003; Martin, 2004; Verrelli, 2008; van Deventer, 2012).

The compressive yield stress, $P_y(\phi)$ (which describes the compressibility) is defined by the network stress (or the strength of the network) when a solids network is formed for the local solids concentration larger than the gel point (Buscall and White, 1987; Landman and White, 1994; de Kretser et al., 2003; van Deventer, 2012; Zhang et al., 2013a,b). For the local solids concentration less than the gel point, the compressive yield stress, $P_y(\phi)$ is nil, but otherwise the compressive yield stress, $P_y(\phi)$ must be considered in the sedimentation model (de Kretser et al., 2003; van Deventer, 2012; Zhang et al.,

2013a,b). The hindered settling function, $R(\phi)$ (which describes the permeability) represents a resistance of flow of the liquid (or the hydrodynamic drag) (Buscall and White, 1987; de Kretser et al., 2003; Northcott et al., 2005; Usher et al., 2009; van Deventer, 2012; Zhang et al., 2013b). The dewaterability of sludges and/or slurries is described by the diffusivity, $D(\phi)$ which combines the compressive yield stress, $P_y(\phi)$ and the hindered settling function, $R(\phi)$ (Landman et al., 1995, 1999; de Kretser et al., 2003; Northcott et al., 2005). It should be noted that the compressive yield stress, $P_y(\phi)$ and the diffusivity, $D(\phi)$ are only determined for the local solids concentration larger than the gel point whilst the hindered settling function, $R(\phi)$ can be determined via a full range of the solids concentration (Northcott et al., 2005; van Deventer, 2012).

1.2.1 Effects of coagulation on sludge rheological properties

The properties of aggregates/flocs (e.g. ionic strength, solids concentrations, and the particle size) and the conditions for coagulation and flocculation (e.g. pH, temperature, dosages, and types of coagulants and flocculants) have significant effects on the determinations of the compressive yield stress, $P_y(\phi)$, the hindered settling function, $R(\phi)$, and the diffusivity, $D(\phi)$ (Northcott et al., 2005; Flatt and Bowen, 2006; Verrelli, 2008; Verrelli et al., 2009, 2010). A mathematical model describing the compressive yield stress has been established by Flatt and Bowen (2006). That mathematical model considered the effects of different particle sizes upon the compressive yield stress.

Effects of pH, temperature, dosages of coagulants, types of coagulants, and the shear stress on the sludge rheological properties have been investigated via experiments (Zhou et al., 1999; Northcott et al., 2005; Verrelli et al., 2009; Franks and Zhou, 2010). All those mentioned parameters influence significantly the determination of the compressive yield stress, the hindered settling function, and hence the diffusivity (Northcott et al., 2005; Verrelli, 2008; Verrelli et al., 2009). The work of Northcott et al. (2005) has suggested the pH value ranges for ferric coagulants used in wastewater treatment plants, and has also investigated the effects of pH, temperature, and the types of coagulants on the determination of sludge rheological properties. Lower dosages of coagulants can increase the compressibility, the permeability, and hence the dewaterability of sludges in wastewater

treatment plants (Verrelli et al., 2009, 2010). The pH value affects the dewaterability, the compressibility, and the permeability significantly for aluminium coagulants but insignificantly for ferric coagulants (Verrelli et al., 2009, 2010). For wastewater treatment plants, pH is suggested to be either approximately 6 for aluminium coagulants or approximately 7.5 for ferric coagulants (Northcott et al., 2005; Verrelli et al., 2009, 2010).

1.2.2 Determination of sludge rheological properties

Knowing the functional forms of the compressive yield stress, $P_y(\phi)$ and the hindered settling function, $R(\phi)$ is essential to establish the sedimentation model and optimise the operation of the sedimentation process (Martin, 2004; Usher and Scales, 2005; Zhang et al., 2013a,b). Experimental data of the compressive yield stress, $P_y(\phi)$ and the hindered settling function, $R(\phi)$ enable researchers and engineers to obtain the functional forms of those two sludge rheological properties via curve fitting techniques (Green et al., 1996; Green and Boger, 1997; Usher, 2002). In general, sludges and slurries are coagulated and/or flocculated before determining the above mentioned sludge rheological properties (Green et al., 1996; Green and Boger, 1997; Usher, 2002). There are several techniques obtaining experimental data for the compressive yield stress, $P_y(\phi)$ and the hindered settling function, $R(\phi)$ (e.g. transient batch sedimentation, equilibrium batch sedimentation, pressure filtration, and centrifugation) (van Deventer, 2012). Batch sedimentation may be used in the determination of the low solids concentration whilst pressure filtration and centrifugation may be used in the determination of the intermediate and/or high solids concentrations (Stickland et al., 2008; Usher et al., 2013).

A simple approach which can be used to obtain experimental data for the compressive yield stress, $P_y(\phi)$ is the use of equilibrium batch sedimentation (Buscall and White, 1987; van Deventer, 2012). However, the drawback of this approach is the long settling time for reaching the equilibrium state in a batch settler, especially for wastewater sludges (Usher et al., 2013). Thus, pressure filtration and centrifugation may be more convenient in obtaining experimental data for the compressive yield stress, $P_y(\phi)$ (Buscall and White, 1987; Green et al., 1996; Green and Boger, 1997; de Kretser et al., 2001; Usher et al., 2013). Transient batch sedimentation which is based on Kynch's theory (Kynch,

1952) and used for low solids concentrations has been employed to determine the hindered settling function, $R(\phi)$ by many researchers (Lester et al., 2005; Diehl, 2007; Grassia et al., 2008, 2011; van Deventer et al., 2011). In addition, pressure filtration is a rapid and accurate technique determining the hindered settling function, $R(\phi)$ for intermediate and high solids concentrations (Landman and White, 1992; de Kretser et al., 2001; Usher et al., 2001; Stickland, 2005).

1.3 Aggregate densification

Rakes are often used in thickeners, due to the need for transportation of solids downwards to the underflow (Rudman et al., 2008; van Deventer, 2012). The presence of the shear stress produced by these rakes affects significantly the sludge rheological properties and hence the dewatering process (Holdich and Butt, 1996; Channell and Zukoski, 1997; Channell et al., 2000; Zhou et al., 1999; Stickland and Buscall, 2009; Usher et al., 2009). One consequence of the action of rakes (which can add the shear stress in suspensions) is to densify aggregates/flocs increasing the density of aggregates/flocs through decreasing the aggregate diameters (Farrow et al., 2000; Selomulya et al., 2003; Verrelli, 2008; Usher et al., 2009; Gladman et al., 2010). The above process is called aggregate densification. The density of aggregates, which is typically smaller than the solids density itself, is an essential parameter when considering aggregate densification. A theoretical derivation of the density of aggregates in terms of the solids density and the solids concentration within the aggregates (or the solidosity of aggregates) has been given in Verrelli (2008) and Usher et al. (2009). A picture showing aggregate densification under the shear stress is presented in Fig. 1.2 which is reproduced from Usher et al. (2009).

As shown in Fig. 1.2, the aggregate diameters are decreased after aggregate densification and hence channels between aggregates are widened (Usher et al., 2009; Zhang et al., 2013a,b; Grassia et al., 2014). Both the solids concentration within the aggregates and the settling velocity expressed in terms of the solids concentration and the sludge rheological properties increase when aggregate densification occurs, due to the decrease of the aggregate diameters and the changes of sludge rheological properties (Usher et al., 2009; van Deventer et al., 2011; Zhang et al., 2013a,b). The gel point also increases dur-

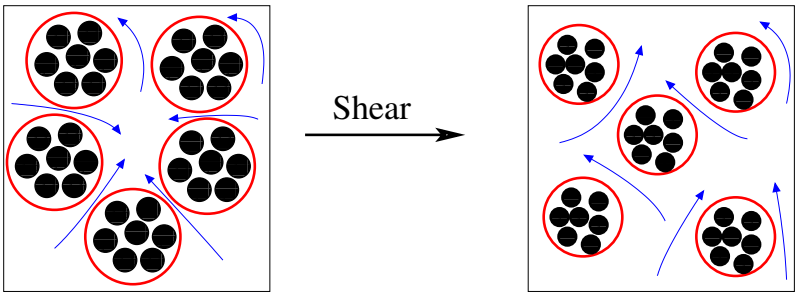

Figure 1.2: The process of aggregate densification – this figure is reproduced from Usher et al. (2009)

ing aggregate densification and hence the compressive yield stress must be altered (Usher et al., 2009; van Deventer et al., 2011; Zhang et al., 2013a,b). Therefore, the permeability and the compressibility of sludges and slurries can be improved via decreasing the hindered settling function and the compressive yield stress, respectively after aggregate densification (Usher et al., 2009; van Deventer, 2012; Zhang et al., 2013a,b; Buratto et al., 2014).

When densifying aggregates/flocs in the settling process, two processes may occur: restructuring and breakage of aggregates (Selomulya et al., 2003; Buratto et al., 2014). For a relatively low shear rate, restructuring of aggregates may occur and there is no breakage of aggregates whilst for a high shear rate, breakage of aggregates may occur (Selomulya et al., 2003; Verrelli, 2008; Gladman et al., 2010; Buratto et al., 2014; Vaxelaire and Olivier, 2014). Aggregate densification led by the action of rakes and/or the shear stress can improve the performance of a piece of dewatering equipment via increasing the solids concentrations obtained at the bottom of the tanks and the underflow solids fluxes, increasing the permeability and the compressibility, and decreasing the height of the consolidation zone (Usher et al., 2009; Gladman et al., 2010; van Deventer et al., 2011; van Deventer, 2012; Zhang et al., 2013a,b; Buratto et al., 2014).

Sludge rheological properties are altered when aggregate densification occurs in the settling process (Usher et al., 2009; Gladman et al., 2010; van Deventer et al., 2011; Zhang et al., 2013a,b). The theory of aggregate densification (Usher et al., 2009; van Deventer et al., 2011; Zhang et al., 2013a,b) assumes that there is no breakage of aggregates during aggregate densification. Under these assumptions, the sludge rheological properties (e.g. the compressive yield stress, $P_y(\phi)$ and the hindered settling function $R(\phi)$) have been

derived theoretically in terms of the solids concentrations and the aggregate diameters, once the suspension has undergone aggregate densification (Usher et al., 2009; Zhang et al., 2013b). The performance of steady state thickeners using the aggregate densification theory has been explored by several researchers (Usher et al., 2009; Gladman et al., 2010; Zhang et al., 2013a,b; Grassia et al., 2014).

In this thesis, aggregate densification is assumed to be only time-dependent. The evolution of aggregate diameters in the settling process is governed by a first order ordinary differential equation which is given by van Deventer et al. (2011). An important parameter given in that first order ordinary differential rate equation is the aggregate densification rate parameter (denoted by A) (van Deventer et al., 2011). This parameter is here assumed to be constant during aggregate densification and independent of the solids concentration in this thesis. Both inertial effects and wall effects are treated as being negligible in this thesis.

1.4 Thesis overview

This thesis is laid out as follows. Chapter 2 introduces batch sedimentation subject to slow aggregate densification. In Chapter 2, interest focusses on long-time scales so that significant settling has already taken placed before the time scales of interest. Any residual solids motion that is then driven by aggregate densification and the hydrodynamic drag induced by this residual solids motion (and the associated residual solids flux) are assumed to be negligible. Chapter 3 extends the aggregate densification theory developed by Usher et al. (2009) and van Deventer et al. (2011) to new parameter regimes, and then predicts thickener performance using the extended aggregate densification theory. In Chapter 3, a fixed aggregate diameter ratio is used to predict thickener performance. However, more generally it is necessary to densify aggregates throughout thickeners, since densification is a time-dependent behaviour. Thus, in Chapter 4, time-dependent aggregate densification is considered. The effects of time-dependent aggregate densification upon the sludge rheological properties (e.g. the compressive yield stress, $P_y(\phi)$ and the hindered settling function, $R(\phi)$) and thickener performance are also explored in Chapter 4. Chapter 5 considers how different underflow solids concentrations obtained at the bottom of thickeners

affect the predictions of thickener performance and sludge rheological properties during time-dependent aggregate densification. In Chapters 3–5, the hindered settling zone is neglected and only the consolidation zone is considered. The hindered settling zone however affects the determinations of sludge rheological properties and thickener performance when time-dependent aggregate densification occurs. Thus, Chapter 6 predicts the sludge rheological properties and thickener performance when the hindered settling zone is present. Chapter 7 gives conclusions and future work.

This thesis contains manuscripts and published papers and is presented in a so called alternative format. Chapters 2 and 6 are manuscripts which are prepared for submission. Chapters 3–4 have been published and are exhibited in the published format. The transient batch settler considered in this thesis is assumed to be initially networked where the initial feed solids volume fraction is larger than the gel point. However, the thickener considered in this thesis is operated at steady state and in addition is assumed to be initially unnetworked where the initially feed solids volume fraction is smaller than the gel point.

Chapter 2

Mathematical modelling of batch sedimentation subject to slow aggregate densification

This chapter is a manuscript that is prepared for submission. This chapter addresses the effects of slow aggregate densification occurring in an initially networked batch settler upon the evolutions of suspension heights and consolidated bed heights, and in addition upon the determinations of consolidated bed structures.

Summary

This chapter considers an initially networked batch settler subjected to very slow aggregate densification. The so called pseudo-steady state theory developed by van Deventer (2012) has been extended. The solids behaviour and the evolutions of the suspension height and the consolidated bed height have been predicted using the extended pseudo-steady state theory. Different formulae for the weight-bearing strength of the consolidated bed (so called weakly gelled and strongly gelled formulae, which differ near the top of the bed) are considered. The effects of weakly and strongly gelled formulae upon the predictions of the solids behaviour, and upon the evolutions of the suspension height as well as the consolidated bed height have been identified. In addition, the effects of the evolutions of the above two gelled formulae during aggregate densification upon the de-

terminations of the heights of the suspension and the consolidated bed have also been explored. This chapter also investigates how the proposed initial feed solids volume fraction and the proposed initial feed suspension height affect the evolutions of the heights of the suspension and the consolidated bed, as well as the determinations of the solids volume fractions obtained at the bottom of the batch settler. Giving a sufficiently tall initial suspension height leads to an insignificant increase in the solids volume fraction obtained at the bottom of the batch settler after densification. The heights of the suspension and the consolidated bed coincide when the gel point becomes larger than the initial feed solids volume fraction.

2.1 Introduction

A batch settler where there is no net flux at the bottom is an important piece of equipment in applications not only of dewatering but also of measuring sludge rheology, obtaining settling velocities of sludges, as well as designing continuous thickeners (thickeners being more in general having non-zero solids flux out the bottom) (Buscall and White, 1987; Font, 1988, 1991; Font and Ruiz, 1993; Fitch, 1993; Rushton et al., 1996; Lester et al., 2005; Diehl, 2007; Grassia et al., 2008, 2011). A sedimentation theory proposed by Kynch (1952) gives a mathematical model describing how the solids volume fraction and the suspension-clear liquor interface change in a batch settler (Bürger and Wendland, 2001a; Lester et al., 2005; Diehl, 2007; Grassia et al., 2008). Kynch's theory has been extended with the consideration of consolidation near the bottom of a batch settler (Tiller, 1981; Fitch, 1983; Font, 1988; Davis and Russel, 1989). A dewatering theory developed by Buscall and White (1987) describes a consolidation mechanism during the settling process using the so called sludge rheological properties (e.g. the compressive yield stress and the hindered settling function). Continuous thickeners, filter presses, and centrifuges are successfully designed using that dewatering theory (Landman et al., 1988; Usher et al., 2001; Martin, 2004,a; Usher and Scales, 2005; Stickland et al., 2006). Prior to designing those pieces of dewatering equipment, one must know the functional forms of the compressive yield stress and the hindered settling function (Martin, 2004; Lester et al., 2005; Usher and Scales, 2005; Zhang et al., 2013a,b). The functional form of the compressive

yield stress can be obtained using filtration tests and/or centrifugation tests (Buscall and White, 1987; Green et al., 1996; Green and Boger, 1997). However batch sedimentation is often used to obtain the functional form of the hindered settling function at low solids concentrations (Lester et al., 2005; Diehl, 2007; Stickland et al., 2008; Grassia et al., 2008, 2011; van Deventer et al., 2011). The gel point, ϕ_g which is the critical solids volume fraction at which the compressive yield stress becomes non-zero can also be determined via experiments (e.g. batch settling tests, filtration tests and/or centrifugation tests) (Usher, 2002; van Deventer, 2012). When the local solids concentration is larger than the gel point, a continuous and compressible solids network is formed (Buscall and White, 1987; de Kretser et al., 2003; Usher et al., 2006).

There are two types of batch sedimentation depending upon the proposed initial feed solids volume fractions: initially unnetworked batch settlers where the proposed initial feed solids volume fraction, ϕ_f is smaller than the gel point, ϕ_g, and initially networked batch settlers where ϕ_f is larger than ϕ_g (Buscall and White, 1987; Howells et al., 1990; Lester et al., 2005; Usher et al., 2006). An initially unnetworked batch settler includes a clear liquor zone where the solids volume fraction is nil, a hindered settling zone where the solids volume fraction is smaller than the gel point, and a consolidation zone where the solids volume fraction is larger than the gel point (Lester et al., 2005; Usher et al., 2006). An initially networked batch settler also contains three zones: a clear liquor zone, an unconsolidated zone where the solids volume fraction equals the initial feed solids volume fraction, ϕ_f, and a consolidation zone where the local solids volume fraction is larger than the gel point (Buscall and White, 1987; Howells et al., 1990). When analysing a batch settler, there are two important heights which must be identified: the suspension height which is defined by the height of the interface between the clear liquor zone and the unconsolidated zone, and the consolidated bed height which is defined by the height of the interface between the unconsolidated zone and the consolidation zone (Buscall and White, 1987; Howells et al., 1990; Lester et al., 2005; Usher et al., 2006). In this work, initially networked batch settlers are the main focus. According to the standard batch settling theories, the interface of the unconsolidated zone *never* meets that of the consolidation zone for an initially networked suspension (whereas for initially unnetworked

cases, the interface of the hindered settling zone eventually meets that of the consolidation zone) (Buscall and White, 1987; Howells et al., 1990; Bürger and Karlsen, 2001; Usher et al., 2006). These standard theories may however need to be modified owing to the process of so called aggregate densification.

Solids in a suspension tend to group together into loose aggregates often produced deliberately as a result of the addition of flocculants which form bridges between solids, leading to a faster settling rate (Usher et al., 2009; van Deventer, 2012; Grassia et al., 2014). Aggregate densification caused by shear stresses and/or the action of raking leads to a decrease in the diameters of aggregates (Channell and Zukoski, 1997; Channell et al., 2000; Usher et al., 2009; Gladman et al., 2010; van Deventer, 2012; Zhang et al., 2013a,b; Grassia et al., 2014). This leads to increases in the solids concentration within the aggregates, increases in the suspension gel point, increases in the underflow solids flux, and changes of the sludge rheological properties (Channell and Zukoski, 1997; Channell et al., 2000; Usher et al., 2009; Gladman et al., 2010; van Deventer et al., 2011; Zhang et al., 2013a,b; Grassia et al., 2014). Full densification is considered to be obtained when the aggregate diameter is densified to a minimum value (the solids volume fraction within the aggregates corresponding to the state designated as full densification typically falls well short of close packing) (Gladman et al., 2010; van Deventer et al., 2011; Zhang et al., 2013a). The ratio between the aggregate diameter in the fully densified state and that in the initially undensified state is denoted by $D_{agg,\infty}$ with the typical value of 0.9 often used in the literature (Usher et al., 2009; van Deventer et al., 2011; Zhang et al., 2013a,b).

Simulations and experiments of batch sedimentation consistent with time-dependent aggregate densification for $\phi_f < \phi_g$ (e.g. initially unnetworked suspensions) have been conducted by van Deventer et al. (2011) and van Deventer (2012). Aggregate densification ordinarily depends on time, up until attainment of the fully densified state (van Deventer et al., 2011). A rate equation that is used to characterise the evolution of the aggregate diameter and is influenced by a so called aggregate densification rate parameter, A has also been developed by van Deventer et al. (2011). If the initial feed solids volume fraction, ϕ_f is less than the gel point, ϕ_g, a shorter consolidated bed height and a larger solids volume fraction obtained at the bottom of a batch settler are achieved after time-

dependent aggregate densification (van Deventer et al., 2011; van Deventer, 2012). For a given solids volume fraction, the hindered settling function and the compressive yield stress become smaller after time-dependent aggregate densification (Usher et al., 2009; van Deventer et al., 2011; van Deventer, 2012; Zhang et al., 2013a,b). Little attention has however focused on cases for $\phi_f > \phi_g$ when time-dependent aggregate densification occurs in a batch settler. It is of particular interest therefore to explore the solids behaviours and to predict the consolidating bed structures in cases for $\phi_f > \phi_g$ when time-dependent aggregate densification occurs. The evolutions of the suspension height and the consolidated bed height during time-dependent aggregate densification are also of particular interest.

van Deventer (2012) used the so called pseudo-steady state model for determining the consolidated bed structure and the heights of the suspension and the consolidation zone in a batch settler subject to time-dependent aggregate densification[1] for $\phi_f < \phi_g$. The hydrodynamic drag forces associated with any residual solids flux and/or the solids motion are assumed to be nil when using this pseudo-steady state model (van Deventer, 2012). Experimental data imply that the results calculated using the pseudo-steady state model are only correct when using a very small aggregate densification rate parameter, A (which is far smaller than the reciprocal of the suspension's characteristic settling time) (van Deventer, 2012). For cases where $\phi_f > \phi_g$ and very slow aggregate densification (or a very small aggregate densification rate parameter, A) are chosen, we are interested in exploring whether this pseudo-steady state model can also be applied and how the heights of the suspension and the consolidation zone evolve with an increase of the densification time when using this pseudo-steady state model. This is one of the aims addressed in this work. For $\phi_f > \phi_g$, the densification-induced increase of the solids volume fraction obtained at the bottom of the batch settler after aggregate densification is also of particular interest.

Several factors influence the pseudo-steady state behaviour including the initial suspension height, H_0, the initial feed solids volume fraction, ϕ_f, the final steady state aggregate diameter ratio, $D_{agg,\infty}$, the aggregate densification rate parameter, A, different functional forms of the compressive yield stress, and the evolution of the compressive yield

[1] Specifically it is the batch settling which is treated as pseudo-steady; the aggregate densification on the other hand remains time-dependent.

stress functional form during time-dependent aggregate densification. The hydrodynamic force (or the friction drag) is neglected when using the pseudo-steady state model (van Deventer, 2012). This implies that the hindered settling function ought to have no effects on the predictions of the solids behaviours, the consolidated bed structures, and the heights of the suspension and the consolidated bed when the pseudo-steady state model is used. If aggregate densification occurs, the evolution of the compressive yield stress functional form and the physical nature of the compressive yield stress have been predicted and explored by many researchers (Gladman et al., 2005; Usher et al., 2009; van Deventer et al., 2011; van Deventer, 2012; Zhang et al., 2013a,b). It is of interest to explore how the evolution of the compressive yield stress functional form during time-dependent aggregate densification affects the consolidated bed structure, and the evolutions of the heights of the suspension and the consolidated bed when using the pseudo-steady state batch settling model. One of the aims of this work is to explore how different initial suspension heights affect the consolidated bed structure and the evolutions of the heights of the suspension and the consolidated bed during time-dependent aggregate densification for a specified initial feed solids volume fraction, ϕ_f, when the pseudo-steady state batch settling model is used. Another aim of this work is to investigate how the evolutions of the heights of the suspension and the consolidated bed are affected by giving different ϕ_f in cases where time-dependent aggregate densification occurs and the pseudo-steady state batch settling model is used.

The structure of this work is as follows. Section 2.2 reviews the sedimentation theory developed by Buscall and White (1987) and the aggregate densification theory developed by Usher et al. (2009) and van Deventer et al. (2011). The analysis of equilibrium states achieved in batch settlers for $\phi_f > \phi_g$ is also given in Section 2.2. Section 2.3 explores the evolutions of the consolidated bed height and the suspension height for both initially unnetworked and networked batch settlers where the hydrodynamic drag forces associated with the solids fluxes are included in the system of equations. Section 2.4 introduces the pseudo-steady state model developed by van Deventer (2012) and then extends this model to predict the consolidated bed structures, and the heights of the suspension and the consolidated bed in initially networked batch settlers. The effects of different pro-

posed initial suspension heights upon the predictions of the consolidated bed structures are also given in Section 2.4. A number of cases are set up in Section 2.5. Section 2.5 also introduces different types of the compressive yield stress functional form and how the compressive yield stress functional form evolves during time-dependent aggregate densification. Simulation results including the evolutions of the heights of the suspension and the consolidated bed, and the consolidated bed structures predicted using the pseudo-steady state model are given in Section 2.6. Section 2.7 provides conclusions.

2.2 Theories for batch sedimentation and aggregate densification

In this section, the theories describing batch sedimentation and aggregate densification (Buscall and White, 1987; Usher et al., 2009; van Deventer et al., 2011) are reviewed. The equilibrium state achieved in batch sedimentation consistent with time-dependent aggregate densification is also analysed in this section. Note that initially networked systems are the main focus of this study.

2.2.1 Batch sedimentation theory

Buscall and White (1987) developed a batch sedimentation theory and derived a force balance equation that can describe the settling process in a batch settler for $\phi_f > \phi_g$:

$$\frac{R(\phi)q_b}{(1-\phi)^2} - \frac{\partial P_s}{\partial z} - \Delta\rho g\phi = 0 \tag{2.2.1}$$

where ϕ is the solids volume fraction, P_s and $R(\phi)$ denote the particle stress and the hindered settling function, respectively, q_b is the solids flux, $\Delta\rho$ represents the density difference[2] between the solids and the liquid, g is the gravity acceleration which is chosen to be $9.8\,\mathrm{m\,s^{-2}}$, and z is the height which is measured upwards. Note that in Eq. (2.2.1),

[2]The variable, $\Delta\rho$ is a constant value during time-dependent densification and consolidation, since the solids and liquid are assumed to be incompressible in this thesis (Kynch, 1952). Typically, the densities of solids and liquid are chosen as $3200\,\mathrm{kg\,m^{-3}}$ and $1000\,\mathrm{kg\,m^{-3}}$, respectively (Usher et al., 2009). Hence, in this thesis, the density difference, $\Delta\rho = 2200\,\mathrm{kg\,m^{-3}}$.

the sign convention is such that the solids flux, q_b is a positive value when solids move downwards.

In some cases, when a suspension is initially networked, it might not be consolidated at all. This tends to occur in the case of a column of suspension that is not particularly tall. There is then a trivial solution to Eq. (2.2.1) in which there is no solids flux whatsoever, and the particle stress, P_s simply grows hydrostatically with depth according to the weight of solids above it. If at no point anywhere in the network does the particle stress ever attain the compressive yield stress of the material, no consolidation need ever occur. In what follows however, we assume that the column is sufficiently tall that this 'trivial' solution does not apply, and the column is tall enough, so that at least in some part of the domain, material must consolidate. In such cases, still considering an initially networked system, a zone where the particle stress is less than the compressive yield stress is designated as the unconsolidated zone and a zone where the particle stress is approximately equal to the compressive yield stress[3] is designated as the consolidation zone (Buscall and White, 1987; Howells et al., 1990). The solids volume fraction and the solids flux in the unconsolidated zone are uniform being equal to the initial feed solids volume fraction, ϕ_f and the solids flux evaluated at the top of the consolidation zone, $q_{b,top}$, respectively (Buscall and White, 1987; Auzerais et al., 1988; Howells et al., 1990). Thus, Eq. (2.2.1) indicates that the particle stress, P_s evaluated in the unconsolidated zone increases with depth up to a value that equals the compressive yield stress evaluated at the top of the consolidation zone (Buscall and White, 1987; Auzerais et al., 1988; Howells et al., 1990). In the consolidation zone however, the solids volume fraction starts to increase with depth but the solids flux starts to decrease with depth. In the consolidation zone, the particle stress is assumed to be equal to the compressive yield stress (Buscall and White, 1987; Auzerais et al., 1988; Howells et al., 1990). Hence, Eq. (2.2.1) can be rewritten as (Buscall and White, 1987; Howells et al., 1990; Lester et al., 2005; Usher et al., 2006):

[3]According to the theory of Buscall and White (1987), the particle stress cannot *exceed* the compressive yield stress by any significant amount, as this would lead to arbitrarily rapid consolidation and hence rapid increases in the compressive yield stress back to the level of the particle stress.

$$\frac{R(\phi)q_b}{(1-\phi)^2} - \frac{\partial P_y(\phi)}{\partial \phi}\frac{\partial \phi}{\partial z} - \Delta\rho g\phi = 0 \tag{2.2.2}$$

where $P_y(\phi)$ denotes the compressive yield stress.

When integrating Eq. (2.2.1) with respect to the height, z across the unconsolidated zone, this can yield an equation connecting the suspension height and the consolidated bed height (Buscall and White, 1987; Howells et al., 1990):

$$P_y(\phi_f) + \left(\frac{R(\phi_f)q_{b,top}}{(1-\phi_f)^2} - \Delta\rho g\phi_f\right)(H - z_c) = 0 \tag{2.2.3}$$

where H is the suspension height, z_c is the consolidated bed height, ϕ_f is the initial feed solids volume fraction, and $q_{b,top}$ is the solids flux evaluated at the top of the consolidation zone.

Meanwhile in the consolidated bed, once the solids flux, q_b is obtained as a function of position via Eq. (2.2.2), consolidation is described by the continuity equation that has been derived by Kynch (1952):

$$\partial\phi/\partial t = \partial q_b/\partial z \tag{2.2.4}$$

where Eq. (2.2.4) indicates that the solids volume fraction increases with time but the solids flux decreases with depth.

2.2.2 Time-dependent aggregate densification theory

Aggregate densification has been observed in settling experiments by many researchers (Farrow et al., 2000; Gladman et al., 2010; Buratto et al., 2014) and mathematical models have also been developed to describe the process of aggregate densification (Usher et al., 2009; van Deventer et al., 2011; Zhang et al., 2013a,b). We assume that there is no

breakage of aggregates (solely densification) in this work. One advantage of aggregate densification is that the performance of a piece of dewatering equipment is enhanced via altering the sludge rheological properties (Usher et al., 2009; Gladman et al., 2010; van Deventer, 2012; Zhang et al., 2013a,b; Grassia et al., 2014). The aggregate densification theory developed by Usher et al. (2009) and van Deventer et al. (2011) describes how the aggregate diameter changes with the densification time and how the sludge rheological properties are affected by changes in the aggregate diameter during aggregate densification (see details in Usher et al. (2009); van Deventer et al. (2011); Zhang et al. (2013a,b); Grassia et al. (2014); Zhang et al. (2014)).

The aggregate diameter ratio, D_{agg} denotes the ratio between the diameter of a densified aggregate and its initially undensified counterpart (Zhang et al., 2013a,b). Regardless of whether the aggregates are densified or undensified, the system gels via packing aggregates together (Usher et al., 2009; Zhang et al., 2013a,b). At the gel point there is invariably some free space between the aggregates, which implies that the overall solids volume fraction at the gel point, ϕ_g is less than the solids volume fraction within the aggregates, ϕ_{agg} (Usher et al., 2009; van Deventer, 2012; Zhang et al., 2013a,b). Moreover, the gel point, ϕ_g and the solids volume fraction within the aggregates, ϕ_{agg} are both increased with a decrease of the aggregate diameter ratio (Usher et al., 2009; van Deventer et al., 2011; Zhang et al., 2013a,b). Expressed in terms of the aggregate diameter ratio, D_{agg} (which itself evolves during the course of time-dependent aggregate densification), we have (Usher et al., 2009; van Deventer et al., 2011; Zhang et al., 2013a,b):

$$\phi_g = \frac{\phi_{g,0}}{D_{agg}^3} \tag{2.2.5}$$

where $\phi_{g,0}$ represents the initially undensified gel point.

$$\phi_{agg} = \frac{\phi_{agg,0}}{D_{agg}^3} \tag{2.2.6}$$

where $\phi_{agg,0}$ denotes the solids volume fraction within the initially undensified aggregates.

One important equation describing how the aggregate diameter ratio evolves during aggregate densification has been developed by van Deventer et al. (2011):

$$\frac{\mathrm{d}D_{agg}}{\mathrm{d}t} = -A(D_{agg} - D_{agg,\infty}) \tag{2.2.7}$$

and

$$D_{agg} = D_{agg,\infty} + (1 - D_{agg,\infty})e^{-At} \tag{2.2.8}$$

where t is the densification time, $D_{agg,\infty}$ is the fully densified aggregate diameter ratio (or the minimum aggregate diameter ratio) that is achieved in the fully densified state, and A is the aggregate densification rate parameter which is assumed to be independent of the solids volume fraction and can be measured via experiments (van Deventer, 2012).

The functional forms of the densified hindered settling function, $R(\phi, t)$ and the densified compressive yield stress, $P_y(\phi, t)$ will be altered with the decrease of the aggregate diameter ratio, D_{agg} for a local solids volume fraction, ϕ less than the solids volume fraction within the aggregates, ϕ_{agg} (Usher et al., 2009; van Deventer et al., 2011; Zhang et al., 2013a,b). For $\phi > \phi_{agg}$ however, those two densified sludge rheological properties are independent of aggregate densification due to elimination of any remaining space between the (now interpenetrating) aggregates which form into a large interlinked network, and hence the functional forms of those two densified sludge rheological properties will be replaced by the undensified ones (Usher et al., 2009; van Deventer et al., 2011; Zhang et al., 2013a,b). We will make extensive use of this result later on.

2.2.3 Analysis of the equilibrium state following batch sedimentation

At the equilibrium state in a batch settler, the solids flux is nil and hence the gravity of solids will balance the gradient of the compressive yield stress in the consolidation zone (Buscall and White, 1987; Howells et al., 1990; Usher et al., 2006; van Deventer, 2012). Hence, Eqs. (2.2.1–2.2.3) can be rewritten in the absence of the solids flux and the

solids motion (Buscall and White, 1987; Howells et al., 1990):

$$\frac{\partial P_s}{\partial z} + \Delta\rho g\phi = 0 \tag{2.2.9}$$

$$\frac{\partial P_y(\phi)}{\partial \phi}\frac{\partial \phi}{\partial z} + \Delta\rho g\phi = 0 \tag{2.2.10}$$

and

$$P_y(\phi_f) - \Delta\rho g\phi_f(H - z_c) = 0. \tag{2.2.11}$$

There are two types of equilibrium states that can be distinguished if time-dependent aggregate densification occurs: the undensified equilibrium state obtained in a batch settler where there is no aggregate densification occurring, and the fully densified equilibrium state eventually achieved in a batch settler subject to time-dependent aggregate densification (van Deventer, 2012). If no aggregate densification whatsoever occurs in a batch settler, the materials are undensified and hence the undensified sludge rheological properties are used to predict the consolidated bed structure in the undensified equilibrium state batch settler (Buscall and White, 1987; Howells et al., 1990; Usher et al., 2006). On the other hand, if time-dependent aggregate densification is complete, the fully densified sludge rheological properties are used provided the local solids volume fraction, ϕ is smaller than that within the fully densified aggregates, $\phi_{agg,\infty}$ determined using Eq. (2.2.6) by setting $D_{agg} = D_{agg,\infty}$, whereas the initially undensified sludge rheological properties are still applied for $\phi > \phi_{agg,\infty}$ in the fully densified equilibrium state batch settler (Zhang et al., 2013b). The above two equilibrium states are two limits for the predictions of the consolidated bed structures and the heights of the suspension and the consolidated bed in a batch settler subject to time-dependent aggregate densification. At the fully densified equilibrium state, the solids volume fraction determined at the top of the consolidated bed is either the initial feed solids volume fraction, ϕ_f if the proposed initial feed solids volume fraction, ϕ_f is larger than the fully densified gel point, $\phi_{g,\infty}$ calculated via Eq. (2.2.5)

by setting $D_{agg} = D_{agg,\infty}$ or the fully densified gel point, $\phi_{g,\infty}$ if $\phi_f < \phi_{g,\infty}$ (Buscall and White, 1987; Howells et al., 1990; van Deventer et al., 2011; Zhang et al., 2013b). In other words, in the former case there is a column of unconsolidated material persisting above the consolidated bed, but in the latter case there is not.

In the undensified equilibrium state where the material properties have not changed, the height of the consolidated bed, $z_{c,0}$ can be deduced via integrating Eq. (2.2.10) (Howells et al., 1990; Usher et al., 2006; van Deventer, 2012):

$$z_{c,0} = \int_{\phi_{be,0}}^{\phi_f} -\frac{\partial P_{y,0}(\phi)/\partial\phi}{\Delta\rho g\phi}\mathrm{d}\phi \tag{2.2.12}$$

where $P_{y,0}(\phi)$ represents the undensified compressive yield stress, and $\phi_{be,0}$ is the solids volume fraction determined at the bottom of the undensified equilibrium state batch settler. Note that the solids volume fraction at the top of the consolidation zone equals the initial feed solids volume fraction, ϕ_f, due to $\phi_f > \phi_{g,0}$.

The value of $\phi_{be,0}$ is not known a priori, but can be measured experimentally or else obtained via a mass balance. Overall mass balance is implied since in a batch settler there is no net solids flux at the bottom. The solids mass balance must be satisfied (Buscall and White, 1987; Howells et al., 1990):

$$P_{y,0}(\phi_{be,0}) = \Delta\rho g\phi_f H_0 \tag{2.2.13}$$

where H_0 is the initial suspension height, and $P_{y,0}(\phi_{be,0})$ denotes the undensified compressive yield stress determined at $\phi = \phi_{be,0}$. Hence, $\phi_{be,0}$ can be calculated using Eq. (2.2.13) once the functional form of the undensified compressive yield stress is given.

The suspension height, H^{unden} determined at the undensified equilibrium state is obtained via rearranging Eq. (2.2.11) (Buscall and White, 1987; Howells et al., 1990):

$$H^{unden} = z_{c,0} + \frac{P_{y,0}(\phi_f)}{\Delta\rho g\phi_f}. \tag{2.2.14}$$

At the fully densified equilibrium state where the aggregate diameter ratio is densified to the minimum value, $D_{agg,\infty}$, the prediction of the consolidated bed height is complicated, due to the need to consider a number of different cases. When the solids volume fraction obtained at the bottom of the fully densified equilibrium state batch settler, $\phi_{be,\infty}$ is smaller than the solids volume fraction within the fully densified aggregates, $\phi_{agg,\infty}$, the consolidated bed height and the solids volume fraction obtained at the bottom of the fully densified equilibrium state batch settler ($z_{c,\infty}$ and $\phi_{be,\infty}$, respectively) can be deduced via Eqs. (2.2.15–2.2.16), respectively (Buscall and White, 1987; Howells et al., 1990; van Deventer et al., 2011; van Deventer, 2012):

$$z_{c,\infty} = \int_{\phi_{be,\infty}}^{\phi_{top}} -\frac{\partial P_{y,\infty}(\phi)/\partial\phi}{\Delta\rho g\phi}\,\mathrm{d}\phi \tag{2.2.15}$$

where ϕ_{top} denotes the solids volume fraction determined at the top of the consolidated bed, $\phi_{be,\infty}$ is the solids volume fraction determined at the bottom of the fully densified equilibrium state batch settler, and $P_{y,\infty}(\phi)$ represents the fully densified compressive yield stress. Note that the solids volume fraction determined at the top of the consolidated bed, ϕ_{top} is either ϕ_f for $\phi_f > \phi_{g,\infty}$ or $\phi_{g,\infty}$ for $\phi_f < \phi_{g,\infty}$.

The solids volume fraction obtained at the bottom of the fully densified equilibrium state batch settler, $\phi_{be,\infty}$ can be deduced via Eq. (2.2.16) when $\phi_{be,\infty} < \phi_{agg,\infty}$ (Buscall and White, 1987; Howells et al., 1990; van Deventer et al., 2011; van Deventer, 2012):

$$P_{y,\infty}(\phi_{be,\infty}) = \Delta\rho g\phi_f H_0. \tag{2.2.16}$$

If $\phi_{be,\infty}$ is larger than $\phi_{agg,\infty}$, the functional form of the *fully densified* compressive yield stress is used for the zone where the local solids volume fraction, ϕ is less than the

solids volume fraction within the fully densified aggregates, $\phi_{agg,\infty}$ whilst the functional form of the *undensified* compressive yield stress must be used for the zone where $\phi > \phi_{agg,\infty}$ (Zhang et al., 2013b). The functional form of the *undensified* compressive yield stress must be included for the determination of $\phi_{be,\infty}$ when $\phi_{be,\infty} > \phi_{agg,\infty}$. Thus, Eqs. (2.2.17–2.2.18) hold:

$$z_{c,\infty} = \left(\int_{\phi_{be,\infty}}^{\phi_{agg,\infty}} -\frac{\partial P_{y,0}(\phi)/\partial\phi}{\Delta\rho g\phi} \mathrm{d}\phi \right) + \left(\int_{\phi_{agg,\infty}}^{\phi_{top}} -\frac{\partial P_{y,\infty}(\phi)/\partial\phi}{\Delta\rho g\phi} \mathrm{d}\phi \right) \tag{2.2.17}$$

and

$$P_{y,0}(\phi_{be,\infty}) = \Delta\rho g\phi_f H_0 \tag{2.2.18}$$

where ϕ_{top} represents the solids volume fraction determined at the top of the consolidated bed which is equal to $\phi_{g,\infty}$ if $\phi_f < \phi_{g,\infty}$ and is equal to ϕ_f if $\phi_f > \phi_{g,\infty}$.

The suspension height determined at the fully densified state, $H^{full\ den}$ can be calculated via Eq. (2.2.19):

$$H^{full\ den} = z_{c,\infty} + \frac{P_{y,\infty}(\phi_f)}{\Delta\rho g\phi_f} \tag{2.2.19}$$

where the second term on the right hand side of Eq. (2.2.19) vanishes in the case where $\phi_f \leq \phi_{g,\infty}$ but is non-zero in the case where $\phi_f > \phi_{g,\infty}$.

2.3 Evolution of the consolidated bed height

Knowing the evolution of the height of the consolidated bed is essential to predict the consolidated bed structure. The physical effects governing the evolution of the height of the consolidated bed must be understood before detailed mathematical modelling and simulation of batch settlers. In this section, the general behaviour of the evolution of the consolidated bed height is introduced for both initially unnetworked and networked

systems. Note that the analysis of the evolution of the consolidated bed height discussed in this section is based, in the interests of generality, not on the pseudo-steady state case but rather on the regular batch settling process where the hydrodynamic effects of the solids flux and the solids motion must be considered. Once the general behaviour of the consolidated bed is established, detailed simulation of the consolidated bed can proceed via various numerical methods[4] for predicting the suspension height and the consolidated bed height.

2.3.1 Initially unnetworked systems

For initially unnetworked systems in the case where no aggregate densification occurs, the height of the consolidated bed always increases from the bottom of a batch settler at early times and then intersects the suspension height at some time evaluated as the solids volume fraction at which the suspension height becomes the gel point (Auzerais et al., 1988; Bürger and Karlsen, 2001; Lester et al., 2005; Usher et al., 2006). The consolidated bed height (which now intersects the suspension height) is then decreased due to further consolidation at large times (Auzerais et al., 1988; Bürger and Karlsen, 2001; Lester et al., 2005; Usher et al., 2006). When time-dependent aggregate densification occurs in initially unnetworked systems, the evolution of the top of the consolidated bed is analogous to that discussed above for initially unnetworked systems in the case where no aggregate densification occurs (van Deventer et al., 2011; van Deventer, 2012).

2.3.2 Initially networked systems

The height of the consolidated bed always increases from the bottom of a batch settler until the equilibrium state is obtained for initially networked systems in the case where no aggregate densification occurs (Buscall and White, 1987; Auzerais et al., 1988; Howells et al., 1990). As discussed in Section 2.2, the suspension height must be higher than the height of the consolidated bed if there is no aggregate densification occurring: i.e. a column of unconsolidated material persists. When time-dependent aggregate densification

[4]The relevant numerical methods include the fully explicit scheme, the semi-implicit scheme, and the fully implicit scheme (Press et al., 1992). Eq. (2.2.2) and Eq. (2.2.4) are solved numerically to determine the solids volume fraction profiles and the heights of the suspension and the consolidated bed (Auzerais et al., 1988; Howells et al., 1990; Bürger et al., 2000; Bürger and Karlsen, 2001).

occurs however, the evolution of the consolidated bed height is more complicated with different behaviours, according to different initial feed solids volume fractions, ϕ_f that are given in initially networked systems.

If the initial feed solids volume fraction, ϕ_f is larger than the fully densified gel point, $\phi_{g,\infty}$, the evolution of the height of the consolidated bed is analogous to that discussed above for initially networked systems in the case where no aggregate densification occurs. Time-dependent aggregate densification might not affect (at least qualitatively) the transient behaviour of the evolution of the height of the consolidated bed in such systems.

On the other hand, if the initial feed solids volume fraction, ϕ_f is larger than the initially undensified gel point, $\phi_{g,0}$ but is smaller than the fully densified gel point, $\phi_{g,\infty}$, the evolution of the height of the consolidated bed is complicated when time-dependent aggregate densification occurs. Eq. (2.2.5) implies that the gel point increases with time during aggregate densification. When the gel point is less than the initial feed solids volume fraction, the height of the consolidated bed still increases with time, since the system is still networked. At a critical time, $t_{g,c}$ where the gel point is exactly equal to the initial feed solids volume fraction, the exact position of the top of the consolidated bed is not clear. The difficulty can be seen by comparing Eqs. (2.2.1-2.2.2). Since ϕ and q_b are continuous across the boundary between the consolidated bed and the unconsolidated column, it follows that the network stress gradient is likewise continuous across this boundary. However, at the point where the gel point, ϕ_g (which is growing in time) approaches the initial feed solids volume fraction, ϕ_f, the network stress at the bottom of the unconsolidated column, $P_y(\phi_f)$ is vanishingly small. If the unconsolidated column has any significant height, the network stress gradient in the unconsolidated column is also vanishingly small. Continuity of the network stress gradient moving into the top of the consolidated bed, then implies via Eq. (2.2.2) a vanishingly small $\mathrm{d}\phi/\mathrm{d}z$ at the top of the bed. Thus the top of the bed separates an upper region of (perfectly) uniform solids volume fractions, from a lower region of (at least locally) near uniform solids volume fractions. Such a boundary is not easily visualised via experiments.

Consider further the situation where the height of the consolidated bed is shorter than the suspension height at the critical time, $t_{g,c}$, i.e. where there is a finite height of the un-

consolidated column which is on the point of losing its gel-like character. A finite height of the unnetworked zone (or the hindered settling zone) is present for the densification time, t larger than the critical time, $t_{g,c}$. It is not clear how the height of the consolidated bed evolves for $t > t_{g,c}$. The height of the consolidated bed might be decreased if aggregate densification is faster than consolidation, a significant amount of just barely networked material (near-uniform solids volume fraction material) just below the top of the consolidated bed might lose its network character. On the other hand, the height of the consolidated bed might be increased if aggregate densification is slower than consolidation. Material situated above the top of the consolidated bed only needs to undergo a very tiny change in solids volume fractions to recover its gelled character. Unsurprisingly (due to the physics of the problem) it is inherently difficult to predict the precise location of the consolidated bed when ϕ_g is in the neighbourhood of ϕ_f, and as a direct result, numerical schemes that try to track the location of the consolidated bed also face challenges.

One situation that is relatively easy to analyse is the case where the approach to full densification is exceedingly rapid (much faster than settling). In that case, the entire initial column of gelled feed material instantaneously loses its gel-like character, and begins to settle into a gelled consolidated bed. The rheological properties of the system no longer exhibit any explicit time dependence, therefore, we are back to a conventional batch settling problem. Another situation that we can compute is that the height of the consolidated bed intersects the suspension height at the critical time, $t_{g,c}$ (i.e. the unconsolidated column vanishes at exactly the same time as it loses its gel-like character). Only a consolidation zone is present at the critical time, $t_{g,c}$. We have still not specified how the height of the consolidated bed evolves for $t > t_{g,c}$. Notice however that the inherent difficulties mentioned above in calculating the consolidated bed height need no longer apply. The network stress gradient in the unconsolidated column at the instant when the column vanishes can be non-zero, thus a non-zero gradient of ϕ is possible at the top of the consolidated bed at that same instant. There is no longer any extensive region containing material which is at or very near the gel point (thereby avoiding the inherent complications, discussed earlier, which that situation would produce).

Although there are various scenarios for the system behaviour as ϕ_g crosses ϕ_f, at

very large times where the gel point increases up to the fully densified gel point, $\phi_{g,\infty}$ ($\phi_{g,\infty} > \phi_f$), the height of the consolidated bed invariably coincides with the suspension height and then decreases until the fully densified equilibrium state is reached – this is analogous to what is observed in initially unnetworked systems for large times.

2.4 Pseudo-steady state analysis

As discussed in Section 2.3, it is difficult to predict the evolution of the consolidated bed height when aggregate densification occurs in an initially networked batch settler. However, if very slow aggregate densification is operated in an initially networked batch settler, the evolution of the consolidated bed height might be predicted using the so-called pseudo-steady state model[5] developed by van Deventer (2012).

The 'initial' state of the pseudo-steady state analysis is actually the *undensified equilibrium state* that is obtained using the undensified materials (van Deventer, 2012). In this state, an unconsolidated zone where the solids volume fraction is uniformly equal to the initial feed solids volume fraction, ϕ_f, and a consolidated bed where the solids volume fraction varies with depth are present in the batch settler (Buscall and White, 1987; Auzerais et al., 1988; Howells et al., 1990). The solids volume fraction at the top of the consolidated bed is equal to the initial feed solids volume fraction, ϕ_f at the undensified equilibrium state (Buscall and White, 1987; Howells et al., 1990). Then time-dependent aggregate densification starts to occur and additional consolidation happens as a result of densification. Note that we assume here that aggregate densification (and hence any additional consolidation associated with it) is very slow. If slow densification drives slow residual consolidation (i.e. $\partial\phi/\partial t$ is small), it follows from Eq. (2.2.4) that the solids flux, q_b associated with this $\partial q_b/\partial z$ must be likewise small (note that q_b vanishes exactly on the bottom boundary). These small q_b values experience negligible hydrodynamic force, leading to an 'equilibrium' profile of solids volume fraction vs. height that balances the gradient of the network stress with gravity.

[5]In the pseudo-steady state case, as the settling is arbitrarily fast compared to the densification, if the densified gel point crosses over the initial feed solids volume fraction, it will always be the case that the column of unconsolidated material vanishes at the same instant when that cross over occurs. Conversely in any other situation (i.e. when settling is not arbitrarily fast compared to densification), a finite unconsolidated column is still present when the densified gel point crosses over the initial feed solids volume fraction.

The equations that are used to describe the pseudo-steady state model can be written in a general form during time-dependent aggregate densification (analogous to the presentation in Section 2.2). For the bed height, z_c, we find:

$$z_c = \left(\int_{\phi_{be}}^{\phi_{agg}} -\frac{\partial P_{y,0}(\phi)/\partial\phi}{\Delta\rho g\phi} \mathrm{d}\phi \right) + \left(\int_{\phi_{agg}}^{\phi_{top}} -\frac{\partial P_y(\phi,t)/\partial\phi}{\Delta\rho g\phi} \mathrm{d}\phi \right) \tag{2.4.1}$$

where ϕ_{be} is the solids volume fraction determined at the bottom of the batch settler, $P_y(\phi,t)$ is the densified compressive yield stress which depends upon the local solids volume fraction and the densification time, $P_{y,0}(\phi)$ is the undensified compressive yield stress, t is the densification time, and ϕ_{top} is the solids volume fraction obtained at the top of the consolidation zone. Note that Eq. (2.4.1) is valid for any ϕ_{be} that is larger than the solids volume fraction within the aggregates, ϕ_{agg}. For $\phi_{be} < \phi_{agg}$, the first term on the right hand side of Eq. (2.4.1) is discarded and the lower bound of the integral, ϕ_{agg} in the second term on the right hand side of Eq. (2.4.1) is replaced by ϕ_{be}. The solids volume fraction obtained at the top of the consolidation zone, ϕ_{top} is equal to either the initial feed solids volume fraction, ϕ_f (if ϕ_f is larger than the densified gel point, ϕ_g) or the densified gel point, ϕ_g (if $\phi_f < \phi_g$). Note that the densified gel point, ϕ_g determined using Eq. (2.2.5) is required to be updated at each time step. Moreover, ϕ_{be} and $P_y(\phi,t)$ also need to be updated at each time step (more details about the time evolution will be given shortly).

The solids volume fraction obtained at the bottom of the batch settler, ϕ_{be} and the suspension height, H can be calculated using Eqs. (2.4.2–2.4.3) during time-dependent aggregate densification:

$$P_y(\phi_{be},t) = \Delta\rho g\phi_f H_0 \tag{2.4.2}$$

and

$$H = z_c + \frac{P_y(\phi_f, t)}{\Delta\rho g \phi_f} \tag{2.4.3}$$

where the functional form of the compressive yield stress used in Eq. (2.4.2) is either the (time-varying) *densified* one if $\phi_{be} < \phi_{agg}$ or the (time-invariant) *undensified* one if $\phi_{be} > \phi_{agg}$. Eq. (2.4.3) uses the functional form of the *densified* compressive yield stress predicting the suspension height. Note that Eq. (2.4.3) is only valid for $\phi_f > \phi_g$. When $\phi_f < \phi_g$, the term in $P_y(\phi_f, t)$ vanishes. Thus, $H = z_c$.

The consolidated bed structure can be obtained at each time step via rearranging Eq. (2.2.10) (Zhang et al., 2013b)

$$\frac{\partial z}{\partial \phi} = -\frac{\partial P_y(\phi, t)/\partial \phi}{\Delta\rho g \phi} \tag{2.4.4}$$

where $P_y(\phi, t)$ is the *densified* compressive yield stress functional form if the local solids volume fraction, ϕ is smaller than that within the aggregates, ϕ_{agg}. Otherwise, the *undensified* compressive yield stress functional form, $P_{y,0}(\phi)$ replaces the *densified* one.

As discussed in Section 2.2, the gel point, ϕ_g will increase from the initially undensified gel point, $\phi_{g,0}$ to the fully densified gel point, $\phi_{g,\infty}$ during time-dependent aggregate densification. When slow aggregate densification occurs and the solids volume fraction profile follows the form described above, the evolution of the consolidated bed height is easy to analyse. If the given initial feed solids volume fraction, ϕ_f is larger than the fully densified gel point, $\phi_{g,\infty}$ ($\phi_f > \phi_{g,\infty}$), the consolidated bed height always increases (at least in the systems under consideration here) from the height predicted at the initially undensified equilibrium state to the height determined at the fully densified equilibrium state, and the suspension height will never intersect the consolidated bed height. In other words, the suspension height must be always taller than the consolidated bed height. Thus, the batch settler includes a clear liquor zone, an unconsolidated zone where the solids volume fraction is equal to ϕ_f, and a consolidation zone where the solids volume fraction at the top of the consolidation zone is still ϕ_f. Eqs. (2.4.1–2.4.4) can be validly applied to

determine the solids behaviours and consolidated bed structures during time-dependent aggregate densification.

On the other hand, for $\phi_f < \phi_{g,\infty}$ but $\phi_f > \phi_{g,0}$, the suspension height will intersect the consolidated bed height at the critical time, $t_{g,c}$ and then the consolidated bed height decreases due to further dewatering. For the densification time, t shorter than $t_{g,c}$, the evolution of the consolidated bed height turns out (as we will see later) to be quite sensitive to the proposed functional forms of the compressive yield stress and in particular how they behave near the gel point. This critical time, $t_{g,c}$ can be calculated using Eq. (2.2.5) by setting $\phi_g = \phi_f$. Recall that the solids volume fraction at the top of the consolidated bed is either equal to the initial feed solids volume fraction, ϕ_f for $\phi_g < \phi_f$ or equal to the densified gel point, ϕ_g for $\phi_g > \phi_f$. At the fully densified equilibrium state, the batch settler only includes a clear liquor zone and a consolidation zone where the solids volume fraction at the top of the consolidation zone is the fully densified gel point, $\phi_{g,\infty}$. Eqs. (2.4.1–2.4.2) and Eq. (2.4.4) are used to predict the consolidated bed structure and the evolution of the consolidated bed height. However, Eq. (2.4.3) only needs to be applied for $\phi_g < \phi_f$. When $\phi_f < \phi_g$, the second term on the right hand side of Eq. (2.4.3) vanishes.

2.4.1 Bounds on the initial suspension height influencing consolidated bed behaviour

The solids mass balance equation (Eq. (2.4.2)) shows that the initial suspension height will influence the determination of the solids volume fraction at the bottom of the batch settler for a specified initial feed solids volume fraction, ϕ_f. At the undensified equilibrium state, it is very easy to obtain the solids volume fraction determined at the bottom of the batch settler, $\phi_{be,0}$ via solving Eq. (2.2.13), once the undensified compressive yield stress functional form is obtained. When time-dependent aggregate densification occurs however, the determination of the solids volume fraction at the bottom of the batch settler at each time step is complicated, due to the fact that different functional forms of the compressive yield stress apply depending on whether or not aggregates interlink and interpenetrate one another so as to fill space, i.e. depending on whether the local solids

volume fraction, ϕ is greater or less than that within the aggregates, ϕ_{agg}.

There are two limiting values of the proposed initial suspension height which will influence the predictions of consolidated bed structures and the evolutions of consolidated bed heights for specified initial feed solids volume fractions, ϕ_f. These limiting values (the interpretation of which will be given very shortly) can be determined using Eq. (2.2.13) by setting $\phi_{be,0} = \phi_{agg,0}$ and $\phi_{be,0} = \phi_{agg,\infty}$, respectively:

$$P_{y,0}(\phi_{agg,0}) = \Delta\rho g \phi_f H^{lower} \tag{2.4.5}$$

and

$$P_{y,0}(\phi_{agg,\infty}) = \Delta\rho g \phi_f H^{upper} \tag{2.4.6}$$

where H^{lower} and H^{upper} represent the lower and upper limiting values for the initial suspension height, respectively.

It is important to note that the functional form of the compressive yield stress used in Eqs. (2.4.5–2.4.6) is the *undensified* one. Eqs. (2.4.5–2.4.6) can be solved if an initial feed solids volume fraction, ϕ_f is specified. When the proposed initial suspension height, $H^{proposed}$ is smaller than the lower limit of the initial suspension height, H^{lower}, ϕ_{be} is smaller than ϕ_{agg} at each time step. For $H^{proposed} < H^{upper}$ but $H^{proposed} > H^{lower}$, the relationship between ϕ_{be} and ϕ_{agg} is complicated: ϕ_{be} is initially greater than ϕ_{agg}, but could finish off smaller than ϕ_{agg}. The actual behaviour of ϕ_{be} will be discussed shortly. If $H^{proposed} > H^{upper}$, then ϕ_{be} is larger than ϕ_{agg} at each time step.

For a specified initial feed solids volume fraction, ϕ_f, if the proposed initial suspension height, $H^{proposed}$ is smaller than the lower limit of the initial suspension height, H^{lower}, the *densified* compressive yield stress functional form should be used in Eq. (2.4.2) for the determination of the solids volume fraction at the bottom of the batch settler, ϕ_{be} for each time step. Since the compressive yield stress, $P_y(\phi, t)$ tends to decrease over time as a result of densification, it follows that ϕ_{be} must increase over time (although it still never exceeds ϕ_{agg}).

If the proposed initial suspension height, $H^{proposed}$ is larger than H^{lower} but is smaller than H^{upper}, the determination of ϕ_{be} is complicated. The solids volume fraction obtained at the bottom of the undensified equilibrium state batch settler, $\phi_{be,0}$ is larger than the solids volume fraction within the undensified aggregates, $\phi_{agg,0}$ but is smaller than the solids volume fraction within the fully densified aggregates, $\phi_{agg,\infty}$ when $H^{proposed}$ is larger than H^{lower} but is smaller than H^{upper}. If aggregate densification occurs, the solids volume fraction obtained at the bottom of the batch settler, ϕ_{be} for each time step should be equal to or larger than $\phi_{be,0}$ calculated from Eq. (2.2.13) for the specified initial feed solids volume fraction and the specified proposed initial suspension height, since consolidation is irreversible. There are two sub-cases for the determinations of ϕ_{be} at each time step. As long as the solids volume fraction within the aggregates, ϕ_{agg} updated at each time step remains smaller than $\phi_{be,0}$, then ϕ_{be} calculated at each time step must continue to be equal to $\phi_{be,0}$ due to the use of the *undensified* compressive yield stress functional form in Eq. (2.4.2). In other words, ϕ_{be} starts off fixed at a constant value $\phi_{be,0}$ for a finite period of time but later on starts to increase if ϕ_{agg} updated at each time step is larger than $\phi_{be,0}$, since the *densified* compressive yield stress functional form is then used in Eq. (2.4.2). A critical time, $t_{be,c}$ which can distinguish the boundary between the above mentioned two sub-cases can be determined via Eqs. (2.2.6–2.2.8) by setting $\phi_{agg} = \phi_{be,0}$:

$$\phi_{be,0} = \frac{\phi_{agg,0}}{(D_{agg,\infty} + (1 - D_{agg,\infty})e^{-At_{be,c}})^3}. \tag{2.4.7}$$

Therefore, when the densification time, t is smaller than this critical time, $t_{be,c}$, the solids volume fraction obtained at the bottom of the batch settler, ϕ_{be} updated at each time step is equal to the solids volume fraction obtained at the bottom of the undensified equilibrium state batch settler, $\phi_{be,0}$. On the other hand, if $t > t_{be,c}$, Eq. (2.4.2) can be used to calculate ϕ_{be} with the use of the *densified* compressive yield stress functional form that is required to be updated at each time step.

If the proposed initial suspension height, $H^{proposed}$ is larger than H^{upper}, the solids volume fraction obtained at the bottom of the undensified equilibrium state batch settler, $\phi_{be,0}$ is larger than the solids volume fraction within the fully densified aggregates, $\phi_{agg,\infty}$.

Hence, the solids volume fraction obtained at the bottom of the batch settler, ϕ_{be} calculated at any time step will be equal to $\phi_{be,0}$, since the *undensified* compressive yield stress functional form is used in Eq. (2.4.2).

2.4.2 Consolidated bed structure

The consolidation zone in a batch settler where aggregate densification occurs might include two sub-zones depending upon the relationship between the solids volume fraction obtained at the bottom of the batch settler, ϕ_{be} and the solids volume fraction within the aggregates, ϕ_{agg}. Only one zone where the *densified* sludge rheological properties are applied can be observed for $\phi_{be} < \phi_{agg}$ whilst two sub-zones (including the upper part of the consolidation zone where the *densified* sludge rheological properties are applied and the lower part of the consolidation zone where the *undensified* sludge rheological properties are used) can be observed for $\phi_{be} > \phi_{agg}$ (Zhang et al., 2013b). Thus, for the proposed initial suspension height, $H^{proposed}$ smaller than H^{lower}, only one zone where the densified sludge rheological properties are used can be found in a batch settler, due to $\phi_{be} < \phi_{agg}$. If the proposed initial suspension height, $H^{proposed}$ is larger than H^{upper}, the consolidation zone must be divided into two sub-zones: the upper sub-zone where the densified sludge rheological properties are applied and the lower sub-zone where the undensified sludge rheological properties are used, due to $\phi_{be} > \phi_{agg,\infty}$. For the proposed initial suspension height, $H^{proposed}$ larger than H^{lower} but smaller than H^{upper}, the consolidation zone might be divided into the upper sub-zone and the lower sub-zone for the densification time, t less than the critical time, $t_{be,c}$, due to $\phi_{be} > \phi_{agg}$. Then the lower sub-zone disappears and the consolidation zone only includes one zone where the densified sludge rheological properties are used for $t > t_{be,c}$, due to $\phi_{be} < \phi_{agg}$.

2.5 Case studies

In this section, the pseudo-steady state model is used to predict the solids behaviours in initially networked systems. Eight cases will be illustrated in this section with two different proposed initial feed solids volume fractions, ϕ_f and with different initial sus-

pension heights, H_0. The functional forms of the compressive yield stress are also given in this section. As discussed in Zhang et al. (2013a,b), there are two classes of the compressive yield stress functional forms that we consider: the weakly gelled formula and the strongly gelled formula. The derivative of the compressive yield stress with respect to the solids volume fraction evaluated at the gel point equals zero when using the weakly gelled formula but is equal to a finite value when using the strongly gelled formula (Zhang et al., 2013a,b). In this section, both the weakly and strongly gelled formulae are introduced.

The initial feed solids volume fraction, ϕ_f is chosen to be 0.105 for Cases 1–6 and 0.14 for Cases 7–8. The initial suspension height, H_0 is chosen to be $0.15\,\mathrm{m}$ for Cases 1–2, $0.5\,\mathrm{m}$ for Cases 3–4 and Cases 7–8, and $0.8\,\mathrm{m}$ for Cases 5–6. Cases 1, 3, 5 and 7 use the weakly gelled formulae whilst other cases use the strongly gelled formulae. The final steady state aggregate diameter ratio (or the fully densified aggregate diameter ratio), $D_{agg,\infty}$ is chosen to be 0.9 in these eight cases (Usher et al., 2009; van Deventer, 2012; Zhang et al., 2013a,b). The implication, for an undensified gel point, $\phi_{g,0}$ of 0.1, is that the fully densified gel point ($\phi_{g,\infty} = \phi_{g,0}/D^3_{agg,\infty}$) becomes 0.1372. A small aggregate densification rate parameter, A is chosen for Cases 1–8 ($A = 0.0001\,\mathrm{s}^{-1}$ (van Deventer, 2012)). In the pseudo-steady state approach considered here, changing the value of A has no effects whatsoever on the sequence of states through which the systems evolve: changing A just changes the rate at which the system evolves through that sequence. Nevertheless selecting an appropriate value of A does make it easier to relate the evolution to a physically meaningful time scale: in our case one unit of dimensionless time corresponds to approximately 2.8 hours. The densities of the solids and the liquid are $3200\,\mathrm{kg\,m}^{-3}$ and $1000\,\mathrm{kg\,m}^{-3}$, respectively, and hence the density difference, $\Delta\rho = 2200\,\mathrm{kg\,m}^{-3}$ (Usher et al., 2009; Zhang et al., 2013a,b). The gravitational acceleration, $g = 9.8\,\mathrm{m\,s}^{-2}$. The solids volume fraction within the undensified aggregates, $\phi_{agg,0}$ is chosen to be 0.1667 (Usher et al., 2009; van Deventer et al., 2011; Zhang et al., 2013a). Hence, the solids volume fraction within the fully densified aggregates, $\phi_{agg,\infty}$ is equal to 0.2286 (Usher et al., 2009; Zhang et al., 2013a). For simplicity, the densification time is set to zero at the undensified equilibrium state. Hence, the densification time increases from $t = 0$ at the undensified equilibrium state to some large value at the fully densified

	Gel formula	ϕ_f	$\phi_{g,0}$	$\phi_{g,\infty}$	$A/\,\mathrm{s}^{-1}$	$D_{agg,\infty}$	$H_0/\,\mathrm{m}$
Case 1	Weak	0.105	0.1	0.1372	0.0001	0.9	0.15
Case 2	Strong	0.105	0.1	0.1372	0.0001	0.9	0.15
Case 3	Weak	0.105	0.1	0.1372	0.0001	0.9	0.5
Case 4	Strong	0.105	0.1	0.1372	0.0001	0.9	0.5
Case 5	Weak	0.105	0.1	0.1372	0.0001	0.9	0.8
Case 6	Strong	0.105	0.1	0.1372	0.0001	0.9	0.8
Case 7	Weak	0.14	0.1	0.1372	0.0001	0.9	0.5
Case 8	Strong	0.14	0.1	0.1372	0.0001	0.9	0.5

Table 2.1: Operating parameters given in eight cases.

equilibrium state. Table 2.1 summaries the operating parameters for Cases 1–8.

2.5.1 Sludge rheological properties

We make a distinction between weakly gelled formulae (which vanish very rapidly near the gel point) and strongly gelled formulae (which vanish much less rapidly). The functional forms of the weakly gelled formulae which have been given in Usher et al. (2009) and Zhang et al. (2013b) are chosen to be

$$P_{wy,0}(\phi) = C_0 \left(\frac{\phi - \phi_{g,0}}{(\phi_{cp} - \phi)(b + \phi - \phi_{g,0})} \right)^{k_0} \tag{2.5.1}$$

where $P_{wy,0}(\phi)$ represents the weakly gelled compressive yield stress evaluated at the undensified state, the curve fitting parameters[6], $C_0 = 3.1866\,\mathrm{Pa}$, $b = 0.002$, and $k_0 = 11$ (Usher et al., 2009; Zhang et al., 2013b), the undensified gel point, $\phi_{g,0}$ and the close packing solids volume fraction, ϕ_{cp} are chosen to be 0.1 and 0.8, respectively (Usher et al., 2009; Zhang et al., 2013b). Note that the close packing solids volume fraction, ϕ_{cp}, and the curve fitting parameter, b are assumed to be independent of aggregate densification and hence are constant values in this work (Usher et al., 2009; van Deventer et al., 2011; Zhang et al., 2013a,b).

Meanwhile

[6]Usher et al. (2009) points out that the fitting parameters values chosen whilst the system specific are typical for suspensions in large-scale industrial thickeners, and points to similarities with experimental data of Gladman (2004).

$$P_{wy,1}(\phi,t) = C_1 \left(\frac{\phi - \phi_g}{(\phi_{cp} - \phi)(b + \phi - \phi_g)} \right)^{k_1} \tag{2.5.2}$$

where $P_{wy,1}(\phi,t)$ represents the weakly gelled compressive yield stress evaluated at the densified state, C_1, and k_1 are curve fitting parameters which are dependent upon the densification time, the aggregate densification rate parameter, and the solids volume fraction within the aggregates, ϕ_g is the densified gel point that is determined using Eq. (2.2.5), $b = 0.002$ and $\phi_{cp} = 0.8$ (Usher et al., 2009; Zhang et al., 2013b).

The parameters C_1 and k_1 that are given in Eq. (2.5.2) can be calculated assuming $P_{wy,0}(\phi_{agg}) = P_{wy,1}(\phi_{agg})$ and the derivatives (with respect to the solids volume fraction) $P'_{wy,0}(\phi_{agg}) = P'_{wy,1}(\phi_{agg})$ (Usher et al., 2009; van Deventer et al., 2011; Zhang et al., 2013a,b). Hence, Eqs. (2.5.3–2.5.4) hold (Usher et al., 2009; Zhang et al., 2013b)

$$C_1 = \frac{P_{wy,0}(\phi_{agg})}{\left(\frac{\phi_{agg} - \phi_g}{(\phi_{cp} - \phi_{agg})(b + \phi_{agg} - \phi_g)} \right)^{k_1}} \tag{2.5.3}$$

and

$$k_1 = k_0 \left(\left(\frac{\phi_{agg} - \phi_g}{\phi_{agg} - \phi_{g,0}} \right) \left(\frac{b + \phi_{agg} - \phi_g}{b + \phi_{agg} - \phi_{g,0}} \right) \left(\frac{(\phi_{agg} - \phi_{g,0})^2 + b(\phi_{cp} - \phi_{g,0})}{(\phi_{agg} - \phi_g)^2 + b(\phi_{cp} - \phi_g)} \right) \right). \tag{2.5.4}$$

The weakly gelled formula evaluated at the fully densified state is also given by (Usher et al., 2009; Zhang et al., 2013b)

$$P_{wy,\infty}(\phi) = C_\infty \left(\frac{\phi - \phi_{g,\infty}}{(\phi_{cp} - \phi)(b + \phi - \phi_{g,\infty})} \right)^{k_2} \tag{2.5.5}$$

where $P_{wy,\infty}(\phi)$ is the weakly gelled compressive yield stress evaluated at the fully densified state, the curve fitting parameters, $C_\infty = 4.8057\,\mathrm{Pa}$, $b = 0.002$ (as before), and $k_2 = 10.3633$ (Usher et al., 2009; Zhang et al., 2013b), the close packing solids volume fraction, $\phi_{cp} = 0.8$ (Usher et al., 2009; Zhang et al., 2013b), and the fully densified gel point, $\phi_{g,\infty}$ can be determined via Eq. (2.2.5) replacing D_{agg} by the final steady state aggregate diameter ratio, $D_{agg,\infty}$.

The strongly gelled formulae are chosen by (Zhang et al., 2013a)

$$P_{sy,0}(\phi) = \frac{c_0(\phi - \phi_{g,0})}{(b_1 + \phi - \phi_{g,0})(\phi_{cp} - \phi)^{k_3}} \tag{2.5.6}$$

where $P_{sy,0}(\phi)$ represents the strongly gelled compressive yield stress evaluated at the initially undensified state, the curve fitting parameters, $c_0 = 3.7914\,\mathrm{Pa}$, $b_1 = 0.0363$, and $k_3 = 10.8302$ (Zhang et al., 2013a), the undensified gel point, $\phi_{g,0} = 0.1$ and the close packing solids volume fraction, $\phi_{cp} = 0.8$ (Zhang et al., 2013a). Again, ϕ_{cp} and b_1 are constant values which are independent of aggregate densification (Zhang et al., 2013a).

Meanwhile

$$P_{sy,1}(\phi, t) = \frac{c_1(\phi - \phi_g)}{(b_1 + \phi - \phi_g)(\phi_{cp} - \phi)^{k_4}} \tag{2.5.7}$$

where $P_{sy,1}(\phi, t)$ represents the strongly gelled compressive yield stress evaluated at the densified state, c_1 and k_4 are dependent upon the densification time, the aggregate densification rate parameter, and the solids volume fraction. Note that $b_1 = 0.0363$ (as before) and $\phi_{cp} = 0.8$ (again as before) (Zhang et al., 2013a).

Again, c_1 and k_4 are calculated assuming $P_{sy,0}(\phi_{agg}) = P_{sy,1}(\phi_{agg})$ and the derivatives (with respect to the solids volume fraction) $P'_{sy,0}(\phi_{agg}) = P'_{sy,1}(\phi_{agg})$ (Usher et al., 2009; van Deventer et al., 2011; Zhang et al., 2013a,b). Hence, Eqs. (2.5.8–2.5.9) hold (Zhang et al., 2013a)

$$c_1 = \frac{P_{sy,0}(\phi_{agg})(b_1 + \phi_{agg} - \phi_g)(\phi_{cp} - \phi_{agg})^{k_4}}{\phi_{agg} - \phi_g} \tag{2.5.8}$$

and

$$k_4 = (\phi_{cp} - \phi_{agg}) \left(\frac{P'_{sy,0}(\phi_{agg})}{P_{sy,0}(\phi_{agg})} + \frac{1}{b_1 + \phi_{agg} - \phi_g} - \frac{1}{\phi_{agg} - \phi_g} \right) \tag{2.5.9}$$

where $P'_{sy,0}(\phi_{agg})$ is the derivative of the undensified strongly gelled compressive yield stress with respect to the solids volume fraction, ϕ evaluated at $\phi = \phi_{agg}$.

The strongly gelled formula obtained at the fully densified state is written as (Zhang et al., 2013a):

$$P_{sy,\infty}(\phi) = \frac{c_\infty(\phi - \phi_{g,\infty})}{(b_1 + \phi - \phi_{g,\infty})(\phi_{cp} - \phi)^{k_5}} \tag{2.5.10}$$

where $P_{sy,\infty}(\phi)$ denotes the fully densified strongly gelled compressive yield stress, $c_\infty = 6.4516\,\mathrm{Pa}$, $b_1 = 0.0363$, $\phi_{cp} = 0.8$, and $k_5 = 10.0335$ (Zhang et al., 2013a). Note that the fully densified gel point, $\phi_{g,\infty}$ can be calculated using Eq. (2.2.5) by setting $D_{agg} = D_{agg,\infty}$.

A figure plotting the above mentioned compressive yield stresses is presented in Fig. 2.1. It is clear from Fig. 2.1 that (except for very large solids volume fraction, ϕ in excess of the solids volume fraction within the fully densified aggregates, $\phi_{agg,\infty}$) the value of $P_y(\phi, t)$ in the densified state is less than that of $P_{y,0}(\phi)$ in the undensified state. As a result, a suspension which consolidates in the undensified state, will undergo additional consolidation due to aggregate densification (Usher et al., 2009). There is however another possibility: recall from Section 2.2.1 that a suspension which is not very tall need not consolidate at all, provided the network stress (throughout the entire network) never exceeds the compressive yield stress. If however the compressive yield stress decreases with time, at some point in time, consolidation could actually commence. In what follows however, we focus

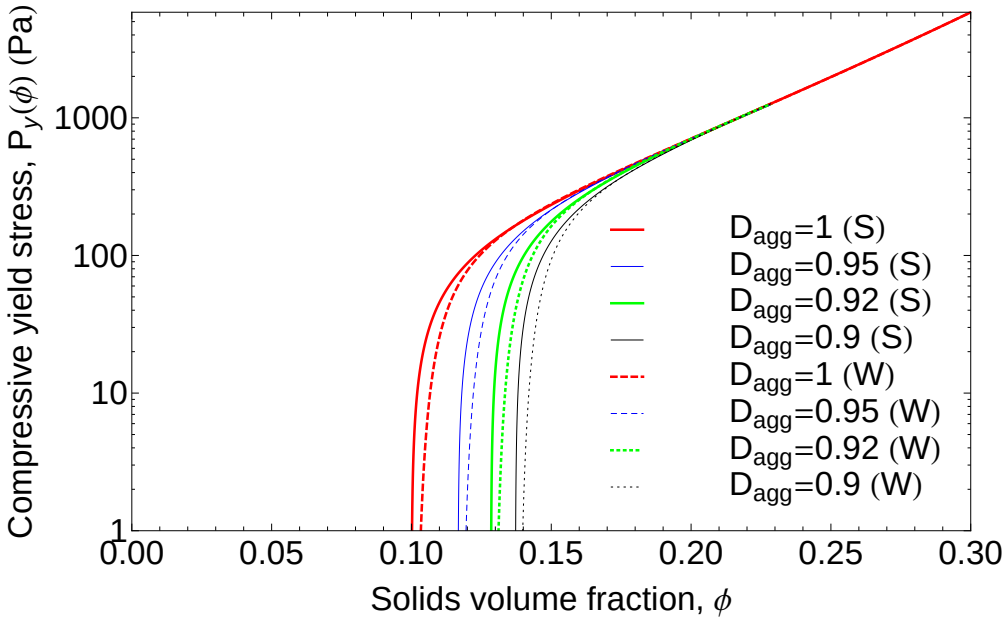

Figure 2.1: Compressive yield stress curves determined using both the strong gel (S) formula and the weak gel (W) formula with different levels of aggregate densification, represented via an aggregate diameter ratio, D_{agg}. Note that the initially undensified state corresponds to the aggregate diameter ratio, $D_{agg} = 1$ and the full densification corresponds to the aggregate diameter ratio, $D_{agg} = 0.9$.

exclusively on the case where the suspension is sufficiently tall that some consolidation happens even with aggregates in the undensified state, with subsequent densification then providing additional consolidation.

2.5.2 Dimensionless equations

We choose $C_0/(\Delta\rho g)$ as a length scale to make the dimensional equations be in dimensionless form (or completely analogously we choose $c_0/(\Delta\rho g)$ according to whether we select the strong or weak gel formulae). Moreover we choose C_0 (or the equivalently c_0) to be the scale of the compressive yield stress. Thus, the initial dimensionless suspension height, L_0, the dimensionless coordinate, Z, the dimensionless bed height, Z_c, the dimensionless compressive yield stress, $p_y(\phi, T)$, and the dimensionless suspension height, L can be defined as (Howells et al., 1990; Grassia et al., 2014; Zhang et al., 2013a, 2014):

$$L_0 = \frac{H_0 \Delta \rho g}{C_0}, \quad Z = \frac{z \Delta \rho g}{C_0}, \quad L = \frac{H \Delta \rho g}{C_0}$$

$$T = At, \quad p_y(\phi, T) = \frac{P_y(\phi, t)}{C_0}.$$

Thus, Eq. (2.2.8), Eqs. (2.4.1–2.4.4), and Eqs. (2.4.7) can be rewritten as follows. The equation for densification of aggregates becomes:

$$D_{agg} = D_{agg,\infty} + (1 - D_{agg,\infty}) e^{-T}. \tag{2.5.11}$$

The equation for predicting the bed height becomes:

$$Z_c = \left(\int_{\phi_{be}}^{\phi_{agg}} -\frac{\partial p_{y,0}(\phi)/\partial \phi}{\phi} \mathrm{d}\phi \right) + \left(\int_{\phi_{agg}}^{\phi_{top}} -\frac{\partial p_y(\phi, T)/\partial \phi}{\phi} \mathrm{d}\phi \right) \tag{2.5.12}$$

where Eq. (2.5.12) can be applied for $\phi_{be} > \phi_{agg}$. For $\phi_{be} < \phi_{agg}$, Eq. (2.5.13) applies:

$$Z_c = \int_{\phi_{be}}^{\phi_{top}} -\frac{\partial p_y(\phi, T)/\partial \phi}{\phi} \mathrm{d}\phi. \tag{2.5.13}$$

The equation for mass balance in a batch settler becomes:

$$p_y(\phi_{be}, T) = \phi_f L_0 \tag{2.5.14}$$

where Eq. (2.5.14) can also be used to determine the solids volume fraction at the bottom of the batch settler for any instant, if the initial feed solids volume fraction, ϕ_f, the dimensionless initial suspension height, L_0, and the compressive yield stress functional

form are all specified.

The equation for predicting the height of the top of the suspension becomes:

$$L = Z_c + \frac{p_y(\phi_f, T)}{\phi_f}. \tag{2.5.15}$$

The equation for determining the solids volume fraction profile becomes:

$$\frac{\partial Z}{\partial \phi} = -\frac{\partial p_y(\phi, T)/\partial \phi}{\phi}. \tag{2.5.16}$$

The equation for determining the critical time $T_{be,c}$ at which ϕ_{be} starts to increase becomes:

$$\phi_{be,0} = \frac{\phi_{agg,0}}{(D_{agg,\infty} + (1 - D_{agg,\infty})e^{-T_{be,c}})^3} \tag{2.5.17}$$

where it should be noted that Eq. (2.5.17) only applies when $\phi_{be,0}$ is between the solids volume fractions within the undensified and fully densified aggregates. If $\phi_{be,0}$ is less than $\phi_{agg,0}$, the value of ϕ_{be} always increases with time. In contrast for $\phi_{be,0} > \phi_{agg,\infty}$, the value of ϕ_{be} is fixed (at $\phi_{be,0}$) for all time. Only for $\phi_{agg,0} < \phi_{be,0} < \phi_{agg,\infty}$ does a finite $T_{be,c}$ result. It turns out that the values of $T_{be,c}$ are only relevant for Cases 3–4 here (and the values are 2.591 and 2.598, respectively).

The equation for determining the critical time, $T_{g,c}$ at which the suspension height intersects the consolidated bed height becomes:

$$\phi_f = \frac{\phi_{g,0}}{(D_{agg,\infty} + (1 - D_{agg,\infty})e^{-T_{g,c}})^3}. \tag{2.5.18}$$

It should be noted that Eq. (2.5.18) only applies when the initial feed solids volume fraction, ϕ_f is less than the fully densified gel point, $\phi_{g,\infty}$. For $\phi_f > \phi_{g,\infty}$, it is not

necessary to determine the critical time, $T_{g,c}$, since the consolidated bed height must be less than the suspension height, and some material remains unconsolidated. In this work, the critical time, $T_{g,c}$ is equal to 0.176 for Cases 1–6 (but is not relevant for Cases 7–8). Recall that for $\phi_f < \phi_{g,\infty}$, Eq. (2.5.15) only applies at $T < T_{g,c}$; otherwise for $T > T_{g,c}$ we have simply $L = Z_c$ (since $p_y(\phi_f, T)$ vanishes once $\phi_f \leq \phi_g$). Although it is convenient to perform the calculations in dimensionless form, in certain cases in what follows, the results are presented in dimensional form for ease of interpretation.

2.6 Results and discussion

The evolutions of the suspension height and the consolidated bed height predicted from Cases 1–8 are the main results of interest here. The simulation results also include the determinations of solids volume fractions obtained at the bottom of the batch settler, ϕ_{be} and the predictions of consolidated bed structures during time-dependent aggregate densification as different initial suspension heights and different initial feed solids volume fractions are given.

2.6.1 Effects of initial suspension heights and initial feed solids volume fractions

Recall that if the initial suspension height is less than a certain lower bound, H^{lower}, the solids volume fraction obtained at the bottom of the batch settler, ϕ_{be} tends to increase with time, whereas, if the initial suspension height is greater than an upper bound, H^{upper}, then ϕ_{be} remains constant. If the initial suspension height is between these two bounds, ϕ_{be} starts off constant, but later begins to increase. Table 2.2 shows, for specified initial feed solids volume fractions, these bounds on the initial suspension height which govern the system behaviour. The initial suspension heights given in Cases 1–2 are less than H^{lower} but given in Cases 5–8 are greater than H^{upper}. For Cases 3–4, the initial suspension height is between H^{lower} and H^{upper}.

As discussed in Section 2.4, the proposed initial suspension height affects the consolidated bed structure significantly. Table 2.3 shows that, for the initially networked system

ϕ_f	Gel formula	H^{lower} / m	H^{upper} / m
0.105	Weak	0.1547	0.5611
0.105	Strong	0.1527	0.5610
0.14	Weak	0.1161	0.4208
0.14	Strong	0.1145	0.4207

Table 2.2: Limits of the initial suspension height with different proposed initial feed solids volume fractions. Note that for ease of interpretation H^{lower} and H^{upper} are presented in dimensional form.

where there is no aggregate densification occurring, the solids volume fraction obtained at the bottom of the initially undensified equilibrium state batch settler, $\phi_{be,0}$ (at any given densification time) increases with an increase of the proposed initial suspension height[7] for a specified initial feed solids volume fraction, ϕ_f. If time-dependent aggregate densification occurs, the solids volume fraction obtained at the bottom of the batch settler, ϕ_{be} is also increased with the increase of the proposed initial suspension height for a given ϕ_f.

As shown in Table 2.3, the solids volume fraction obtained at the bottom of the fully densified equilibrium state batch settler, $\phi_{be,\infty}$ is less than the solids volume fraction within the fully densified aggregates, $\phi_{agg,\infty}$, provided the solids volume fraction obtained at the bottom of the initially undensified equilibrium state batch settler, $\phi_{be,0}$ is less than $\phi_{agg,\infty}$ (this applies to Cases 1–4). On the other hand, $\phi_{be,\infty}$ is larger than $\phi_{agg,\infty}$ if $\phi_{be,0} > \phi_{agg,\infty}$: indeed $\phi_{be,\infty}$ equals $\phi_{be,0}$ in that case (see Cases 5–8).

Table 2.3 also presents the solids volume fractions obtained at the bottom of the batch settler and the heights of the suspension and the consolidated bed predicted at both the initially undensified and fully densified states. The heights of the suspension in the fully densified state are invariably smaller than their undensified counterparts. Nevertheless the heights of the consolidated bed predicted at the fully densified equilibrium state are taller than those determined at the undensified equilibrium state for Cases 7–8 (contrast with the bed heights in e.g. Cases 1–6), due to a larger initial feed solids volume fraction, ϕ_f given in Cases 7–8 leading to a quite significant amount of unconsolidated column being retained above the consolidated bed for an undensified system (most of this mass then

[7]Reflecting this change in the solids volume fraction, the settled suspension height relative to the initial suspension height undergoes (in Table 2.3) a corresponding decrease.

	$\phi_{be,0}$	$\phi_{be,\infty}$	$\phi_{agg,0}$	$\phi_{agg,\infty}$
Case 1	0.1653	0.1725	0.1667	0.2286
Case 2	0.1659	0.1723	0.1667	0.2286
Case 3	0.22305	0.22308	0.1667	0.2286
Case 4	0.22309	0.22312	0.1667	0.2286
Case 5	0.2458	0.2458	0.1667	0.2286
Case 6	0.2457	0.2457	0.1667	0.2286
Case 7	0.2370	0.2370	0.1667	0.2286
Case 8	0.2370	0.2370	0.1667	0.2286

	$Z_{c,0}/L_0$	L^{unden}/L_0	$Z_{c,\infty}/L_0$	$L^{full\ den}/L_0$
Case 1	0.767	0.780	0.671	0.671
Case 2	0.717	0.787	0.682	0.682
Case 3	0.601	0.605	0.569	0.569
Case 4	0.586	0.606	0.572	0.572
Case 5	0.543	0.5455	0.523	0.523
Case 6	0.533	0.5465	0.525	0.525
Case 7	0.6196	0.739	0.720	0.721
Case 8	0.6195	0.738	0.7035	0.7235

Table 2.3: The predictions of solids volume fractions determined at the bottom of the batch settler, and heights of the suspension and the consolidated bed (normalised by the dimensionless initial suspension height L_0) in both the initially undensified equilibrium state and the fully densified equilibrium state batch settlers. Recall from Table 2.1, that Cases 1–2 have a shorter initial suspension height than Cases 3–4, whereas Cases 5–6 have a taller initial suspension height. Meanwhile Cases 7–8 have a higher initial feed solids volume fraction than any of the others. Odd numbered cases correspond to weak gels and even numbered cases correspond to strong gels.

entering the consolidated bed in the fully densified system). As also shown in Table 2.3, the solids volume fractions obtained at the bottom of the batch settler determined using the weakly gelled formula are very similar compared to those determined using the strongly gelled formula for both the initially undensified and fully densified equilibrium state batch settlers. Table 2.3 also shows that $\phi_{be,0}$ tends to increase with an increase in the initial feed solids volume fraction for an identical initial suspension height, due to more total solids mass that is given in the batch settler.

For Cases 1–6, the suspension heights and the consolidated bed heights calculated in the fully densified equilibrium state batch settler are smaller than those calculated in the initially undensified equilibrium state batch settler as shown in Table 2.3. Moreover, the fully densified suspension height equals the fully densified consolidated bed height since the initial feed solids volume fraction, ϕ_f given in those cases are smaller than the

fully densified gel point, $\phi_{g,\infty}$. Although the consolidated bed heights determined in the initially undensified equilibrium state batch settler using the weakly gelled formula are taller than those using the strongly gelled formula (e.g. odd vs. even numbered cases), the suspension heights determined in the undensified equilibrium state batch settler using the weakly gelled formula are shorter, due to the differing behaviours of the compressive yield stress formulae evaluated at or near ϕ_f when ϕ_f is itself not too far from ϕ_g.

In spite of these differences just noted, the suspension heights and the consolidated bed heights calculated using the weakly gelled formula are broadly similar compared to those determined using the strongly gelled formula in Cases 7–8, due to comparatively good agreement of the strong and weak gel functional forms (see e.g. Fig. 2.1) over much of the local solids volume fraction domain (i.e. away from the neighbourhood of the gel point; the solids volume fractions everywhere being a finite amount above the gel point in Cases 7–8).

2.6.2 Evolutions of the heights of the suspension and the consolidated bed

Figs. 2.2–2.5 show the evolutions of the heights of the suspension and the consolidated bed for Cases 1–8. For Cases 1–6, the suspension heights intersect the consolidated bed heights at the critical time, $T_{g,c}$, since the initial feed solids volume fraction, ϕ_f is smaller than the fully densified gel point, $\phi_{g,\infty}$. This time $T_{g,c}$ can be determined using Eq. (2.5.18). When the densification time, T is larger than the critical time, $T_{g,c}$, the consolidated bed heights become the suspension heights and then decrease until the fully densified equilibrium state is obtained for Cases 1–6. From this point onwards, the solids volume fraction at the top of the consolidated bed is the densified gel point which is required to be updated at each time step for $T > T_{g,c}$ in Cases 1–6. On the other hand, for Cases 7–8, the consolidated bed heights are always shorter than the suspension heights, due to a larger specified initial feed solids volume fraction, ϕ_f that exceeds the fully densified point, $\phi_{g,\infty}$. Hence, the solids volume fraction at the top of the consolidated bed is equal to the specified initial feed solids volume fraction, ϕ_f for Cases 7–8.

The functional form of the compressive yield stress affects the evolution of the consol-

idated bed height significantly for Cases 1–8. Figs. 2.2–2.5 present that the consolidated bed heights determined in Cases 1–6 always decrease for the densification time, T larger than the critical time, $T_{g,c}$, since the materials require more dewatering in order to achieve the fully densified equilibrium state. As also shown in Figs. 2.2–2.4, the consolidated bed heights determined for those cases using the strongly gelled formula always increase until the densification time, T equals the critical time, $T_{g,c}$ (e.g. Cases 2, 4, and 6) whilst the consolidated bed heights determined for those cases using the weakly gelled formula increase up to a maximum value at some time that is shorter than the critical time, $T_{g,c}$, and then decrease until the densification time, T equals the critical time, $T_{g,c}$ (e.g. Cases 1, 3, and 5). The reason for observing the decreases in the (weakly gelled) consolidated bed heights for $T < T_{g,c}$ in Figs. 2.2–2.4 is due to the very poor weight bearing abilities of the weak gel for the solids volume fractions close to the gel point: locally there tends to be a very significant amount of compression near the top of the bed as a result. This is also reflected in the amount of material that remains in the unconsolidated column. Eq. (2.5.15) indicates that this is proportional to $p_y(\phi_f, T)$, a function which collapses very dramatically in the weak gel case as the gel point, ϕ_g approaches the initial feed solids volume fraction, ϕ_f at the critical time $T_{g,c}$. Indeed when the suspension heights and the consolidated bed heights meet in Figs. 2.2–2.4, they do so tangentially for weak gels, reflecting the fact that the unconsolidated layer is exceedingly thin for quite some time on the approach to $T_{g,c}$.

The feature (in the weakly gelled case) of having a maximum in the consolidated bed height prior to the suspension height and the consolidated bed height coinciding is particular to slowly densifying systems. In the opposite limit of rapid densification, in which a suspension might switch from being gelled to ungelled, and attain full densification even before significant settling has occurred, this feature is not observed. That limit corresponds to a conventional batch settling problem but starting from an *unnetworked* system, in which the consolidated bed height tends to grow, up until the point that it coincides with the suspension height and to decrease thereafter. Thus, the qualitative curve shapes plotted in Figs. 2.2–2.4 using the strongly gelled formula with slow densification might be also observed when densification is more rapid. However, the curve shapes plotted

in Figs. 2.2–2.4 using the weakly gelled formula and slow densification (which exhibit a decrease in the consolidated bed height even for $T < T_{g,c}$) differ qualitatively from their rapid densification counterparts. It is not clear whether it is possible to observe a decrease in the consolidated bed height for $T < T_{g,c}$ in experiments. One might anticipate that these effects on the consolidated bed height could be observed in experiments, although the consolidation zone cannot always be readily visualised in experiments: rather it is the top of the suspension that is more easily detected.

For Cases 7–8, the consolidated bed heights always increase until the fully densified equilibrium state is achieved. When the weakly gelled formula is used to predict the heights of the suspension and the consolidated bed, the difference between the consolidated bed height and the suspension height near the fully densified state is smaller, compared to that determined using the strongly gelled formula as shown in Fig. 2.5, since the compressive yield stress determined at $\phi = \phi_f$ using the weakly gelled formula is substantially smaller than that determined at $\phi = \phi_f$ using the strongly gelled formula for Cases 7–8.

Although the graphs for the consolidated bed height and the suspension height given in Figs. 2.2–2.5 show clearly how the system responds to densification, there is another aspect of these figures which is worth mentioning. In Fig. 2.2, sedimentation (on a rapid time scale that is left unsolved here) takes the system from an initial normalised height of unity down to 0.78, whereas densification only takes it from the normalised height of 0.78 down to roughly 0.68. Moreover, Figs. 2.2–2.5 show even more modest from benefits from densification. Even though dewatering is clearly enhanced by aggregate densification, for these data at least, much of the dewatering was already achieved during the initial settling phase before the onset of densification.

2.6.3 Consolidated bed structure

As discussed in Section 2.4.2, the consolidated bed structure is influenced significantly by the functional forms of the compressive yield stress. It is necessary to know whether the consolidation zone determined at each time step has a sub-zone where the undensified sludge rheological properties are used. Thus, the critical time, $T_{be,c}$ deter-

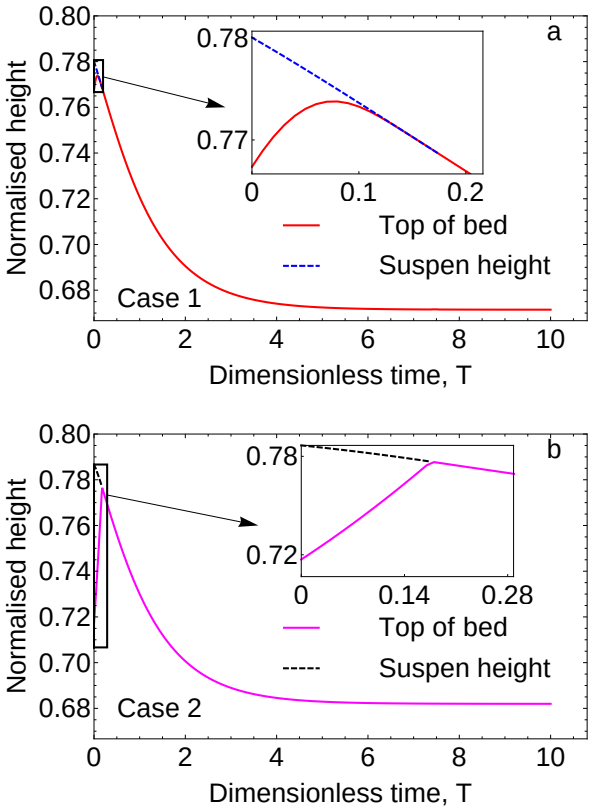

Figure 2.2: Evolutions of the heights of the suspension and the consolidated bed for Cases 1–2 (both normalised by the dimensionless initial suspension height, L_0). Note that the sub-plot labelled 'a' denotes the heights plotted for Case 1 (weak gel) whilst the sub-plot labelled 'b' represents the heights plotted for Case 2 (strong gel). Recall that the initial feed solids volume fraction, ϕ_f equals 0.105 in Cases 1–2, and this is less than the fully densified gel point, $\phi_{g,\infty}$ which equals 0.1372. Recall also that the time scale is set to zero at the undensified equilibrium state and thereafter the time scale increases when time-dependent densification and consolidation occur in parallel.

mined via Eq. (2.5.17) for each case and illustrated in Table 2.4 is very important, since it determines the densification time at which such a sub-zone, if initially present, tends to disappear.

Table 2.4 shows the critical time, $T_{be,c}$ determined for each case. The critical time, $T_{be,c}$ is not available for Cases 1–2, since $\phi_{be,0}$ is smaller than $\phi_{agg,0}$. Hence, the solids volume fraction obtained at the bottom of the batch settler, ϕ_{be} determined for each time step will be smaller than the solids volume fraction within the aggregates, ϕ_{agg} updated at each time step for Cases 1–2. Eq. (2.5.14) is used to calculate ϕ_{be} with the densified compressive yield stress for Cases 1–2. The consolidated bed just contains one zone and the densified compressive yield stress is used throughout the consolidation zone for Cases 1–

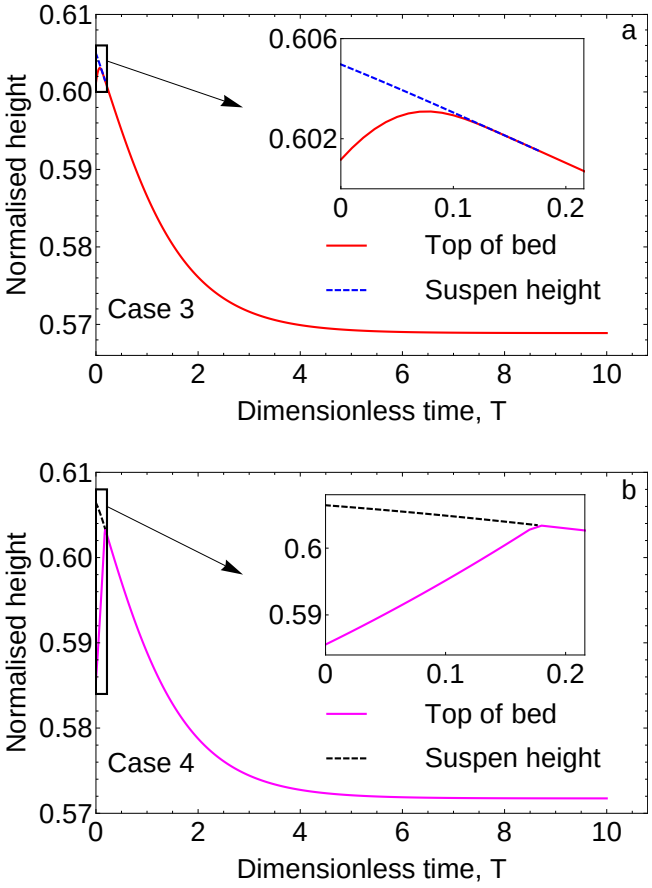

Figure 2.3: Evolutions of the suspension heights and the consolidated bed heights for Cases 3–4 (both normalised by the dimensionless initial suspension height, L_0). Note that the sub-plots labelled 'a' and 'b' denote the heights plotted for Case 3 (weak gel) and Case 4 (strong gel), respectively. Recall that the initial feed solids volume fraction, ϕ_f equals 0.105 in Cases 3–4, and this is less than the fully densified gel point, $\phi_{g,\infty}$ which equals 0.1372.

	$\phi_{be,0}$	$\phi_{be,\infty}$	$\phi_{agg,0}$	$\phi_{agg,\infty}$	$T_{be,c}$
Case 1	0.1653	0.1725	0.1667	0.2286	N/A
Case 2	0.1659	0.1723	0.1667	0.2286	N/A
Case 3	0.22305	0.22308	0.1667	0.2286	2.591
Case 4	0.22309	0.22312	0.1667	0.2286	2.598
Case 5	0.2458	0.2458	0.1667	0.2286	N/A
Case 6	0.2457	0.2457	0.1667	0.2286	N/A
Case 7	0.2370	0.2370	0.1667	0.2286	N/A
Case 8	0.2370	0.2370	0.1667	0.2286	N/A

Table 2.4: Determinations of the critical time, $T_{be,c}$ for Cases 1–8. In Cases 1–2, as ϕ_{be} starts varying from the initial instant, formally $T_{be,c}$ is zero; likewise in Cases 5–8, as ϕ_{be} never varies, formally $T_{be,c}$ is infinite.

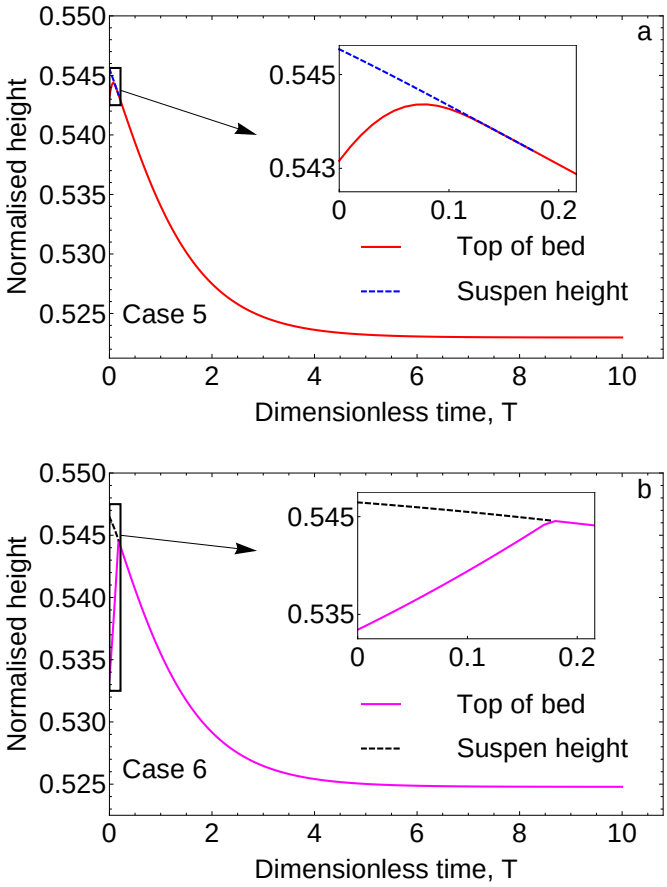

Figure 2.4: Determinations of the suspension heights and the consolidated bed heights for Cases 5–6 (both normalised by the dimensionless initial suspension height, L_0). Note that Case 5 (weak gel) and Case 6 (strong gel) are plotted in the sub-plots labelled 'a' and 'b', respectively. Recall that the initial feed solids volume fraction, ϕ_f equals 0.105 in Cases 5–6, and this is less than the fully densified gel point, $\phi_{g,\infty}$ which equals 0.1372.

2. The critical time, $T_{be,c}$ is likewise unavailable for Cases 5–8, since $\phi_{be,0}$ is larger than $\phi_{agg,\infty}$. Thus, ϕ_{be} determined at each time step will be equal to $\phi_{be,0}$ for Cases 5–8. The consolidated bed contains an upper sub-zone where the densified compressive yield stress is used, and a lower sub-zone where the undensified compressive yield stress is used for Cases 5–8. For Cases 3–4, ϕ_{be} determined at each time step equals $\phi_{be,0}$ if $T < T_{be,c}$ whilst ϕ_{be} will be determined using Eq. (2.5.14) at each time step if $T > T_{be,c}$. Thus, the consolidated bed contains both lower and upper sub-zones if $T < T_{be,c}$ in Cases 3–4. For $T > T_{be,c}$, the consolidated bed only contains one zone and the densified compressive yield stress is then used in Cases 3–4.

Figs. 2.6–2.9 show the solids volume fraction profiles for the suspension. The solids volume fractions predicted in the consolidation zone increase moving downwards into the

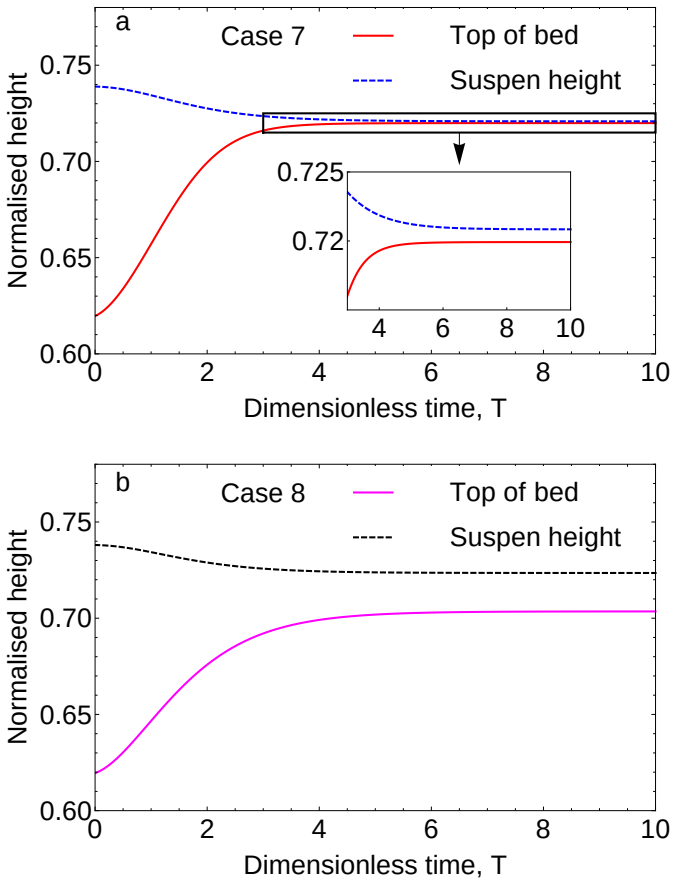

Figure 2.5: Predictions of the heights of the suspension and the consolidated bed for Cases 7–8 (both normalised by the dimensionless initial suspension height, L_0). Note that the sub-plot labelled 'a' represents the heights plotted for Case 7 (weak gel) and the sub-plot labelled 'b' denotes the heights plotted for Case 8 (strong gel). Recall that the initial feed solids volume fraction, ϕ_f equals 0.14 in Cases 7–8, and this is greater than the fully densified gel point, $\phi_{g,\infty}$ which equals 0.1372.

consolidated bed as shown in Figs. 2.6–2.9. When the local solids volume fraction, ϕ is larger than the solids volume fraction within the aggregates, ϕ_{agg}, the densified compressive yield stress functional form used in Eq. (2.5.16) is replaced by the undensified one. Thus, the same slope of the curves might be observed, at least low down in the consolidated bed, particularly in Figs. 2.6–2.9 (e.g. Cases 3–8). In cases where either the initial suspension is very tall (e.g. Cases 5–6) or the initial suspension has a comparatively high solids volume fraction (e.g. Cases 7–8), undensified sludge rheological properties actually continue to apply in quite a significant part of the consolidated bed, thus there is only very marginal benefit of densification. Near the top of the consolidated bed when predicted using the weakly gelled formula (and when the unconsolidated zone

has already disappeared), flat segments of the curves are observed in Figs. 2.6–2.9 (e.g. Cases 1, 3, and 5). This is due to both the compressive yield stress and the derivative of the compressive yield stress with respect to the local solids volume fraction determined using the weakly gelled formula approaching zero near the gel point (Zhang et al., 2013b). The implication is that the solids volume fraction obtained near the top of the consolidated bed changes significantly as the precise position in the consolidated bed changes slightly (Zhang et al., 2013b). This corroborates our statements about local collapse of the consolidated bed near the gel point. The similar behaviour is also predicted in Zhang et al. (2013b).

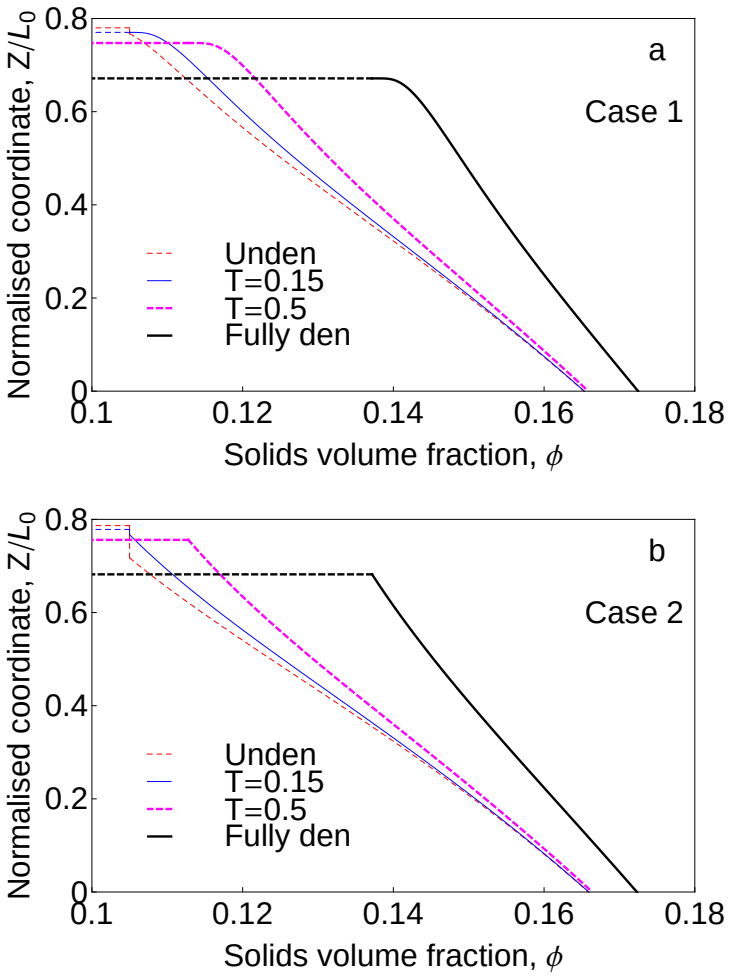

Figure 2.6: The solids volume fraction profiles predicted for Cases 1–2. Note that the sub-plot labelled 'a' denotes the consolidated bed structures predicted for Case 1 (weak gel) whilst the sub-plot labelled 'b' represents the consolidated bed structures determined for Case 2 (strong gel). Recall that the initial feed solids volume fraction, ϕ_f equals 0.105 in Cases 1–2. At sufficiently early times there can be an unconsolidated column of the uniform solids volume fraction, ϕ_f (here $\phi_f = 0.105$), although this disappears at later times.

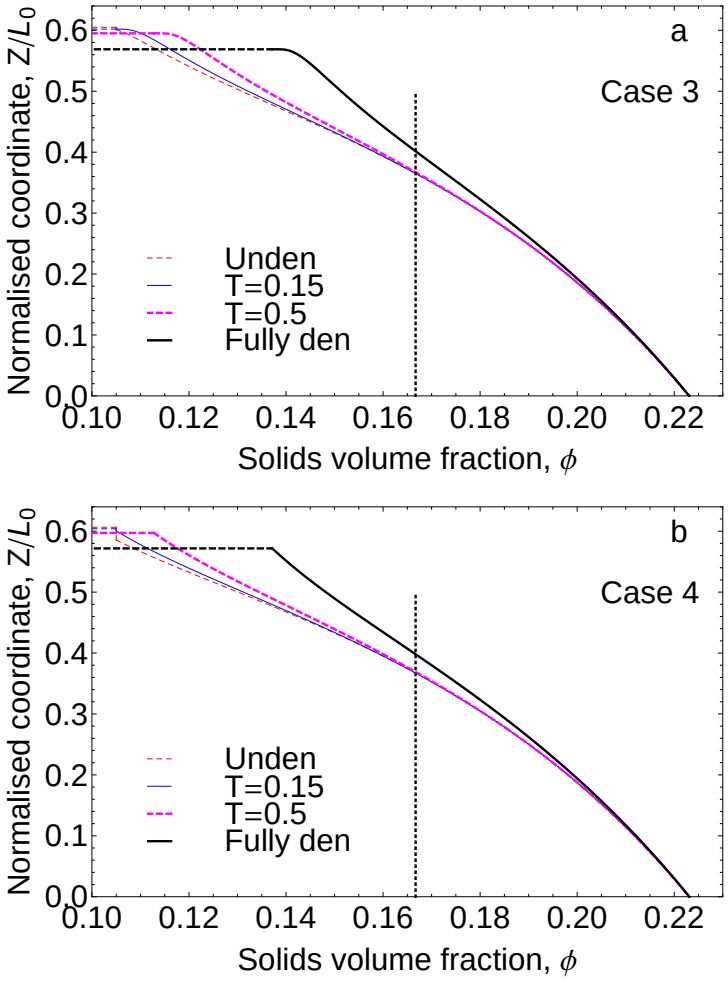

Figure 2.7: The solids volume fraction profiles determined for Cases 3–4. Note that the sub-plots labelled 'a' and 'b' denote the consolidated bed structures predicted for Case 3 (weak gel) and Case 4 (strong gel), respectively. The dotted line represents for $T = 0$ (the undensified state), the boundary between the upper part and the lower part of the consolidation zone, at which ϕ crosses ϕ_{agg} (which governs whether densified or undensified suspension properties are utilised). The boundary migrates downward over time reaching the bottom of the suspension at the critical time $T_{be,c}$ given in Table 2.4. Recall that the initial feed solids volume fraction, ϕ_f equals 0.105 in Cases 3–4.

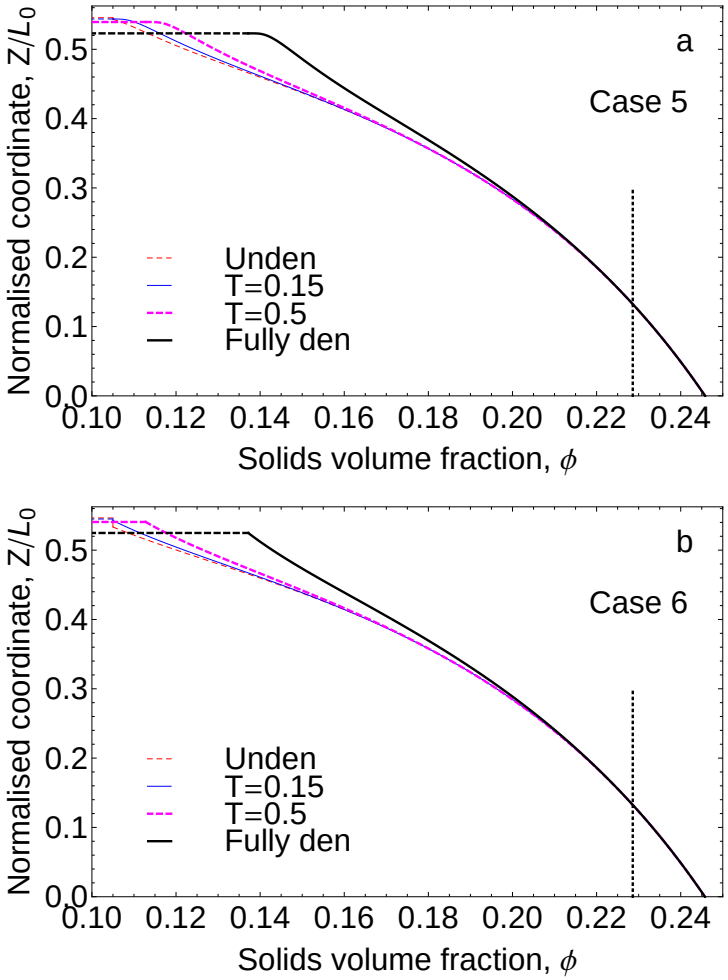

Figure 2.8: Predictions of the solids volume fraction profiles for Cases 5–6. Note that the consolidated bed structures predicted for Case 5 (weak gel) and Case 6 (strong gel) are shown in the sub-plots labelled 'a' and 'b', respectively. The dotted vertical lines represent the boundary between the upper part and lower part of the consolidation zone in a fully densified state. This boundary moves at any instant depending upon different levels of aggregate densification. At early times, with less densification this boundary would be higher up in the bed. Recall that the initial feed solids volume fraction, ϕ_f equals 0.105 in Cases 5–6.

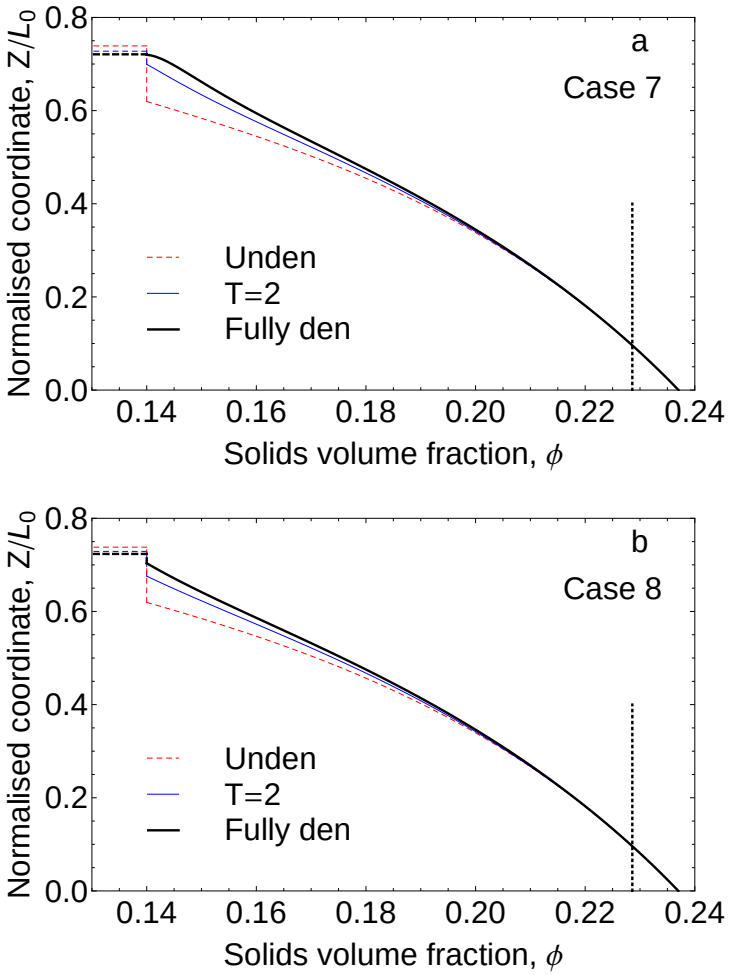

Figure 2.9: Determinations of the solids volume fraction profiles for Cases 7–8. Note that the sub-plot labelled 'a' represents the consolidated bed structures predicted for Case 7 (weak gel) and the sub-plot labelled 'b' denotes the consolidated bed structures determined for Case 8 (strong gel). The dotted vertical lines represent the boundary between the upper part of the consolidated bed (where the densified sludge rheological properties are used) and the lower part of the consolidated bed (where the undensified sludge rheological properties are used) in the case of the fully densified state. Again, at early times, with less densification this boundary would be higher up in the bed. An unconsolidated zone can be seen above the top of the bed, and this shrinks but does not disappear altogether at long times. Recall that the initial feed solids volume fraction, ϕ_f equals 0.14 in Cases 7–8.

2.7 Conclusions

In an initially networked batch setter where slow aggregate densification occurs, the pseudo-steady state model which neglects hydrodynamic drag forces associated with the solids flux is used to predict the evolutions of the heights of the suspension and the consolidated bed, and the consolidated bed structures. For the initial feed solids volume fraction, ϕ_f less than the fully densified gel point, $\phi_{g,\infty}$, different compressive yield stress functional forms can affect the evolutions of the consolidated bed heights with marked differences for times immediately before the critical time at which the suspension height and the consolidated bed height intersect. When aggregate densification occurs, the evolution of the functional form of the compressive yield stress significantly affects the prediction of the consolidated bed structure. It is possible to have either slight increases or no increase whatsoever in the solids volume fraction achieved at the bottom of the batch settler, ϕ_{be} after aggregate densification, the latter scenario occurring if the proposed initial suspension height, H_0 is comparatively tall and/or the initial feed solids volume fraction, ϕ_f is comparatively large. Decreasing the initial suspension height and/or the initial feed solids volume fraction leads to more marked increases in ϕ_{be} as the aggregates densify. If $\phi_f < \phi_{g,\infty}$ (with $\phi_{g,\infty}$ here being the gel point for a suspension that is considered fully densified), the consolidated bed height will intersect the suspension height at a critical time. Otherwise, if $\phi_f > \phi_{g,\infty}$, the suspension height is always taller than the consolidated bed height. The consolidated bed height determined at the fully densified equilibrium state is typically shorter than that calculated at the undensified equilibrium state for $\phi_f < \phi_{g,\infty}$ but can be taller than that determined at the undensified equilibrium state for $\phi_f > \phi_{g,\infty}$: this reflects a significantly higher amount of solids (in the undensified case compared to the densified one) that are retained in an unconsolidated column with the initial feed solids volume fraction, ϕ_f.

Chapter 3

Prediction of thickener performance with aggregate densification

This chapter has been published in Chemical Engineering Science: 101, 346–358 (2013). The aims of this chapter are to determine thickener performance and explore the evolutions of sludge rheological properties in a fully densified thickener.

Improving thickener performance is the main task and objective when designing and optimising a thickener (Diehl, 2006, 2012). One approach for improving thickener performance is to rake and/or shear the suspension leading to aggregate densification (Usher et al., 2009; Gladman et al., 2010; Buratto et al., 2014). In this chapter, the aggregates are assumed to be raked and/or sheared to attain a fixed constant diameter (smaller than their initial diameter) and then enter a thickener. The aggregate diameter is uniform throughout the thickener. This implies that aggregate densification considered in this chapter is neither time-dependent nor height-dependent. Thus, one limit of aggregate densification (specifically arbitrarily rapid densification) is considered in this chapter. An important assumption made in this chapter is that the aggregates are stable throughout the thickener (Usher et al., 2009; van Deventer et al., 2011), i.e. no break up of aggregates is observed.

The cross-sectional area is a very important parameter which must be considered when designing a thickener. A sufficiently large cross-sectional area provides enough space for solids settling in a tank (Talmage and Fitch, 1955; Rushton et al., 1996). There are three important interlinked operating parameters: namely the underflow solids volume fraction,

the underflow solids flux (which for a given volumetric flow rate scales inversely with the thickener cross-sectional area), and the consolidated bed height. All those three operating parameters are controllable. Engineers and researchers can determine one of those three operating parameters via specifying the other two operating parameters. If engineers and researchers aim to design and optimise a thickener successfully, the constraints on the above three operating parameters must be understood a priori.

Two interesting research questions can be asked: How do engineers and researchers determine the limits of the underflow solids flux and the consolidated bed height in a fully densified thickener as the underflow solids volume fraction is specified? Moreover how do engineers and researchers predict the consolidated bed structures and explore the evolutions of sludge rheological properties in a fully densified thickener? These two research questions are addressed in this chapter.

Chemical Engineering Science 101 (2013) 346–358

Contents lists available at ScienceDirect

Chemical Engineering Science

journal homepage: www.elsevier.com/locate/ces

Prediction of thickener performance with aggregate densification

Yi Zhang, Alastair Martin, Paul Grassia*

CEAS, The Mill, The University of Manchester, Oxford Road, Manchester M13 9PL, UK

HIGHLIGHTS

- Aggregate densification in thickeners is considered via theory of Usher et al. (2009).
- Access to much larger solids fluxes in a densified thickener is demonstrated.
- Solids fraction profiles near the top of thickener are sensitive to suspension rheology.
- Thickening enhanced if underflow solids fraction is less than that in aggregates.

GRAPHICAL ABSTRACT

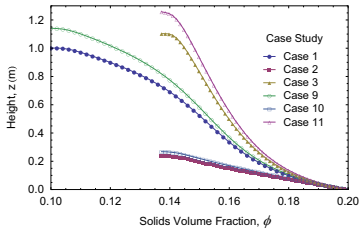

ARTICLE INFO

Article history:
Received 29 November 2012
Received in revised form
16 June 2013
Accepted 30 June 2013
Available online 9 July 2013

Keywords:
Gels
Rheology
Suspension
Mathematical modelling
Compressive yield stress
Hindered settling function

ABSTRACT

This paper aims at investigating the effects of densification of aggregates within a suspension on thickener dewatering performance. The comparisons of the maximum permitted underflow solids flux calculated from both an initial undensified thickener and a densified thickener were achieved. Large underflow solids fluxes were attained in densified thickeners. The effects of densification on the bed heights and on the solids residence times required to achieve a given underflow solids flux and a given underflow solids volume fraction were also computed and compared. Substantial reductions in the bed heights and the solids residence times are possible in densified cases. Previous studies have assumed the functional form of the compressive yield stress in the suspension so as to give an exceedingly weak gel in the neighbourhood of the solids volume fraction at the top of the bed. The implications of considering a different gel rheology with a rather stronger gel were considered. The effects of this new rheology lead to a slightly less sharp spatial gradient in the solids volume fraction near the top of the bed. In addition, the effect of varying the underflow solids volume fraction was considered. The observations of substantial increases in underflow solids fluxes and substantial reductions in bed heights and solids residence times were only achieved when the underflow solids volume fraction was less than or comparable with the solids volume fraction within the aggregates. However, if the underflow solids volume fraction was considerably larger, aggregates were considered to be overlapping and interpenetrating. As a result, the improvements in thickener performance due to densification were insignificant.

1. Introduction

A large amount of waste in the form of liquid with suspended solids is produced by the minerals industries and wastewater plants each year (Boger, 2009). Water needs to be removed from these suspensions by using dewatering devices (Bustos et al., 1999; Bürger and Wendland, 2001). In particular, thickeners are devices commonly used in the minerals industries and wastewater plants, due to low operating costs (Stickland et al., 2008). However, robust design and operation of a device such as a thickener rely on understanding the rheological behaviour of the suspension that it is used to process.

Detailed understanding of suspension rheology entails detailed models for the microstructure and micromechanics of that suspension,

* Corresponding author. Tel.: +44 161 306 8851; fax: +44 161 306 9321.
E-mail address: paul.grassia@manchester.ac.uk (P. Grassia).

0009-2509/$ - see front matter © 2013 Elsevier Ltd. All rights reserved.
http://dx.doi.org/10.1016/j.ces.2013.06.055

which have been studied by Brady and Bossis (1985, 1988), Phillips et al. (1988), and Marchioro and Acrivos (2001). Models at this level of microstructural detail tend however to be computationally intensive. Buscall and White (1987) have developed a suspension dewatering theory based on phenomenological sludge rheological properties: a so-called 'hindered settling function' and a so-called 'compressive yield stress' (both quantities to be defined shortly). This theory operates on a *continuum* rather than on a microstructural level.

The above-mentioned sludge rheological properties have been commonly used to design a thickener and predict the thickener performance[1] via this phenomenological theory over the last several years (Landman et al., 1988; Martin, 2004; Usher and Scales, 2005). Experiments and mathematical simulation models for extracting the relevant sludge rheological properties have also been developed by many authors (Kynch, 1952; Buscall and White, 1987; Landman and White, 1994; Green et al., 1998; Bürger and Concha, 1998; Lester et al., 2005; Diehl, 2007). Indeed it could be argued that the Buscall and White (1987) theory for predicting the behaviour of dewatering equipment has enjoyed wide take up owing in large part to the development of reliable and inexpensive bench-scale experimental techniques (using small suspension samples), that determine the material properties (Stickland et al., 2008; de Kretser et al., 2001; Usher et al., 2001; Landman et al., 1999; Green et al., 1998) subsequently needed for engineering design of thickeners (and/or other dewatering equipment) on a phenomenological level.

The above-mentioned theoretical and mathematical models used for the predictions of thickener performance did not however account for shear stress which could be important in thickeners due to the presence of rakes which shear the suspensions in order to improve the thickener performance. Thus, discrepancies still exist between theoretical models and industrial thickener operations (Usher et al., 2009; van Deventer et al., 2011).

A complete understanding of how suspensions might dewater in the presence of shear again involves detailed descriptions of suspension microstructure, and how such microstructure is influenced by changes in solids volume fraction as well as by shear (Brady and Bossis, 1985, 1988; Phillips et al., 1988; Marchioro and Acrivos, 2001; Bossis and Brady, 1984; Graham and Bird, 1984). What has become apparent is that, in the presence of shear, there is not only a Buscall and White (1987) type 'compressive yield stress' term (driving suspended solids from high to low concentrations, Landman et al., 1999; Fang et al., 2002), but also a 'shear-induced diffusion' effect, driving solids from zones of high to low shear (Leighton and Acrivos, 1987a, 1987b; Acrivos, 1995). The phenomenon of shear-induced diffusion is considered to arise as a result of solids in the suspension acquiring a random component to their velocity due to hydrodynamic interactions with other (randomly positioned) solids (Acrivos, 1995). There have been numerous studies quantifying these effects (Breedveld et al., 1998; Wang et al., 1996, 1998; Husband et al., 1994; Graham et al., 1991; Abbott et al., 1991; Foss and Brady, 1999; Brady and Morris, 1997). Shear-induced diffusion has also been introduced into continuum level models of suspension mechanics (Phillips et al., 1992; Subia et al., 1998; Fang et al., 2002; Kapoor and Acrivos, 1995). Such continuum models can be considered to be informed by processes occurring at the microscale, but certainly do not require detailed microstructural information to be employed. In the works cited above, the models have been used to good effect in various geometries (e.g. pipe flows, rotating cylinder flows, inclined-settler flows, etc.).

The work of Usher et al. (2009) however chose to incorporate shear in a somewhat more empirical fashion which can nonetheless be adapted conveniently and readily onto the framework of the dewatering calculations from the Buscall and White (1987) theory. Usher et al. (2009) focussed on suspensions containing bound aggregates of solids known as flocs, and in particular considered systems that are flocculated using polymers, the role of the polymers being to bridge solid particles and thereby to bind solids together into the aforementioned aggregates. Given that binding by polymer bridges may be considered irreversible (on time scales of interest), Usher et al. (2009) speculated that shear stress produced by rakes or rotors might change the microstructure of a suspension by leading to further binding and thereby aggregate densification[2]; individual aggregates may become more tightly bound and simultaneously wider channels open up between aggregates (a process which could potentially be considered as being very loosely analogous to shear-induced diffusion driving solids away from the neighbourhood of the rake, and opening up channels near it). This aggregate densification then affects the suspension settling process and thereby the thickener performance (Usher et al., 2009; Gladman et al., 2010; van Deventer et al., 2011).

The aggregate densification theory developed by Usher et al. (2009) quantified the extent to which the shear-induced change of aggregate diameters during the settling process affected the sludge rheological properties. The ability of the suspension to form a weight bearing gel relies on maintaining contacts between adjacent aggregates. However, these contacts become fewer as the individual aggregates densify, which can lead (as noted above) to wider channels between aggregates. Viscous drag between the solids and adjacent fluid tends also to be reduced, owing to these wider channels.

As a development of the aggregate densification theory, the performance of a densified thickener must be predicted. Usher et al. (2009) presented the significant improvement possible for the performance of a densified thickener based on the predictions of the solids flux and the solids settling rate in a thickener with a given bed height. In the case of a thickener that processes material beyond the solids fraction at which the suspension forms a weight bearing gel, it was not made explicit by Usher et al. (2009) how closely the solids flux in these fixed bed height cases approached the maximum possible solids flux (which is only realised for an arbitrarily tall bed). Thus, the possibility of accessing an underflow solids flux which is demonstrably much larger than the maximum permitted underflow solids flux in an undensified thickener has not been explicitly investigated in such cases. Moreover, the possibility of dramatic reductions in the solids residence time and the bed height required to achieve a given underflow solids volume fraction in a densified thickener have not been explored.

Whenever studying a densified thickener, an important parameter is the ratio of the solids residence time to the characteristic time scale for densifying aggregates. Residence time is evidently an important parameter used for the prediction of the performance of a densified thickener, since the evolution of the aggregate diameter depends on the residence time (van Deventer et al., 2011): aggregates can potentially densify to attain a final steady state diameter, but the final steady state aggregate diameter is

[1] More generally the theory can be used to design and predict the performance of other types of dewatering equipment including e.g. batch settlers and pressure filters (Buscall and White, 1987; Howells et al., 1990; Landman and Russel, 1993; Landman and White, 1994; Davis and Russel, 1989; Green et al., 1998; Landman et al., 1999; de Kretser et al., 2001). The overarching theory is the same, although the boundary conditions required depend on the particular type of equipment under consideration.

[2] This is a different physical picture from one where weak aggregates might be formed due to electrostatic and van der Waals forces between particles (Kralchevsky et al., 2008), in the absence of any bridging polymer. The microstructure of an aggregate which involves polymer bridging is arguably more complex than that of one where e.g. spherical particles are subject to electrostatic, van der Waals and possibly also Brownian forces (Brady and Bossis, 1988; Davis and Russel, 1989) (in addition to hydrodynamic forces and gravity which would be present in either case).

only achieved when the solids residence time is longer than the characteristic densification time (Gladman et al., 2010). This is the particular limit to be studied here.

The bed height is also an important parameter used to design a thickener with the bed height being required to exceed a minimum permitted value. A significant reduction in the bed height may lead to a significant reduction in the solids residence time and thereby a failure to attain a final steady state aggregate diameter within the solids residence time available, although this is not an issue we shall address here.

In addition to studying the thickener bed heights for densified and undensified sludges, it is interesting to understand how the solids volume fraction varies across the bed, which previous studies did not specifically examine (Usher et al., 2009). The properties of the solids volume fraction versus height location in densified thickeners have not been previously reported. Predictions of the profiles of the solids volume fraction in thickeners are useful to understand how these profiles change with respect to the underflow solids flux. The influence upon the thickener design of different underflow solids volume fractions is of particular interest. Usher et al. (2009) demonstrated a weak improvement in the thickener performance due to densification in the case of a high underflow solids volume fraction, specifically for the case when the underflow solids volume fraction, ϕ_u, is much larger than the solids volume fraction within the aggregates, ϕ_{agg}. The reasons for a weak performance improvement, which were not examined in detail by Usher et al. (2009), need to be discussed. The findings need to be contrasted with the case where the underflow solids volume fraction, ϕ_u, and the solids volume fraction within the aggregates, ϕ_{agg}, are comparable.

This paper uses the densified sludge rheological properties as determined by the theory of Usher et al. (2009) as inputs to predict the performance of a densified thickener. The calculated results include the actual bed height, h_b, the minimum possible bed height, $h_{b,min}$, the maximum permitted underflow solids flux, $q_{\max}$, and the solids residence time, t_{res}. The sensitivity of the thickener design to the precise functional forms of the sludge rheological properties is also explored. Section 2 describes how sludge rheological properties are affected by densification. Section 3 outlines a number of case studies used to predict the above-mentioned parameters (i.e. the actual bed height, h_b, the minimum possible bed height, $h_{b,min}$, the maximum permitted underflow solids flux, $q_{\max}$, and the solids residence time, t_{res}). Section 4 presents the calculated results and discusses how aggregate densification affects the thickener performance. Section 5 gives the conclusions.

2. Sludge dewatering theory

Here, the densification theory developed by Usher et al. (2009) is reviewed and extended. Based on the physical picture alluded to earlier, i.e. solids joined together irreversibly into flocs by polymer bridging, suspension rheological properties in terms of the solids volume fraction, ϕ, and the solids volume fraction within the aggregates, ϕ_{agg}, are discussed. In particular, the densified sludge properties including the densified hindered settling function, $R(\phi,\phi_{agg})$ (a measure of the frictional drag between the solids and liquid), and the densified compressive yield stress, $P_y(\phi,\phi_{agg})$ (a measure of gel strength[3]) are discussed. A mathematical model used for predicting the variation of the solids volume fraction across the consolidation zone (where suspension dewatering occurs) is also introduced.

Aggregate densification leads to the decrease in the aggregate diameter. The solids volume fraction within the aggregates is not constant, but rather increases with the decrease in the aggregate diameter. A mass balance within the aggregates developed by Usher et al. (2009) is used to determine the solids volume fraction within the aggregates

$$\phi_{agg} = \frac{\phi_{agg,0}}{D_{agg}^3} \tag{1}$$

where $\phi_{agg,0}$ is the initial undensified solids volume fraction within the aggregates and D_{agg} is the aggregate diameter ratio defined as the densified-to-undensified diameter ratio.

During aggregate densification, the so-called aggregate volume fraction, Φ, is an important parameter that is used for the determination of the densified hindered settling function, $R(\phi,\phi_{agg})$, and the compressive yield stress, $P_y(\phi,\phi_{agg})$. Usher et al. (2009) defined the aggregate volume fraction

$$\Phi = \frac{\phi}{\phi_{agg}} \tag{2}$$

where ϕ is the solids volume fraction and ϕ_{agg} is the solids volume fraction within the aggregates. Clearly if $\Phi<1$, then free space exists between aggregates, whilst if $\Phi\geq 1$, then the aggregates overlap and interpenetrate.

2.1. Densified hindered settling function

The densified hindered settling function, $R(\phi,\phi_{agg})$, is measured in principle via the solids free settling velocity for an arbitrarily tall suspension with spatially uniform solids volume fraction. The initial undensified dewatering theory developed by Buscall and White (1987) presents that the hydrodynamic drag force in the suspension is balanced by a gravity force, since all the solids settle uniformly in the absence of any particle pressure gradient. Specifically, if the density difference between solid and liquid is $\Delta\rho$, gravity is g, solids fraction is ϕ, and the solids settling speed (in a spatially uniform system) is u, then R is defined as $(1-\phi)^2\Delta\rho g/u$. The reason for including the $(1-\phi)^2$ factor here comes from consideration of both the governing momentum and continuity equations for the system. In the momentum balance (Landman and White, 1994), hydrostatic pressure in the liquid cooperates with drag on settling solids, tending to reduce settling speed by a factor $1-\phi$. Meanwhile, the continuity equation (Buscall and White, 1987) ensures that (in a batch settler with a closed base) the settling speed itself is an extra factor $1-\phi$ smaller than the solid–liquid velocity difference.

The aggregate densification theory (Usher et al., 2009) assumes that the densified solids settling velocity has two contributions: the velocity of aggregates associated with the liquid flow *around* the aggregates and the velocity of aggregates associated with the liquid flow *through* the aggregates. Here, we reformulate the theory from Usher et al. (2009) in an equivalent way that elucidates some of the key physical ideas that were left implicit in Usher et al. (2009). Specifically, as the effects of liquid flow *around* the aggregates and liquid flow *through* the aggregates act in parallel, the densified hindered settling function, $R(\phi,\phi_{agg})$, is described by

$$\frac{(1-\phi)^2}{R(\phi,\phi_{agg})} = \frac{\phi_{agg}(1-\Phi)^2}{R_{Stokes}r_{agg}(\Phi)} + \frac{\Phi(1-\phi_{agg})^2}{R_0(\phi_{agg})} \tag{3}$$

where $R_0(\phi_{agg})$ is the undensified hindered settling function evaluated at $\phi=\phi_{agg}$, R_{Stokes} denotes the densified hindered

[3] For a system involving flocculation of solid particles by bridging polymers forming a network, the compressive yield stress can be thought of as being an analogue of the osmotic pressure (in the case of a system where instead solids experience electrostatic, van der Waals and/or Brownian forces (Davis and Russel, 1989)). There are nevertheless some subtleties involved in demonstrating this analogy: see Buscall and White (1987) for details.

settling function of an isolated aggregate, and $r_{agg}(\Phi)$ is the aggregate hindered settling factor which is defined shortly.

The first term with the prefactor ϕ_{agg} on the right hand side of Eq. (3) denotes the influence of resistance associated with the liquid flow around the aggregates. The prefactor ϕ_{agg} represents the fact that the aggregates are less dense than the solids and hence would experience less buoyancy in the free settling zone. In addition, the second term with the prefactor Φ on the right hand side of Eq. (3) denotes the influence of resistance associated with liquid flow through the aggregates. The prefactor Φ represents that flow through the aggregates only occurs in the fraction of space that the aggregates actually occupy. Note that Eq. (3) is only valid for $\Phi<1$. In the event that $\Phi>1$, the aggregates are all overlapping and interpenetrating. There is then no space remaining between aggregates and hence only flow through the aggregates can occur. In that case, $R(\phi,\phi_{agg})=R_0(\phi)$.

The densified hindered settling function of an isolated aggregate, R_{Stokes}, is determined as

$$R_{Stokes}=\frac{R_{Stokes,0}}{D_{agg}^2} \tag{4}$$

where $R_{Stokes,0}$ denotes the hindered settling function of an isolated undensified aggregate.

The undensified hindered settling function of an isolated aggregate can also be obtained as

$$R_{Stokes,0}=\phi_{agg,0}R_0(0) \tag{5}$$

where $R_0(0)$ denotes the undensified hindered settling function for the suspension in the limit as $\phi\to 0$.

Usher et al. (2009) assumed that the aggregate hindered settling factor, $r_{agg}(\Phi)$, was independent of densification. Consequently, $r_{agg}(\Phi)$ is determined by substituting Eq. (1) and Eqs. (4) and (5) into Eq. (3) and then rearranging Eq. (3) in the initial undensified state

$$r_{agg}(\Phi)=\frac{\phi_{agg,0}(1-\Phi)^2R_0(\phi_{agg,0})R_0(\phi_{agg,0}\Phi)/(R_{Stokes,0}D_{agg,0})}{(R_0(\phi_{agg,0})(1-\phi_{agg,0}\Phi)^2-\Phi(1-\phi_{agg,0})^2R_0(\phi_{agg,0}\Phi))} \tag{6}$$

where by definition $D_{agg,0}=1$.

Substituting Eq. (1) and Eqs. (4)–(6) into Eq. (3) and then rearranging Eq. (3) yields the densified hindered settling function

$$R(\phi,\phi_{agg})=\frac{(1-\phi)^2R_0(\phi_{agg})R_{Stokes,0}D_{agg}}{\dfrac{\phi_{agg,0}R_0(\phi_{agg})\left(1-\dfrac{\phi}{\phi_{agg}}\right)^2}{r_{agg}\left(\dfrac{\phi}{\phi_{agg}}\right)}+R_{Stokes,0}D_{agg}\left(\dfrac{\phi}{\phi_{agg}}\right)(1-\phi_{agg})^2}. \tag{7}$$

Whilst the above represents a 'complete' formula for $R(\phi,\phi_{agg})$, Usher et al. (2009) stated that the first term on the right hand side of Eq. (3) (flow around the aggregates) played the dominant contribution to determine the densified hindered settling function, $R(\phi,\phi_{agg})$, at least when the local solids volume fraction was considerably smaller than that within the aggregates. In other words, the second term on the right hand side of Eq. (3) can be neglected in that case. Therefore, Eq. (3) can be rewritten as

$$\frac{(1-\phi)^2}{\tilde{R}(\phi,\phi_{agg})}\approx\frac{\phi_{agg,0}(1-\Phi)^2}{R_{Stokes,0}D_{agg}\tilde{r}_{agg}(\Phi)} \tag{8}$$

where $\tilde{R}(\phi,\phi_{agg})$ is the approximated densified hindered settling function and $\tilde{r}_{agg}(\Phi)$ is the approximated aggregate hindered settling factor which is also assumed to be independent of densification.

We derive $\tilde{r}_{agg}(\Phi)$ by rearranging Eq. (8) in the initial undensified state

$$\tilde{r}_{agg}(\Phi)\approx\frac{\phi_{agg,0}(1-\Phi)^2R_0(\Phi\phi_{agg,0})}{R_{Stokes,0}D_{agg,0}(1-\Phi\phi_{agg,0})^2} \tag{9}$$

where $R_0(\Phi\phi_{agg,0})$ denotes the initial undensified hindered settling function (evaluated at $\phi=\Phi\phi_{agg,0}$) and where again $D_{agg,0}=1$ by definition.

Substituting Eq. (9) into Eq. (8) and then rearranging Eq. (8) gives the approximated densified hindered settling function

$$\tilde{R}(\phi,\phi_{agg})\approx\frac{D_{agg}(1-\phi)^2R_0(\phi_{agg,0}\phi/\phi_{agg})}{(1-\phi_{agg,0}\phi/\phi_{agg})^2}. \tag{10}$$

This can also be derived directly from a settling velocity equation given by van Deventer et al. (2011), itself based on the work of Usher et al. (2009). When ϕ is rather smaller than ϕ_{agg}, the first term in the settling velocity equation of van Deventer et al. (2011) dominates, and corresponds identically to Eq. (10) given here.

As ϕ_{agg} changes, the main change in $\tilde{R}(\phi,\phi_{agg})$ is due to the change in the value of $R_0(\phi_{agg,0}\phi/\phi_{agg})$ (i.e. the function R_0 is evaluated at a smaller value of its argument). In other words, the approximated densified hindered settling function, $\tilde{R}(\phi,\phi_{agg})$, is similar to the undensified hindered settling function evaluated at a lower solids volume fraction. Note that Eq. (10) will lose accuracy when the local solids volume fraction is close to that within the aggregates, ϕ_{agg}, since Eq. (8), from which it was derived, is invalid in that regime. In such cases we must return to the 'complete' formula Eq. (7).

2.2. Densified gel point and compressive yield stress

During thickening, solids tend to be compressed and consolidated to the extent that the solids volume fraction is equal to or greater than the so-called gel point at which a networked suspension is formed. In that case, the compressive yield stress must be considered in the suspension force balance equation. The value of the gel point is therefore important for determining the compressive yield stress which itself represents a measure of the strength of the networked solids. According to the definition, the compressive yield stress is zero up to the gel point.

Aggregate densification leads to an increase in the gel point, due to the decrease in individual aggregate diameters causing aggregates to lose contact with their neighbours. The aggregate densification theory (Usher et al., 2009; van Deventer et al., 2011) indicates that the evolution of the densified gel point, ϕ_g, with the change of the aggregate diameter ratio, D_{agg}, is

$$\phi_g=\frac{\phi_{g,0}}{D_{agg}^3} \tag{11}$$

where $\phi_{g,0}$ is the initial undensified gel point.

Having now specified how the gel point varies with densification, we are able to determine how the compressive yield stress varies in the densified system. Specifically, we shall look for a functional form, $P_y(\phi,\phi_{agg})$, similar to that[4] in the undensified case, $P_{y,0}(\phi)$, but now being zero at the new gel point. The aggregate densification theory (Usher et al., 2009; van Deventer et al., 2011) also indicates a requirement that the densified and undensified formulae agree in the limit as $\phi\to\phi_{agg}$, since the aggregates are all overlapping and interpenetrating in that limit, making it

[4] The basis for looking for a similar functional form is that the compressive yield stresses in both the densified and the undensified systems arise due to packing together networks of aggregates, merely with the size of the aggregates having changed upon densification.

effectively impossible to distinguish any individual aggregate within the gel network as a whole. Full details of the functional form of $P_y(\phi,\phi_{agg})$ will be given later in this paper.

2.3. Model for the consolidation zone

For a densified thickener, the consolidated bed may be composed of two parts according to the ratio between the local solids volume fraction, ϕ, and the solids volume fraction within the aggregates, ϕ_{agg}. In the upper part of the consolidated bed where $\phi<\phi_{agg}$, the densified sludge properties are applied. In the lower part of the consolidated bed where it is possible that the local solids volume fraction, ϕ, is larger than the solids volume fraction within the aggregates, ϕ_{agg}, sludge properties are unchanged from those of the initial undensified sludge. This latter case only occurs if the underflow solids volume fraction, ϕ_u, exceeds the solids volume fraction within the aggregates, ϕ_{agg}. Typically, the aggregates densify from the initial solids volume fraction within the aggregates, $\phi_{agg,0}$, to some final value, $\phi_{agg,\infty}$, which cannot subsequently be surpassed by shearing and/or raking the aggregates (Usher et al., 2009). Here, we make the assumption that densification is a rapid process compared to the solids residence time in a thickener, so that (if densification occurs at all) aggregates densify to the final steady state solids volume fraction within the aggregates, $\phi_{agg,\infty}$, immediately upon entering the thickener. When the underflow solids volume fraction, ϕ_u, exceeds the final steady state solids volume fraction within the aggregates, $\phi_{agg,\infty}$, it is therefore of interest to know how much of the bed has $\phi<\phi_{agg,\infty}$ and how much of the bed has $\phi>\phi_{agg,\infty}$. Thus, it is necessary to establish how the solids volume fraction, ϕ, changes with the height within the bed.

A one-dimensional model describing the consolidation zone in thickeners has been already developed by many authors (Landman et al., 1988; Martin, 2004; Usher and Scales, 2005). The formulation is simplest (reducing to an ordinary differential equation model) when used to describe a thickener operating at steady state. Unsteady state thickener operation is mathematically more complex (requiring the use of partial differential, Bürger and Concha, 1998; Bürger et al., 1999). Since our aim here is understanding how dewatering equipment design might be influenced by aggregate densification, we elect to study the simpler (steady-state) case here. The resulting governing equation is

$$\frac{\mathrm{d}z}{\mathrm{d}\phi}=-\frac{P'_y(\phi,\phi_{agg})}{\Delta\rho g\phi(1-(R(\phi,\phi_{agg})/(\Delta\rho g(1-\phi)^2))q(1/\phi-1/\phi_u))} \tag{12}$$

where $\Delta\rho$ is the density difference between the solids and liquid, g is the gravitational acceleration, q is the underflow solids flux, $P_y(\phi,\phi_{agg})$ is the compressive yield stress, $P'_y(\phi,\phi_{agg})$ denotes the derivative[5] with respect to the solids volume fraction, ϕ, and z denotes the height within the bed which is measured upwards.

There is a maximum possible value of the underflow solids flux corresponding to an arbitrarily tall thickener. This can be obtained by setting the denominator of Eq. (12) to zero at some value of the local solids volume fraction, ϕ. Specifically, we are interested in the value of ϕ that causes the denominator of Eq. (12) to vanish at the smallest value of the underflow solids flux. The maximum permitted underflow solids flux, q_{max}, which would be able to operate at all the possible solids volume fractions in a thickener is given as (Usher and Scales, 2005)

$$q_{max}=\min_{\phi_g\le\phi\le\phi_u}\frac{\Delta\rho g(1-\phi)^2}{R(\phi,\phi_{agg})\left(\frac{1}{\phi}-\frac{1}{\phi_u}\right)} \tag{13}$$

where we typically search for the minimum value of Eq. (13) between the gel point, ϕ_g (corresponding to the top of the bed) and the underflow solids volume fraction, ϕ_u (corresponding to the bottom of the bed).

For any $q<q_{max}$, Eq. (12) can be solved. In the aggregate densification system, the densified hindered settling function, $R(\phi,\phi_{agg})$, and the densified compressive yield stress, $P_y(\phi,\phi_{agg})$, must be determined, corresponding to the given aggregate diameter ratio, D_{agg}, and hence the solids volume fraction within the aggregates, ϕ_{agg}, given by Eq. (1). Whereas $q\to q_{max}$ corresponds to an arbitrarily tall thickener, in the opposite limit where $q\ll q_{max}$, one obtains a bed of minimum height

$$h_{b,min}=\int_{\phi_g}^{\phi_u}\frac{P'_y(\phi,\phi_{agg})}{\Delta\rho g\phi}\,\mathrm{d}\phi. \tag{14}$$

This corresponds to the height of a final steady state bed which would have been obtained had the material that is in the bed settled within a batch settler (as opposed to a continuous thickener).

In addition to the bed heights, and also the solids volume fraction versus height profiles described above, the solids residence time is also a vital operating parameter in the design of thickeners. The solids residence time, t_{res}, depends on both the solids volume fraction and the underflow solids flux. Usher and Scales (2005) gave the equation for determining the solids residence time for a thickener at steady state across a bed:

$$\frac{\mathrm{d}t_{res}}{\mathrm{d}z}=-\frac{\phi}{q} \tag{15}$$

where z is the height within the bed.

3. Thickener performance prediction

All the foregoing analysis in Section 2 has been kept general. We discussed the densified and undensified suspension material properties, but never specified the values of those properties. Now we begin to specify the material property values that we will employ in our calculations. In Eq. (12), the solids and liquid densities are chosen as $\rho_{sol}=3200\ \mathrm{kg\ m^{-3}}$ and $\rho_{liq}=1000\ \mathrm{kg\ m^{-3}}$, respectively (Usher and Scales, 2005). Gravitational acceleration is $g=9.8\ \mathrm{m\ s^{-2}}$. The sludge properties including the compressive yield stress, $P_y(\phi,\phi_{agg})$, and the hindered settling function, $R(\phi,\phi_{agg})$, used for the predictions of thickener performance are given later (in Section 3.2).

The aggregate diameter ratio is chosen as $D_{agg,0}=1$ (by definition) for the initial undensified cases and $D_{agg,\infty}=0.9$ for the densified cases (a value also considered by Usher et al., 2009 and van Deventer et al., 2011). In cases where densification occurs, recall our assumption here that $D_{agg,\infty}$ is attained immediately upon entering the bed. The initial undensified solids volume fraction within the aggregates, $\phi_{agg,0}$, is assumed to be 0.1667 (Usher et al., 2009). Therefore, the densified solids volume fraction within the aggregates, $\phi_{agg,\infty}$, determined by Eq. (1) is 0.2286.

3.1. Case studies

Sixteen cases are presented to predict the thickener performance. The actual bed height, h_b, the minimum bed height, $h_{b,min}$, the maximum permitted underflow solids flux, $q_{\max}$, and the solids residence time, t_{res}, are the main outputs. Cases 1–8 are

[5] We reiterate the important assumption here that ϕ_{agg} saturates at the value $\phi_{agg,\infty}$ over a time scale much less than the solids residence time in the bed. In effect $\phi_{agg,\infty}$ is attained immediately upon entering the bed. Thus, spatial changes in $P_y(\phi,\phi_{agg})$ arise solely from the derivative of $P_y(\phi,\phi_{agg})$ with respect to ϕ, as ϕ itself changes across the bed. Hence, the derivative notation $P'_y(\phi,\phi_{agg})$ is unambiguous here, despite the fact that $P_y(\phi,\phi_{agg})$ strictly speaking has two arguments.

presented by using the compressive yield stress functional form developed by Usher et al. (2009). Cases 9–16 are presented by using a new compressive yield stress functional form. This allows us to explore which aspects of thickener performance are generic and which are sensitive to the particular rheology of suspensions being processed. Cases 1, 4, 7, 9, 12, and 15 are operated without densification. The remaining cases are determined in the presence of densification. A summary of all the various cases is presented in a tabular form later (see Tables 1–3).

Cases 1–3 and Cases 9–11 are chosen to have a small underflow solids fraction, ϕ_u, which is smaller than the final steady state solids volume fraction within the aggregates, $\phi_{agg,\infty}$ (specifically $\phi_u=\phi_{u,1}\equiv 0.2$). Cases 4–6 and Cases 12–14 are chosen with an intermediate underflow solids fraction, ϕ_u (specifically $\phi_u=\phi_{u,2}\equiv 0.24$), which is slightly larger than $\phi_{agg,\infty}$. Cases 7–8 and Cases 15–16 are chosen with a large underflow solids fraction, ϕ_u (specifically $\phi_u=\phi_{u,3}\equiv 0.3$), which is substantially larger than $\phi_{agg,\infty}$.

Table 1
For the various underflow solids fractions ϕ_u (corresponding to the various cases discussed in Section 3.1), the dimensionless maximum permitted underflow solids flux, Q_{max}, and the ϕ value obtained via Eq. (13) (and here denoted ϕ_{corres}) to which Q_{max} corresponds for each given underflow solids fraction, ϕ_u. Values of ϕ_{agg} are given for comparison.

Case(s)	ϕ_u	Densified	Q_{max}	ϕ_{corres}	ϕ_{agg}
Cases 1, 9	0.2	No	0.0004231	0.1514	0.1667
Cases 2–3, 10–11	0.2	Yes	0.001449	0.1531	0.2286
Cases 4, 12	0.24	No	0.0002338	0.1854	0.1667
Cases 5–6, 13–14	0.24	Yes	0.0005332	0.2286	0.2286
Cases 7, 15	0.3	No	0.0001054	0.2368	0.1667
Cases 8, 16	0.3	Yes	0.0001054	0.2368	0.2286

Table 2
The values of the dimensionless minimum bed height, $H_{b,min}$, calculated by using the original 'USS' compressive yield stress functional form and the new compressive yield stress functional form. Data are grouped by their underflow solids fraction ϕ_u (utilised in the various cases studied which are numbered according to the numbering scheme of Section 3.1).

Yield stress function	ϕ_u	Undensified $H_{b,min}$	Densified $H_{b,min}$
'USS' functional form (Cases 1–3)	0.2	34.9	31.2
New functional form (Cases 9–11)	0.2	39.5	35.1
'USS' functional form (Cases 4–6)	0.24	66.1	62.9
New functional form (Cases 12–14)	0.24	71.9	68.1
'USS' functional form (Cases 7–8)	0.3	184.9	181.6
New functional form (Cases 15–16)	0.3	192.2	188.3

Table 3
Ratio of the dimensionless underflow solids flux, Q, to the dimensionless maximum permitted underflow solids flux, Q_{max}, for Cases 1–8 as described in Section 3.1. Cases 9–16 (which are not shown in the table) have the same Q/Q_{max} values as Cases 1–8, respectively, but slightly different $H_b/H_{b,min}$ values.

Case	Densified	ϕ_u	Q/Q_{max} (undensified)	Q/Q_{max} (densified)	$H_b/H_{b,min}$
Case 1	No	0.2	90.2%	N/A	4.77
Case 2	Yes	0.2	N/A	26.3%	1.28
Case 3	Yes	0.2	N/A	90.2%	5.86
Case 4	No	0.24	75.9%	N/A	2.52
Case 5	Yes	0.24	N/A	33.3%	1.32
Case 6	Yes	0.24	N/A	75.9%	2.46
Case 7	No	0.3	61%	N/A	1.8
Case 8	Yes	0.3	N/A	61%	1.65

Case 1 predicts the solids residence time, $t_{res,1}$, and the underflow solids flux, q_1, for the given bed height, $h_{b,1}$, and the given underflow solids volume fraction, $\phi_{u,1}$. Note that the given bed height, $h_{b,1}$, is chosen as 1 m. The corresponding underflow solids flux, q_1, is 90.2% of the undensified maximum permitted underflow solids flux, $q_{max,1}$.

Case 2 calculates the solids residence time, $t_{res,2}$, and the bed height, $h_{b,2}$, with the same given underflow solids volume fraction, $\phi_{u,1}$, as chosen in Case 1 and also the same given underflow solids flux, q_1, as chosen in Case 1. The bed height $h_{b,2}$ is shorter than $h_{b,1}$ owing to densification.

Case 3 determines the solids residence time, $t_{res,3}$, and the bed height, $h_{b,3}$, given the same underflow solids fraction, $\phi_{u,1}$, as in Case 1 but a larger underflow solids flux, q_2, than that in Case 2. Note that this given underflow solids flux, q_2, which is not even accessible with undensified Case 1, accounts for 90.2% of the densified maximum permitted underflow solids flux, $q_{max,2}$.

Case 4 predicts the solids residence time, $t_{res,4}$, and the underflow solids flux, q_3, for the given bed height, $h_{b,4}$, and the given underflow solids volume fraction, $\phi_{u,2}$, which exceeds $\phi_{u,1}$. Note that the given bed height, $h_{b,4}$, is chosen as 1 m. The corresponding underflow solids flux, q_3, is 75.9% of the undensified maximum permitted underflow solids flux, $q_{max,3}$.

Case 5 calculates the solids residence time, $t_{res,5}$, and the bed height, $h_{b,5}$, with the same given underflow solids volume fraction, $\phi_{u,2}$, as chosen in Case 4 and also the same given underflow solids flux, q_3, as chosen in Case 4. The calculated bed height $h_{b,5}$ is shorter than $h_{b,4}$ owing to densification.

Case 6 determines the solids residence time, $t_{res,6}$, and the bed height, $h_{b,6}$, given the same underflow solids volume fraction, $\phi_{u,2}$, as chosen in Case 4 but a larger underflow solids flux, q_4, than that in Case 5. This given underflow solids flux, q_4, which is not even accessible with undensified Case 4, accounts for 75.9% of the densified maximum permitted underflow solids flux, $q_{max,4}$.

Case 7 predicts the solids residence time, $t_{res,7}$, and the underflow solids flux, q_5, for the given underflow solids fraction, $\phi_{u,3}$, which is larger still than $\phi_{u,1}$ and $\phi_{u,2}$ and for a given bed height, $h_{b,7}$. Note that this given bed height, $h_{b,7}=2$ m, is chosen larger than either $h_{b,1}$ or $h_{b,4}$ in view of the high underflow solids volume fraction. The corresponding underflow solids flux, q_5, is 61% of the undensified maximum permitted underflow solids flux, $q_{max,5}$.

Case 8 determines the solids residence time, $t_{res,8}$, and the bed height, $h_{b,8}$, with the same given underflow solids flux, q_5, chosen in Case 7 and the same given underflow solids volume fraction, $\phi_{u,3}$, as chosen in Case 7. Clearly, $h_{b,8}$ should be lower than $h_{b,7}$ owing to densification. We did not explore the related problem of using densification to raise the underflow solids flux for this case of high underflow solids volume fraction, since for a high underflow solids volume fraction, the maximum permitted underflow solids flux calculated from the densified case turns out to be equal to that determined for the undensified case (a point we will return to later).

Cases 9–16 repeat the same procedures and choose the same thickener operating parameters (in particular the same underflow solids fluxes albeit with slightly different bed heights) outlined in Cases 1–8, respectively. However, a new compressive yield stress functional form is used in Cases 9–16 instead of that used in Cases 1–8. This new functional form has somewhat different rheological behaviours in the neighbourhood of the gel point (the gel now being rather stronger in this neighbourhood). Some of the features of Cases 1–8 and Cases 9–16 are summarised in a tabular form in Section 4. In particular, Tables 1 and 2 report for each underflow solids fraction, respectively, the maximum flux and the minimum bed height permissible. The various cases are then listed in Table 3 in terms of how closely flux approaches the maximum and how closely bed height approaches the minimum.

3.2. Sludge properties

Before proceeding any further with our case studies, we first must specify the sludge rheological properties. The rheological properties we consider here are the hindered settling function and the compressive yield stress. We follow Usher et al. (2009) in choosing property values which are 'representative of a flocculated mineral tailings slurry'. Further discussion of suitable functional forms that fit rheological property data can be found in Usher and Scales (2005) and van Deventer et al. (2011), and more data are available in Usher (2002) and Gladman (2006) (including sheared system data). Recently Usher et al. (2013) also used similar functional forms (albeit with rather different fitted parameter values) to describe sewage sludges based on the data of Studer (2008). Thus we can expect that the general functional forms we shall employ (despite involving a certain level of empiricism) could be reasonable for analysing a variety of different suspension types.

3.2.1. Hindered settling function

The undensified hindered settling function, $R_0(\phi)$, is chosen with the same functional form and parameters as used by Usher et al. (2009)

$$R_0(\phi) = \frac{R_{Stokes,0}}{\phi_{agg,0}}(\phi + r_g)^{r_n} r_g^{-r_n} \tag{16}$$

where r_g, r_n, and $R_{Stokes,0}$ are the functional parameters which are assumed to be 0.05, 5, and 260469 Pa s m^{-2}, respectively (Usher et al., 2009).

We are now in a position to compute the aggregate hindered settling factor, $r_{agg}(\Phi)$, and the densified hindered settling function, $R(\phi, \phi_{agg})$, using the theory presented in Section 2.1. We choose to express $r_{agg}(\Phi)$ in terms of $(1-\Phi)^2/r_{agg}(\Phi)$ which can be related to the flow around the aggregates. The curves of the so-called 'complete' function $(1-\Phi)^2/r_{agg}(\Phi)$ and the approximated function $(1-\Phi)^2/\tilde{r}_{agg}(\Phi)$ are shown in Fig. 1. They agree well for Φ values substantially smaller than unity, but differ as $\Phi \to 1$. As the aggregate volume fraction, Φ tends towards unity, $(1-\Phi)^2/r_{agg}(\Phi)$ tends towards zero. In other words, for $\Phi \to 1$, the liquid only flows *through* the aggregates and no liquid flows *around* the aggregates. However, the approximated function $(1-\Phi)^2/\tilde{r}_{agg}(\Phi)$ reaches a small but finite limit, implying that flow leaks around the aggregates, which technically should not be observed.

As previously noted, the 'complete' densified hindered settling function, $R(\phi, \phi_{agg})$, determined by Eq. (7) is valid for $\phi < \phi_{agg}$. For $\phi > \phi_{agg}$, the 'complete' densified hindered settling function, $R(\phi, \phi_{agg})$ equals the undensified hindered settling function, $R_0(\phi)$. The curves of the initial undensified hindered settling function, $R_0(\phi)$, the 'complete' densified hindered settling function, $R(\phi, \phi_{agg})$, and the approximated densified hindered settling function, $\tilde{R}(\phi, \phi_{agg})$, are shown in Fig. 2. The curves of $R_0(\phi)$ and $R(\phi, \phi_{agg})$ are constructed such that the two curves intersect at $\phi = \phi_{agg,\infty}$. Fig. 2 shows that the approximated Eq. (10) has good accuracy when the local solids volume fraction, ϕ, is not too close to that within the aggregates, ϕ_{agg}.

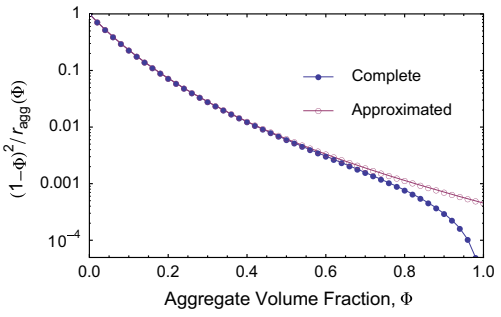

Fig. 1. $(1-\Phi)^2/r_{agg}(\Phi)$ and $(1-\Phi)^2/\tilde{r}_{agg}(\Phi)$ curves determined by Eqs. (6) ('complete' function) and (9) (approximated function), respectively.

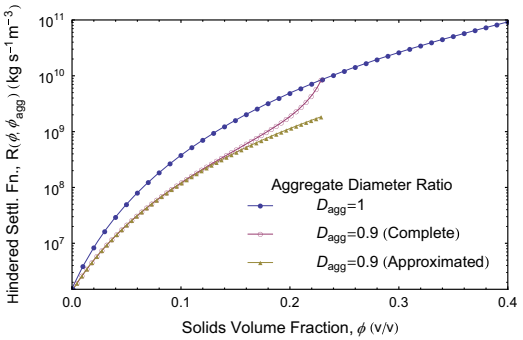

Fig. 2. The hindered settling function, $R(\phi, \phi_{agg})$, curves determined using Eqs. (16) (undensified function), (7) ('complete' function in the densified case) and (10) (approximated function in the densified case), respectively.

3.2.2. Compressive yield stress

Usher et al. (2009) proposed a formula[6] for $P_{y,0}(\phi)$ which involved the initial undensified gel point, $\phi_{g,0}$, and a close packing solids volume fraction, ϕ_{cp}, at which $P_y(\phi) \to \infty$. The value of ϕ_{cp} (which the solids volume fraction, ϕ can *never* exceed) is substantially larger than the solids volume fraction within the aggregates, ϕ_{agg}. Indeed the maximum solids volume fraction permitted in the suspension, ϕ_{cp}, is quite distinct from the final steady state solids volume fraction within the aggregates, $\phi_{agg,\infty}$. The local solids volume fraction, ϕ, in a suspension can exceed $\phi_{agg,\infty}$ in which case the aggregates overlap and interpenetrate, but ϕ can *never* exceed ϕ_{cp}. In fact, a typical thickening operation would not approach the solids volume fractions anywhere near the close packing solids volume fraction, ϕ_{cp}. Here, following Usher et al. (2009), the initial undensified gel point, $\phi_{g,0}$, and the closed packing solids volume fraction, ϕ_{cp}, are assumed[7] to be 0.1 and 0.8, respectively. Moreover Usher et al. (2009) proposed the initial undensified compressive yield stress functional form which we denote (utilising the initials of the three authors in question: Usher, Spehar and Scales), $P^{USS}_{y,0}(\phi)$, and the densified compressive yield stress functional form denoted, $P^{USS}_{y,1}(\phi, \phi_{agg})$, respectively.

For the initial undensified compressive yield stress

$$P^{USS}_{y,0}(\phi) = A_0 \left(\frac{\phi - \phi_{g,0}}{\phi_{g,0}} \frac{\phi_{cp} - \phi_{g,0}}{\phi_{cp} - \phi} \frac{b + \phi_{g,0}}{b + \phi - \phi_{g,0}} \right)^{k_0} \tag{17}$$

where A_0, b, and k_0 are the curve fitting parameters which are assumed as 129.614 Pa, 0.002, and 11, respectively (Usher et al., 2009).

[6] Davis and Russel (1989) have proposed a rather different formula from that of Usher et al. (2009). The formula of Davis and Russel (1989) was however proposed specifically for the case of the osmotic pressure (considered to be analogous to $P_y(\phi)$) in a system of hard spheres subject to the Brownian motion. It does not however exhibit the feature that pressure vanishes for solids fraction less than a critical gel point, which is a key feature (Landman and White, 1994) of the polymer flocculated suspension system that we consider here.

[7] Note that based on our chosen values of $\phi_{g,0} = 0.1$ and $\phi_{agg,0} = 0.1667$, the fraction of space filled by aggregates at the gel point is $\Phi_g = \phi_{g,0}/\phi_{agg,0} \sim 0.6$ (Usher et al., 2009).

For the densified compressive yield stress (with $\phi_{g,\infty}$ as the new gel point)

$$P_{y,1}^{USS}(\phi,\phi_{agg,\infty}) = A_1\left(\frac{\phi-\phi_{g,\infty}}{\phi_{g,\infty}}\frac{\phi_{cp}-\phi_{g,\infty}}{\phi_{cp}-\phi}\frac{b+\phi_{g,\infty}}{b+\phi-\phi_{g,\infty}}\right)^{k_1} \tag{18}$$

where A_1 and k_1 are the curve fitting parameters, but b and ϕ_{cp} are unchanged from the undensified case.

The final densified gel point (as determined by Eq. (11) using $D_{agg}=D_{agg,\infty}=0.9$ and $\phi_{g,0}=0.1$) is $\phi_{g,\infty}=0.1372$.

The values of A_1 and k_1 are given so that not only $P_{y,0}^{USS}(\phi)=P_{y,1}^{USS}(\phi)$ at $\phi=\phi_{agg,\infty}$ but also the derivatives match at $\phi=\phi_{agg,\infty}$ (Usher et al., 2009)

$$k_1 = k_0\left(\frac{\frac{1}{\phi_{agg,\infty}-\phi_{g,0}}+\frac{1}{\phi_{cp}-\phi_{agg,\infty}}-\frac{1}{b+\phi_{agg,\infty}-\phi_{g,0}}}{\frac{1}{\phi_{agg,\infty}-\phi_{g,\infty}}+\frac{1}{\phi_{cp}-\phi_{agg,\infty}}-\frac{1}{b+\phi_{agg,\infty}-\phi_{g,\infty}}}\right) \tag{19}$$

$$A_1 = \frac{P_{y,0}^{USS}(\phi_{agg,\infty})}{\left(\frac{\phi_{agg,\infty}-\phi_{g,\infty}}{\phi_{g,\infty}}\frac{\phi_{cp}-\phi_{g,\infty}}{\phi_{cp}-\phi_{agg,\infty}}\frac{b+\phi_{g,\infty}}{b+\phi_{agg,\infty}-\phi_{g,\infty}}\right)^{k_1}} \tag{20}$$

where $\phi_{agg,\infty}$ and $\phi_{g,\infty}$ in Eqs. (19) and (20) are determined by Eqs. (1) and (11), respectively.

The values of A_1 and k_1 determined by Eqs. (19) and (20) are computed as 292.312 Pa and 10.3667, respectively (Usher et al., 2009).

One feature of Eqs. (17) and (18) is that they approach zero very rapidly at the top of the bed as $\phi\to\phi_g$ (the gel is extremely weak in that limit) which may affect the local bed structure significantly. We are therefore interested in considering another rheology which is expected to alter the bed structure near the top of the bed. A new undensified compressive yield stress, $P_{y,0}(\phi)$, based on the formula given by Usher et al. (2009) has been considered:

$$P_{y,0}(\phi) = P_{y,0}^{USS}(\phi) + a_0\frac{\phi-\phi_{g,0}}{\phi_{g,0}} \tag{21}$$

where a_0 is a fitting parameter.

Similarly, the densified compressive yield stress, $P_{y,1}(\phi,\phi_{agg})$, is given as

$$P_{y,1}(\phi,\phi_{agg,\infty}) = P_{y,1}^{USS}(\phi,\phi_{agg,\infty}) + a_1\frac{\phi-\phi_{g,\infty}}{\phi_{g,\infty}} - c_1\frac{(\phi-\phi_{g,\infty})^2}{\phi_{g,\infty}^2} \tag{22}$$

where a_1 and c_1 represent the fitting parameters (the reason why two parameters a_1 and c_1 are needed will be explained shortly).

In order that P_y only differs significantly from P_y^{USS} in the neighbourhood of the gel point, ϕ_g, we assume that $P_{y,0}^{USS}(\phi)$ equals $a_0(\phi-\phi_{g,0})/\phi_{g,0}$ at $\phi=\phi_{g,0}+\Delta\phi$, where $\Delta\phi$ is assumed to be 0.005. Thus

$$a_0\frac{\Delta\phi}{\phi_{g,0}} = P_{y,0}^{USS}(\phi_{g,0}+\Delta\phi) \tag{23}$$

where Eq. (23) determines a_0.

As previously noted, the compressive yield stress functional forms are continuous with continuous derivatives at $\phi=\phi_{agg,\infty}$ in this work. Hence

$$a_0\frac{\phi_{agg,\infty}-\phi_{g,0}}{\phi_{g,0}} = a_1\frac{\phi_{agg,\infty}-\phi_{g,\infty}}{\phi_{g,\infty}} - c_1\frac{(\phi_{agg,\infty}-\phi_{g,\infty})^2}{\phi_{g,\infty}^2} \tag{24}$$

$$\frac{a_0}{\phi_{g,0}} = \frac{a_1}{\phi_{g,\infty}} - 2c_1\frac{\phi_{agg,\infty}-\phi_{g,\infty}}{\phi_{g,\infty}^2}. \tag{25}$$

Thus we have two equations to solve for two unknowns a_1 and c_1 – hence the reason why these two parameters a_1 and c_1 were included in Eq. (22).

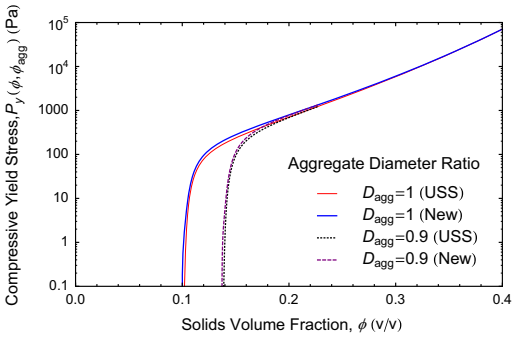

Fig. 3. The new compressive yield stress curves determined using Eqs. (17)–(25).

The values of a_0, a_1 and c_1 determined by Eqs. (23), (24) and (25) are given as 86.123 Pa, 214.345 Pa, and 72.191 Pa, respectively. The new initial undensified compressive yield stress, $P_{y,0}(\phi)$, and the new densified compressive yield stress, $P_{y,1}(\phi,\phi_{agg,\infty})$, curves determined by Eqs. (21)–(25) (alongside the initial undensified and densified, Usher et al., 2009, formulae (Eqs. (17)–(20))) are shown in Fig. 3.

3.3. Maximum permitted underflow solids flux

Identifying the maximum permitted underflow solids flux is important in any parametric study of thickener design, since a tall thickener design results from operating at a large underflow solids flux which is very close to the maximum permitted underflow solids flux, whereas a shorter thickener design results from operating at a small underflow solids flux which is far below the maximum permitted underflow solids flux.

Usher and Scales (2005) have already developed the method used for the prediction of the maximum permitted underflow solids flux, q_{max}, in an initial undensified thickener. That method is readily adapted to the case of a densified thickener provided aggregates reach a steady state diameter ratio, $D_{agg,\infty}$ (and hence the solids volume fraction within the aggregates achieves a steady state $\phi_{agg,\infty}$) immediately upon entering the consolidated bed.

Recall that the maximum permitted underflow solids flux corresponds to the minimum sought in Eq. (13). It is unlikely that this minimum sought will occur at the top of the bed where the solids volume fraction, ϕ, is the smallest (around ϕ_g). This is due to the nature of the hindered settling function, $R(\phi)$, which appears in the denominator of Eq. (13) and which tends to increase very rapidly with ϕ. Likewise the minimum sought in Eq. (13) cannot occur near the bottom of the bed where $\phi\to\phi_u$ as the denominator in Eq. (13) vanishes there. Thus, the minimum sought in Eq. (13) tends to be determined somewhere in the interior of the bed. As a result, cases for which the underflow solids volume fraction, ϕ_u, exceeds the solids volume fraction within the aggregates, ϕ_{agg}, need to be considered carefully, due to the non-smooth nature of the hindered settling function at $\phi=\phi_{agg}$.

For an underflow solids volume fraction, ϕ_u less than the solids volume fraction within the aggregates, ϕ_{agg}, the maximum permitted underflow solids flux, q_{max}, determined in a densified thickener is much larger than that determined in an initial undensified thickener, since the maximum permitted underflow solids flux scales inversely with the densified hindered settling function, and the densified hindered settling function, $R(\phi,\phi_{agg})$, is much smaller than the initial undensified hindered settling function, $R_0(\phi)$. In this case, for the purposes of finding the minimum sought in Eq. (13), we would be permitted to replace $R(\phi,\phi_{agg})$ by

the approximated densified hindered settling function, $\tilde{R}(\phi,\phi_{agg})$ (see Eq. (10)).

For an intermediate underflow solids volume fraction, ϕ_u, which is slightly larger than the solids volume fraction within the aggregates, ϕ_{agg}, the densified hindered settling function, $R(\phi,\phi_{agg})$, also governs the maximum permitted underflow solids flux, $q_{\max}$, via Eq. (13). Consequently, the maximum permitted underflow solids flux, q_{max}, predicted in a densified thickener is still somewhat larger than that predicted in an initial undensified thickener, since the densified hindered settling function, $R(\phi,\phi_{agg})$, remains smaller than the initial undensified hindered settling function, $R_0(\phi)$. For the purposes of computing $q_{\max}$, it would not however generally be permitted to replace $R(\phi,\phi_{agg})$ by the approximated formula $\tilde{R}(\phi,\phi_{agg})$ in this case.

For an underflow solids volume fraction, ϕ_u, much larger than the solids volume fraction within the aggregates, ϕ_{agg}, the minimum sought in Eq. (13) tends to occur at $\phi>\phi_{agg}$. The initial undensified hindered settling function, $R_0(\phi)$, then determines the maximum permitted underflow solids flux, $q_{\max}$. Therefore, the maximum permitted underflow solids flux, $q_{\max}$, determined in a densified thickener equals that determined in an initial undensified thickener (a point we have already made previously – see Section 3.1). Hence, for cases with very large ϕ_u, we have explored densification primarily as a way of reducing consolidated bed height rather than as a means of increasing the underflow solids flux. Computations of $q_{\max}$ with and without densification for the cases of small, intermediate and large ϕ_u relative to ϕ_{agg} will be presented in Section 4.

3.4. Minimum bed height

The discussion of Section 3.3 corresponded to a very tall thickener operated at a very high underflow solids flux ($q\to q_{max}$). As stated previously, there is also an opposite limit corresponding to a very short thickener operated at a very low underflow solids flux ($q\to 0$). In this latter case, the minimum bed height, $h_{b,min}$, satisfies Eq. (14).

The minimum bed height, $h_{b,min}$, will increase as the underflow solids fraction, ϕ_u, increases and may actually increase quite substantially with ϕ_u, since $P'_y(\phi,\phi_{agg})$ in Eq. (14) tends to be a rapidly increasing function of ϕ.

The minimum bed height, $h_{b,min}$, also tends to increase if we change the gel rheology (e.g. from an exceedingly weak gel in the neighbourhood of the gel point to a substantially stronger gel). Moreover, the minimum bed height, $h_{b,min}$, will decrease as the aggregates densify, since the gel point, ϕ_g, then changes from a comparatively small value, $\phi_{g,0}$, to a rather larger value, $\phi_{g,\infty}$. This increases the denominator of Eq. (14) and hence decreases minimum bed height, despite the fact that, had we considered the numerator alone, $\int_{\phi_g}^{\phi_u} P'_y(\phi,\phi_{agg})\,d\phi$ would be independent of densification whenever $\phi_u>\phi_{agg}$. The results of $h_{b,min}$ computed with different rheologies and different underflow solids volume fractions, with and without densification, are presented in Section 4.

3.5. Dimensionless equations

Dimensionless equations are convenient to describe and compute the solids behaviours in the bed and are slightly simpler to deal with their dimensional analogues. The dimensionless scheme based on Howells et al. (1990) and Martin (2004) has been developed with dimensionless coordinate, Z, bed height, H_b, rheological functions, $p_y(\phi,\phi_{agg})$ and $R_s(\phi,\phi_{agg})$, underflow solids flux, Q, and solids residence time, T_{res}

$$Z=\frac{z}{H_0},\quad H_b=\frac{h_b}{H_0}$$

$$p_y(\phi,\phi_{agg})=\frac{P_y(\phi,\phi_{agg})}{A_0},\quad R_s(\phi,\phi_{agg})=\frac{R(\phi,\phi_{agg})u_{Stokes,0}}{\Delta\rho g}$$

$$Q=\frac{q}{u_{Stokes,0}},\quad T_{res}=\frac{t_{res}u_{Stokes,0}}{H_0}$$

where $H_0=A_0/(\Delta\rho g)$ is the characteristic length scale and $u_{Stokes,0}$ denotes the Stokes' velocity of an isolated aggregate, as defined by Usher et al. (2009)

$$u_{Stokes,0}=\frac{\Delta\rho g}{R_0(0)}=\frac{\Delta\rho g\phi_{agg,0}}{R_{Stokes,0}} \tag{26}$$

where Eq. (5) has also been used. For the parameter values reported in Sections 3.1–3.2, $H_0=0.00601$ m and $u_{Stokes,0}=0.0138$ m s^{-1}.

Eqs. (12) and (15) become, when converted to a dimensionless form

$$\frac{dZ}{d\phi}=-\frac{p'_y(\phi,\phi_{agg})/\phi}{1-R_s(\phi,\phi_{agg})Q(1/\phi-1/\phi_u)/(1-\phi)^2} \tag{27}$$

$$\frac{dT_{res}}{dZ}=-\frac{\phi}{Q}. \tag{28}$$

Regarding the dimensionless sludge rheological properties ($R_s(\phi,\phi_{agg})$ and $p_y(\phi,\phi_{agg})$), these are formally the same as the expressions given previously, except that, for the initial undensified hindered settling function, $R_0(\phi)$, the prefactor $R_{Stokes,0}$ must be replaced by $\phi_{agg,0}$. Specifically, $R_{s,0}(\phi)$ becomes in lieu of Eq. (16):

$$R_{s,0}(\phi)=(\phi+r_g)^{r_n}r_g^{-r_n} \tag{29}$$

where r_g and r_n are the parameters which have been given in Section 3.2.1 (see also Usher et al., 2009). Eq. (6) still applies subject to the above-mentioned replacements as does Eq. (3). For the dimensionless undensified compressive yield stresses, $p_{y,0}(\phi)$, Eqs. (17) and (21) still apply with prefactors A_0 and a_0 replaced by 1 and a_0/A_0. Dimensionless densified compressive yield stresses, $p_{y,1}(\phi,\phi_{agg})$, are formally the same as Eqs. (18) and (22) but with the prefactors A_1, a_1, and c_1 replaced by A_1/A_0, a_1/A_0, and c_1/A_0, respectively.

4. Results and discussion

As mentioned previously, the results presented here include the maximum permitted underflow solids fluxes, the minimum possible bed heights, the actual bed heights, and the solids residence times. Calculations are most simply carried out in a dimensionless form and the maximum permitted underflow solids fluxes and the minimum bed heights are presented in this form (e.g. Section 4.1). However, for the purposes of presenting the actual bed heights and the solids residence times (e.g. Sections 4.2–4.4), we reconverted back to a dimensional form using typical parameter values supplied in Section 3.

4.1. Maximum underflow solids flux and minimum bed height predictions

The operating inputs, which may include the target bed height, h_b, the underflow solids flux, q, and the underflow solids volume fraction, ϕ_u, have been described in Section 3. The dimensionless maximum permitted underflow solids flux, Q_{max}, predicted in each case is shown in Table 1. Results are presented for various underflow solids volume fractions, ϕ_u, and for both densified and undensified cases. We are primarily interested here not so much in the individual reported values of $Q_{\max}$, but rather in how Q_{max} changes due to changes in ϕ_u and/or due to densification. As the underflow solids volume fraction, ϕ_u increases, we tend to see an

increase in the value of the corresponding solids volume fraction, denoted ϕ_{corres} that corresponds to Q_{max}. That leads to a large increase in the hindered settling function $R(\phi, \phi_{agg})$ in Eq. (13) and thereby a decrease in Q_{max}. The effects of densification upon Q_{max} are exactly as already anticipated in Section 3.3. Densified cases tend to have higher Q_{max} than undensified ones at least when the desired ϕ_u is not too large. For a large ϕ_u however, Q_{max} remains the same regardless of whether or not densification occurs.

In Eq. (27), we are allowed to use any dimensionless underflow solids flux, Q, value ranging from 0 to Q_{max}. The dimensionless minimum bed height, $H_{b,min}$, is determined by using Eq. (27) with $Q=0$ and integrating up to the desired underflow solids volume fraction. Table 2 shows the values of $H_{b,min}$ calculated from both undensified and densified cases. Again the focus is not so much on the individual reported values of $H_{b,min}$, but on how $H_{b,min}$ changes with changing conditions. Table 2 bears out the discussion of Section 3.4. The dimensionless minimum bed height, $H_{b,min}$, is increased with increasing underflow solids volume fraction, ϕ_u. Densification can decrease the dimensionless minimum bed height, $H_{b,min}$, for a given underflow solids fraction, ϕ_u. In addition, the values of $H_{b,min}$ calculated by using the new compressive yield stress functional form are slightly larger than those calculated by using the original 'USS' compressive yield stress functional form.

For the various case studies mentioned in Section 3.1, Table 3 presents the ratio of the dimensionless underflow solids flux, Q, to the dimensionless maximum permitted solids flux, $Q_{\max}$, and also the ratio of the dimensionless bed height, H_b, to the dimensionless minimum bed height, $H_{b,min}$.

For a comparatively small underflow solids volume fraction, $\phi_u = 0.2$, and/or an intermediate underflow volume fraction, $\phi_u = 0.24$, Table 3 indicates how a large underflow solids flux can be achieved in a densified thickener. This is because Cases 1 and 2 actually have the same dimensionless underflow solids flux, Q, but very different dimensionless maximum permitted underflow solids fluxes, $Q_{\max}$, whereas Cases 2 and 3 have the same dimensionless maximum permitted underflow solids flux, $Q_{\max}$, but very different dimensionless underflow solids fluxes, Q. In fact Q in densified Case 3, actually exceeds $Q_{\max}$ in undensified Case 1. Analogous flux parameter settings apply for Cases 4–6. Despite the fact that Q/Q_{max} values in Cases 4 and 6 are chosen to be rather smaller than in Cases 1 and 3, respectively, it is still in fact the case that Q chosen in densified Case 6 exceeds $Q_{\max}$ calculated in undensified Case 4. However, for Cases 7–8 with a larger underflow solids volume fraction, $\phi_u = 0.3$, the dimensionless underflow solids flux chosen in a densified thickener cannot exceed the dimensionless maximum permitted underflow solids flux calculated in an initial undensified thickener, since the densified and the undensified maximum permitted underflow solids fluxes are then the same. In general, the values of Q/Q_{max} presented in Table 3 show the scope available for operating a thickener at a higher underflow solids flux (subject to increasing its height). Meanwhile, the values of $H_b/H_{b,min}$ show the scope for designing a thickener of lesser height (subject to decreasing its underflow solids flux). Cases 9–16 which are not shown in the table have the same dimensionless underflow solids flux ratio chosen in Cases 1–8, respectively. However, $H_b/H_{b,min}$ values calculated from Cases 9–16 differ slightly compared with those calculated from Cases 1–8, owing to the slightly different rheological properties (Eqs. (21) and (22) instead of Eqs. (17) and (18)).

4.2. Solids volume fraction profile prediction

Figs. 4–6 show the solids volume fraction profiles determined by using Eq. (27) with the initial inputs given by Tables 1–3. In Fig. 4 for instance, Cases 1 and 3 both show a typical curve shape including flat near the top of the bed, steeper in the middle and less steep at the bottom. Cases 9 and 11 likewise both show a typical curve shape including not quite flat near the top of the bed, steeper in the middle, and less steep at the bottom of the bed.

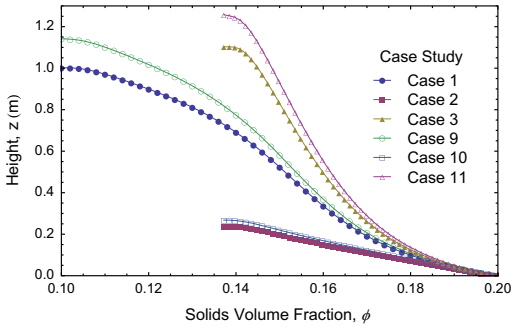

Fig. 4. The solids volume fraction profile – Small underflow solids volume fraction, $\phi_u = 0.2$. For simplicity of interpretation, we have converted dimensionless coordinate Z back into dimensional coordinate z here. Details of the various cases can be found in Section 3.1 but briefly Cases 1 and 9 are undensified, whilst the remaining cases are densified. Cases 1–3 use the original (Usher et al., 2009) functional form for the yield stress, and remaining cases use a new form.

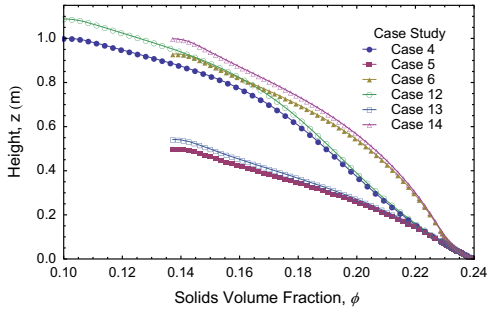

Fig. 5. The solids volume fraction profile – Intermediate underflow solids volume fraction, $\phi_u = 0.24$. Cases 4 and 12 are undensified, whilst remaining cases are densified. Cases 4–6 use the original functional form for the yield stress, and remaining cases use a new form.

Indeed looking at Figs. 4–6, the curves of Cases 1–8 are all flat near the top of the bed, a manifestation of the network strength being incredibly weak (exceedingly small $dp_y(\phi)/d\phi$ in the neighbourhood of the gel point) and hence, small $|dZ/d\phi|$ in the neighbourhood of the gel point. Significant increase in the solids volume fraction over a comparatively small height near the top of the bed occurs in all these cases. However, the new dimensionless compressive yield stress, $p_y(\phi)$ functional form used in Cases 9–16 leads to a somewhat stronger network near the top of the bed, due to finite $dp_y(\phi)/d\phi$ in the neighbourhood of the gel point. Consequently, the curves of Cases 9–16 shown in Figs. 4–6 manage to have finite $|dZ/d\phi|$ near the top of the bed, but otherwise are quite similar to their Cases 1–8 counterparts. Moreover, the slightly stronger gel leads to a slightly higher bed overall.

The typical feature of steep curves in the middle (e.g. Cases 1, 3, 9 and 11) is due to the large $|dZ/d\phi|$ in the interior of the bed. The denominator of Eq. (27) decreases with the increase in the local solids volume fraction moving deeper into the bed, due to the increase of $R_s(\phi, \phi_{agg})$. However, the minimum value which the denominator of Eq. (27) can reach is only exceedingly small when the dimensionless underflow solids flux, Q, is very close to the dimensionless maximum permitted underflow solids flux, $Q_{\max}$. Thus, $|dZ/d\phi|$ can only become large in the interior of the bed when the dimensionless underflow solids flux, Q is very close to the dimensionless maximum permitted underflow solids flux, Q_{max}. This observation can be seen in Cases 1, 3,

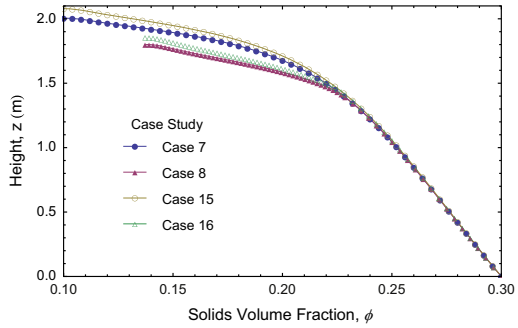

Fig. 6. The solids volume fraction profile – Large underflow solids volume fraction, $\phi_u = 0.3$. Cases 7 and 15 are undensified, whilst Cases 8 and 16 are densified. Cases 7 and 8 use the original functional form for the yield stress, whilst Cases 15 and 16 use a new form.

9, and 11, whereas Cases 2 and 10 for which $Q \ll Q_{max}$ did not have the steep section of curve for instance. As $\phi \to \phi_u$, the denominator of Eq. (27) invariably approaches unity. Thus $|dZ/d\phi|$ cannot remain large as $\phi \to \phi_u$ even if $Q \to Q_{max}$ which is why curves such as Cases 1, 3, 9 and 11 become less steep right at the bottom.

Other details of the curves also become apparent. The densified sludge rheological properties can be replaced by the undensified sludge rheological properties at $\phi > \phi_{agg}$. Thus, for $\phi > \phi_{agg}$ (which will occur towards the bottom of the bed whenever $\phi_u > \phi_{agg}$), $|dZ/d\phi|$ evaluated for the densified cases and the undensified cases, respectively, have the same slope, given the same dimensionless underflow solids flux, Q, and the same underflow solids volume fraction, ϕ_u. This is particularly noticeable in Fig. 6.

Eq. (27) indicates clearly that the dimensionless hindered settling function, $R_s(\phi, \phi_{agg})$, and the dimensionless underflow solids flux, Q, affect the value of $|dZ/d\phi|$ only slightly near the bottom of the bed, since the local solids volume fraction, ϕ, is then very close to the desired underflow solids volume fraction, ϕ_u. Physically, this comes about because the solids and liquid leave the thickener at the same velocity at the bottom of the bed. Therefore, the hydrodynamic drag forces between the solids and liquid are irrelevant there. The dimensionless compressive yield stress, $p_y(\phi, \phi_{agg})$ is the main influence upon $|dZ/d\phi|$ near the bottom of the bed. Hence, given the same dimensionless functional form of $p_y(\phi, \phi_{agg})$ and the same underflow solids volume fraction, ϕ_u, we obtain the same slope of $|dZ/d\phi|$ near the bottom of the bed, regardless of the value of Q or $R_s(\phi, \phi_{agg})$. That is very apparent in Figs. 4–6.

4.3. Prediction of bed height

Having now described the shapes of the solids volume fraction versus height profiles, we turn to matters of thickener performance enhancement, due to densification. Table 4 shows that the bed height required to achieve the comparatively small underflow solids volume fraction, $\phi_u = 0.2$, in a densified thickener is much shorter than that in an initial undensified thickener, since densification affects the entire consolidated bed (i.e. $\phi_u < \phi_{agg,\infty}$). A very large dimensionless underflow solids flux which is not accessible to the initial undensified thickener can also be achieved in a densified thickener with only modest increases in bed height (compared to the undensified case).

For $\phi_u > \phi_{agg}$, densification is relevant in the upper part of the consolidated bed whereas the initial undensified sludge rheological properties apply to the lower part of the consolidated bed. Moreover, densification only affects the thickener performance significantly when the upper part of the consolidation zone accounts for a large proportion of the consolidated bed (e.g. as in Table 5). Further increasing the underflow solids volume fraction, ϕ_u can decrease the proportion of the upper part of the consolidated bed in which densification is relevant and this proportion could be quite small when the underflow solids fraction, ϕ_u is rather larger than the solids volume fraction within the aggregates, ϕ_{agg} (e.g. as in Table 6).

In line with the above observations, Table 5 shows that the bed height calculated in a densified thickener can be considerably shorter than that calculated in an initial undensified thickener given the same dimensionless underflow solids flux, Q, and the same (intermediate) underflow solids volume fraction, $\phi_u = 0.24$, due to the upper part of the consolidated bed being comparatively large. Moreover, the underflow solids flux in the densified case can be increased substantially and still return a bed height comparable with the undensified bed height. Nevertheless, for larger $\phi_u = 0.3$, as shown in Table 6, the bed height decreases only slightly in a densified thickener with the same operating parameters as used in an initial undensified thickener, due to the upper part of the consolidated bed being now comparatively small.

Table 4
Bed heights, h_b, and total solids residence times, t_{res}, calculated by using Eqs. (27) and (28) at the comparatively small underflow solids volume fraction, $\phi_u = 0.2$. For simplicity (i.e. ease of interpretation), we present results in a dimensional form rather than a dimensionless form. Recall from Section 3.1 that bed height was set to 1 m exactly in Case 1, but calculated in the other cases. Recall also that Cases 1–2 and 9–10 all operate at the same underflow solids flux, but Cases 3 and 11 operate at a much larger underflow solids flux.

Case	Densified	h_b/m	Total t_{res}/h
Case 1	No	1	7.95
Case 2	Yes	0.24	2.12
Case 3	Yes	1.1	2.73
Case 9	No	1.14	9.02
Case 10	Yes	0.27	2.39
Case 11	Yes	1.26	3.11

Table 5
Bed heights, h_b, and total solids residence times, t_{res}, calculated by using Eqs. (27) and (28) at the intermediate underflow solids volume fraction, $\phi_u = 0.24$. Recall from Section 3.1 that bed height was set to 1 m exactly in Case 4, but calculated in the other cases. Recall also that Cases 4–5 and Cases 12–13 all operate at the same underflow solids flux, but Cases 6 and 14 operate at a substantially larger underflow solids flux. In densified cases, where a distinction is made between upper and lower parts of the bed, the solids fraction in the upper region is less than the aggregate solids fraction (and hence suspension material properties are affected by densification), whereas the solids fraction in the lower region exceeds the aggregate solids fraction (and hence suspension properties remain uninfluenced by densification in the lower region).

Case	Densified	h_b/m	t_{res}/h (upper)	t_{res}/h (lower)	Total t_{res}/h
Case 4	No	1	N/A	N/A	20.96
Case 5	Yes	0.5	9.04	2.16	11.2
Case 6	Yes	0.93	7.78	1.48	9.26
Case 12	No	1.09	N/A	N/A	22.62
Case 13	Yes	0.54	9.81	2.23	12.04
Case 14	Yes	1.00	8.38	1.52	9.9

4.4. Solids residence time prediction

The solids residence time is another important operating parameter in the design of thickeners. Table 4 shows (alongside bed heights, h_b) the solids residence time, t_{res}, calculated for a comparatively small underflow solids volume fraction, $\phi_u = 0.2$.

As shown in Table 4, the total solids residence time, t_{res}, calculated in a densified thickener can be much smaller than that calculated in an initial undensified thickener. The total solids residence time, t_{res}, determined in undensified Case 9 is also

Table 6
Bed heights and total dimensionless solids residence times, t_{res}, calculated by using Eqs. (27) and (28) at the large underflow solids volume fraction, $\phi_u = 0.3$. Recall from Section 3.1 that bed height was set to 2 m exactly in Case 7, but calculated in the other cases. All of these cases have the same underflow solids flux. Note the unit of t_{res} is now days rather than hours.

Case	Densified	h_b/m	t_{res}/days (upper)	t_{res}/days (lower)	Total t_{res}/days
Case 7	No	2	N/A	N/A	6.33
Case 8	Yes	1.8	1.02	4.84	5.86
Case 15	No	2.08	N/A	N/A	6.52
Case 16	Yes	1.86	1.11	4.91	6.02

slightly larger than that determined in undensified Case 1, due to a taller bed obtained in undensified Case 9. Although the bed heights calculated in densified Cases 3 and 11 are slightly higher than those determined in undensified Cases 1 and 9, respectively, both the total solids residence times, t_{res}, determined in densified Cases 3 and 11 are decreased significantly, due to the larger dimensionless underflow solids fluxes, Q chosen in densified Cases 3 and 11, respectively. Densified Cases 2 and 10 are also operated at short residence times, due to the short bed heights obtained in those two cases. The solids residence times, t_{res}, calculated from densified Cases 3 and 11 are slightly *larger* than those determined from densified Cases 2 and 10 respectively (which have the lower underflow solids flux), since the dimensionless underflow solids flux, Q, chosen in densified Cases 3 and 11 is very close to the dimensionless maximum permitted underflow solids flux, $Q_{\max}$, making the ratio $H_b/H_{b,min}$ really quite large (see e.g. Table 3).

Table 5 presents the total solids residence times, t_{res}, calculated at the intermediate underflow solids volume fraction, $\phi_u = 0.24$. The total solids residence time, t_{res}, calculated in a densified thickener is still substantially smaller than that calculated in an initial undensified thickener, since the upper part of the bed for which $\phi < \phi_{agg}$ (where densification is relevant), accounts for a much larger proportion of the total consolidated bed than the lower part where $\phi > \phi_{agg}$ (and densification has no effect). Due to a higher underflow solids flux, Q, in densified Cases 6 and 14 (compared to densified Cases 5 and 13), the solids residence times calculated in densified Cases 6 and 14 are slightly *smaller* than those calculated in densified Cases 5 and 13. Admittedly the beds for Cases 6 and 14 are rather taller than in Cases 5 and 13, but the intermediate value of Q/Q_{max} chosen for Cases 6 and 14 does not lead to excessive $H_b/H_{b,min}$ values (see Table 3) and this ensures that the solids residence times for Cases 6 and 14 are likewise not excessive.

Results calculated from the cases of the underflow solids volume fraction, $\phi_u = 0.3$, which is much larger than the solids volume fraction within the aggregates, ϕ_{agg}, are shown in Table 6. The total solids residence time, t_{res}, calculated in a densified thickener is only slightly smaller than that calculated in an initial undensified thickener. This is because the dominant contribution to determine the total solids residence time, t_{res}, then comes from the lower part of the consolidated bed throughout which the initial undensified hindered settling function, $R_0(\phi)$ applies.

A final observation from Tables 4 to 6 is that a weaker network quantified via the compressive yield stress (Eqs. (17) and (18) applied in Cases 1–8 in lieu of Eqs. (21) and (22) for Cases 9–16) leads to shorter bed heights, h_b, and shorter total solids residence times, t_{res}, in an undensified or a densified thickener. Hence, networks that are weak tend to be relatively easier to dewater.

5. Conclusions

Phenomenological, continuum-scale models for suspension dewatering are immensely valuable for designing (and predicting the performance of) dewatering equipment e.g. thickeners (Landman et al., 1988; Martin, 2004; Usher and Scales, 2005). Even though the continuum models considered herein do not formally consider small scale microstructural details within the suspension, the phenomenological material properties utilised by them should nevertheless evolve if and when the suspension microstructure evolves. Here, we have discussed how densification of (microscale) aggregates within a suspension (Usher et al., 2009) (in particular for aggregates formed by polymer flocculation with polymers bridging between solid particles) can affect continuum-scale material parameters, and have determined the consequences for suspension dewatering in a steady-state thickener (considered here, as it is far easier to model than an unsteady state operation, such as a batch settler and/or a transient thickener, Bürger and Concha, 1998; Bürger et al., 1999).

Aggregate densification (assumed to occur here by raking/shearing the suspension as it dewaters) affects the thickener performance significantly when the underflow solids volume fraction in an initial undensified thickener is less than the solids volume fraction within the aggregates. Larger maximum permitted underflow solids fluxes can be achieved in a densified thickener. Moreover, a shorter thickener (associated with a significantly shorter residence time) can be achieved, and one can also operate at high underflow solids fluxes which are inaccessible to the undensified thickener. The thickener performance is still enhanced significantly given an intermediate underflow solids volume fraction which is slightly larger than the solids volume fraction within the aggregates. When the required thickening duty is more demanding (large underflow solids volume fraction), the thickener performance enhancement owing to densification is however comparatively modest. The reason is that, for a solids volume fraction above that within the aggregates (accounting now for much of the height of the thickener), the sludge rheological properties are unaffected by densification. The thickener performance enhancements predicted here are somewhat sensitive to different functional forms of the suspension rheological properties (i.e. the form of the compressive yield stress function near the suspension gel point). Specifically, the bed heights, the total solids residence times and fine details of how the solids volume fractions vary near the top of the bed are sensitive to the compressive yield stress functional form.

The above findings offer useful insights to a chemical engineer faced with designing a thickener or similar item of dewatering equipment. Nevertheless our findings still constitute an incomplete picture of a suspension being processed under simultaneous compression and shear (Lester et al., 2010; Stickland and Buscall, 2009). Aggregates in the suspension are assumed here to densify instantaneously in the presence of shear, whereas in fact they may densify on time scales comparable those with for dewatering (van Deventer et al., 2011). Moreover, whereas compression forces in the suspension drive solids from high concentration regions to low concentrations ones, shear itself may drive solids from high shear regions to low shear regions (Leighton and Acrivos, 1987a,b; Acrivos, 1995), and such effects are missing from the models analysed here.

Acknowledgements

Part of this work also was carried out whilst Paul Grassia was a Royal Academy of Engineering/Leverhulme Trust Senior Research Fellow and funding from the fellowship is gratefully acknowledged.

References

Abbott, J.R., Tetlow, N., Graham, A.L., Altobelli, S.A., Fukushima, E., Mondy, L.A., Stephens, T.S., 1991. Experimental observations of particle migration in concentrated suspensions: Couette-flow. J. Rheol. 35, 773–795.

Acrivos, A., 1995. Shear-induced particle diffusion in concentrated suspensions of noncolloidal particles. J. Rheol. 39, 813–826.
Boger, D.V., 2009. Rheology and the resource industries. Chem. Eng. Sci. 64, 4525–4536.
Bossis, G., Brady, J.F., 1984. Dynamic simulation of sheared suspensions. 1. General method. J. Chem. Phys. 80, 5141–5154.
Brady, J.F., Bossis, G., 1985. The rheology of concentrated suspensions of spheres in simple shear-flow by numerical simulation. J. Fluid Mech. 155, 105–129.
Brady, J.F., Bossis, G., 1988. Stokesian dynamics. Annu. Rev. Fluid Mech. 20, 111–157.
Brady, J.F., Morris, J.F., 1997. Microstructure of strongly sheared suspensions and its impact on rheology and diffusion. J. Fluid Mech. 348, 103–139.
Breedveld, V., van den Ende, D., Tripathi, A., Acrivos, A., 1998. The measurement of the shear-induced particle and fluid tracer diffusivities in concentrated suspensions by a novel method. J. Fluid Mech. 375, 297–318.
Bürger, R., Bustos, M.C., Concha, F., 1999. Settling velocities of particulate systems: 9. Phenomenological theory of sedimentation processes: numerical simulation of the transient behavior of flocculated suspensions in an ideal batch or continuous thickener. Int. J. Mineral. Proc. 55, 267–282.
Bürger, R., Concha, F., 1998. Mathematical model and numerical simulation of the settling of flocculated suspensions. Int. J. Multiphase Flow 24, 1005–1023.
Bürger, R., Wendland, W.L., 2001. Sedimentation and suspension flows: historical perspective and some recent developments. J. Eng. Math. 41, 101–116.
Buscall, R., White, L.R., 1987. The consolidation of concentrated suspensions: Part 1. The theory of sedimentation. J. Chem. Soc. – Faraday Trans. 83, 873–891.
Bustos, M.C., Concha, F., Bürger, R., Tory, E.M., 1999. Sedimentation and Thickening: Phenomenological Foundation and Mathematical Theory. Kluwer Academic, Dordrecht, Netherlands.
Davis, K.E., Russel, W.B., 1989. An asymptotic description of transient settling and ultrafiltration of colloidal dispersions. Phys. Fluids A 1, 82–100.
de Kretser, R.G., Usher, S.P., Scales, P.J., Boger, D.V., Landman, K.A., 2001. Rapid filtration measurement of dewatering design and optimisation parameters. AIChE J. 47, 1758–1769.
Diehl, S., 2007. Estimation of the batch-settling flux function for an ideal suspension from only two experiments. Chem. Eng. Sci. 62, 4589–4601.
Fang, Z.W., Mammoli, A.A., Brady, J.F., Ingber, M.S., Mondy, L.A., Graham, A.L., 2002. Flow-aligned tensor models for suspension flows. Int. J. Multiphase Flow 28, 137–166.
Foss, D.R., Brady, J.F., 1999. Self-diffusion in sheared suspensions by dynamic simulation. J. Fluid Mech. 401, 243–274.
Gladman, B.R., 2006. The Effect of Shear on Dewatering of Flocculated Suspensions. Ph.D. Thesis, University of Melbourne.
Gladman, B.R., Rudman, M., Scales, P.J., 2010. The effect of shear on gravity thickening: pilot scale modelling. Chem. Eng. Sci. 65, 4293–4301.
Graham, A.L., Altobelli, S.A., Fukushima, E., Mondy, L.A., Stephens, T.S., 1991. NMR imaging of shear-induced diffusion and structure in concentrated suspensions undergoing Couette-flow. J. Rheol. 35, 191–201.
Graham, A.L., Bird, R.B., 1984. Particle clusters in concentrated suspensions. 1. Experimental-observations of particle clusters. Ind. Eng. Chem. Fundam. 23, 406–410.
Green, M.D., Landman, K.A., de Kretser, R.G., Boger, D.V., 1998. Pressure filtration technique for complete characterization of consolidating suspensions. Ind. Eng. Chem. Res. 37, 4152–4156.
Howells, I., Landman, K.A., Panjkov, A., Sirakoff, C., White, L.R., 1990. Time-dependent batch settling of flocculated suspensions. Appl. Math. Modell. 14, 77–86.
Husband, D.M., Mondy, L.A., Ganani, E., Graham, A.L., 1994. Direct measurements of shear-induced particle migration in suspensions of bimodal spheres. Rheol. Acta 33, 185–192.
Kapoor, B., Acrivos, A., 1995. Sedimentation and sediment flow in settling tanks with inclined walls. J. Fluid Mech. 290, 39–66.
Kralchevsky, P.A., Danov, K.D., Denkov, N.D., 2008. Chemical physics of colloids systems and interfaces. In: Birdi, K.S. (Ed.), Handbook of Surface and Colloid Chemistry, 3rd edition CRC Press, Boca Raton, FL, pp. 197–377.
Kynch, G.J., 1952. A theory of sedimentation. Trans. Faraday Soc. 48, 166–176.
Landman, K.A., Russel, W.B., 1993. Filtration at large pressures for strongly flocculated suspensions. Phys. Fluids A 5, 550–560.
Landman, K.A., Stankovich, J.M., White, L.R., 1999. Measurement of the filtration diffusivity $D(\phi)$ of a flocculated suspension. AIChE J. 45, 1875–1882.
Landman, K.A., White, L.R., 1994. Solid/liquid separation of flocculated suspensions. Adv. Colloid Interface Sci. 51, 175–246.
Landman, K.A., White, L.R., Buscall, R., 1988. The continuous-flow gravity thickener: steady state behavior. AIChE J. 34, 239–252.
Leighton, D., Acrivos, A., 1987a. Measurement of shear-induced self-diffusion in concentrated suspensions of spheres. J. Fluid Mech. 177, 109–131.
Leighton, D., Acrivos, A., 1987b. The shear-induced migration of particles in concentrated suspensions. J. Fluid Mech. 181, 415–439.
Lester, D.R., Rudman, M., Scales, P.J., 2010. Macroscopic dynamics of flocculated colloidal suspensions. Chem. Eng. Sci. 65, 6362–6378.
Lester, D.R., Usher, S.P., Scales, P.J., 2005. Estimation of the hindered settling function $R(\phi)$ from batch-settling tests. AIChE J. 51, 1158–1168.
Marchioro, M., Acrivos, A., 2001. Shear-induced particle diffusivities from numerical simulations. J. Fluid Mech. 443, 101–128.
Martin, A.D., 2004. Optimisation of clarifier-thickeners processing stable suspensions for turn-up/turn-down. Water Res. 38, 1568–1578.
Phillips, R.J., Armstrong, R.C., Brown, R.A., Graham, A.L., Abbott, J.R., 1992. A constitutive equation for concentrated suspensions that accounts for shear-induced particle migration. Phys. Fluids A 4, 30–40.
Phillips, R.J., Brady, J.F., Bossis, G., 1988. Hydrodynamic transport-properties of hard-sphere dispersions. 1. Suspensions of freely mobile particles. Phys. Fluids 31, 3462–3472.
Stickland, A.D., Burgess, C., Dixon, D.R., Harbour, P.J., Scales, P.J., Studer, L.J., Usher, S.P., 2008. Fundamental dewatering properties of wastewater treatment sludges from filtration and sedimentation testing. Chem. Eng. Sci. 63, 5283–5290.
Stickland, A.D., Buscall, R., 2009. Whither compressional rheology? J. non-Newtonian Fluid Mech. 157, 151–157.
Studer, L.J., 2008. New Approaches to the Optimisation of Wastewater Dewatering and Processing. Ph.D. Thesis, University of Melbourne.
Subia, S.R., Ingber, M.S., Mondy, L.A., Altobelli, S.A., Graham, A.L., 1998. Modelling of concentrated suspensions using a continuum constitutive equation. J. Fluid Mech. 373, 193–219.
Usher, S.P., 2002. Suspension Dewatering: Characterisation and Optimisation. Ph.D. Thesis, University of Melbourne.
Usher, S.P., de Kretser, R.G., Scales, P.J., 2001. Validation of a new filtration technique for dewaterability characterization. AIChE J. 47, 1561–1570.
Usher, S.P., Scales, P.J., 2005. Steady state thickener modelling from the compressive yield stress and hindered settling function. Chem. Eng. J. 111, 253–261.
Usher, S.P., Spehar, R., Scales, P.J., 2009. Theoretical analysis of aggregate densification: impact on thickener performance. Chem. Eng. J. 151, 202–208.
Usher, S.P., Studer, L.J., Wall, R.C., Scales, P.J., 2013. Characterisation of dewaterability from equilibrium and transient centrifugation test data. Chem. Eng. Sci. 93, 277–291.
van Deventer, B.B.G., Usher, S.P., Kumar, A., Rudman, M., Scales, P.J., 2011. Aggregate densification and batch settling. Chem. Eng. J. 171, 141–151.
Wang, Y., Mauri, R., Acrivos, A., 1996. The transverse shear-induced liquid and particle tracer diffusivities of a dilute suspension of spheres undergoing a simple shear flow. J. Fluid Mech. 327, 255–272.
Wang, Y., Mauri, R., Acrivos, A., 1998. Transverse shear-induced gradient diffusion in a dilute suspension of spheres. J. Fluid Mech. 357, 279–287.

Chapter 4

Mathematical modelling of time-dependent densified thickeners

This chapter has been published in Chemical Engineering Science: 99 103–112 (2013). This chapter addresses how thickener performance and sludge rheological properties are affected by time-dependent aggregate densification occurring in a continuous steady state thickener.

Chapter 3 considered one limit of aggregate densification where the aggregates are densified to have a fixed diameter before entering a thickener. Due to continuous raking of suspensions, the aggregate diameter is changing throughout a thickener (Gladman et al., 2010; van Deventer et al., 2011; van Deventer, 2012). This implies that aggregate densification is time-dependent and/or height-dependent. In this chapter, only aggregate densification is assumed to be time-dependent but the thickener itself is assumed to be at steady state. This implies that the solids flux operated in the thickener is spatially uniform. The aggregates are also assumed to be stable throughout the thickener in this chapter (Usher et al., 2009; van Deventer et al., 2011). In addition, the aggregates are also assumed to enter the consolidating bed immediately and instantaneously. This implies that the hindered settling zone (located above the consolidating bed) can be neglected in this chapter.

Due to time-dependent aggregate densification occurring in a thickener, three interesting research questions can be asked. How do engineers and researchers determine the operating limits of the underflow solids flux in a thickener with time-dependent aggregate

densification when the underflow solids volume fraction is specified? How do different specified underflow solids fluxes affect the predictions of thickener performance and sludge rheological properties? How does the rate of densification of aggregates affect the predictions of consolidated bed structures and the evolutions of sludge rheological properties in a thickener? The above mentioned research questions are of particular interest in this chapter.

Chemical Engineering Science 99 (2013) 103–112

Contents lists available at SciVerse ScienceDirect

Chemical Engineering Science

journal homepage: www.elsevier.com/locate/ces

Mathematical modelling of time-dependent densified thickeners

Yi Zhang, Alastair Martin, Paul Grassia *

CEAS, The Mill, The University of Manchester, Oxford Road, Manchester M13 9PL, UK

HIGHLIGHTS

- Suspension dewatering is considered with simultaneous aggregate/floc densification.
- Suspension rheology evolves between initial undensified and fully densified states.
- For modest solids fluxes, initial undensified gel point achieved at top of solids bed.
- For higher solids fluxes, gel point at the top of the bed must increase.
- Rule of thumb formulae available for determining gel points and/or critical fluxes.

GRAPHICAL ABSTRACT

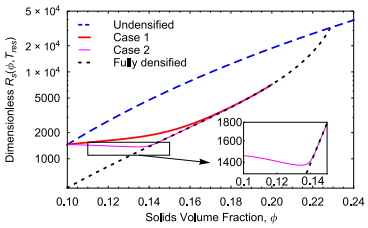

ARTICLE INFO

Article history:
Received 14 March 2013
Received in revised form
16 May 2013
Accepted 23 May 2013
Available online 1 June 2013

Keywords:
Gels
Mathematical modelling
Rheology
Suspension
Dewatering
Densification

ABSTRACT

A one dimensional dewatering model for a thickener consistent with time-dependent densification of aggregates within a sludge suspension has been developed in this paper. The effects of different densification rate parameters and different underflow solids fluxes on the predictions of the sludge rheological properties and thickener performance have been explored. Pre-shearing of aggregates (which leads to the aggregates densifying to some extent before entering the thickener consolidating bed) must occur if a large underflow solids flux is required in a densified thickener. This increases the suspension gel point, and hence the solids volume fraction at the top of the bed. The solids volume fraction at the top of the bed will however be the initial undensified gel point in the case of a small underflow solids flux, where no pre-shearing of aggregates needs to occur. The effects of densification and/or pre-shearing on the sludge rheological properties and thickener performance have been predicted. For a densified thickener, an algorithm has been developed to determine the maximum permitted underflow solids flux, q_{max}, assuming any possible solids volume fraction at the top of the bed and the maximum underflow solids flux, q_{mu}, constraining to the initial undensified gel point at the top of the bed. Regarding the aggregate densification rate parameter, as this parameter was increased, the sludge rheological properties evolved significantly during thickening and thickener performance was substantially enhanced. Moreover, the total solids residence time required to achieve the desired underflow solids volume fraction was significantly reduced both for a higher densification rate parameter and in the presence of pre-shearing in a densified thickener.

1. Introduction

Thickeners are urgently needed to process the significant amounts of sludge produced in the world (Boger, 2009). The aims of improving thickener design are to decrease the thickener bed height (over which the suspension consolidation takes place), increase the underflow solids flux and increase the underflow solids volume fraction. Knowing the sludge rheological material properties which include the so called hindered settling function, $R(\phi)$ and the compressive yield stress, $P_y(\phi)$, engineers will be able to simulate and improve the thickening process. A dewatering theory developed by Buscall and White (1987) has been used to

* Corresponding author. Tel.: +44 161 306 8851; fax: +44 161 306 9321.
E-mail address: paul.grassia@manchester.ac.uk (P. Grassia).

0009-2509/$ - see front matter © 2013 Elsevier Ltd. All rights reserved.
http://dx.doi.org/10.1016/j.ces.2013.05.046

extract the sludge rheological properties and simulate thickener performance. That theory however did not consider shear stress which is often present in thickeners due to the action of rakes and which substantially affects the thickening process.

Channell et al. (2000) conducted experiments investigating the effects of shear on the sludge rheological properties. They found that the sludge rheological properties were significantly influenced by the presence of shear. Adding shear to a sludge suspension dewatering operation can lead to densification of loose solids-containing aggregates (flocs) within the sludge which causes the decrease of the aggregate diameter throughout the dewatering device (Usher et al., 2009; van Deventer et al., 2011; Zhang et al., 2013). Such a dewatering operation in which suspension rheological properties depend not just on local solids fraction, but also explicitly on residence time and/or position in the dewatering device can be expected to be more difficult to model than one in which such explicit time and/or position dependence is absent (Usher et al., 2013). Densification in particular tends over time to reduce the hindered settling function (wider channels open up between flocs facilitating settling) and reduce the compressive yield stress (flocs lose contact with neighbours, limiting a sludge's ability to support stress). Densified aggregate diameters are however believed to saturate to an eventual final value in the presence of shear, meaning that the sludge rheological material properties should likewise saturate. Usher et al. (2009) developed a mathematical model to extract the densified sludge rheological properties given different final aggregate diameters, and applied that model to study the case of a thickener. That mathematical model assumed the aggregates had evolved to a final densified steady state before entering the consolidation zone of the thickener. However, densification and the associated evolution of the aggregate diameter which both depend on the solids residence time can in principle occur throughout the consolidating bed in industrial thickeners. As densification occurs throughout the consolidation zone, both the solids volume fraction within the aggregates, ϕ_{agg} and the suspension gel point, ϕ_g, which can affect the sludge rheological properties, increase with the decrease of the aggregate diameter. The effects of densification as it occurs throughout the consolidating bed upon the sludge rheological properties must therefore be simulated and explored.

The work of van Deventer et al. (2011) assumed a densification rate equation which described the evolution of the aggregate diameter. An important parameter used in that rate equation is the densification rate parameter, A, the reciprocal of which determines the characteristic densification time required to approach the final steady state aggregate diameter. The densification rate parameter, A also affects the rate of change of the gel point, ϕ_g and the rate of change of the solids volume fraction within the aggregates, ϕ_{agg}, which in turn influence the hindered settling function, $R(\phi)$ and the compressive yield stress, $P_y(\phi)$. Thus, for the simulation and computation of the sludge rheological properties in the presence of densification, the densification rate parameter, A must be considered explicitly in the dewatering models for thickeners: this was not tackled by Usher et al. (2009). Previous work by ourselves (Zhang et al., 2013) widened considerably the parameter space investigated by Usher et al. (2009), but still did not address the question of time-dependent densification.

When addressing how densification influences thickening, we must of course identify the thickener operating parameters that are affected. The underflow solids flux is a crucial operating parameter in the design of a densified thickener. Usher and Scales (2005) showed that there was a maximum permitted underflow solids flux which could not be surpassed in a (undensified) thickener for a given underflow solids volume fraction. Experiments conducted by Gladman et al. (2010) argued that a larger underflow solids flux could be achieved for a given underflow solids volume fraction at a given bed height in densified thickeners. There is therefore an interest in finding how densification affects the maximum permitted underflow solids flux in a densified thickener. For an unnetworked feed to a thickener, the solids volume fraction at the top of the bed, which is generally the suspension gel point, has a bearing upon the maximum underflow solids flux permissible in that thickener. We are interested here in whether and how the chosen underflow solids flux imposes conditions upon the solids volume fraction at the top of the bed during densification. When a sufficiently large underflow solids flux is given in a densified thickener, it may be necessary to preshear aggregates which leads to the decrease of the aggregate diameter to some extent before the material enters the consolidation zone. The aggregates will also continue to densify in the consolidation zone. In such a case, the actual height of the consolidation zone and the solids volume fraction at the top of the bed must be computed and explored. The effects of preshearing of aggregates on the sludge rheological properties and thickener performance also must be simulated and predicted.

Thickener performance characteristics including the bed height, the solids residence time and the maximum permitted underflow solids flux have already been predicted in terms of the sludge rheological properties for both initial undensified thickeners and fully densified thickeners (Landman et al., 1988; Bürger et al., 2000; Bürger and Karlsen, 2001; Martin, 2004; Usher and Scales, 2005; Usher et al., 2009; Gladman et al., 2010; Zhang et al., 2013). As the new sludge rheological properties are extracted and computed in the presence of time-dependent densification, we are interested here in predicting and computing the performance of densified thickeners where the densification and consolidation/dewatering occur simultaneously. We are also interested here in the time-evolution in situ of the sludge rheological properties themselves. These are the main novel aspects of the work presented here.

This paper therefore investigates the effects of different densification rate parameters and different underflow solids fluxes on the sludge rheological properties and thickener performance in the presence of densification. Section 2 introduces a dewatering model consistent with time-dependent densification, thereby extending the earlier models presented by Usher et al. (2009). The densification rate equation and an algorithm used to predict the effects of the densification rate parameters and the underflow solids fluxes on the requisite solids volume fraction at the top of the bed are also introduced in Section 2. Section 3 illustrates different cases given different operating parameters in a densified thickener. The functional forms of the densified hindered settling function, $R(\phi, t_{res})$ and the densified compressive yield stress, $P_y(\phi, t_{res})$ are also given in Section 3, being now functions of the solids residence time in the system t_{res} in addition to the solids volume fraction ϕ. Section 4 considers and compares the simulated results by giving different densification rate parameters and different underflow solids fluxes. Section 5 highlights the conclusions.

2. Modelling of the consolidation zone in the presence of time-dependent densification

As the aggregates enter the consolidation zone, the sludge will be dewatered and the solids volume fraction in the bed will be increased. The compressive yield stress which measures the strength of the gel is a vital parameter in this zone and must be considered in the force balance equation (the other forces present being buoyancy and frictional drag). A one dimensional force balance equation governing the consolidation zone is written as

(Buscall and White, 1987; Landman et al., 1988):

$$\frac{R(\phi,t_{res})q(1-\phi/\phi_u)}{(1-\phi)^2}-\frac{\mathrm{d}P_y(\phi,t_{res})}{\mathrm{d}\phi}\frac{\mathrm{d}\phi}{\mathrm{d}z}-\Delta\rho g\phi=0 \tag{1}$$

where ϕ_u is the underflow solids volume fraction, $R(\phi,t_{res})$ is the densified hindered settling function, $P_y(\phi,t_{res})$ is the densified compressive yield stress, $\Delta\rho$ is the density difference between the solids and liquid, g is the gravitational acceleration, t_{res} is the solids residence time, q is the steady and spatially uniform underflow solids flux which is measured downward, and z is the height in the bed which is measured upward.

Due to time-dependent densification that occurs throughout the consolidation zone, the sludge rheological properties including the densified hindered settling function, $R(\phi,t_{res})$, and the densified compressive yield stress, $P_y(\phi,t_{res})$, depend upon both the solids residence time, t_{res}, and the local solids volume fraction, ϕ. Thus, the gradient of the densified compressive yield stress, $P_y(\phi,t_{res})$, with respect to the local solids volume fraction, ϕ becomes

$$\frac{\mathrm{d}P_y(\phi,t_{res})}{\mathrm{d}\phi}=\frac{\partial P_y(\phi,t_{res})}{\partial\phi}+\frac{\partial P_y(\phi,t_{res})}{\partial t_{res}}\frac{\mathrm{d}t_{res}}{\mathrm{d}\phi}. \tag{2}$$

The second term on the right hand side of Eq. (2) is neglected when the aggregates reach the final steady state aggregate diameter, since the compressive yield stress is irrelevant to the solids residence time in that case and this has been the basis of previous modelling by Usher et al. (2009) and Zhang et al. (2013). Here however that term is retained.

The rate of change of the local solids volume fraction in the consolidating bed, $\mathrm{d}\phi/\mathrm{d}t_{res}$ can be written as

$$\frac{\mathrm{d}\phi}{\mathrm{d}t_{res}}=\frac{\mathrm{d}\phi}{\mathrm{d}z}\frac{\mathrm{d}z}{\mathrm{d}t_{res}}. \tag{3}$$

In addition, the solids settling rate in the consolidating bed in terms of the underflow solids flux, q and the local solids volume fraction, ϕ has been given by Usher and Scales (2005):

$$\frac{\mathrm{d}z}{\mathrm{d}t_{res}}=-\frac{q}{\phi} \tag{4}$$

where the sign on the right hand side indicates that the coordinate z is measured upward and the solids residence time, t_{res} is increased from $t_{res}=0$ in the feed at or above the top of the bed to some positive value at the bottom of the densified thickener.

Substituting Eq. (2) into Eq. (1) yields

$$\frac{\mathrm{d}\phi}{\mathrm{d}z}=-\frac{\Delta\rho g\phi-\frac{R(\phi,t_{res})}{(1-\phi)^2}q\left(1-\frac{\phi}{\phi_u}\right)}{\frac{\partial P_y(\phi,t_{res})}{\partial\phi}+\frac{\partial P_y(\phi,t_{res})}{\partial t_{res}}\frac{\mathrm{d}t_{res}}{\mathrm{d}\phi}}. \tag{5}$$

Therefore, substituting Eqs. (4) and (5) into Eq. (3) and then rearranging Eq. (3) yields

$$\frac{\mathrm{d}\phi}{\mathrm{d}t_{res}}=\frac{\Delta\rho gq-\frac{R(\phi,t_{res})}{(1-\phi)^2}q^2\left(\frac{1}{\phi}-\frac{1}{\phi_u}\right)-\frac{\partial P_y(\phi,t_{res})}{\partial t_{res}}}{\frac{\partial P_y(\phi,t_{res})}{\partial\phi}}. \tag{6}$$

Eq. (6) can be solved easily for ϕ vs t_{res} by the midpoint rule.[1] Then z vs t_{res} (via Eq. (4)) and hence ϕ vs z (parametrically in terms of t_{res}) are solved easily.

For an unnetworked system in which the initial solids volume fraction at the inlet of the thickener is less than the gel point, the solids volume fraction at the top of the bed is either the initial undensified gel point, $\phi_{g,0}$ or else the final saturated steady state gel point, $\phi_{g,\infty}$, respectively in initial undensified thickeners or fully densified thickeners (with necessarily $\phi_{g,\infty}>\phi_{g,0}$). When densification occurs throughout the consolidation zone however, the solids volume fraction at the top of the bed is possibly some a priori unknown densified gel point ϕ_g which needs to be determined and computed. Thus, it is vital to obtain the actual value of the densified gel point at the top of the bed in densified thickeners.

Moving into the bed, the rate of increase of the solids volume fraction ϕ in a consolidating and densifying bed tends to be more rapid than that of the gel point ϕ_g if a small underflow solids flux is selected in a densified thickener. Thus, all the aggregates introduced to the thickener can be considered to enter the consolidating bed immediately and no pre-shearing of aggregates needs to occur at early times: the gel point at the top of the bed is the initial undensified gel point in that case. When the underflow solids flux is however selected large enough, the rate of increase of the solids volume fraction may fall and could potentially become slower than that of the gel point itself at early times. This leads to a paradoxical situation whereby a suspension which starts to gel as the solids volume fraction, ϕ surpasses $\phi_{g,0}$, could then "ungel" as individual aggregates densify and lose contact with one another. Hence to avoid this, pre-shearing of aggregates must occur (which has the effect of slowing down further densification occurring in the bed itself). The solids volume fraction at the top of the bed is the densified gel point which needs to be calculated.

2.1. Evolution of the aggregate diameter ratio and the gel point

As mentioned previously, the aggregate diameter is decreased when densification occurs. The densification rate parameter, A, which affects the rate of decrease of the aggregate diameter, is an important parameter for the predictions of thickener performance and the bed structure. Moreover, the predictions of the densified hindered settling function, $R(\phi,t_{res})$, and the densified compressive yield stress, $P_y(\phi,t_{res})$, depend on the densification rate parameter, A. The evolution of the aggregate diameter in terms of the densification rate parameter, A has been developed by van Deventer et al. (2011)

$$\frac{\mathrm{d}D_{agg}}{\mathrm{d}t_{res}}=-A(D_{agg}-D_{agg,\infty}) \tag{7}$$

$$D_{agg}=(1-D_{agg,\infty})\mathrm{e}^{-At_{res}}+D_{agg,\infty} \tag{8}$$

where A is the densification rate parameter, D_{agg} is the aggregate diameter ratio defined as the ratio of the densified aggregate diameter to the undensified aggregate diameter, and $D_{agg,\infty}$ is a final steady state aggregate diameter ratio which is defined as the minimum aggregate diameter ratio obtained in densified thickeners. Note that this final steady state aggregate diameter ratio, $D_{agg,\infty}$ is independent of the densification rate parameter, A. We assume $D_{agg,\infty}=0.9$ here (Usher et al., 2009; van Deventer et al., 2011). Mass balance for the solids volume fraction within the aggregates must obey (van Deventer et al., 2011):

$$\phi_{agg}=\frac{\phi_{agg,0}}{D_{agg}^3} \tag{9}$$

where $\phi_{agg,0}$ is the initial undensified solids volume fraction within the aggregates which is assumed to be 0.1667 in this paper (Usher et al., 2009).

The densification theory (Usher et al., 2009; van Deventer et al., 2011) indicated that the gel point increased with the decrease of the aggregate diameter ratio. The densified gel point, ϕ_g formula which is expressed in terms of the initial undensified gel point, $\phi_{g,0}$ and the aggregate diameter ratio, D_{agg} has been developed by

[1] The 4th order Runge–Kutta method is normally a more accurate method. However as has been discussed in the literature (Usher et al., 2009; Zhang et al., 2013), the functions $R(\phi,t_{res})$ and $P_y(\phi,t_{res})$ are not perfectly smooth at the point where the solids volume fraction, ϕ equals the solids volume fraction within the aggregates, ϕ_{agg}, meaning that 4th order Runge–Kutta method tends not to perform any better than simpler algorithms such as the midpoint rule.

van Deventer et al. (2011)

$$\phi_g = \frac{\phi_{g,0}}{D_{agg}^3} \tag{10}$$

where ϕ_g is the densified gel point, and $\phi_{g,0}$ is the initial undensified gel point which is assumed to be 0.1 in this paper (Usher et al., 2009). According to the above equations, ϕ_g is simply a fixed fraction of ϕ_{agg}—corresponding to the fraction of space that must be filled by aggregates for them to gel into a network.

2.2. Sludge rheological properties

As has been discussed previously, the sludge rheological properties including the densified compressive yield stress, $P_y(\phi, t_{res})$ and the densified hindered settling function, $R(\phi, t_{res})$ are influenced if densification occurs, since the gel point, ϕ_g and the solids volume fraction within the aggregates, ϕ_{agg} increase with the decrease of the aggregate diameters. Surprisingly perhaps, the sludge rheological properties are also influenced by the underflow solids flux, since the value of q we select determines whether the aggregates need to be pre-sheared prior to entering the consolidated bed. The precise details of how the sludge rheological properties change with the above mentioned parameters will be discussed later. We will also identify certain critical values of the underflow solids flux in the following sections.

2.3. Maximum permitted underflow solids flux

As mentioned above, the underflow solids flux affects the consolidating bed structure and the actual bed height of a densified thickener. Usher and Scales (2005) developed an algorithm used to determine the maximum permitted underflow solids flux for an undensified thickener. This balances buoyancy of the solids to the hydrodynamic drag on them and is only realised for an exceedingly tall thickener where the network stresses are very weak. The undensified maximum permitted underflow solids flux, $q_{max}^{undensified}$ is equal to the minimum possible free settling solids flux determined by application of all possible solids volume fractions in the bed (Usher and Scales, 2005). This (minimum) free settling solids flux, q_{fs} can be written as (Usher and Scales, 2005)

$$q_{max}^{undensified} = q_{fs} \equiv \min_{\phi_{g,0} \le \phi \le \phi_u} \frac{\Delta\rho g \phi (1-\phi)^2}{R_0(\phi)\left(1-\frac{\phi}{\phi_u}\right)} \tag{11}$$

where $R_0(\phi)$ is the undensified hindered settling function.

In both an initial undensified thickener and a fully densified thickener, the minimum free settling solids flux is determined at some point in the interior of the bed where, as mentioned previously, the gravity force balances the hydrodynamic drag. The location of the minimum free settling solids flux is set largely by a rapid increase of $R_0(\phi)$ with respect to ϕ and a slow decrease of $(1-\phi/\phi_u)$ with respect to ϕ in the denominator of Eq. (11). However, in a densified thickener (where the hindered settling function depends on both the solids residence time and the solids volume fraction and where $R(\phi, t_{res})$ will replace $R_0(\phi)$ in Eq. (11)), the minimum sought of Eq. (11) can shift, due to the decrease of the aggregate diameter throughout the bed. For a sufficiently low densification rate parameter, A, the rate of evolution of the aggregate diameter ratio is also extremely slow and the minimum free settling solids flux is again determined at some point in the interior of the bed, since the solids behaviour in that case is very similar to that in an initial undensified thickener. However, for a densification rate parameter, A, which is rather larger, the minimum sought of Eq. (11) tends to occur at the top of the bed. This is because any sharp increase in $R(\phi, t_{res})$ with respect to ϕ (drag increases with the solids volume fraction) tends to be offset by a sharp decrease in $R(\phi, t_{res})$ with respect to t_{res} (drag decreases as the aggregates densify and wider channels open up between them).

In the presence of densification, we define two maximum permitted underflow solids fluxes: the maximum permitted underflow solids flux, q_{mu} assuming the initial undensified gel point at the top of the bed and the maximum permitted underflow solids flux, q_{max} for access to any possible solids volume fractions in a densified thickener, corresponding to the densified case with an arbitrarily large amount of pre-shearing.

Specifically, q_{mu} and q_{max} are written as

$$q_{mu} = \frac{\Delta\rho g \phi_{g,0}(1-\phi_{g,0})^2}{R_0(\phi_{g,0})\left(1-\frac{\phi_{g,0}}{\phi_u}\right)} \tag{12}$$

$$q_{max} = \min_{\phi_{g,\infty} \le \phi \le \phi_u} \frac{\Delta\rho g \phi (1-\phi)^2}{R_\infty(\phi)\left(1-\frac{\phi}{\phi_u}\right)} \tag{13}$$

where $\phi_{g,0}$ is the initial undensified gel point, $\phi_{g,\infty}$ is the fully densified gel point, $R_0(\phi_{g,0})$ is the initial undensified hindered settling function evaluated at $\phi = \phi_{g,0}$, $R_\infty(\phi)$ is equal to $\lim_{t_{res}\to\infty} R(\phi, t_{res})$ and ϕ_u is the underflow solids volume fraction.

Evidently q_{max}, which can never be exceeded for a given underflow solids volume fraction in a densified thickener, is larger[2] than q_{mu} which is likewise larger than the undensified maximum permitted underflow solids flux. If the proposed underflow solids flux, q is smaller than q_{mu}, the solids volume fraction at the top of the bed will be the initial undensified gel point, $\phi_{g,0}$. For the case where the proposed underflow solids flux, q is larger than q_{mu}, pre-shearing of aggregates must occur and the solids volume fraction at the top of the bed will be some densified gel point which needs to be computed.

We emphasise that Eqs. (12) and (13) should be viewed as engineering rules of thumb for defining the maximum permitted underflow solids fluxes rather than comprehensive laws. They work well for cases we shall consider here with densification rate parameters of the same order of magnitude as those seen in van Deventer et al. (2011), but it is always possible to envisage a densification rate parameter sufficiently small whereby the densified maximum permitted underflow solids flux moves back arbitrarily close to the undensified value.

Indeed it is not even unambiguous what physical criterion one would use to define the maximum permitted underflow solids fluxes in the time-dependent densified case—is the aim to avoid points where $d\phi/dz \to 0$ (on the grounds that these lead to tall thickeners) or should one be trying to avoid regions where $dP_y(\phi)/dz$ changes sign (to ensure a dynamically stable situation where network stresses oppose suspension buoyancy)? These two criteria are identical in an undensified case and are again unambiguous in a fully densified case, but differ in the case of time-dependent densification – the latter criterion (which is what we have used) turns out to be the more stringent one.

2.3.1. Algorithm for determining the gel point at the top of the bed

A simple formula is available to determine the maximum permitted underflow solids flux, q_{mu} assuming the initial undensified gel point at the top of the bed (see Eq. (12)). For cases where

[2] The claim that typically q_{max} exceeds q_{mu}, is supported by arguments detailed in Zhang et al. (2013) suggesting that the value of $(1-\phi_{g,\infty})^2/R_\infty(\phi_{g,\infty})$ is well approximated by the value of $(1-\phi_{g,0})^2/(D_{agg,\infty}R_0(\phi_{g,0}))$.

$q_{mu} < q < q_{max}$, the densified gel point at the top of the bed is also determined via a simple algorithm described below.

We have already stated that for a sufficiently small densification rate parameter, A, the maximum permitted underflow solids flux accessible in a densified thickener corresponds to that in an undensified thickener, but for a larger densification rate parameter, A (comparable with the values actually encountered in practice by van Deventer et al., 2011), the maximum permitted underflow solids flux assuming the initial undensified gel point, $\phi_{g,0}$ at the top of the bed instead approaches the rule of thumb value q_{mu} given by Eq. (12).

If the proposed underflow solids flux, q now exceeds q_{mu} (but is less than q_{max} given by Eq. (13)), then we have to search for a new gel point, ϕ_g (which is larger than $\phi_{g,0}$) at the top of the bed. The equation for searching for this new gel point, ϕ_g can be written as

$$q = \frac{\Delta\rho g \phi_g (1-\phi_g)^2}{R(\phi_g, t_{res}(\phi_g))\left(1-\frac{\phi_g}{\phi_u}\right)} \tag{14}$$

where q denotes the proposed underflow solids flux, and $t_{res}(\phi_g)$ denotes the amount of pre-shearing time computed via Eqs. (8) and (10) needed to shift the gel point from $\phi_{g,0}$ to ϕ_g. Again the rule of thumb assumption[3] applies here that, at $t_{res}(\phi_g)$, aggregates are still densifying sufficiently quickly that increases in $R(\phi, t_{res})$ with respect to ϕ moving down into the consolidated bed are offset by decreases in $R(\phi, t_{res})$ with respect to t_{res}.

For a given underflow solids volume fraction, the maximum permitted underflow solids flux that can ever be delivered is of course q_{max}, which corresponds to pre-shearing all the way to a final steady state aggregate diameter ratio given in a fully densified thickener. Then, the solids volume fraction at the top of the bed is the final steady state gel point, $\phi_{g,\infty}$ whereas q_{max} is equal to the minimum sought in Eq. (13) considering the solids volume fractions ranging between the final steady state gel point, $\phi_{g,\infty}$ and the proposed underflow solids volume fraction, ϕ_u in a fully densified thickener.

3. Case studies

Four cases are illustrated in this section. Two cases operate a comparatively small underflow solids flux, including either a small densification rate parameter or a large densification rate parameter (with a value as chosen by van Deventer et al., 2011), respectively. The imposed underflow solids flux is smaller than q_{mu} given by Eq. (12) in those two cases. Another two cases include the same small densification rate parameter and the same large densification rate parameter as given in the previous two cases, respectively, but a different underflow solids flux which is larger than q_{mu}. The operating parameters given in each case are shown in Table 1.

The underflow solids volume fraction, ϕ_u is assumed to be 0.2 in all cases, the initial undensified gel point, $\phi_{g,0}$ is chosen as 0.1 (Usher et al., 2009) and the initial solids volume fraction within the aggregates, $\phi_{agg,0}$ is assumed to be 0.1667 (Usher et al., 2009). In addition, the final steady state aggregate diameter ratio, $D_{agg,\infty}$ is assumed to be 0.9 (a value used previously in computations by both Usher et al. (2009) and van Deventer et al. (2011), and moreover not too far from an experimentally determined value 0.846 of van Deventer et al. (2011) for a calcite suspension). Hence, the final steady state gel point, $\phi_{g,\infty}$, determined by Eq. (10) is 0.1372 and the final steady state solids volume fraction within the aggregates, $\phi_{agg,\infty}$, determined by Eq. (9) is 0.2286. The densities of solids and liquid are chosen as 3200 kg m^{-3} and 1000 kg m^{-3}, respectively (Usher et al., 2009). The gravitational acceleration, g is chosen as 9.8 m s^{-2}.

3.1. Sludge properties

As densification occurs right throughout the consolidating bed, the sludge rheological properties depend on the solids volume fraction, ϕ, and the solids volume fraction within the aggregates, ϕ_{agg}, which itself depends on the densification rate parameter, A, and the solids residence time, t_{res}. In order to simulate and compute the sludge rheological properties, we must choose appropriate functional forms for the densified hindered settling function, $R(\phi, t_{res})$, and the densified compressive yield stress, $P_y(\phi, t_{res})$ in terms of their undensified counterparts.

3.1.1. Hindered settling function

The initial undensified hindered settling function, $R_0(\phi)$ is chosen here as (Usher et al., 2009; Zhang et al., 2013)

$$R_0(\phi) = \frac{R_{Stokes,0}}{\phi_{agg,0}}(\phi + r_g)^{r_n} r_g^{-r_n} \tag{15}$$

where $R_{Stokes,0}$ is the initial undensified hindered settling function of an isolated aggregate which is chosen as 2, 60, 469 Pa s m^{-2} (Zhang et al., 2013), r_g and r_n are the functional parameters which are chosen as 0.05 and 5, respectively (van Deventer et al., 2011; Usher et al., 2009).

The densified hindered settling function has been developed by Usher et al. (2009) and Zhang et al. (2013). The reader is referred to those papers for full details of the derivation, but briefly the formula accounts for the fact that flow can go both around and through aggregates, and moreover in the case of flow around aggregates, it is necessary to recognise that the aggregates themselves are less buoyant than pure solids would be. The result is

$$R(\phi, t_{res}) = \frac{(1-\phi)^2 R_0(\phi_{agg}) R_{Stokes,0} D_{agg}}{\phi_{agg,0} R_0(\phi_{agg})(1-\phi/\phi_{agg})^2 / r_{agg}(\phi/\phi_{agg}) + (R_{Stokes,0} D_{agg}\phi/\phi_{agg})(1-\phi_{agg})^2} \tag{16}$$

where ϕ_{agg} represents the solids volume fraction within the aggregates, D_{agg} denotes the aggregate diameter ratio, and $r_{agg}(\phi/\phi_{agg})$ is the aggregate hindered settling factor which is a function of ϕ/ϕ_{agg} and which will be defined later. Note that both ϕ_{agg} and D_{agg} depend upon the solids residence time, t_{res} and the densification rate parameter, A.

The aggregate hindered settling factor, $r_{agg}(\phi/\phi_{agg})$ is assumed to be independent of densification and hence can be evaluated in the initial undensified state (Usher et al., 2009; Zhang et al., 2013). A suitable functional form of $r_{agg}(\phi/\phi_{agg})$ is given by Zhang et al. (2013):

$$r_{agg}(\phi/\phi_{agg}) = \frac{\phi_{agg,0}\left(1-\frac{\phi}{\phi_{agg}}\right)^2 R_0(\phi_{agg,0}) R_0\left(\phi_{agg,0}\frac{\phi}{\phi_{agg}}\right)}{\left(R_0(\phi_{agg,0})\left(1-\phi_{agg,0}\frac{\phi}{\phi_{agg}}\right)^2 - \frac{\phi}{\phi_{agg}}(1-\phi_{agg,0})^2 R_0\left(\phi_{agg,0}\frac{\phi}{\phi_{agg}}\right)\right) R_{Stokes,0}}. \tag{17}$$

3.1.2. Compressive yield stress

For an initial undensified system, previous work (Zhang et al., 2013) considered two functional forms for the compressive yield

[3] This rule of thumb procedure for relating ϕ_g to q breaks down when the solids residence times are sufficiently long as to bring ϕ_g into the neighbourhood of $\phi_{g,\infty}$, since $R(\phi, t_{res})$ then ceases to change with t_{res}, and identification of the maximum permitted underflow solids flux corresponding to a given $\phi_g \approx \phi_{g,\infty}$ then reverts to an interval search analogous to Eq. (13). As a consequence, for q values which are very close to q_{max}, the values of ϕ_g vary more rapidly with respect to q than the solution of Eq. (14) would suggest. However for the values of the densification rate parameter, A and the underflow solids flux, q to be considered here, Eq. (14) works well in practice.

Table 1
Operating parameters given in each case. Note that the proposed underflow solids flux operated in each case is larger than the undensified maximum permitted underflow solids flux, but smaller than the (fully) densified maximum underflow solids flux. The values of $q_{max}^{undensified}$, q_{mu}, and $q_{max}^{densified}$ are determined via Eqs. (11)–(13), respectively. Observe that $q < q_{mu}$ in Cases 1 and 2, but $q > q_{mu}$ in Cases 3 and 4.

	Case 1	Case 2	Case 3	Case 4
Small A/s^{-1}	0.001	N/A	0.001	N/A
Large A/s^{-1}	N/A	0.01	N/A	0.01
Small $q/m\ s^{-1}$	6×10^{-6}	6×10^{-6}	N/A	N/A
Large $q/m\ s^{-1}$	N/A	N/A	1×10^{-5}	1×10^{-5}
$q_{mu}/m\ s^{-1}$	9.2×10^{-6}	9.2×10^{-6}	9.2×10^{-6}	9.2×10^{-6}
$q_{max}^{undensified}/m\ s^{-1}$	5.84×10^{-6}	5.84×10^{-6}	5.84×10^{-6}	5.84×10^{-6}
$q_{max}^{densified}/m\ s^{-1}$	2×10^{-5}	2×10^{-5}	2×10^{-5}	2×10^{-5}
ϕ_u	0.2	0.2	0.2	0.2
$D_{agg,\infty}$	0.9	0.9	0.9	0.9

stress. One had a comparatively weak network in the neighbourhood of the gel point – as $\phi\to\phi_g$, $P_y(\phi,t_{res})$ approached zero as a high power of $\phi-\phi_g$. The other was comparatively strong in the neighbourhood of the gel point – as $\phi\to\phi_g$, $P_y(\phi,t_{res})$ approached zero linearly in $\phi-\phi_g$. The weak gel had $d\phi/dz\to\infty$ at the top of the bed where $\phi\to\phi_g$, in order to keep $dP_y(\phi,t_{res})/dz$ finite at the top of the bed. The strong gel however had $d\phi/dz$ finite there. In the presence of densification, we expect the bed height to shrink, therefore $d\phi/dz$ is likely to increase throughout the bed – and the larger the densification rate parameter, A, the more $d\phi/dz$ should increase. Clearly for a weak gel where $d\phi/dz$ is already large near the top of the bed, it is difficult to detect a local increase in $d\phi/dz$. Therefore in this study, we choose to consider the case of a strong gel where the effects of varying densification rate parameter, A will be more apparent. The undensified compressive yield stress data presented in Usher et al. (2009) are used here, but slightly different gel strength formulae are developed to fit the data to the strong gel case. Thus, the functional forms of the initial undensified compressive yield stress, $P_{y,0}(\phi)$, and the densified compressive yield stress, $P_{y,1}(\phi,t_{res})$ are chosen as

$$P_{y,0}(\phi)=\frac{a_0(\phi-\phi_{g,0})}{(m+\phi-\phi_{g,0})(\phi_{cp}-\phi)^{n_0}} \tag{18}$$

and

$$P_{y,1}(\phi,t_{res})=\frac{a_1(\phi-\phi_g)}{(m+\phi-\phi_g)(\phi_{cp}-\phi)^{n_1}} \tag{19}$$

where a_0, m, n_0, a_1, and n_1 are the fitting parameters. The close packing solids volume fraction, ϕ_{cp} at which $P_{y,0}(\phi)$ and $P_{y,1}(\phi,t_{res})$ are considered to become infinite regardless of whether or not densification occurs is assumed to be 0.8 (Usher et al., 2009).

In this paper, the values of a_0, m, and n_0 are assumed[4] to be 3.7914 Pa, 0.0363, and 10.8302, respectively. Due to a requirement that the densified and undensified cases join up continuously with continuous derivative at $\phi=\phi_{agg}$, the densified fitting parameters, a_1 and n_1, which depend on the aggregate diameter ratio, D_{agg} and need to be updated in each time step, are given by

$$n_1=(\phi_{cp}-\phi_{agg})\left(\frac{P'_{y,0}(\phi_{agg})}{P_{y,0}(\phi_{agg})}+\frac{1}{m+\phi_{agg}-\phi_g}-\frac{1}{\phi_{agg}-\phi_g}\right) \tag{20}$$

and

$$a_1=\frac{P_{y,0}(\phi_{agg})(m+\phi_{agg}-\phi_g)(\phi_{cp}-\phi_{agg})^{n_1}}{(\phi_{agg}-\phi_g)}. \tag{21}$$

The values of n_1 and a_1 can be calculated via using the chosen parameters which have already been mentioned above. The value of n_1 ranges from $n_1=10.8302$ determined initially at $D_{agg}=1$ down to $n_1=10.0288$ determined at $D_{agg}=0.91$. Meanwhile the value of a_1 ranges from $a_1=3.7914$ Pa determined initially at $D_{agg}=1$ up to $a_1=6.4516$ Pa determined at $D_{agg}=D_{agg,\infty}=0.9$.

Eliminating a_1 yields a new expression of the densified compressive yield stress, $P_{y,1}(\phi,t_{res})$:

$$P_{y,1}(\phi,t_{res})=P_{y,0}(\phi_{agg})\frac{m+\phi_{agg}-\phi_g}{m+\phi-\phi_g}\left(\frac{\phi_{cp}-\phi_{agg}}{\phi_{cp}-\phi}\right)^{n_1}\frac{\phi-\phi_g}{\phi_{agg}-\phi_g}. \tag{22}$$

In Eq. (22), ϕ_{agg}, ϕ_g, and n_1 are all well-defined functions of the solids residence time, t_{res}. Thus, it is easy to evaluate the derivative, $\partial P_{y,1}(\phi,t_{res})/\partial t_{res}$ (required in Eq. (6)) using any standard mathematical software (e.g. MATLAB and Mathematica). Note that by construction $\partial P_{y,1}(\phi,t_{res})/\partial t_{res}$ vanishes when evaluated at any instantaneous $\phi=\phi_{agg}$ value.

3.2. Dimensionless equations

It is possible to convert the systems of equations to dimensionless form by defining a characteristic velocity scale, $\Delta\rho g/R_{Stokes,0}$ and a characteristic length scale, $a_0/(\Delta\rho g)$ (Zhang et al., 2013). The dimensionless sludge rheological properties, denoted now $p_y(\phi)$ and $R_s(\phi)$, the dimensionless location, Z, the dimensionless underflow solids flux, Q, the dimensionless solids residence time, T_{res}, and the dimensionless densification rate parameter, α are also easily defined as (Zhang et al., 2013)

$$p_y(\phi,T_{res})=\frac{P_y(\phi,t_{res})}{a_0},\quad R_s(\phi,T_{res})=\frac{R(\phi,t_{res})}{R_{Stokes,0}}$$

$$Z=\frac{\Delta\rho gz}{a_0},\quad Q=\frac{R_{Stokes,0}q}{\Delta\rho g}$$

$$T_{res}=\frac{(\Delta\rho g)^2t_{res}}{a_0R_{Stokes,0}},\quad \alpha=\frac{a_0R_{Stokes,0}A}{(\Delta\rho g)^2}$$

where as noted earlier $a_0=3.7914$ Pa, $R_{Stokes,0}=260469$ Pa s m^{-2}, $\Delta\rho=2200$ kg m^{-3}, and $g=9.8$ m s^{-2}. Thus, the characteristic velocity scale now becomes 0.08277 m s^{-1}, the characteristic length scale now becomes 1.7585×10^{-4} m, and the characteristic time scale is 2.125×10^{-3} s. Hence, based on the values given in Table 1, the dimensionless densification rate parameter, α is evaluated to 2.125×10^{-6} in Cases 1 and 3 and to 2.125×10^{-5} in Cases 2 and 4. In addition, the dimensionless imposed underflow solids flux, Q is determined to be 7.25×10^{-5} in Cases 1 and 2 and is determined to be 1.21×10^{-4} in Cases 3 and 4. The dimensionless undensified maximum permitted underflow solids flux, $Q_{max}^{undensified}$, the dimensionless maximum permitted underflow solids flux, Q_{mu} assuming the initial undensified gel point at the top of the bed, and the dimensionless densified maximum permitted underflow solids flux, $Q_{max}^{densified}$ are determined to be 7.06×10^{-5}, 1.11×10^{-4}, and 2.42×10^{-4}, respectively.[5]

[4] Typically m is a small parameter – smaller than $\phi_u-\phi_g$. Thus, except very close to the top of the bed (where ϕ is near ϕ_g) we deduce $(\phi-\phi_g)/(m+\phi-\phi_g)\approx1$. Therefore, $P_{y,0}(\phi)\approx a_0/(\phi_{cp}-\phi)^{n_0}$ and $P_{y,1}(\phi,t_{res})\approx a_1/(\phi_{cp}-\phi)^{n_1}$. This behaviour was also seen in the strong gel formulae of Zhang et al. (2013) – although Eqs. (18) and (19) are not identical to the formulae utilised there.

[5] These dimensionless values are surprisingly small, but such small values arise because the chosen characteristic length and velocity scales become atypical of suspensions significantly beyond the gel point, owing partly to the comparatively weak buoyancy of flocs compared to pure solids, but primarily due to the rapid increase in hindrance between flocs and in gel strength as the solids volume fraction increases. As in Zhang et al. (2013) however, we are primarily interested in relative changes of these dimensionless values between different cases, rather than the actual dimensionless values in any particular case.

Eqs. (4), (6) and (8) can be easily converted to dimensionless form using the above dimensionless scales:

$$\frac{dZ}{dT_{res}} = -\frac{Q}{\phi} \tag{23}$$

$$\frac{d\phi}{dT_{res}} = \frac{Q - \frac{R_s(\phi,T_{res})}{(1-\phi)^2}Q^2\left(\frac{1}{\phi}-\frac{1}{\phi_u}\right) - \frac{\partial p_y(\phi,T_{res})}{\partial T_{res}}}{\frac{\partial p_y(\phi,T_{res})}{\partial \phi}} \tag{24}$$

$$D_{agg} = (1-D_{agg,\infty})e^{-\alpha T_{res}} + D_{agg,\infty}. \tag{25}$$

In the above expressions, $R_s(\phi, T_{res})$ obeys the same equations ass given in Eqs. (15)–(17) provided we replace $R_{Stokes,0}$ by $\phi_{agg,0}$ (see details in Zhang et al. (2013)). Likewise $p_y(\phi, T_{res})$ obeys Eqs. (18) and (19) provided we replace a_0 by unity and a_1 by a_1/a_0 (again see details in Zhang et al., 2013). Finally, At_{res} in Eq. (8) can be replaced by αT_{res}. Although computations are most conveniently done in dimensionless form, in what follows, we will convert many of our results back to dimensional form for ease of interpretation.

4. Results and discussion

The sludge rheological properties including the densified hindered settling function, $R(\phi, t_{res})$, and the densified compressive yield stress, $P_y(\phi, t_{res})$, were predicted consistent with time-dependent densification throughout the bed in this section. Moreover, the solids concentration profiles, the bed heights and the total solids residence times required to achieve the desired underflow solids volume fractions were also obtained via integration of the governing equations with the midpoint rule.

4.1. Densified gel point

As discussed previously, the densified gel point at the top of the bed can be increased to some extent via pre-shearing of aggregates permitting values of Q/Q_{mu} in excess of unity (e.g. Cases 3 and 4). No pre-shearing of aggregates is required in Cases 1 and 2, so the solids volume fraction at the top of the bed is the initial undensified gel point, $\phi_{g,0}$ in those two cases. Table 2 shows the densified gel points at the top of the bed determined via Eq. (14) in Cases 3 and 4, respectively.

As shown in Table 2, the densified gel point calculated from Cases 3 and 4, respectively remains the same value for a given underflow solids flux (with a fixed underflow solids volume fraction), regardless of the densification rate parameter, since the aggregates are pre-sheared to a specific aggregate diameter ratio such that Eq. (14) is satisfied. If a smaller densification rate parameter is given, the solids residence time required to pre-shear the aggregates is correspondingly longer.

4.2. Densified compressive yield stress

The dimensionless densified compressive yield stress, $p_{y,1}(\phi, T_{res})$ is an important parameter which determines the network strength. Figs. 1 and 2 indicate the evolution of the dimensionless densified compressive yield stress, $p_{y,1}(\phi, T_{res})$ given different dimensionless densification rate parameters and different dimensionless underflow solids fluxes, recognising that (in the bed) ϕ is a function of T_{res} and hence equivalently T_{res} is a function of ϕ. For a given dimensionless underflow solids flux and a given underflow solids volume fraction (as in Fig. 1), the dimensionless densified compressive yield stress, $p_{y,1}(\phi, T_{res})$ determined in the case of a larger dimensionless densification rate parameter, α (in Case 2) is considerably smaller than that determined in the case of a smaller dimensionless densification rate parameter, α (in Case 1), due to a rapid decrease of the aggregate diameter ratio, D_{agg} and a rapid increase of the solids volume fraction within the aggregates, ϕ_{agg} in Case 2. Also comparing Figs. 1 and 2, the dimensionless densified compressive yield stress, $p_{y,1}(\phi, T_{res})$ determined in Case 3 is smaller than that determined in Case 1, since the aggregates are pre-sheared before entering the bed. A similar observation can be obtained by comparing Case 4 with Case 2. The dimensionless fully densified compressive yield stress is obtained at late times, as the aggregate diameter ratio reaches the final steady state aggregate diameter ratio, $D_{agg,\infty}$.

Table 2
The updated densified gel points at the top of the bed determined in Cases 3 and 4, respectively and the corresponding amount of pre-shearing time calculated in those two cases. Cases 1 and 2 have $Q/Q_{mu} < 1$ and consequently do not require pre-shearing. Thus, in those two cases $\phi_g = \phi_{g,0} = 0.1$.

	Q/Q_{mu}	ϕ_g	$\alpha T_{res}^{pre-shear}$	$t_{res}^{pre-shear}$/s
Case 3	1.09	0.1043	0.1491	149.1
Case 4	1.09	0.1043	0.1491	14.91

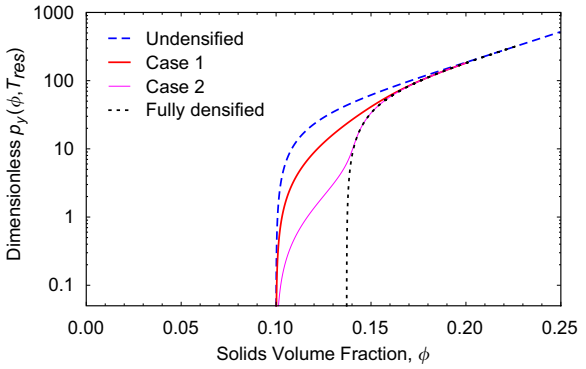

Fig. 1. The determination of the dimensionless densified compressive yield stress, $p_y(\phi, T_{res})$, with a small dimensionless underflow solids flux, $Q = 7.25 \times 10^{-5}$ (Case 1—slow densification ($\alpha = 2.125 \times 10^{-6}$) and Case 2—rapid densification ($\alpha = 2.125 \times 10^{-5}$).

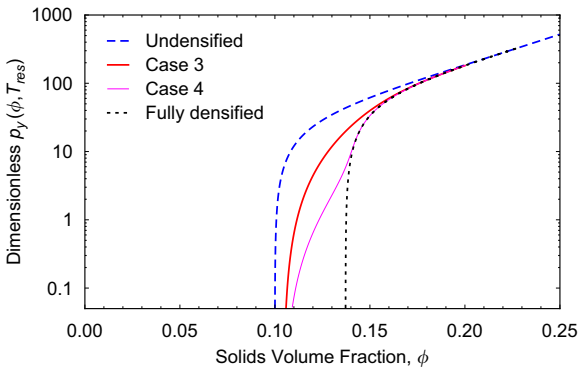

Fig. 2. The determination of the dimensionless densified compressive yield stress, $p_y(\phi, T_{res})$, with a comparatively 'large' dimensionless underflow solids flux, $Q = 1.21 \times 10^{-4}$ (Case 3—slow densification ($\alpha = 2.125 \times 10^{-6}$) and Case 4—rapid densification ($\alpha = 2.125 \times 10^{-5}$)).

4.3. Densified hindered settling function

Figs. 3–5 show the dimensionless densified hindered settling function, $R_s(\phi, T_{res})$ predicted in each case. Those figures indicate how the dimensionless densified hindered settling function, $R_s(\phi, T_{res})$ changes with given different dimensionless densification rate parameter, α and different dimensionless underflow solids flux, Q in the consolidating bed of a densified thickener. Again the calculations recognise that within the consolidated bed, ϕ is a function of T_{res}, and hence T_{res} is a function of ϕ. The dimensionless densified hindered settling function, $R_s(\phi, T_{res})$, calculated in Case 1 increases from the top of the bed to the bottom of the densified thickener. This is the same qualitative behaviour as observed in an undensified bed with $Q < Q_{max}^{undensified}$. However, the dimensionless densified hindered settling function, $R_s(\phi, T_{res})$, determined in Case 2 (with more rapid densification than in Case 1) decreases for the solids volume fraction, ϕ between 0.1 and 0.14, and is then increased for $\phi > 0.14$. In Case 3 (with a higher underflow solids flux than in Case 1), the dimensionless densified hindered settling function, $R_s(\phi, T_{res})$ decreases with the increase of the solids volume fraction for $\phi < 0.108$ and then increases with the increase of the solids volume fraction for $\phi > 0.108$. Note however that the amount of the initial decrease is extremely tiny in this particular case. The dimensionless densified hindered settling function, $R_s(\phi, T_{res})$, predicted in Case 4 (again corresponding to comparatively rapid densification) has a similar curve shape as that achieved in Case 2.

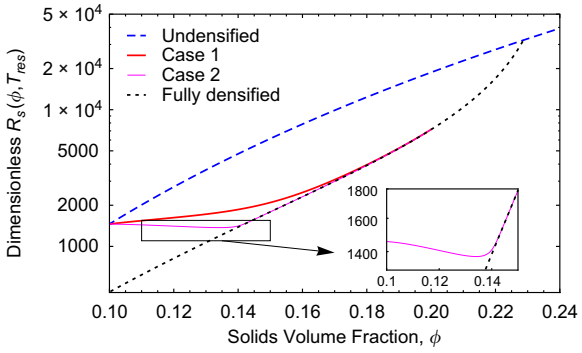

Fig. 3. The determination of the dimensionless densified hindered settling function, $R_s(\phi, T_{res})$, with a small dimensionless underflow solids flux, $Q = 7.25 \times 10^{-5}$—(Case 1—slow densification ($\alpha = 2.125 \times 10^{-6}$) and Case 2—rapid densification ($\alpha = 2.125 \times 10^{-5}$).

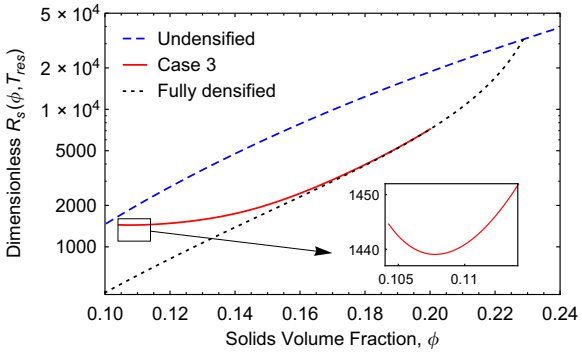

Fig. 4. The determination of the dimensionless densified hindered settling function, $R_s(\phi, T_{res})$, with a comparatively 'large' dimensionless underflow solids flux ($Q = 1.21 \times 10^{-4}$) and a small dimensionless densification rate parameter, α – Case 3 – slow densification ($\alpha = 2.125 \times 10^{-6}$).

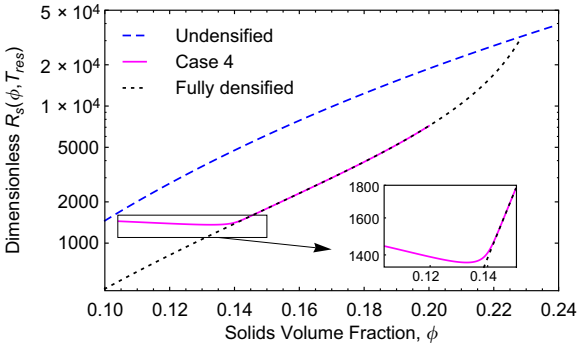

Fig. 5. The determination of the dimensionless densified hindered settling function, $R_s(\phi, T_{res})$, with a comparatively 'large' dimensionless underflow solids flux ($Q = 1.21 \times 10^{-4}$) and a comparatively 'large' dimensionless densification rate parameter, α – Case 4 – rapid densification ($\alpha = 2.125 \times 10^{-5}$).

Zhang et al. (2013) made a good approximation of $R_s(\phi, T_{res})$ which can be used to explain the behaviour of $R_s(\phi, T_{res})$ vs ϕ in a densified thickener:

$$R_s(\phi, T_{res}) \approx D_{agg} \frac{(1-\phi)^2 R_{s0}(\phi_{agg,0}\phi/\phi_{agg})}{(1-\phi_{agg,0}\phi/\phi_{agg})^2} \tag{26}$$

where $R_{s0}(\phi_{agg,0}\phi/\phi_{agg})$ represents the undensified hindered settling function in dimensionless form.

If ϕ/ϕ_{agg} increases significantly moving down from the top of the bed, then $R_s(\phi, T_{res})$ will increase (as the given $R_{s0}(\phi_{agg,0}\phi/\phi_{agg})$ is a rapidly increasing function). If however ϕ/ϕ_{agg} is more or less constant moving down into the bed, then $R_s(\phi, T_{res})$ will decrease slightly, since the factor $D_{agg}(1-\phi)^2$ in Eq. (26) is a decreasing function. The behaviour of $R_s(\phi, T_{res})$ vs ϕ depends therefore on whether ϕ/ϕ_{agg} is an increasing or a nearly steady function. This in turn depends on the value of $((d\phi/dT_{res})-(\phi/\phi_{agg})(d\phi_{agg}/dT_{res}))/\phi_{agg}$. Due to $(\phi_g/\phi_{g,0}) = (\phi_{agg}/\phi_{agg,0}) = 1/D_{agg}^3$, the value of $((d\phi/dT_{res})-(\phi/\phi_{agg})(d\phi_{agg}/dT_{res}))/\phi_{agg}$ is equivalent to the value of $((d\phi/dT_{res})-(\phi/\phi_g)(d\phi_g/dT_{res}))/\phi_{agg}$. Near the top of the bed where $\phi \approx \phi_g$, we must examine $((d\phi/dT_{res})-(d\phi_g/dT_{res}))/\phi_{agg}$.

If the dimensionless underflow solids flux, Q is not too large and the dimensionless densification rate parameter, α is small (e.g. Case 1), then $d\phi/dT_{res}$ tends to exceed $d\phi_g/dT_{res}$, meaning that (according to Eq. (26)), $R_s(\phi, T_{res})$ will increase. If however the dimensionless densification rate parameter, α is increased (e.g. Case 2), then it is clear from Eq. (24) that $d\phi/dT_{res} \approx -(\partial p_{y,1}(\phi, T_{res})/\partial T_{res})/(\partial p_{y,1}(\phi, T_{res})/\partial \phi)$. This implies that ϕ increases moving into the bed in such a way as to keep $p_{y,1}(\phi, T_{res})$ nearly fixed. However, $p_{y,1}(\phi, T_{res})$ at the top of the bed vanishes. Hence fixing $p_{y,1}(\phi, T_{res})$ at or near zero then implies $\phi \approx \phi_g$ moving down into the bed. Large α indicates a rapid change in ϕ_g and hence a rapid change in ϕ. Moreover, Eq. (26) reduces to a new expression:

$$R_s(\phi, T_{res}) \approx D_{agg} \frac{(1-\phi_g)^2 R_{s0}(\phi_{g,0})}{(1-\phi_{g,0})^2} \tag{27}$$

where $\phi_{g,0}$ is the undensified gel point.

The evolution of the factor $D_{agg}(1-\phi_g)^2$ explains the slight decrease in $R_s(\phi, T_{res})$ at early times. After a particular time, T_{res} (of order α^{-1}), ϕ_{agg} saturates at a final value $\phi_{agg,\infty}$. Beyond this point, any further increase in ϕ and hence in $R_{s0}(\phi_{agg,0}\phi/\phi_{agg})$ implies that $R_s(\phi, T_{res})$ will increase again (according to Eq. (26)).

The above arguments explain how $R_s(\phi, T_{res})$ changes due to an increase in the dimensionless densification rate parameter, α. Now we turn to how $R_s(\phi, T_{res})$ changes in response to the increasing dimensionless underflow solids flux Q, which approaching the dimensionless maximum permitted underflow solids flux, Q_{max} tends to lead to very tall beds. For a sufficiently tall bed and a small α (e.g. Case 3), $d\phi/dT_{res}$ must decrease—making it again comparable with $d\phi_g/dT_{res}$ at early times. Thus, this can lead (as before) to a very slight decrease in $R_s(\phi, T_{res})$ at early times. If the dimensionless underflow solids flux Q is large and the dimensionless densification rate parameter α is also large (e.g. Case 4), the gel point, ϕ_g increases rapidly and then the local solids volume fraction, ϕ also increases rapidly. This is conceptually similar to Case 2 which has already been discussed. Thus, a slight initial decrease in $R_s(\phi, T_{res})$ is also observed in Case 4.

4.4. Thickener performance predictions

Predictions of thickener performance in the presence of densification are very important for improving the thickener design. As mentioned previously, the main variables of interest include the bed height, h_b and the total solids residence time, t_{res}^{total} (given here for convenience in dimensional form). These data determined in each case are presented in Table 3. Figs. 6 and 7 meanwhile show the solids volume fraction vs height in the thickeners. For a given underflow solids flux, the bed height required to achieve the desired underflow solids volume fraction decreases with the increase of the dimensionless densification rate parameter rate, α, due to the more rapid evolution of the sludge rheological properties. As shown in Figs. 6 and 7, for a given dimensionless densification rate, α and a given underflow solids volume fraction, ϕ_u, the bed height determined by operating a smaller underflow solids flux is smaller than that determined by using a larger underflow solids flux.

Table 3
The total solids residence time and the corresponding bed height determined in each case. Note that in Cases 3 and 4 (which require pre-shearing) the total solids residence time includes the solids residence time required for pre-shearing of aggregates and the solids residence time required for consolidating the bed, although the former time is typically just a very small fraction of the latter.

	Case 1	Case 2	Fully densified
t_{res}^{total}/hours	2.092	1.944	1.931
αT_{res}^{total}	7.531	69.984	N/A
h_b/m	0.286	0.253	0.249

	Case 3	Case 4	Fully densified
t_{res}^{total}/hours	1.832	1.520	1.489
αT_{res}^{total}	6.595	54.720	N/A
$t_{res}^{pre-shear}/t_{res}^{total}$	0.0226	2.725×10^{-3}	N/A
h_b/m	0.418	0.332	0.323

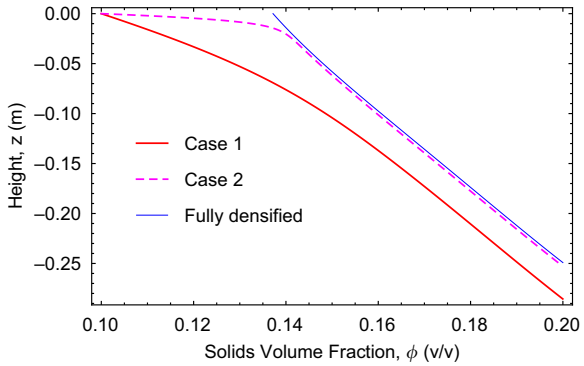

Fig. 6. The profile of the height in the bed vs the solids volume fraction – for a small underflow solids flux (Case 1—small densification rate parameter and Case 2—comparatively 'large' densification rate parameter). Data are compared with the fully densified case. No comparison data are shown for the undensified case, since the imposed underflow solids flux chosen in Cases 1 and 2 is larger than the undensified maximum permitted underflow solids flux (see Table 1).

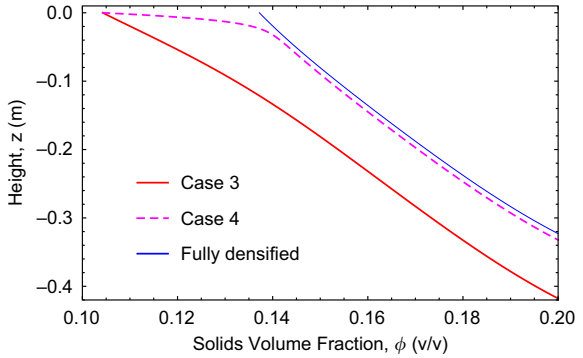

Fig. 7. The profile of the height in the bed vs the solids volume fraction—for a comparatively 'large' underflow solids flux (Case 3—small densification rate parameter and Case 4—comparatively 'large' densification rate parameter). Fully densified data are also shown for comparison. As the imposed underflow solids flux is larger than the undensified maximum permitted underflow solids flux, no comparison has been made with undensified data.

For Case 2, Fig. 6 shows that a nearly flat line profile can be observed near the top of the bed and then a sharp change in the gradient can be obtained in the interior of the bed. A similar curve shape can be observed for Case 4 in Fig. 7. For a comparatively 'large' dimensionless densification rate parameter, α, the ratio of the solids volume fraction, ϕ, to the densified gel point, ϕ_g remains roughly unity as long as the gel point, ϕ_g is still changing significantly. Rapid changes in ϕ_g then imply rapid changes in ϕ (in order to avoid any tendency of the system to "ungel"), hence the flat line profile (i.e. ϕ changes significantly over a small distance) near the top of the bed can be observed in the cases of a large dimensionless densification rate parameter, α (e.g. Cases 2 and 4). Further down in the interior of the bed, the densified gel point, ϕ_g reaches the fully densified gel point, $\phi_{g,\infty}$ and thereafter remains constant. Whilst ϕ still continues to increase in the interior of the bed, it is no longer tied to rapid increases in ϕ_g, hence the sharp changes in the gradient can be seen in Figs. 6 and 7.

Table 3 shows the total solids residence time required to obtain the desired underflow solids volume fraction. Although taller bed heights are required to achieve the desired underflow solids volume fraction in Case 3 and 4, the total solids residence times calculated in those two cases are shorter compared to those determined in Case 1 and 2, respectively, due to the presence of pre-shearing of aggregates permitting a large underflow solids flux given in Case 3 and 4. Thus, the rate of dewatering is also improved via pre-shearing of aggregates in a densified thickener.

5. Conclusions

Thickening/dewatering with simultaneous in situ densification is far more challenging to model than an undensified thickener and/or a system where densification is effectively completed before significant dewatering starts. Despite these modelling challenges useful insights into systems with simultaneous dewatering and

densification can be obtained. When a comparatively small underflow solids flux (which, by a simple rule of thumb formula valid in cases of practical interest, can be up to the free settling solids flux, corresponding to the initial undensified gel point) is operated in a densified thickener, the solids volume fraction at the top of the bed is the initial undensified gel point. A larger underflow solids flux however requires pre-shearing of aggregates at early times in a densified thickener. The solids volume fraction at the top of the bed is then a densified gel point (again readily obtained by a simple rule of thumb formula in cases of practical interest) which is larger than the initial undensified gel point owing to this pre-shearing. That densified gel point at the top of the bed depends on the imposed underflow solids flux and the imposed underflow solids volume fraction, but is independent of the densification rate parameter that determines how rapidly aggregates densify. Nevertheless the densification rate parameter and the evolution of the solids volume fraction within the aggregates substantially affect the sludge rheological properties and thickener performance in a densified thickener. A large densification rate parameter can decrease the densified hindered settling function and reduce the densified compressive yield stress for a given underflow solids flux and a given underflow solids volume fraction. Thickening operations can then achieve higher underflow solids fluxes and/or shorter bed heights. The sludge rheological properties and the associated thickener performance are further affected by pre-shearing of aggregates. Moreover, densification in situ and/or pre-shearing of aggregates can increase the dewatering performance by decreasing the total solids residence time.

Nomenclature

A	aggregate densification rate parameter (s^{-1})
a_0	curve fitting parameter for the undensified compressive yield stress function (Pa)
a_1	curve fitting parameter for the densified compressive yield stress function (Pa)
D_{agg}	aggregate diameter ratio
$D_{agg,\infty}$	final steady state aggregate diameter ratio
g	gravitational acceleration ($m\ s^{-2}$)
h_b	bed height (m)
m	curve fitting parameter for the undensified and densified compressive yield stress functions
n_0	curve fitting parameter for the undensified compressive yield stress function
n_1	curve fitting parameter for the densified compressive yield stress function
$P_{y,0}$	undensified compressive yield stress (Pa)
$P_{y,1}$	densified compressive yield stress (Pa)
$p_{y,1}$	dimensionless densified compressive yield stress
q	imposed underflow solids flux ($m\ s^{-1}$)
q_{fs}	free settling solids flux ($m\ s^{-1}$)
q_{mu}	maximum underflow solids flux assuming the initial undensified gel point at the top of the bed ($m\ s^{-1}$)
q_{max}	maximum permitted underflow solids flux in densified thickeners ($m\ s^{-1}$)
Q	dimensionless imposed underflow solids flux
Q_{mu}	dimensionless maximum underflow solids flux assuming the initial undensified gel point at the top of the bed
Q_{max}	dimensionless maximum permitted underflow solids flux in densified thickeners
r_n, r_g	curve fitting parameters for the undensified hindered settling function
r_{agg}	aggregate hindered settling factor
R_0	undensified hindered settling function ($Pa\ s\ m^{-2}$)
R	densified hindered settling function ($Pa\ s\ m^{-2}$)
R_∞	fully densified hindered settling function ($Pa\ s\ m^{-2}$)
$R_{Stokes,0}$	initial undensified hindered settling function of an isolated aggregate which has the same density as that of the solids ($Pa\ s\ m^{-2}$)
R_{s0}	dimensionless undensified hindered settling function
R_s	dimensionless densified hindered settling function
t_{res}	solids residence time (s)
$t_{res}^{pre-shear}$	solids residence time required for pre-shearing of aggregates (s)
t_{res}^{total}	total solids residence time (s)
T_{res}	dimensionless solids residence time
$T_{res}^{pre-shear}$	dimensionless solids residence time required for pre-shearing of aggregates
T_{res}^{total}	dimensionless total solids residence time
z	height in the bed (m)
Z	dimensionless height in the bed
α	dimensionless aggregate densification rate parameter
$\Delta\rho$	density difference between the solids and liquid ($kg\ m^{-3}$)
ϕ	local solids volume fraction
$\phi_{agg,0}$	initial solids volume fraction within the aggregates
ϕ_{agg}	solids volume fraction within the aggregates
$\phi_{agg,\infty}$	solids volume fraction within fully densified aggregates
$\phi_{g,0}$	initial undensified gel point
ϕ_g	densified gel point
$\phi_{g,\infty}$	fully densified gel point
ϕ_u	underflow solids volume fraction
ϕ_{cp}	close packing solids volume fraction at which the compressive yield stress becomes infinite

Acknowledgements

This work was carried out whilst Paul Grassia was a Royal Academy of Engineering/Leverhulme Trust Senior Research Fellow and funding from the fellowship is gratefully acknowledged.

References

Boger, D.V., 2009. Rheology and the resource industries. Chem. Eng. Sci. 64, 4525–4536.
Bürger, R., Evje, S., Karlsen, K.H., Lie, K.A., 2000. Numerical methods for the simulation of the settling of flocculated suspensions. Chem. Eng. J. 80, 91–104.
Bürger, R., Karlsen, K.H., 2001. On some upwind difference schemes for the phenomenological sedimentation-consolidation model. J. Eng. Math. 41, 145–166.
Buscall, R., White, L.R., 1987. The consolidation of concentrated suspensions: part 1. The theory of sedimentation. J. Chem. Soc. Faraday Trans. 83, 873–891.
Channell, G.M., Miller, K.T., Zukoski, C.F., 2000. Effects of microstructure on the compressive yield stress. AIChE J. 46, 72–78.
Gladman, B.R., Rudman, M., Scales, P.J., 2010. The effect of shear on gravity thickening: pilot scale modelling. Chem. Eng. Sci. 65, 4293–4301.
Landman, K.A., White, L.R., Buscall, R., 1988. The continuous-flow gravity thickener: steady state behavior. AIChE J. 34, 239–252.
Martin, A.D., 2004. Optimisation of clarifier-thickeners processing stable suspensions for turn-up/turn-down. Water Res. 38, 1568–1578.
Usher, S.P., Scales, P.J., 2005. Steady state thickener modelling from the compressive yield stress and hindered settling function. Chem. Eng. J. 111, 253–261.
Usher, S.P., Spehar, R., Scales, P.J., 2009. Theoretical analysis of aggregate densification: impact on thickener performance. Chem. Eng. J. 151, 202–208.
Usher, S.P., Studer, L.J., Wall, R.C., Scales, P.J., 2013. Characterisation of dewaterability from equilibrium and transient centrifugation test data. Chem. Eng. Sci. 93, 277–291.
van Deventer, B.B.G., Usher, S.P., Kumar, A., Rudman, M., Scales, P.J., 2011. Aggregate densification and batch settling. Chem. Eng. J. 171, 141–151.
Zhang, Y., Martin, A., Grassia, P., 2013. Prediction of thickener performance with aggregate densification. Chem. Eng. Sci. Submitted for publication.

Chapter 5

Effects of underflow solids volume fractions on thickener performance subject to aggregate densification

Summary

This chapter considers the operation of a thickener processing a solid-liquid sludge suspension, where loose solid aggregates contained within the suspension are subjected to shear-induced densification. Specifically this chapter considers the effect of varying the underflow solids volume fraction in such a system upon the prediction of thickener performance. The effects of different underflow solids volume fractions upon the determination of the underflow solids flux permitted in a thickener has also been explored. Moreover, the effects of different proposed underflow solids volume fractions upon the evolution of sludge rheological properties have been addressed. Pre-shearing of aggregates proposed in Zhang et al. (2013a) influences the prediction of thickener performance and the evolution of sludge rheological properties. In this chapter, whether or not pre-shearing of aggregates needs to occur when giving different proposed underflow solids volume fractions has been investigated. Pre-shearing of aggregates is not required if a very large underflow solids volume fraction is given, the thickener then being operated at a comparatively small underflow solids flux. Different values of the so called aggregate densification rate parameters which are believed to have significant effects on the evolu-

tion of sludge rheological properties and on the prediction of thickener performance have been considered in this chapter. The extent in the improvement of thickener performance due to aggregate densification has been explored. Thickener performance is significantly enhanced when the underflow solids volume fraction is comparatively small. With the increase in the underflow solids volume fraction, there is less improvement in thickener performance.

5.1 Introduction

One advantage of densified thickeners where aggregates/flocs within sludge suspensions become smaller in diameter throughout thickeners due to the presence of rakes is to improve the performance of thickeners (e.g. shorter heights required for the consolidation zone and larger underflow solids fluxes given in thickeners) (Usher et al., 2009; Gladman et al., 2010; Zhang et al., 2013a,b). An important finding is that the underflow solids flux operated in a steady state thickener can be increased for a given underflow solids volume fraction after aggregate densification (Usher et al., 2009; Gladman et al., 2010; Zhang et al., 2013a,b). Knowing different underflow solids flux operating ranges which were discussed in the literature (Usher and Scales, 2005; Zhang et al., 2013a,b) is useful for the design and control of a thickener with time-dependent densification, since the underflow solids flux can influence the height and the solids residence time required for the consolidation zone. In a fully densified thickener, the consolidation zone can be divided into 2 sub-zones depending upon the ratio of the underflow solids volume fraction, ϕ_u to the solids volume fraction within the final steady state aggregates, $\phi_{agg,\infty}$: $Zone^{upper}$ where the densified sludge rheological properties are applied and which is determined from the top of the consolidation zone to some height predicted at $\phi = \phi_{agg,\infty}$, and $Zone^{lower}$ where the initially undensified sludge rheological properties are applied and which is underneath $Zone^{upper}$ (Zhang et al., 2013b). Densification still occurs in $Zone^{lower}$ but the sludge rheological properties determined in $Zone^{lower}$ are exactly the same as the undensified ones, due to the overlapping and interpenetration of aggregates (Zhang et al., 2013b). The presence of $Zone^{lower}$ affects significantly the determination of the maximum permitted underflow solids flux and may have effects on the prediction of thickener

performance (Zhang et al., 2013b). We are interested in exploring how the presence of $Zone^{lower}$ affects the predictions of the maximum permitted underflow solids flux and thickener performance in a thickener subject to time-dependent densification.

When considering time-dependent aggregate densification, one important operating parameter is the aggregate densification rate parameter, A which governs how the aggregate diameters evolve in a thickener, and affects the evolutions of sludge rheological properties and hence the prediction of thickener performance (Gladman et al., 2010; van Deventer et al., 2011; Zhang et al., 2013a; Grassia et al., 2014). The works of Zhang et al. (2013a,b) show that the largest extent in the improvement of thickener performance is achieved at a fully densified state where aggregates/flocs are densified to the minimum diameter. If time-dependent densification occurs, the faster the densification rate parameter, A that is given, the more significant improvements of the performance of thickeners that have been achieved for a given underflow solids volume fraction and a given underflow solids flux (Zhang et al., 2013a).

The underflow solids volume fraction, ϕ_u determined at the bottom of a thickener is expected to be a comparatively large value (which is much larger than the initial feed solids volume fraction) and the underflow solids flux which is uniform in a steady state thickener is also expected to be reasonably large (so as to cope with the incoming feed flux) in practice (Diehl, 2006, 2012). Previous works (Usher and Scales, 2005; Usher et al., 2009; Zhang et al., 2013a,b), albeit ignoring aggregate densification, show that the limits imposed on the underflow solids flux are influenced significantly by the proposed underflow solids volume fraction. When time-dependent densification occurs however, we still need to explore how the limits imposed on the underflow solids flux are affected by different proposed underflow solids volume fractions.

This chapter includes six sections in total which are introduced as follows. Section 5.2 reviews the mathematical model consistent with time-dependent densification. The sludge rheological properties are also introduced in Section 5.2. Section 5.3 describes the effects of different proposed underflow solids volume fractions upon the determinations of the limits of the underflow solids flux. Different cases with different operating parameters are considered in Section 5.4. The main outputs including the analysis of maximum permit-

ted underflow solids fluxes, the evolutions of densified sludge rheological properties, the bed heights, and the total solids residence times required for the consolidation zone are illustrated in Section 5.5. Section 5.6 gives conclusions.

5.2 Mathematical model for thickeners subject to time-dependent densification

This section reviews the suspension dewatering theory consistent with time-dependent densification (Buscall and White, 1987; Usher et al., 2009; van Deventer et al., 2011; Zhang et al., 2013a,b; Grassia et al., 2014). The functional forms of sludge rheological properties are also given in this section. When the functional forms of sludge rheological properties are given, an ordinary differential equation describing densification and consolidation which occur in parallel in a thickener can be written as (Zhang et al., 2013a)

$$\frac{\mathrm{d}\phi}{\mathrm{d}t_{res}} = \frac{\Delta\rho g q_u - \dfrac{R(\phi, t_{res})}{(1-\phi)^2} q_u^2 \left(\dfrac{1}{\phi} - \dfrac{1}{\phi_u}\right) - \dfrac{\partial P_y(\phi, t_{res})}{\partial t_{res}}}{\dfrac{\partial P_y(\phi, t_{res})}{\partial \phi}} \tag{5.2.1}$$

where $R(\phi, t_{res})$ is the densified hindered settling function (a measure of the viscous resistance to settling), $P_y(\phi, t_{res})$ is the densified compressive yield stress (a measure of the weight bearing strength of the suspension), t_{res} is the solids residence time, $\Delta\rho$ is the density difference between the solids and liquid which is chosen as $2200\,\mathrm{kg\,m^{-3}}$ (Usher et al., 2009), g is the gravitational acceleration which is chosen as $9.8\,\mathrm{m\,s^{-2}}$, q_u is a constant and uniform underflow solids flux, due to the operation of steady state thickening. Note that in this equation, our sign convention is such that the underflow solids flux is positive whilst the z coordinate is measured upward. The hindered settling zone is neglected in this chapter. In other words, the solids are assumed to enter the consolidation zone immediately and instantaneously. We define the z coordinate so that it is zero at the top of the bed, and the solids residence time increasing from $t_{res} = 0$ at the top of the bed to the

maximum value required to achieve the desired underflow solids volume fraction. Due to $\partial P_y(\phi, t_{res})/\partial\phi$ and $\partial P_y(\phi, t_{res})/\partial t_{res}$ being known, Eq. (5.2.1) can be solved easily via classical numerical methods (e.g. Runge–Kutta methods, midpoint rules, and higher–order Taylor methods) (Press et al., 1992). Here, the midpoint rule which is implemented in Mathematica is utilised.

The determination of the solids velocity in a steady state thickener with time-dependent aggregate densification is written as (Usher et al., 2009; Zhang et al., 2013a)

$$\frac{\mathrm{d}z}{\mathrm{d}t_{res}} = -\frac{q_u}{\phi} \tag{5.2.2}$$

where the minus sign on the right hand side of Eq. (5.2.2) refers to a decreasing height in the bed and an increase of the solids residence time.

If densification occurs, the aggregate diameter is decreasing with the solids residence time (van Deventer et al., 2011; van Deventer, 2012; Zhang et al., 2013a,b). The rate equation for the decrease of aggregate diameter is given by van Deventer et al. (2011):

$$\frac{\mathrm{d}D_{agg}}{\mathrm{d}t_{res}} = -A(D_{agg} - D_{agg,\infty}) \tag{5.2.3}$$

and

$$D_{agg} = (1 - D_{agg,\infty})e^{-At_{res}} + D_{agg,\infty} \tag{5.2.4}$$

where D_{agg} is the dimensionless aggregate diameter ratio, A is the densification rate parameter, $D_{agg,\infty}$ is the minimum dimensionless aggregate diameter ratio that is taken to be 0.9 in this chapter (Usher et al., 2009; Zhang et al., 2013a,b), and t_{res} is the solids residence time.

As shown in Eq. (5.2.4), the rate of the evolution of the aggregate diameter ratio depends upon the densification rate parameter, A which is a vital parameter in a time-dependent densified system. Operating a large densification rate parameter leads to a significant improvement of thickener performance (e.g. a significant decrease in the bed

height) for a specified underflow solids volume fraction, unless that volume fraction is exceedingly large (Zhang et al., 2013a). Hence, two different typical values of A which are used in previous studies ($A = 0.001\,\mathrm{s}^{-1}$ and $A = 0.01\,\mathrm{s}^{-1}$, respectively) are given in this chapter (van Deventer et al., 2011; Zhang et al., 2013a).

Sludge rheological properties that are key parameters in the fundamental dewatering theory developed by Buscall and White (1987) and in the densification theory developed by Usher et al. (2009) are very important for the design of thickeners and the prediction of thickener performance. Knowing the functional forms of sludge rheological properties can help engineers predict thickener performance as densification occurs in a thickener. A general strongly gelled undensified compressive yield stress functional form for which the derivative evaluated at $\phi = \phi_g$ is some finite value is written as (Zhang et al., 2013a)

$$P_{y,0}(\phi) = \frac{a_0(\phi - \phi_{g,0})}{(m + \phi - \phi_{g,0})(\phi_{cp} - \phi)^{n_0}} \tag{5.2.5}$$

where typical values might be $a_0 = 3.7914\,\mathrm{Pa}$, $n_0 = 10.8302$, m which is assumed to be independent of densification is chosen to be 0.0363 (Zhang et al., 2013a), $\phi_{g,0}$ is the undensified gel point which is chosen as 0.1 (Usher et al., 2009; Zhang et al., 2013a), and ϕ_{cp} which is also assumed to be independent of densification is chosen as 0.8 (Usher et al., 2009; Zhang et al., 2013a).

In addition, the strongly gelled densified compressive yield stress functional form is written as (Zhang et al., 2013a)

$$P_{y,1}(\phi, t_{res}) = \frac{a_1(\phi - \phi_g)}{(m + \phi - \phi_g)(\phi_{cp} - \phi)^{n_1}} \tag{5.2.6}$$

where a_1 and n_1 are fitting parameters, and ϕ_g is the densified gel point that is determined by $\phi_g = \phi_{g,0}/D_{agg}^3$.

The curve fitting parameters, n_1 and a_1 in the functional form of the densified compressive yield stress are determined by Zhang et al. (2013a):

$$n_1 = (\phi_{cp} - \phi_{agg}) \left(\frac{P'_{y,0}(\phi_{agg})}{P_{y,0}(\phi_{agg})} + \frac{1}{m + \phi_{agg} - \phi_g} - \frac{1}{\phi_{agg} - \phi_g} \right) \tag{5.2.7}$$

and

$$a_1 = \frac{P_{y,0}(\phi_{agg})(m + \phi_{agg} - \phi_g)(\phi_{cp} - \phi_{agg})^{n_1}}{\phi_{agg} - \phi_g}. \tag{5.2.8}$$

The hindered settling function, $R(\phi, t_{res})$ that governs the solids settling velocity and hence the solids flux is a key parameter when predicting the performance of thickeners with time-dependent densification. A general functional form of the undensified hindered settling function which only depends on the solids volume fraction is written as (Usher et al., 2009; Zhang et al., 2013a,b)

$$R_0(\phi) = \frac{R_{Stokes,0}}{\phi_{agg,0}} (\phi + r_g)^{r_n} r_g^{-r_n} \tag{5.2.9}$$

where $R_{Stokes,0}$ which is the initially undensified hindered settling function of an isolated aggregate is chosen as $260469\,\mathrm{Pa\,s\,m^{-2}}$ (Zhang et al., 2013a,b), $\phi_{agg,0}$ is the solids volume fraction within the initially undensified aggregates which is chosen as 0.1667 (Usher et al., 2009; Zhang et al., 2013a,b), r_g and r_n are constant fitting parameters which are chosen to be 0.05 and 5, respectively (Usher et al., 2009; Zhang et al., 2013a,b).

The densified hindered settling function that depends both on the solids volume fraction and the solids residence time is written as (Zhang et al., 2013a,b)

$$R(\phi, t_{res}) = \frac{(1-\phi)^2 R_0(\phi_{agg}) R_{Stokes,0} D_{agg}}{\phi_{agg,0} R_0(\phi_{agg})(1 - \phi/\phi_{agg})^2 / r_{agg}(\phi/\phi_{agg}) + (R_{Stokes,0} D_{agg} \phi/\phi_{agg})(1 - \phi_{agg})^2} \tag{5.2.10}$$

where $r_{agg}(\phi/\phi_{agg})$ is the aggregate hindered settling factor determined by (Usher et al., 2009; van Deventer et al., 2011; Zhang et al., 2013a,b)

$$r_{agg}(\phi/\phi_{agg}) = \frac{\phi_{agg,0}\left(1-\frac{\phi}{\phi_{agg}}\right)^2 R_0(\phi_{agg,0}) R_0\left(\phi_{agg,0}\frac{\phi}{\phi_{agg}}\right)}{R_{Stokes,0}\left(R_0(\phi_{agg,0})\left(1-\phi_{agg,0}\frac{\phi}{\phi_{agg}}\right)^2 - \frac{\phi}{\phi_{agg}}(1-\phi_{agg,0})^2 R_0\left(\phi_{agg,0}\frac{\phi}{\phi_{agg}}\right)\right)}. \tag{5.2.11}$$

5.3 Analysis of maximum underflow solids fluxes permitted in a thickener

In this section, the maximum permitted underflow solids flux is analysed for a wide range of the underflow solids volume fraction. The works of Usher et al. (2009) and Zhang et al. (2013b) explored the criterion for the determination of the maximum permitted underflow solids flux (assuming an arbitrarily tall thickener) in a fully densified thickener. When the proposed underflow solids volume fraction, ϕ_u is larger than the solids volume fraction within the final steady state aggregates, $\phi_{agg,\infty}$, the maximum permitted underflow solids flux is equal to the *minimum* free settling solids flux (minimised over the solids volume fraction) determined either using the fully densified sludge rheological properties or using the initially undensified sludge rheological properties, depending upon the proposed underflow solids volume fraction, ϕ_u and its relation to $\phi_{agg,\infty}$ (Zhang et al., 2013b). This criterion can also be applied in a time-dependent densified system. Before analysing the maximum permitted underflow solids fluxes operated in a thickener subject to time-dependent aggregate densification, it is useful to choose a velocity scale ($R_{Stokes,0}/(\Delta\rho g)$) making the underflow solids flux be in dimensionless form. Thus, the dimensionless underflow solids flux is defined by (Zhang et al., 2013a,b)

$$Q_u = \frac{R_{Stokes,0} q_u}{\Delta\rho g}. \tag{5.3.1}$$

The determinations of the limits of the underflow solids flux depend on the proposed

underflow solids volume fraction, ϕ_u. Here, the underflow solids volume fraction, ϕ_u is assumed to be larger than the initially undensified gel point, $\phi_{g,0}$ but smaller than the close packing solids volume fraction, ϕ_{cp}. Three solids volume fraction ranges are distinguished: a small solids volume fraction range which is between the initially undensified gel point, $\phi_{g,0}$ and the fully densified gel point, $\phi_{g,\infty}$, an intermediate solids volume fraction range which is between $\phi_{g,\infty}$ and the solids volume fraction within the final steady state aggregates, $\phi_{agg,\infty}$, and a large solids volume fraction range which is between $\phi_{agg,\infty}$ and ϕ_{cp}.

In the case where a large underflow solids volume fraction, ϕ_u (much larger than $\phi_{agg,\infty}$) is given, Eq. (5.3.2) holds for the determination of the maximum permitted underflow solids flux, Q_{max} (Zhang et al., 2013b)

$$Q_{max} = \min_{\phi_{agg,\infty} \leq \phi \leq \phi_u} \frac{\phi(1-\phi)^2}{R_{s,0}(\phi)\left(1 - \dfrac{\phi}{\phi_u}\right)} \tag{5.3.2}$$

where $\phi_{agg,\infty}$ is the solids volume fraction within the final steady state aggregates which is chosen as 0.2286 (Usher et al., 2009; Zhang et al., 2013a,b), and $R_{s,0}(\phi)$ is the dimensionless undensified hindered settling function which is itself defined by $R_{s,0}(\phi) = R_0(\phi)/R_{Stokes,0}$.

On the other hand, for an underflow solids volume fraction that is just slightly larger than $\phi_{agg,\infty}$, the maximum permitted underflow solids flux[1] is written as (Zhang et al., 2013a,b)

[1]The fact that we are restricting the search for a minimum to the values in excess of a gel point is indicative of our neglect of the hindered settling zone. One could extend the search all the way down to a feed solids volume fraction, although this seldom has any bearing on the minimum in Eq. (5.3.3), except for ϕ_u values exceedingly close to the gel point. Throughout this chapter we do not specify a feed solids volume fraction, as this has no bearing on the bed. Indeed regardless of the feed, the solids volume fraction determined at the top of the bed is the gel point, and this is varied (between $\phi_{g,0}$ and $\phi_{g,\infty}$) by pre-shearing the suspension, rather than by varying the feed solids volume fraction.

$$Q_{max} = \min_{\phi_{g,\infty} \leq \phi \leq \phi_{agg,\infty}} \frac{\phi(1-\phi)^2}{R_{s,\infty}(\phi)\left(1 - \dfrac{\phi}{\phi_u}\right)} \tag{5.3.3}$$

where $\phi_{g,\infty}$ is the fully densified gel point determined at the final steady state aggregates ($\phi_{g,\infty} = 0.1372$ (Usher et al., 2009; Zhang et al., 2013b)) and $R_{s,\infty}(\phi)$ represents the dimensionless fully densified hindered settling function defined by $R_{s,\infty}(\phi) = R_{\infty}(\phi)/R_{Stokes,0}$.

In the case for $\phi_u < \phi_{agg,\infty}$ but $\phi_u > \phi_{g,\infty}$, the maximum permitted underflow solids flux, Q_{max} can be determined using Eq. (5.3.4) (Zhang et al., 2013a,b)

$$Q_{max} = \min_{\phi_{g,\infty} \leq \phi \leq \phi_u} \frac{\phi(1-\phi)^2}{R_{s,\infty}(\phi)\left(1 - \dfrac{\phi}{\phi_u}\right)}. \tag{5.3.4}$$

In the case for $\phi_u > \phi_{g,0}$ but $\phi_u < \phi_{g,\infty}$, it turns out that there is no upper limit to the maximum permitted underflow solids flux. When the proposed underflow solids volume fraction, ϕ_u lies between $\phi_{g,0}$ and $\phi_{g,\infty}$, the system (if it is to gel) can only densify from the initial aggregate diameter ($D_{agg} = D_{agg,0} = 1$) to some aggregate diameter which must be larger than the minimum aggregate diameter ($D_{agg} > D_{agg,\infty}$). In other words, the densifying system never becomes simultaneously fully densified and gelled when a small underflow solids volume fraction is given. Under this circumstance, the lower and upper limits for the underflow solids flux are nil and infinity, respectively. Thus, for a suitably chosen ϕ_u, and provided one is able to pre-shear the system to prevent gelation, the underflow solids flux can be chosen as an arbitrarily large value[2].

For the case of $\phi_{g,\infty} < \phi_u < \phi_{agg,\infty}$, the system can be densified to the fully densified state, even before reaching the bed. Thus, the maximum permitted underflow solids

[2]Note that to achieve this arbitrarily large underflow solids flux, it may also be necessary to choose a feed very close to the gel point, but this aspect is not explicitly studied here, since we focus on the consolidated bed, the structure of which can be determined without prior knowledge of the feed solids volume fraction.

flux is determined using Eq. (5.3.4) – this is the case which has been reported by Zhang et al. (2013a). For the case of $\phi_{agg,\infty} < \phi_u < \phi_{cp}$, both $Zone^{upper}$ and $Zone^{lower}$ are present. Zhang et al. (2013b) analysed the maximum permitted underflow solids flux that was determined either in the interior of $Zone^{upper}$ using Eq. (5.3.3) or in the interior of $Zone^{lower}$ using Eq. (5.3.2), depending on the proposed underflow solids volume fraction, ϕ_u. In this chapter, it turns out that for $\phi_u < 0.2905$ but $\phi_u > \phi_{agg,\infty}$ ($\phi_{agg,\infty} = 0.2286$), the maximum permitted underflow solids flux is determined in the interior of $Zone^{upper}$. If $\phi_u > 0.2905$, it is determined in the interior of $Zone^{lower}$.

Another important limit for the underflow solids flux which is defined by Zhang et al. (2013a) is the maximum underflow solids flux requiring an undensified gel point at the top of the bed, q_{mu}. As discussed in Zhang et al. (2013a), the criterion for imposition of pre-shearing of aggregates is whether the proposed underflow solids flux is larger or smaller than q_{mu}. The determination of Q_{mu} (a dimensionless form of q_{mu}) is given by (Zhang et al., 2013a)

$$Q_{mu} = \frac{\phi_{g,0}(1-\phi_{g,0})^2}{R_{s,0}(\phi_{g,0})\left(1-\dfrac{\phi_{g,0}}{\phi_u}\right)}. \tag{5.3.5}$$

Note that Eq. (5.3.5) uses the initially undensified sludge rheological properties, since aggregates are assumed to enter the consolidating bed immediately and hence there is no densification at the top of the bed (Zhang et al., 2013a). Eq. (5.3.5) also uses the concept that as a rule of thumb in time-dependent densification, increases in the hindered settling function as the local solids volume fraction increases are often offset by decreases in the hindered settling function as the solids volume fraction within the aggregates increases, which is why the undensified gel point, $\phi_{g,0}$ at the top of the bed controls the underflow solids flux (Zhang et al., 2013a).

5.4 Case studies

Eight cases are illustrated in this section. Cases 1–4 consider a comparatively small underflow solids volume fraction, Cases 5–6 give an intermediate underflow solids volume fraction, and Cases 7–8 consider a comparatively large underflow solids volume fraction. Two densification rate parameters are given in this chapter ($A = 0.001\mathrm{s}^{-1}$ and $A = 0.01\mathrm{s}^{-1}$, respectively (van Deventer et al., 2011; Zhang et al., 2013a)). Different underflow solids flux ratios are also given in Cases 1–8. Recall that the minimum aggregate diameter ratio which is assumed to be fixed, $D_{agg,\infty} = 0.9$ here. The hindered settling zone is not explicitly modelled in this chapter. Thus, we only focus on the consolidation zone. Table 5.1 shows the operating details of those cases.

	ϕ_u	solids flux ratios	$A/\,\mathrm{s}^{-1}$	$D_{agg,\infty}$	$\phi_{g,0}$	$\phi_{g,\infty}$	$\phi_{agg,0}$	$\phi_{agg,\infty}$
Case 1	0.12	0.3	0.001	0.9	0.1	0.1372	0.1667	0.2286
Case 2	0.12	0.3	0.01	0.9	0.1	0.1372	0.1667	0.2286
Case 3	0.12	1.5	0.001	0.9	0.1	0.1372	0.1667	0.2286
Case 4	0.12	1.5	0.01	0.9	0.1	0.1372	0.1667	0.2286
Case 5	0.24	0.6	0.001	0.9	0.1	0.1372	0.1667	0.2286
Case 6	0.24	0.6	0.01	0.9	0.1	0.1372	0.1667	0.2286
Case 7	0.3	0.6	0.001	0.9	0.1	0.1372	0.1667	0.2286
Case 8	0.3	0.6	0.01	0.9	0.1	0.1372	0.1667	0.2286

Table 5.1: Operating details of Cases 1–8. Note that the underflow solids flux ratio given for Cases 1–4 is defined as the ratio between the proposed underflow solids flux, Q_u and the maximum permitted underflow solids flux, Q_{mu} imposing an *undensified* gel point at the top of the bed. For Cases 5–8, the underflow solids flux ratio is defined as the ratio between the proposed underflow solids flux, Q_u and the maximum permitted underflow solids flux, Q_{max} determined for the underflow solids volume fraction, ϕ_u that is specified. Eq. (5.3.5) is used to determine Q_{mu} for Cases 1–4 and Eqs. (5.3.2–5.3.3) are used to determine the maximum permitted underflow solids flux, Q_{max} for Cases 5–8. Specifically in Cases 5–6, Q_{max} turns out to correspond to $\phi = \phi_{agg,\infty}$ whereas for Cases 7–8, it corresponds to a ϕ value greater than $\phi_{agg,\infty}$.

5.5 Results and discussion

This section describes the analysis of whether pre-shearing of aggregates occurs and the simulation results including the maximum permitted underflow solids fluxes determined as different underflow solids volume fractions are given, the evolutions of sludge rheological properties, and the predictions of thickener performance. In this section, some

of the results (e.g. the maximum underflow solids flux and sludge rheological properties) are presented in dimensionless form (for computational convenience) but other results (e.g. bed heights and solids residence times) are presented in dimensional form to give a better idea of scale. The dimensional compressive yield stress, $P_y(\phi, t_{res})$ is converted to dimensionless $p_y(\phi, T_{res})$ by defining $p_y(\phi, T_{res}) = P_y(\phi, t_{res})/a_0$. Recall that $R_s(\phi, T_{res}) = R(\phi, t_{res})/R_{Stokes,0}$ and $Q_u = R_{Stokes,0}q_u/(\Delta\rho g)$.

5.5.1 Maximum underflow solids flux and pre-shearing of aggregates

Fig. 5.1 shows the relationships of Q_{mu} and Q_{max} with different underflow solids volume fractions, ϕ_u. As shown in Fig. 5.1, Q_{mu} is *smaller* than Q_{max} for $\phi_u < 0.2392$ but is *larger* than Q_{max} for $\phi_u > 0.2392$. This can be interpreted as follows. When the underflow solids volume fraction, ϕ_u is smaller than 0.2392, a small proposed underflow solids flux up to Q_{mu} can be delivered from the top of the bed to the bottom of a thickener without increasing the gel point at the top of the bed. If a larger underflow solids flux (which is larger than Q_{mu}) is operated however, in order to deliver the operated larger underflow solids flux throughout the consolidating bed, the solids volume fraction at the top of the bed (which generally is the gel point) must be altered (e.g. by pre-shearing the suspension prior to thickening). The algorithm for calculating the densified gel point at the top of the bed when a large underflow solids flux is given has been developed in Zhang et al. (2013a). In this chapter, the densified gel point determined at the top of the bed for a given large underflow solids flux in excess of Q_{mu} (e.g. Cases 3–4) turns out to be 0.10948 (instead of the undensified gel point of 0.1). Note that Zhang et al. (2013a) argued that this densified gel point determined at the top of the bed is independent of the aggregate densification rate parameter, A, but depends on the proposed underflow solids flux. On the other hand, for $\phi_u > 0.2392$, the curve of Q_{max} is underneath the curve of Q_{mu} implying that it is not normally necessary to pre-shear aggregates in order to deliver any proposed underflow solids flux which is already constrained to be smaller than the maximum permitted underflow solids flux (e.g. Cases 5–8).

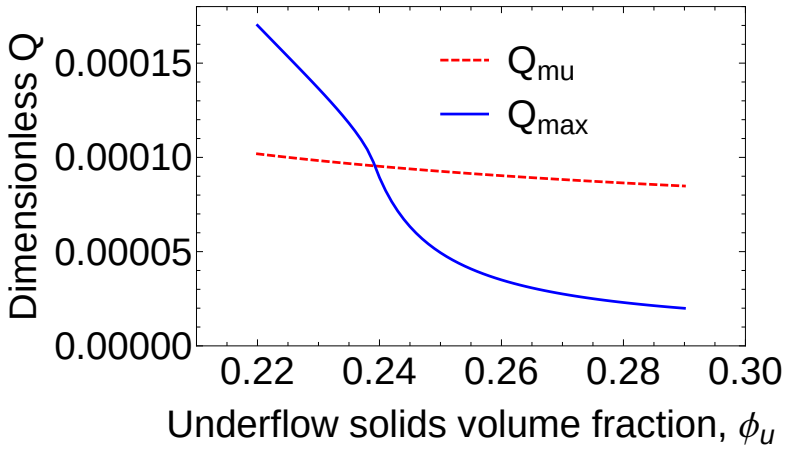

Figure 5.1: Relationships of the dimensionless maximum permitted underflow solids flux, Q_{max} and the dimensionless maximum permitted underflow solids flux, Q_{mu} required for altering the solids volume fraction at the top of the bed. Note that the intersection point is the critical underflow solids volume fraction which defines whether the system is necessary to pre-shear. Recall that the solids volume fraction within the fully densified aggregates, $\phi_{agg,\infty} = 0.2286$. Q_{max} and Q_{mu} are determined using Eq. (5.3.3) and Eq. (5.3.5), respectively.

5.5.2 Sludge rheological properties

In this section, the evolutions of sludge rheological properties in a time-dependent densified system for a wide range of proposed underflow solids volume fractions are discussed. The densification theory (Usher et al., 2009; van Deventer et al., 2011; Zhang et al., 2013a,b; Grassia et al., 2014) implies that sludge rheological properties evaluated for $\phi > \phi_{agg,\infty}$ turn out to be unchanged from the initially undensified ones. Thus, sludge rheological properties evaluated in $Zone^{lower}$ are still the initially undensified ones. The evolution of sludge rheological properties determined in $Zone^{upper}$ is therefore of particular interest in this section.

Figs. 5.2–5.4 present the evolutions of the dimensionless compressive yield stress, $p_y(\phi, T_{res})$ for each case. As shown in Figs. 5.2–5.4, for a constant local solids volume fraction, the dimensionless compressive yield stress, $p_y(\phi, T_{res})$ is decreased with an increase of the densification rate parameter, A, since the aggregate diameter decreases more rapidly as a larger densification rate parameter, A is given (corresponding to even numbered cases). Fig. 5.2 shows that the dimensionless compressive yield stress, $p_y(\phi, T_{res})$ is smaller for a given local solids volume fraction when pre-shearing of aggregates occurs,

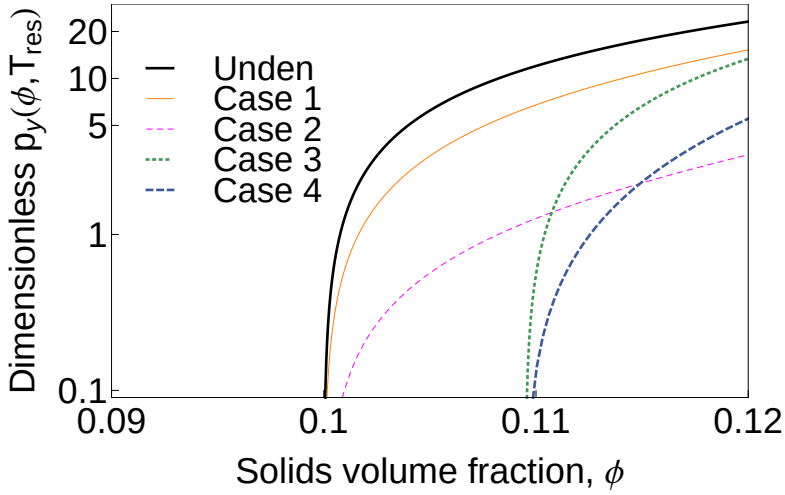

Figure 5.2: Evolutions of the dimensionless compressive yield stresses for Cases 1–4, all of which have $\phi_u = 0.12$. Note that the fully densified compressive yield stress is not relevant, due to the underflow solids volume fraction that is smaller than the fully densified gel point. The curves of Cases 1–2 start from the same undensified gel point at $\phi = \phi_{g,0}$ (pre-shearing of aggregates does not occur in Cases 1–2) and the curves of Cases 3–4 start from the same densified gel point at $\phi_g = 0.10948$ (pre-shearing of aggregates occurs in Cases 3–4).

due to smaller aggregate diameters. The tendency of the dimensionless compressive yield stress, $p_y(\phi, T_{res})$ predicted in this chapter is the same as that analysed in Zhang et al. (2013a).

Figs. 5.5–5.7 show the evolutions of the dimensionless hindered settling function, $R_s(\phi, T_{res})$ for each case. The analysis of the evolutions of $R_s(\phi, T_{res})$ presented in Zhang et al. (2013a) can also be used here for explanations of $R_s(\phi, T_{res})$ behaviours for each case. For larger underflow solids fluxes operated in a densfied system, the ratio between the local solids volume fraction, ϕ and the densified gel point, ϕ_g which depends on the solids residence times is approximately unity near the top of the bed (see detailed explanations in Zhang et al. (2013a)). As a consequence (again explained in Zhang et al. (2013a)), decreasing segments of $R_s(\phi, T_{res})$ curves near the top of the bed can be observed in Figs. 5.5–5.7 (e.g. Case 6 and Case 8).

The $R_s(\phi, T_{res})$ curves of Case 1, and Cases 3–5 always increase between ϕ_g determined at the top of the bed and ϕ_u determined at the bottom of the thickener, since not only does the local solids volume fraction, ϕ increase somewhat, but the ratio ϕ/ϕ_g also increases significantly (see details in Zhang et al. (2013a)). On the other hand, $R_s(\phi, T_{res})$ determined in Case 2 increases near the top of the bed and then decreases (albeit by tiny

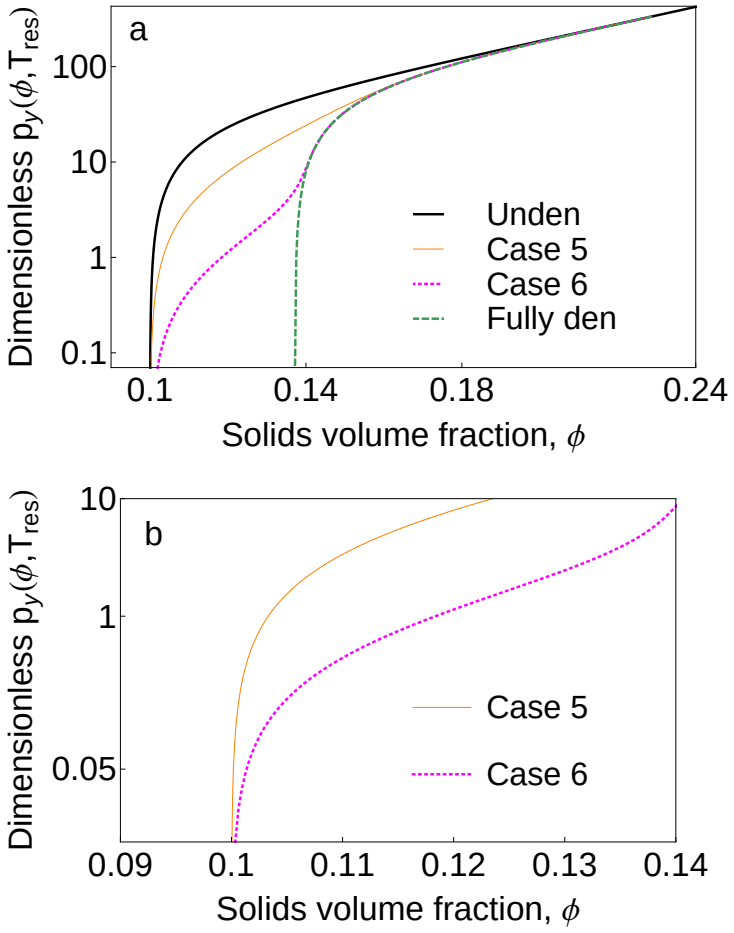

Figure 5.3: Evolutions of the dimensionless compressive yield stresses for Cases 5–6 – $\phi_u = 0.24$. The sub-plot labelled 'b' is the zoomed figure of the sub-plot labelled 'a'. Note that the curves of Cases 5–6 start from the same undensified gel point at $\phi = \phi_{g,0}$.

amounts), since the solids volume fraction, ϕ seems to increase rather rapidly near the top of the bed and then increases at roughly the same rate as that of the densified gel point, ϕ_g (Zhang et al., 2013a). A similar tendency of $R_s(\phi, T_{res})$ is also observed in Case 7.

5.5.3 Thickener performance

In this section, thickener performance is considered in terms of the bed height, z_b and the total solids residence time, t_{res}^{total}. Whether there is an improvement of thickener performance due to aggregate densification might depend upon the proposed underflow solids volume fractions. In this section, the effects of different proposed underflow solids volume fractions on the predictions of thickener performance have been analysed. Figs. 5.8–5.10 present the solids volume fraction profiles for each case. For a given underflow solids

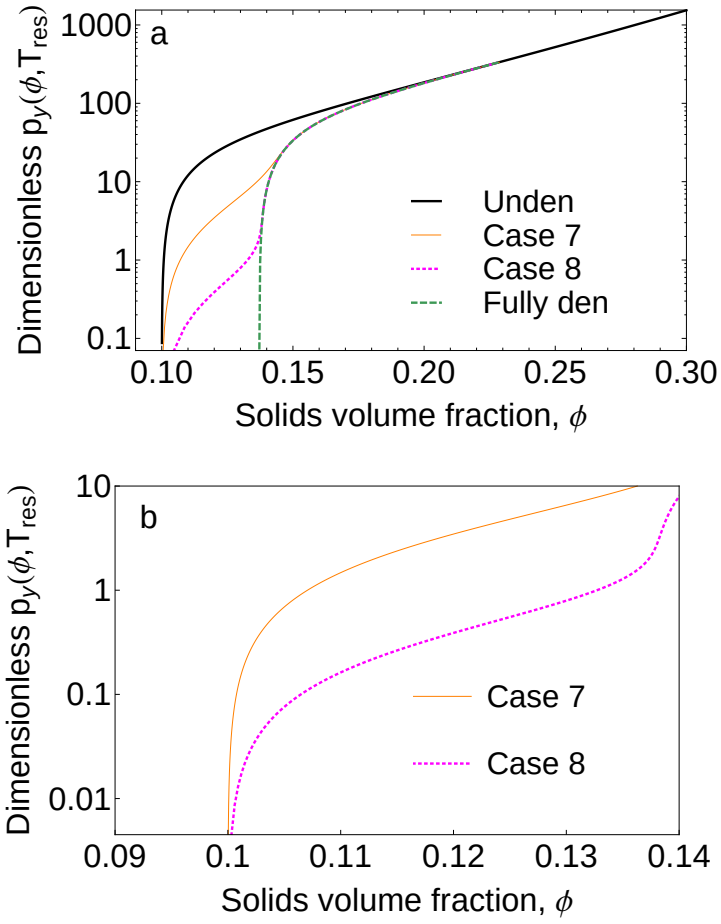

Figure 5.4: Evolutions of the dimensionless compressive yield stresses for Cases 7–8. Recall that the underflow solids volume fraction, $\phi_u = 0.3$ in these cases. Again the sub-plot 'b' is the zoomed figure of the sub-plot 'a'. The curves of Cases 7–8 also start from the same undensified gel point at $\phi = \phi_{g,0}$.

flux, q_u, and a small underflow solids volume fraction, ϕ_u which is smaller than $\phi_{agg,\infty}$, as shown in Fig. 5.8, the bed height calculated using a larger densification rate parameter, A is much shorter than that predicted using a smaller densification rate parameter, A (e.g. Cases 1–2 and Cases 3–4). If the given underflow solids flux increases but the underflow solids volume fraction, ϕ_u and the densification rate parameter, A are not changed, the bed height also needs to increase, since the local solids volume fraction, ϕ increases more rapidly with position as a smaller underflow solids flux is given, and a tall bed is required for delivering a larger underflow solids flux through the consolidation zone (e.g. Case 1 vs Case 3, Case 2 vs Case 4). For intermediate and large underflow solids volume fractions (e.g. Figs 5.9–5.10), the bed heights also shorten (albeit not by quite so much) as larger densification rate parameters are given (see Case 5 vs Case 6; Case 7 vs Case 8) for

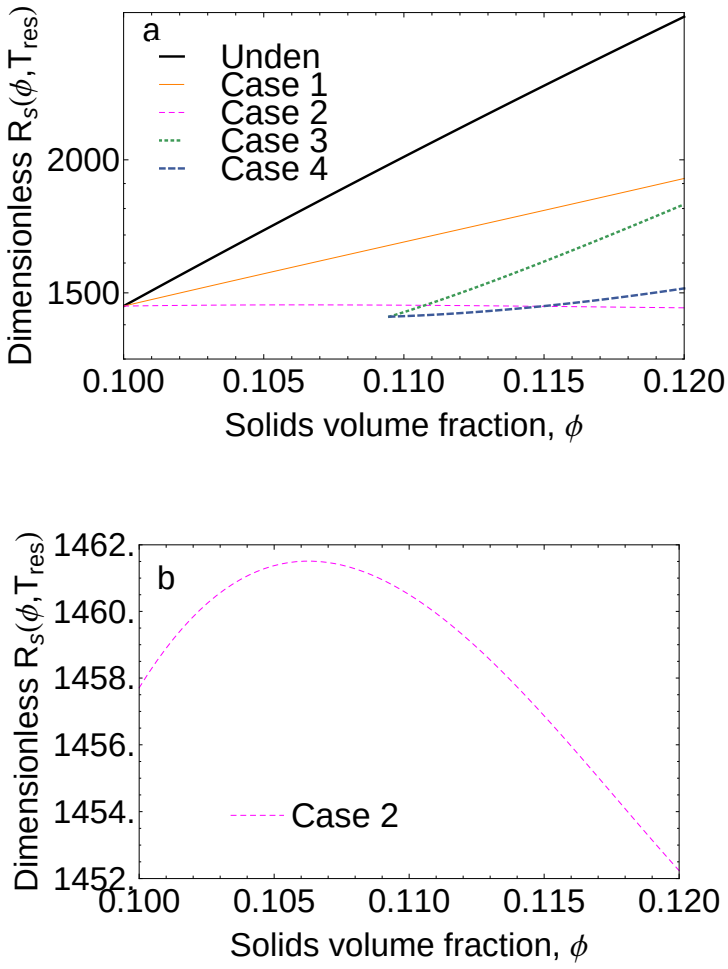

Figure 5.5: Evolutions of the dimensionless hindered settling functions, $R_s(\phi, T_{res})$ for Cases 1–4. Note that the sub-plot labelled 'b' is a zoomed figure of Case 2.

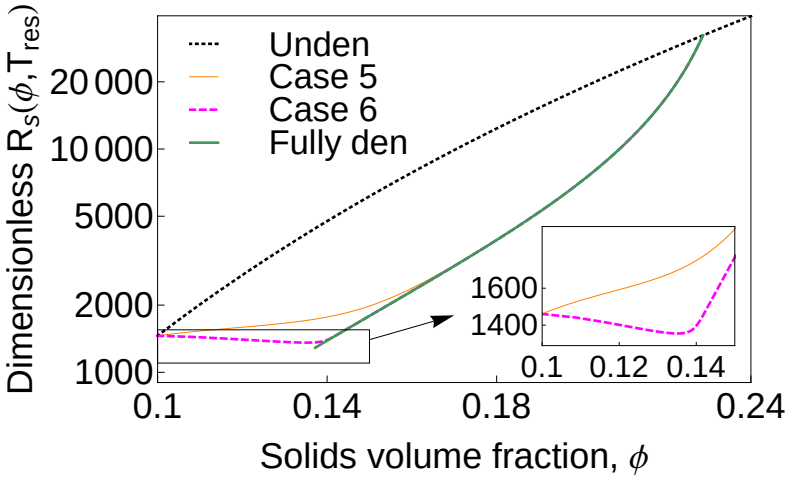

Figure 5.6: Evolutions of the dimensionless hindered settling functions, $R_s(\phi, T_{res})$ for Cases 5–6.

specified underflow solids fluxes.

Near the top of the bed, flat segments of the curves (e.g. Case 6 and Case 8) can be observed in Figs. 5.9–5.10, due to the rate of increase of the local solids volume fraction, ϕ that needs to keep up with that of the densified gel point, ϕ_g (Zhang et al., 2013a). Similar results are also observed in Zhang et al. (2013a). If a large densification rate parameter, A is given for an intermediate or a large underflow solids volume fraction, the system is densifying to the fully densified state rapidly – this is the reason why the subsequent slopes of curves plotted for Case 6 and Case 8 are the same as those of curves plotted for the fully densified cases.

Tables 5.2–5.3 show the bed heights and the solids residence times required for achieving the desired underflow solids volume fractions. As shown in Table 5.2, the magnitude of the bed height decreases dramatically when a small underflow solids volume fraction and a large densification rate parameter are given. For an intermediate underflow solids volume fraction, the height required for $Zone^{upper}$ makes the dominant contribution to the entire height of the consolidation zone and there is scope for reducing this height through aggregate densification. On the other hand, the height required for $Zone^{lower}$ (unaffected by aggregate densification) makes the dominant contribution to the entire height of the consolidation zone implying that less improvement in thickener performance is achieved for a large underflow solids volume fraction[3].

Table 5.3 shows that the solids residence time in the consolidated bed calculated in Case 1 is longer than that determined in Case 3, since a much larger underflow solids flux is operated in Case 3. This is however offset by time needed for pre-shearing of aggregates which must occur in Case 3. The total solids residence time required for Case 2 is longer than that required for Case 4, due to a much larger underflow solids flux operated in Case 4 and comparatively little pre-shear time in the rapidly densifying Case 4. Table 5.3 also presents that the solids residence time required for the consolidation zone is shorter for a specified underflow solids flux when a large aggregate densification rate parameter is given (e.g. Case 2 vs Case 1 and Case 4 vs Case 3). This happens because

[3]The fact that we see in Table 5.2 the same $Zone^{lower}$ heights in Cases 5–6 and the fully densified case (and likewise the same situation in Cases 7–8) is a manifestation of the system becoming already virtually fully densified whilst still in $Zone^{upper}$. This is easy to check in Table 5.3 which computes the solids residence times spent in $Zone^{upper}$, which greatly exceed the reciprocals of the densification rate parameter either $A = 0.001\,\mathrm{s}^{-1}$ or $A = 0.01\,\mathrm{s}^{-1}$.

	ϕ_u	$\lvert z_b^{total}\rvert$/ m	$\lvert z_b^{upper}\rvert$/ m	$\lvert z_b^{lower}\rvert$/ m
Unden	0.12	0.0462	N/A	0.0462
Case 1	0.12	0.0288	0.0288	N/A
Case 2	0.12	0.00592	0.00592	N/A
Case 3	0.12	0.0367	0.0367	N/A
Case 4	0.12	0.0132	0.0132	N/A
Case 5	0.24	0.724	0.621	0.103
Case 6	0.24	0.702	0.599	0.103
Ful den	0.24	0.699	0.596	0.103
Unden	0.3	1.975	N/A	1.975
Case 7	0.3	1.781	0.41	1.371
Case 8	0.3	1.779	0.408	1.371
Ful den	0.3	1.778	0.407	1.371

Table 5.2: Determinations of bed heights for Cases 1–8. $|z_b^{upper}|$ represents the bed height determined in $Zone^{upper}$ and $|z_b^{lower}|$ represents the bed height determined in $Zone^{lower}$. Note that the total bed height, $|z_b^{total}|$ is equal to $|z_b^{upper}| + |z_b^{lower}|$ for Cases 5–8. The bed height determined in the initially undensified thickener for $\phi_u = 0.12$ is calculated using the small underflow solids flux operated in Cases 1–2. The undensified cases formally assign *all* the bed height to $Zone^{lower}$ (by definition, since the sludge rheological properties in $Zone^{lower}$ are defined as being the undensified ones).

the local solids volume fraction changes faster moving through the consolidation zone in a case of a larger aggregate densification rate parameter. As shown in Table 5.3, the same trend is seen for the total solids residence time because any additional time required for pre-shearing of aggregates decreases with the increase of the aggregate densification rate parameter, A (e.g. Cases 3–4). Due to the same undensified sludge rheological properties applying in $Zone^{lower}$ regardless of densification, the solids residence time required for $Zone^{lower}$ must be the same[4] regardless of densification if the underflow solids flux and the underflow solids volume fraction are specified (e.g. Cases 5–6, and Cases 7–8). However, for a specified large ϕ_u, the relative decrease in the solids residence time originating now from $Zone^{upper}$ is marginal.

[4]Strictly speaking for equal time in $Zone^{lower}$, we require all cases studied to leave $Zone^{upper}$ virtually at full densification, so that they all enter $Zone^{lower}$ with a common $\phi_{agg,\infty}$, but this is certainly true for the relevant data of Table 5.3 (i.e. Cases 5–8) with a densification rate parameter either $A = 0.001\,\mathrm{s}^{-1}$ or $A = 0.01\,\mathrm{s}^{-1}$.

	ϕ_u	t_{res}^{total} / hr	t_{res}^{pre} / hr	t_{res}^{upper} / hr	t_{res}^{lower} / hr
Unden	0.12	0.168	N/A	N/A	0.168
Case 1	0.12	0.106	N/A	0.106	N/A
Case 2	0.12	0.0219	N/A	0.0219	N/A
Case 3	0.12	0.126	0.098	0.028	N/A
Case 4	0.12	0.020	0.0098	0.0102	N/A
Case 5	0.24	8.811	N/A	7.304	1.507
Case 6	0.24	8.692	N/A	7.185	1.507
Ful den	0.24	8.681	N/A	7.174	1.507
Unden	0.3	152.104	N/A	N/A	152.104
Case 7	0.3	141.2	N/A	24.937	116.263
Case 8	0.3	141.185	N/A	24.922	116.263
Ful den	0.3	141.179	N/A	24.916	116.263

Table 5.3: Determinations of solids residence times for Cases 1–8. t_{res}^{pre} represents the solids residence time required for pre-shearing of aggregates which is predicted using the algorithm presented in Zhang et al. (2013a). t_{res}^{upper} represents the solids residence time determined in $Zone^{upper}$ and t_{res}^{lower} represents the solids residence time determined in $Zone^{lower}$. Note that the total solids residence time, t_{res}^{total} for Cases 3–4 includes the solids residence time required for pre-shearing of aggregates ($t_{res}^{total} = t_{res}^{pre} + t_{res}^{upper}$) and for Cases 5–8 is equal to $t_{res}^{upper} + t_{res}^{lower}$.

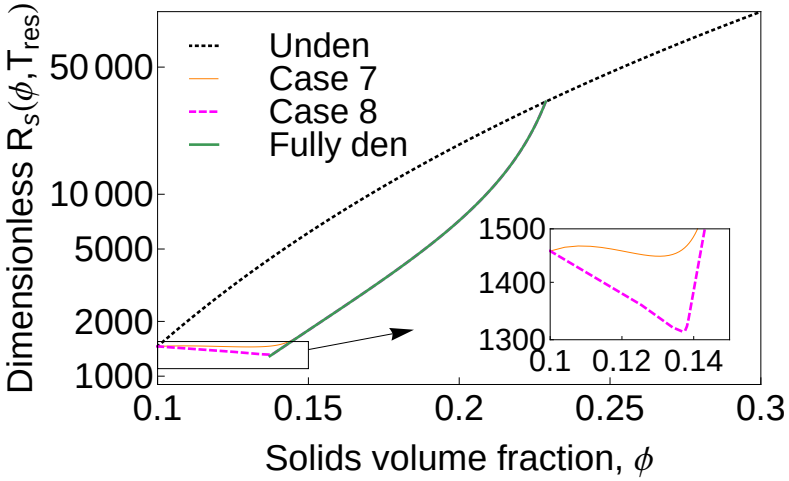

Figure 5.7: Evolutions of the dimensionless hindered settling functions, $R_s(\phi, T_{res})$ for Cases 7–8.

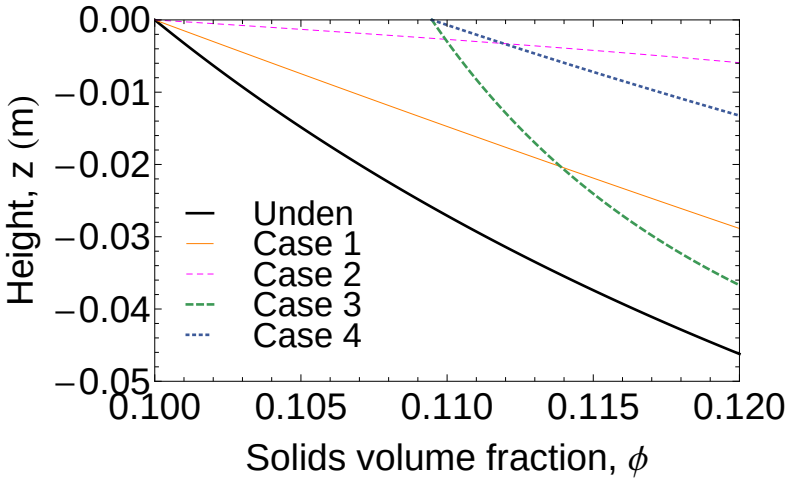

Figure 5.8: The solids volume fraction profiles for $\phi_u = 0.12$. Note that the corresponding profile for the fully densified system is not available, since the fully densified system would not gel for $\phi_u = 0.12$. The bed height required for the undensified system is only determined using the smaller of the two given underflow solids fluxes (i.e. the underflow solids flux is given in Cases 1–2), since the larger underflow solids flux which is given in Cases 3–4 cannot be operated for the undensified system at $\phi_u = 0.12$.

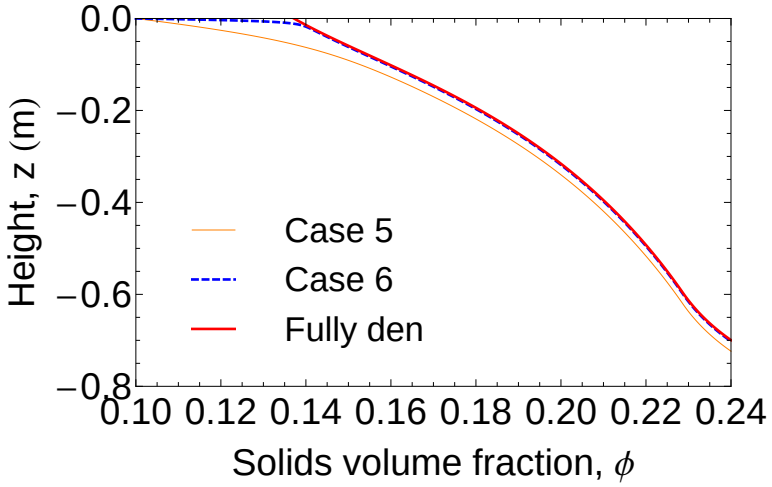

Figure 5.9: The solids volume fraction profiles for $\phi_u = 0.24$. Note that the profile for the undensified system is not available, due to a chosen large underflow solids flux which, whilst substantially less than the maximum permitted underflow solids flux for a densified system, nevertheless remains greater than the maximum permitted underflow solids flux for an undensified system.

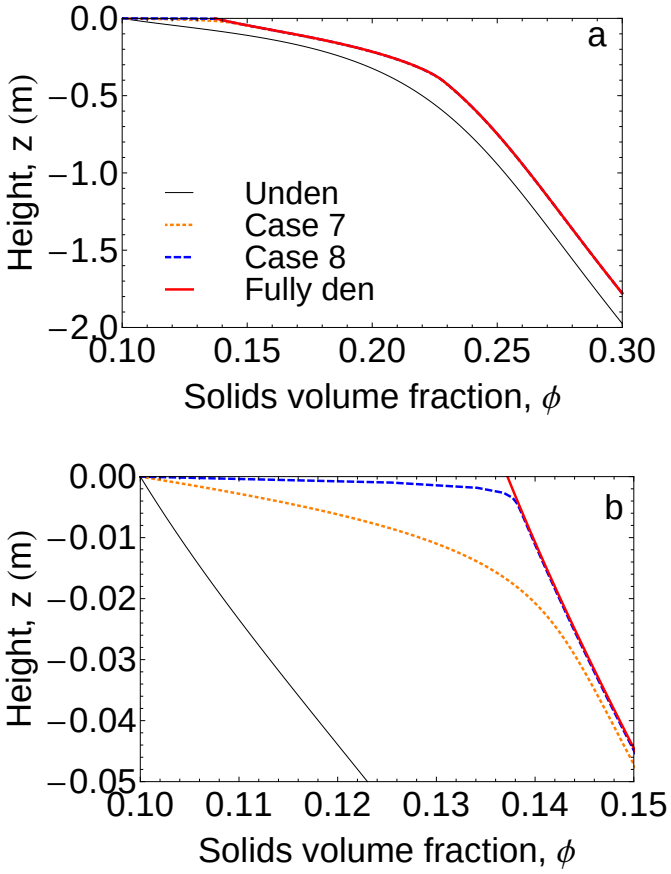

Figure 5.10: The solids volume fraction profiles for $\phi_u = 0.3$. Note that the sub-plot labelled 'b' is a zoomed figure of the sub-plot 'a'.

5.6 Conclusions

Underflow solids volume fractions affect thickener performance and the determinations of the limits of the underflow solids flux significantly. When a comparatively small underflow solids volume fraction is given, the maximum permitted underflow solids flux can be set arbitrarily large[5] in a time-dependent densified system – this improves the performance of thickeners dramatically. If the underflow solids volume fraction is increased to a sufficiently large value, the maximum permitted underflow solids flux will never be improved by densification but will maintain the same value determined in terms of the initially undensified state, regardless of aggregate densification. This leads to little improvement of the performance of a thickener with time-dependent densification. In cases which admit more scope for increasing the underflow solids flux in a thickener with time-dependent densification, the performance of the thickener can be enhanced significantly via aggregate densification.

[5]We have not discussed the role of the feed solids volume fraction here, since in many cases it does not impact on the consolidated bed, but in the special case where the underflow solids flux is pushed to arbitrarily high values, it is possible to show that constraints also appear for the feed, which must then have a solids volume fraction just very slightly less than the underflow solids volume fraction.

Chapter 6

Analysis and control of thickeners subject to aggregate densification

This chapter is a manuscript that is prepared for submission. This chapter explores how the presence of the hindered settling region affects the determinations of consolidated bed structures, and the evolutions of sludge rheological properties.

Summary

This chapter considers the effects of the presence of the hindered settling region upon the consolidation region in a steady state thickener with time-dependent densification. The modified solids flux theory consistent with time-dependent densification extended by Grassia et al. (2014) has been used to predict the consolidated bed structures in this work coupling them to the hindered settling region. Different aggregate densification rate parameters which will affect the evolutions of aggregate diameters during aggregate densification have been considered in this chapter. The evolutions of the solids volume fractions in the hindered settling region have also been analysed. This chapter also investigates how the presence of the hindered settling region affects the evolutions of sludge rheological properties. Moreover, the effects of the extent of densification occurring in the hindered settling region upon the predictions of solids residence times and bed heights determined in the consolidation region for different specified suspension fluxes have been investigated. For smaller proposed suspension fluxes, the focus is primarily upon the

consolidated bed (i.e., the height and the solids residence time required for the hindered settling region is neglected). For larger proposed suspension fluxes however, the hindered settling region might need to be considered. For a specified suspension flux and a specified aggregate densification rate parameter, *taller* beds are achieved when *more* densification occurs in the hindered settling region, but this is associated with higher underflow solids volume fractions.

6.1 Introduction

A steady state thickener is an indispensable unit whose main objective is to increase solids concentrations within suspensions in many industries including chemical engineering plants, minerals plants, food industries, and wastewater treatment plants (Stickland et al., 2008; Boger, 2009; Diehl, 2012). Proper design and control of steady state thickeners are essential to engineers and researchers, since the failure of thickeners may lead to huge environmental disasters and economic losses (Boger, 2009; Jones and Boger, 2012; Diehl, 2012). In practice, engineers often aim to operate thickeners at or near steady state with continuous incoming feeds as well as with continuous thickened sludges drawn off the bottom of thickeners (Keinath, 1985; Chancelier et al., 1997a; Bürger and Narváez, 2007). The so-called solids flux theory which is based on the theory developed by Kynch (1952) is widely used for the design and control of steady state thickeners (Fitch, 1966; Keinath, 1985; Lev et al., 1986; Chancelier et al., 1997a,b; Diehl, 2001, 2005, 2006, 2008a,b; Bürger and Narváez, 2007; Grassia et al., 2014). One limitation of the solids flux theory is that it cannot predict the height of the consolidation region where the local solids tend to form into a weight bearing gel. The solids flux theory however predicts the thickener area required for achieving the desired underflow solids volume fraction, and the underflow solids flux which is permitted in thickeners (Coe and Clevenger, 1916; Talmage and Fitch, 1955; Fitch, 1966). On the other hand, the height of the consolidation region can be predicted via the Buscall and White theory which incorporated sludge rheological properties in a networked suspension into the description (Buscall and White, 1987). Many published papers can be found in the literature which predict the height of the consolidation region using the Buscall and White theory for gelled suspensions (Land-

man et al., 1988; Martin, 2004; Usher and Scales, 2005; Zhang et al., 2013a,b).

In general, two zones are found inside a thickener: the clarification zone and the thickening zone (Martin, 2004; Bürger and Narváez, 2007). A thickener is operated ideally in such a way that the solids volume fraction in the clarification zone is nil and no solids are observed in effluents (Bürger and Narváez, 2007; Diehl, 2006, 2008a,b). The clarification zone exhibits no complex rheology and is not therefore of interest in this work. The thickening zone includes two regions: the hindered settling region where the suspension's weight-bearing strength is nil and the solids volume fraction is less than the so-called gel point, ϕ_g (which is a critical solids volume fraction at which a solids network is formed (Buscall and White, 1987; de Kretser et al., 2003; Bürger and Narváez, 2007)), and the consolidation region where significant dewatering occurs and the solids volume fraction is larger than the gel point, ϕ_g (Martin, 2004; Bürger and Narváez, 2007). In practice, engineers must avoid the so-called thickening failure and clarification failure, in order to operate thickeners successfully. For a specified suspension flux, feeding an excessively large solids flux to the thickener could lead (depending on the feed solids volume fraction) to the failure of thickening such that the solids will flow upwards to the clarification zone and effluents (Keinath, 1985; Chancelier et al., 1997a; Diehl, 2001). The thickening failure can potentially occur if the proposed underflow solids flux is larger than a local *minimum* value determined on the underflow solids flux vs. the solids volume fraction curve (Laquidara and Keinath, 1983; Keinath, 1985). In addition, the clarification failure (which occurs at even larger underflow solids fluxes) leads (regardless of the feed solids volume fraction) to the effluents containing a large amount of solids (Laquidara and Keinath, 1983). This happens if the proposed underflow solids flux is larger than the *maximum* value (or the peak) determined from the underflow solids flux vs. the solids volume fraction curve (Laquidara and Keinath, 1983). However, failures of thickening and clarification are not considered in this work.

The so-called operating charts developed by Diehl (2001) for analysing the behaviours of steady state thickeners where the underflow solids volume fraction is less than the gel point give comprehensive solids volume fraction predictions in the hindered settling region for different locations of the feed solids volume fractions and the feed underflow

solids fluxes on the curve of the underflow solids flux vs. the local solids volume fraction. If the underflow solids volume fraction increases to a larger value (e.g. larger than the gel point), and/or the specified suspension flux is small enough that consolidation occurs near the bottom of thickeners, the solids behaviours in both the hindered settling region and the consolidation region for steady state thickeners have been analysed by Bürger and Narváez (2007).

Fine particles and/or solids in suspensions will gather to produce larger aggregates/flocs after flocculation or aggregation (Usher et al., 2009; Grassia et al., 2014). Due to the presence of rakes which shear those aggregates/flocs in a thickener, the diameters of aggregates/flocs decrease over time (for a fixed solids mass in an aggregate) which can increase the suspension dewatering rates via altering the so-called sludge rheological properties and also increasing the gel point (Usher et al., 2009; Gladman et al., 2010; van Deventer et al., 2011; Zhang et al., 2013a,b; Grassia et al., 2014). The above process is called aggregate densification and is dependent on time. The sludge rheological properties including specifically the so-called hindered settling function and the so-called compressive yield stress are altered in the presence of aggregate densification (Channell and Zukoski, 1997; Channell et al., 2000; Usher et al., 2009; Gladman et al., 2010; van Deventer et al., 2011; Zhang et al., 2013a,b). When considering aggregate densification in a thickener, it is possible to identify a rate parameter which governs the rate of decrease of aggregate diameters during aggregate densification (van Deventer et al., 2011; van Deventer, 2012; Zhang et al., 2013a,b). This rate parameter is the so called aggregate densification rate parameter which is assumed to be a specified constant value and in addition independent of the solids volume fraction during time-dependent aggregate densification (van Deventer et al., 2011; Zhang et al., 2013a,b). van Deventer et al. (2011) proposed an approach to determine the final steady state aggregate diameter (or the minimum aggregate diameter) after aggregate densification using equilibrium batch settling tests. Moreover an approach for the determination of the aggregate densification rate parameter can be found in van Deventer (2012). In situations where the aggregate diameter remains the initial value (without shearing by rakes) or attains the minimum value after shearing, thickeners are described as initially undensified or fully densified, respectively (Usher et al., 2009;

Zhang et al., 2013a,b).

If time-dependent densification[1] occurs in a thickener, there are two important time scales: the densification time which relates to the changes of aggregate diameters from the initially undensified value to the final steady state value, and the solids residence time which relates to travel of aggregates from the feed point to the bottom of the thickener (Gladman et al., 2010). Grassia et al. (2014) predicted the solids behaviours in the hindered settling region of steady state thickeners using the modified solids flux theory consistent with time-dependent densification by assuming that the total solids residence time spent in a thickener is dominated by time spent in the hindered settling region for aggregates continuously densifying from the initially undensified aggregate diameter to some aggregate diameter obtained at the bottom of the hindered settling region. The height of the hindered settling region may be determined during the course of aggregate densification whilst the heights required for the hindered settling regions in an undensified thickener fed initially undensified materials and in a fully densified thickener fed fully densified materials remain undetermined as in standard Kynch theory (Grassia et al., 2014). The solids volume fraction profiles calculated for different suspension fluxes and different total solids residence times spent in the hindered settling region during aggregate densification have also been explored in Grassia et al. (2014). However, the work of Grassia et al. (2014) did not consider the consolidation region which is underneath the hindered settling region. One of the aims of this work is to explore effects of the presence of the hindered settling region upon the consolidation region during aggregate densification. Another aim of this work is to explore effects of the extent of densification that occurs in the hindered settling region upon the predictions of solids behaviours in the consolidation region.

Consolidation which occurs in a gelled suspension bed is of course a very important process where suspensions can be dewatered to obtain larger solids volume fractions. The solids behaviours in the consolidation regions of undensified steady state thickeners and fully densified steady state thickeners have already been predicted by many authors (Martin, 2004; Usher and Scales, 2005; Bürger and Narváez, 2007; Usher et al., 2009; Zhang

[1]Time-dependent here means time dependent in the Lagrangian sense following the progress of the aggregates through the thickener; the system is still steady state in Eulerian sense.

et al., 2013b). For cases where time-dependent densification occurs, Zhang et al. (2013a) simulated the consolidation region neglecting the hindered settling region. For an undensified system and a fully densified system, the solids volume fractions at the top of the bed are fixed (being the undensified gel point, $\phi_{g,0}$ and the fully densified gel point, $\phi_{g,\infty}$, respectively), regardless of the presence of the hindered settling region, since the gel points are then invariant during consolidation (Buscall and White, 1987; Usher and Scales, 2005; Usher et al., 2009; Zhang et al., 2013a,b). If time-dependent densification occurs in a thickener *where the hindered settling region is not explicitly modelled*, the solids volume fraction at the top of the bed could be any value between $\phi_{g,0}$ and $\phi_{g,\infty}$, according to the proposed underflow solids flux (Zhang et al., 2013a). However, if the hindered settling region is explicitly included and lies above the consolidation region, then as time-dependent densification occurs in a thickener, the evolution of the densified gel point at the top of the bed must be calculated and this is of particular interest in this work. One aim of this work is to determine the densified gel point at the top of the bed as the hindered settling region lies above the consolidation region. Another aim of this work is to analyse whether or not consolidation occurs for different specified suspension fluxes, underflow solids fluxes, and solids residence times.

Pre-shearing of aggregates which increases the densified gel point at the top of the bed is required before entering the consolidation region if a large underflow solids flux is chosen (Zhang et al., 2013a). Some of this pre-shearing can be realised in the hindered settling region. Nevertheless, under certain circumstances, pre-shearing may even be required prior to material entering the hindered settling region. This situation would occur when an underflow solids flux is specified which is larger than the *maximum* value for the *undensified* system (Grassia et al., 2014). This maximum permitted undensified solids flux is readily determined by plotting the underflow solids flux vs. the local solids volume fraction curve for the initially undensified state and finding the local *maximum* (Laquidara and Keinath, 1983; Grassia et al., 2014). It so happens that the underflow solids flux at which one needs to pre-shear prior to entering the hindered settling region corresponds to the same underflow solids flux for which the undensified system would exhibit the clarification failure.

The structure of this work is presented as follows. Sections 6.2–6.3 review the solids flux theory consistent with time-dependent densification, and in addition review the consolidation theory consistent with time-dependent densification. Sludge rheological properties including the functional forms of the compressive yield stresses and the hindered settling functions are also introduced in Sections 6.2–6.3. Section 6.4 introduces different operating limits in undensified thickeners, thickeners with time-dependent densification, and fully densified thickeners. The evolutions of the solids volume fractions in the hindered settling regions of undensified thickeners, thickeners with time-dependent densification, and fully densified thickeners, respectively are analysed in Section 6.5. The determination of the densified gel point at the top of the bed, and the analysis of the consolidation region are given in Section 6.6: the analysis of Section 6.6 takes proper account of the fact that a hindered settling region is present. Case studies are set up in Section 6.7. The main simulation results including the solids volume fraction profiles, sludge rheological properties, and the heights required for both the hindered settling regions and the consolidation regions are discussed in Section 6.8. Section 6.9 gives conclusions.

6.2 Solids flux theory consistent with time-dependent densification

In this section, we review both the undensified solids flux theory and the densified solids flux theory. When addressing the solids flux theory, it is necessary to describe the functional form of the so-called hindered settling function, since the solids flux can be expressed in terms of the hindered settling function (Usher and Scales, 2005; Usher et al., 2009; van Deventer et al., 2011; Zhang et al., 2013a,b; Grassia et al., 2014). For initially undensified cases, the hindered settling function only depends on the local solids volume fraction, ϕ but is independent of the solids residence time, t_{res}, whilst for time-dependent densified cases, the hindered settling function is dependent on both the local solids volume fraction, ϕ, and the solids residence time, t_{res} (van Deventer et al., 2011; Zhang et al., 2013a; Grassia et al., 2014). Many published papers (Landman and White, 1992; Lester et al., 2005; Diehl, 2007; Grassia et al., 2008, 2011) have described mathemati-

cal models and have conducted experiments measuring the initially undensified hindered settling function, $R_0(\phi)$. The densified hindered settling function, $R(\phi, t_{res})$ can be expressed in terms of the solids residence time, t_{res}, the local solids volume fraction, ϕ, and the initially undensified hindered settling function, $R_0(\phi)$. In this work, we choose the functional form of the initially undensified hindered settling function presented in Zhang et al. (2013a,b)

$$R_0(\phi) = \frac{R_{Stokes,0}}{\phi_{agg,0}}(\phi + r_g)^{r_n} r_g^{-r_n} \tag{6.2.1}$$

where $\phi_{agg,0}$ is the solids volume fraction within the initially undensified aggregates, r_g and r_n are the fitting parameters, and $R_{Stokes,0}$ represents the initially undensified hindered settling function of an isolated aggregate/floc which is defined in Zhang et al. (2013b). The constant parameters, $\phi_{agg,0}$, r_n, r_g, and $R_{Stokes,0}$ are chosen as 0.1667, 5, 0.05, and $260469\,\mathrm{Pa\,s\,m^{-2}}$, respectively (Usher et al., 2009; Zhang et al., 2013a,b).

Subsequently, the densified hindered settling function, $R(\phi, t_{res})$ which is also chosen from Zhang et al. (2013a,b) is

$$R(\phi, t_{res}) = \frac{(1-\phi)^2 R_0(\phi_{agg}) R_{Stokes,0} D_{agg}}{\phi_{agg,0} R_0(\phi_{agg})(1-\phi/\phi_{agg})^2 / r_{agg}(\phi/\phi_{agg}) + (R_{Stokes,0} D_{agg}\phi/\phi_{agg})(1-\phi_{agg})^2} \tag{6.2.2}$$

where D_{agg} is the ratio of the densified aggregates to the undensified aggregates, ϕ_{agg} is the solids volume fraction within the densified aggregates, and $r_{agg}(\phi/\phi_{agg})$ is the aggregate hindered settling factor. Note that this aggregate hindered settling factor, $r_{agg}(\phi/\phi_{agg})$ is assumed to be independent of densification and hence defined as follows (Usher et al., 2009; Zhang et al., 2013a,b)

$$r_{agg}(\phi/\phi_{agg}) = \frac{\phi_{agg,0}(1-\phi/\phi_{agg})^2 R_0(\phi_{agg,0}) R_0(\phi\phi_{agg,0}/\phi_{agg})}{R_{Stokes,0}\left(R_0(\phi_{agg,0}\left(1-\phi_{agg,0}\frac{\phi}{\phi_{agg}}\right)^2 - \frac{\phi}{\phi_{agg}}(1-\phi_{agg,0})^2 R_0\left(\phi_{agg,0}\frac{\phi}{\phi_{agg}}\right)\right)\right.}. \tag{6.2.3}$$

The solids volume fraction within the densified aggregates, ϕ_{agg} and the evolution of the aggregate diameter, D_{agg} with the solids residence time are defined by Usher et al. (2009) and van Deventer et al. (2011), respectively

$$\phi_{agg} = \frac{\phi_{agg,0}}{D_{agg}^3} \tag{6.2.4}$$

$$\frac{\mathrm{d}D_{agg}}{\mathrm{d}t_{res}} = -A(D_{agg} - D_{agg,\infty}) \tag{6.2.5}$$

and

$$D_{agg} = (1 - D_{agg,\infty})e^{-At_{res}} + D_{agg,\infty} \tag{6.2.6}$$

where $D_{agg,\infty}$ is the minimum aggregate diameter ratio which is selected to be a commonly chosen value of 0.9 in this work (van Deventer et al., 2011; Zhang et al., 2013a,b), and A is the aggregate densification rate parameter (i.e. various different possible values for A will be considered in this work). Note that the minimum aggregate diameter ratio, $D_{agg,\infty}$ can be measured using equilibrium batch sedimentation tests (van Deventer et al., 2011) and the aggregate densification rate parameter, A can also be determined by experiments (van Deventer, 2012).

The solids volume fraction within the final steady state aggregates, $\phi_{agg,\infty}$ can be calculated using Eq. (6.2.4) by setting $D_{agg} = D_{agg,\infty}$. The fully densified hindered settling function, $R_\infty(\phi)$ is evaluated at $D_{agg} = D_{agg,\infty}$ and $\phi_{agg} = \phi_{agg,\infty}$ via using

Eqs. (6.2.2)–(6.2.3).

Steady state thickeners, regardless of densification or lack thereof, will have the suspension flow balance and the solids mass balance (Bürger and Narváez, 2007; Diehl, 2008b)

$$f_0 = f_s + f_e \tag{6.2.7}$$

and

$$f_0\phi_f = f_s\phi_u + f_e\phi_e \tag{6.2.8}$$

where f_0 is the feed volumetric rate, f_s is the suspension volumetric flow rate, f_e is the volumetric overflow rate, ϕ_f is the initial feed solids volume fraction, ϕ_u is the underflow solids volume fraction, ϕ_e is the overflow solids volume fraction.

When modelling a thickener, it is important to define the suspension flux, q_s as the sum of the solids flux and the liquid flux (Bürger and Narváez, 2007). The feed velocity, q_0, the suspension velocity, u_{sb} determined at the bottom of the thickener, and the overflow velocity, q_e which flows upward between the feed point and the overflow outlet are defined as (Diehl, 2001, 2007, 2008a)

$$q_0 = \frac{f_0}{B} \tag{6.2.9}$$

$$u_{sb} = \frac{f_s}{B} \tag{6.2.10}$$

and

$$q_e = \frac{f_e}{B} \tag{6.2.11}$$

where B is the cross sectional area.

The suspension velocity, u_{sb} determined at the bottom of the thickener equals the suspension flux, q_s, due to no slip condition at the bottom of the thickener (Martin, 2004; Grassia et al., 2014). Hence, substituting Eqs. (6.2.9)–(6.2.11) into Eq. (6.2.8) yields (Diehl, 2001):

$$q_0\phi_f = q_s\phi_u + q_e\phi_e. \tag{6.2.12}$$

Ideally, engineers expect that ϕ_e is nil and then Eq. (6.2.12) reduces (Bürger and Narváez, 2007; Diehl, 2008b):

$$q_0\phi_f = q_s\phi_u. \tag{6.2.13}$$

At steady state, the solids and liquid at the bottom of the thickener have the same velocity (Martin, 2004; Grassia et al., 2014). One may express the underflow solids flux, q_u in terms of the underflow solids volume fraction, ϕ_u and the suspension flux, q_s (Martin, 2004; Grassia et al., 2014)

$$q_u = q_s\phi_u \tag{6.2.14}$$

where q_s represents the suspension flux including the solids flux and the liquid flux.

Substituting Eq. (6.2.9) into Eq. (6.2.13) and then rearranging yields an approach determining the cross sectional area, B (Coe and Clevenger, 1916; Vesilind, 1979)

$$B = \frac{f_0\phi_f}{q_s\phi_u}. \tag{6.2.15}$$

Determining the cross-sectional area B is obviously important for thickener design, however it is evident from Eq. (6.2.15) that this can only be achieved once the denomina-

tor of that equation, namely $q_s\phi_u$ (or equivalently by Eq. (6.2.14), q_u) is known. As stated in Grassia et al. (2014), in the hindered settling region, the underflow solids flux, q_u can be expressed in terms of the suspension flux, q_s and the local solids volume fractions, ϕ

$$q_u = q_s\phi + q_{fs}(\phi, t_{res}) \tag{6.2.16}$$

where $q_{fs}(\phi, t_{res})$ is the free settling solids flux evaluated in the batch settling tests and is independent of the underflow solids volume fraction. Note that the compressive yield stress and/or the particle stress must be neglected when determining q_{fs} in this fashion.

The functional form of q_{fs} is proposed by Usher and Scales (2005)

$$q_{fs}(\phi, t_{res}) = \frac{\Delta\rho g\phi(1-\phi)^2}{R(\phi, t_{res})} \tag{6.2.17}$$

where $\Delta\rho$ is the density difference between the solids and liquid which will be specified shortly, g is the gravity acceleration, which is chosen as $9.8\,\mathrm{m\,s^{-2}}$. Note that, the densified hindered settling function, $R(\phi, t_{res})$ is replaced by the initially undensified hindered settling function, $R_0(\phi)$ if the system is initially undensified and is replaced by the fully densified hindered settling function, $R_\infty(\phi)$ if the system is fully densified.

Eqs. (6.2.16)–(6.2.17) are important to analyse the solids behaviours and operating conditions of a thickener. For a specified q_s which is easily controlled in practice, there is a minimum underflow solid flux achieved via plotting Eq. (6.2.16) in the undensified and fully densified system, respectively. This minimum underflow solids flux is called the limiting solids flux which is the *maximum* permitted underflow solids flux and hence the *maximum* feed loading operated in a thickener for a specified q_s (Vesilind, 1979; Diehl, 2001, 2008b). Note that as a very large q_s is operated in a thickener, the limiting solids flux may be determined at the feed solids volume fraction (Chancelier et al., 1997a; Grassia et al., 2014). If an intermediate and/or a small q_s is operated in a thickener, the limiting solids flux may actually be determined at some point of the underflow solids flux vs. the local solids volume fraction curve which lies to the right of the feed point (in other words,

the critical solids volume fraction which corresponds to determine the limiting solids flux is larger than the feed solids volume fraction) (Bürger and Narváez, 2007; Diehl, 2001, 2008b).

If time-dependent densification occurs however, a family of the densified underflow solids flux vs. the local solids volume fraction curves must be plotted for different aggregate diameters ranging between the initially undensified value and the fully densified value (Grassia et al., 2014). Theoretically, for a specified q_s, the upper bound of the densified limiting solids flux is evaluated at the fully densified state using the fully densified hindered settling function, $R_\infty(\phi)$.

6.3 Consolidation theory consistent with time-dependent densification

The theory presented in Section 6.2 is adequate for describing the hindered settling region, but must be extended for describing the consolidation region. We wish to progress beyond design criteria that solely fix the cross sectional area of a thickener (see Eq. (6.2.15)) so as also to determine required thickener heights. Thus, in this section, the focus is mainly on the predictions of the bed height and the solids volume fraction profile via combining the fundamental consolidation theory developed by Buscall and White (1987) with the densification theory developed by Usher et al. (2009) and van Deventer et al. (2011), and extended by Zhang et al. (2013a,b). The consolidation theory and the densification theory have been described by many researchers in the literature (Buscall and White, 1987; Usher et al., 2009; van Deventer et al., 2011; Zhang et al., 2013a,b; Grassia et al., 2014). Hence, we briefly review these theories in this section. One feature of the consolidation theory and the densification theory is the use of the so-called compressive yield stress, $P_y(\phi, t_{res})$ (see details in Buscall and White (1987); Usher et al. (2009); van Deventer (2012); Zhang et al. (2013a,b)). As the local solids volume fraction exceeds the gel point, ϕ_g where the solids contact each other, the solids enter the consolidation region where the compressive yield stress, $P_y(\phi, t_{res})$ must be taken into account (de Kretser et al., 2003; van Deventer, 2012; Zhang et al., 2013a,b). If consolidation occurs, the solids

volume fraction can increase dramatically, which is the aim of the thickening process.

Knowing the functional form of the compressive yield stress, $P_y(\phi, t_{res})$ is vital to design and control a thickener. Experiments and mathematical models have been established to determine the undensified compressive yield stress, $P_{y,0}(\phi)$ (Buscall and White, 1987; Green and Boger, 1997; Usher et al., 2001; de Kretser et al., 2001). The densified compressive yield stress, $P_y(\phi, t_{res})$ can be expressed in terms of the undensified functional form. In this chapter, we choose both the undensified and densified functional forms of the compressive yield stresses from Zhang et al. (2013a)

$$P_{y,0}(\phi) = \frac{a_0(\phi - \phi_{g,0})}{(m + \phi - \phi_{g,0})(\phi_{cp} - \phi)^{n_0}} \tag{6.3.1}$$

and

$$P_y(\phi, t_{res}) = P_{y,0}(\phi_{agg}) \frac{(m + \phi_{agg} - \phi_g)}{(m + \phi - \phi_g)} \frac{(\phi - \phi_g)}{(\phi_{agg} - \phi_g)} \left(\frac{\phi_{cp} - \phi_{agg}}{\phi_{cp} - \phi} \right)^{n_1} \tag{6.3.2}$$

where $\phi_{g,0}$ is the initially undensified gel point, m is a constant value which is assumed to be independent of densification, a_0 and n_0 are the curve fitting parameters for the undensified functional form, ϕ_{cp} is the close packing solids volume fraction which is also assumed to be independent of densification, ϕ_g is the densified gel point, ϕ_{agg} is the solids volume fraction within the densified aggregates (see Eq. (6.2.4)), and n_1 is the curve fitting parameter for the densified functional form. The constant parameters $\phi_{g,0}$, a_0, n_0, m, and ϕ_{cp} are assumed to be 0.1, $3.7914\,\mathrm{Pa}$, 10.8302, 0.0363, and 0.8, respectively (Usher et al., 2009; Zhang et al., 2013a,b).

The densified gel point, ϕ_g and the curve fitting parameter, i.e. the exponent n_1 are given by (van Deventer et al., 2011; Zhang et al., 2013a)

$$\phi_g = \frac{\phi_{g,0}}{D_{agg}^3} \tag{6.3.3}$$

and

$$n_1 = (\phi_{cp} - \phi_{agg}) \left(\frac{P'_{y,0}(\phi_{agg})}{P_{y,0}(\phi_{agg})} + \frac{1}{m + \phi_{agg} - \phi_g} - \frac{1}{\phi_{agg} - \phi_g} \right) \tag{6.3.4}$$

where $P'_{y,0}(\phi_{agg})$ is the derivative of the initially undensified compressive yield stress with respect to the local solids volume fraction evaluated at $\phi = \phi_{agg}$.

The fully densified compressive yield stress, $P_{y,\infty}(\phi)$ has the same functional form as Eq. (6.3.1) replacing $\phi_{g,0}$ by $\phi_{g,\infty}$, and replacing the curve fitting parameters from the undensified form to the fully densified form (Zhang et al., 2013a,b):

$$P_{y,\infty}(\phi) = \frac{a_\infty(\phi - \phi_{g,\infty})}{(m + \phi - \phi_{g,\infty})(\phi_{cp} - \phi)^{n_\infty}} \tag{6.3.5}$$

where $\phi_{g,\infty}$ is the fully densified gel point, a_∞ and n_∞ are the curve fitting parameters evaluated in the fully densified state: these depend on the aggregate diameter ratio, $D_{agg,\infty}$ in the fully densified state; for $D_{agg,\infty} = 0.9$ as considered here, $a_\infty = 6.4516\,\mathrm{Pa}$ and $n_\infty = 10.0335$. Note that these rather complicated formulae for $P_y(\phi, t_{res})$, and $P_{y,\infty}(\phi)$ ensure that both $P_y(\phi, t_{res})$, and $P_{y,\infty}(\phi)$ and their derivatives with respect to ϕ, match those of $P_{y,0}(\phi)$ when $\phi = \phi_{agg}$ (Usher et al., 2009; van Deventer et al., 2011; Zhang et al., 2013a,b).

Now we turn to the force balance equations. In the absence of densification, the force balance equation is written as (Buscall and White, 1987; Landman et al., 1988; Usher and Scales, 2005; Zhang et al., 2013a,b)

$$\frac{\mathrm{d}z}{\mathrm{d}\phi} = -\frac{\mathrm{d}P_{y,0}(\phi)/\mathrm{d}\phi}{\Delta\rho g\phi(1 - (R_0(\phi)/(\Delta\rho g(1-\phi)^2))q_u(1/\phi - 1/\phi_u))} \tag{6.3.6}$$

where $P_{y,0}(\phi)$ is the undensified compressive yield stress, z is the height of the bed which is measured upwards, and q_u is the underflow solids flux which is measured downwards. Note that the *denominator* on the right hand side of Eq. (6.3.6) is positive (on the grounds

that hydrodynamic drag is smaller than gravity) (Zhang et al., 2013a,b). Hence the leading minus sign on the right hand side of Eq. (6.3.6) ensures that the solids volume fraction increases moving into the bed (i.e. ϕ increases as z decreases with our sign convention).

If the system is fully densified, the force balance equation has the same form as Eq. (6.3.6) replacing $R_0(\phi)$ and $P_{y,0}(\phi)$ by $R_\infty(\phi)$ and $P_{y,\infty}(\phi)$, respectively (Zhang et al., 2013b)

$$\frac{\mathrm{d}z}{\mathrm{d}\phi} = -\frac{\mathrm{d}P_{y,\infty}(\phi)/\mathrm{d}\phi}{\Delta\rho g\phi(1-(R_\infty(\phi)/(\Delta\rho g(1-\phi)^2))q_u(1/\phi-1/\phi_u))}. \tag{6.3.7}$$

For a thickener with time-dependent densification, the local solids volume fraction can be written in terms of either the height, z or the solids residence time, t_{res} (Zhang et al., 2013a; Grassia et al., 2014). Thus, it is convenient to write the rate equation for the change of the local solids volume fraction (Zhang et al., 2013a)

$$\frac{\mathrm{d}\phi}{\mathrm{d}t_{res}} = \frac{\Delta\rho g q_u - \dfrac{R(\phi,t_{res})}{(1-\phi)^2}q_u^2\left(\dfrac{1}{\phi}-\dfrac{1}{\phi_u}\right) - \dfrac{\partial P_y(\phi,t_{res})}{\partial t_{res}}}{\dfrac{\partial P_y(\phi,t_{res})}{\partial\phi}} \tag{6.3.8}$$

where $\partial P_y(\phi,t_{res})/\partial t_{res}$ in the numerator of Eq. (6.3.8) represents that the densified compressive yield stress depends not only on the solids volume fraction, but also on the solids residence time when time-dependent densification occurs.

It is easy to predict the bed heights via integrating Eq. (6.3.6) with the solids volume fraction ranging between $\phi_{g,0}$ and ϕ_u for an undensified system and via integrating Eq. (6.3.7) with the solids volume fraction ranging between $\phi_{g,\infty}$ and ϕ_u for a fully densified system. Eq. (6.3.8) could be also easily solved via using the midpoint rule, if the densified gel point at the top of the bed is identified (Press et al., 1992). We will analyse the evolution of the densified gel point at the top of the bed in the presence of the hindered settling region for a thickener with time-dependent densification shortly. Before doing that however, we wish to cast our equations in dimensionless form and also take a

closer look at the undensified and fully densified cases.

6.3.1 Dimensionless equations

A dimensionless system of equations is convenient to analyse the behaviours of aggregates/flocs in a thickener with time-dependent densification and hence we convert the dimensional system of equations to dimensionless form by defining a scale, α (Zhang et al., 2013a; Grassia et al., 2014):

$$\alpha = a_0 A/(\Delta\rho g u_{Stokes,0}), \quad u_{Stokes,0} = \frac{\Delta\rho g}{R_{Stokes,0}}$$

$$Z = \frac{z\Delta\rho g\alpha}{a_0} = \frac{zA}{u_{Stokes,0}}, \quad R_s(\phi, T_{res}) = \frac{R(\phi, t_{res})}{R_{Stokes,0}}$$

$$Q = \frac{q}{u_{Stokes,0}}, \quad T_{res} = \frac{t_{res} u_{Stokes,0}\Delta\rho g\alpha}{a_0} = t_{res}A, \quad p_y(\phi, T_{res}) = \frac{P_y(\phi, t_{res})}{a_0}$$

where $u_{Stokes,0}$ denotes the Stokes settling velocity. Using these dimensionless forms, the effect of densification rate parameter, A has been scaled out of the hindered settling region, but retains importance in the consolidated bed.

The evolution of the aggregate diameter ratio can be expressed using the above mentioned dimensionless scalings:

$$D_{agg} = (1 - D_{agg,\infty})e^{-T_{res}} + D_{agg,\infty}. \tag{6.3.9}$$

The dimensionless free settling solids flux, Q_{fs} determined in the batch settling test is written as:

$$Q_{fs} = \frac{\phi(1-\phi)^2}{R_s(\phi, T_{res})}. \tag{6.3.10}$$

The dimensionless underflow solids flux, Q_u which is expressed in terms of the dimensionless free settling solids flux, Q_{fs} and the dimensionless suspension flux, Q_s is written as:

$$Q_u = Q_{fs} + \phi Q_s. \tag{6.3.11}$$

The dimensionless rate equation for the solids velocity which is expressed in terms of the dimensionless underflow solids flux, Q_u, and the local solids volume fraction is written as:

$$\frac{\mathrm{d}Z}{\mathrm{d}T_{res}} = -\frac{Q_u}{\phi} \tag{6.3.12}$$

where the minus sign on the right hand side of Eq. (6.3.12) represents the dimensionless solids residence time, T_{res} increasing from $T_{res} = 0$ at the feed point and the dimensionless height, Z being measured upwards and $Z = 0$ being at the feed point of the thickener.

The underflow solids volume fraction, ϕ_u is determined:

$$\phi_u = \frac{Q_u}{Q_s}. \tag{6.3.13}$$

The dimensionless force balance equations for initially undensified thickeners, thickeners subject to time-dependent densification, and fully densified thickeners are given by Eqs. (6.3.14–6.3.16), respectively:

$$\frac{\mathrm{d}\phi}{\mathrm{d}Z} = -\frac{\phi - \dfrac{R_{s,0}(\phi)Q_u(1-\phi/\phi_u)}{(1-\phi)^2}}{\alpha\,\partial p_{y,0}(\phi)/\partial\phi} \tag{6.3.14}$$

$$\frac{\mathrm{d}\phi}{\mathrm{d}T_{res}} = \frac{Q_u - \dfrac{Q_u^2 R_s(\phi,T_{res})}{(1-\phi)^2}\left(\dfrac{1}{\phi}-\dfrac{1}{\phi_u}\right) - \alpha\dfrac{\partial p_y(\phi,T_{res})}{\partial T_{res}}}{\alpha\,\partial p_y(\phi,T_{res})/\partial\phi} \tag{6.3.15}$$

and

$$\frac{\mathrm{d}\phi}{\mathrm{d}Z} = -\frac{\phi - \dfrac{R_{s,\infty}(\phi)Q_u(1-\phi/\phi_u)}{(1-\phi)^2}}{\alpha\,\partial p_{y,\infty}(\phi)/\partial\phi}. \tag{6.3.16}$$

6.4 Theory for operation and control of a thickener

In this section, we analyse the operating limits including the maximum permitted dimensionless underflow solids flux, $Q_{u,max}$ (for a given suspension flux), the maximum permitted dimensionless suspension flux, $Q_{s,max}$ (for a given underflow solids flux), and the underflow solids volume fraction, $\phi_{u,max}$ determined using Eq. (6.3.13) with the maximum permitted dimensionless underflow solids flux, $Q_{u,max}$ calculated for a specified dimensionless suspension flux, Q_s. These limits can be determined using the solids flux theory, regardless of the compressive yield stress.

A general formula determining the dimensionless underflow solids flux, Q_u in the absence of the compressive yield stress is expressed in terms of the underflow solids volume fraction, ϕ_u (Usher and Scales, 2005; Usher et al., 2009; Zhang et al., 2013a):

$$Q_u = \frac{\phi(1-\phi)^2}{R_s(\phi,T_{res})(1-\phi/\phi_u)} \equiv \frac{Q_{fs}}{1-\phi/\phi_u}. \tag{6.4.1}$$

Substituting Eq. (6.4.1) into Eq. (6.3.13) and rearranging yields a formula for the determination of the dimensionless suspension flux, Q_s:

$$Q_s = \frac{\phi(1-\phi)^2}{R_s(\phi, T_{res})(\phi_u - \phi)} \equiv \frac{Q_{fs}}{\phi_u - \phi}. \tag{6.4.2}$$

In an undensified system and a fully densified system, $R_s(\phi, t_{res})$ in the denominators of Eqs. (6.4.1)–(6.4.2) will be replaced by $R_{s,0}(\phi)$ and $R_{s,\infty}(\phi)$, respectively. For a given underflow solids volume fraction, ϕ_u, the maximum permitted dimensionless underflow solids flux, $Q_{u,max}$, and the maximum permitted dimensionless suspension flux, $Q_{s,max}$ are equal to the *minimum* values of Eq. (6.4.1) and Eq. (6.4.2), respectively (Fitch, 1966; Usher and Scales, 2005). For a given dimensionless underflow solids flux, Q_u, the maximum permitted dimensionless suspension flux, $Q_{s,max}$ is equal to the *maximum* value obtained via the dimensionless solids flux formula (Eq. (6.3.11)) subject to satisfying the constraint given on Q_u. For a given dimensionless suspension flux, Q_s, the maximum permitted dimensionless underflow solids flux, $Q_{u,max}$ equals the *minimum* value of Eq. (6.3.11) (Keinath, 1985; Bürger and Narváez, 2007; Grassia et al., 2014).

6.4.1 Undensified and fully densified thickeners

The theory presented up to now can be used to model and control thickener operation, but is considerably complicated by the presence of time-dependent aggregate densification. Looking at either the initially undensified or fully densified cases is simpler, and we do this in the first instance. The controllable operating parameters include the feed velocity (or the feed volumetric rate), the overflow volumetric rate, and the suspension flux (or the suspension volumetric rate). In this work, we only focus on the behaviours of the thickening zone (ignoring the clarification zone), and for the purposes of the immediate discussion, we focus on the hindered settling region only, rather than the entire thickening zone, including the consolidated bed. When controlling a thickener, there are three important operating states: the underloaded state where the proposed underflow solids flux is smaller than the limiting solids flux, the critically loaded state where the proposed under-

flow solids flux is exactly equal to the limiting solids flux, and the overloaded state where the proposed underflow solids flux is larger than the limiting solids flux and hence the solids flow upwards entering the clarification zone and effluents (Keinath, 1985; Chancelier et al., 1997a; Diehl, 2001, 2008b). Ideally, engineers may expect to operate a critically loaded and/or an underloaded thickener in practice. Thus, the dimensionless underflow solids flux, Q_u equals $Q_0\phi_f$.

Fig. 6.1 shows the maximum permitted dimensionless underflow solids fluxes determined in both undensified and fully densified systems, for a specified suspension flux. As shown in Fig. 6.1, the maximum permitted dimensionless underflow solids flux, $Q_{u,max}$ increases with the increase of the suspension flux, Q_s in both undensified and fully densified systems. For a specified suspension flux, Q_s, the maximum permitted dimensionless underflow solids flux, $Q_{u,max}$ can be read off from Fig. 6.1. Hence, the maximum permitted dimensionless feed velocity, $Q_{0,max}$ ($Q_{0,max} \equiv Q_{u,max}/\phi_f$) can also be available for a specified dimensionless suspension flux, Q_s and a given initial solids volume fraction, ϕ_f. We can also explain Fig. 6.1 in such a way that a maximum permitted dimensionless suspension flux, $Q_{s,max}$ is determined for a specified dimensionless underflow solids flux, Q_u (and/or a specified dimensionless feed velocity, Q_0).

For a specified dimensionless suspension flux, Q_s as shown in Fig. 6.1, the maximum permitted dimensionless underflow solids flux, $Q_{u,max}$ determined in a fully densified system is larger than that determined in an undensified system. For a specified dimensionless underflow solids flux, Q_u (and/or a specified dimensionless feed velocity, Q_0), the required suspension flux, Q_s determined in a fully densified system is smaller than that determined in an undensified system. The reason for the above observations is due to the much smaller aggregate diameter ratio and hence the much smaller dimensionless hindered settling function in a fully densified system which leads to a faster settling rate. If a comparatively large dimensionless suspension flux, Q_s is given in a fully densified system, the dimensionless fully densified hindered settling function, $R_{s,\infty}(\phi)$ is used in Eq. (6.3.11). On the other hand, for a sufficiently small dimensionless suspension flux, Q_s operated in a fully densified system, the minimum point of Eq. (6.3.11) will be achieved using the initially undensified hindered settling function, $R_{s,0}(\phi)$, due to a large under-

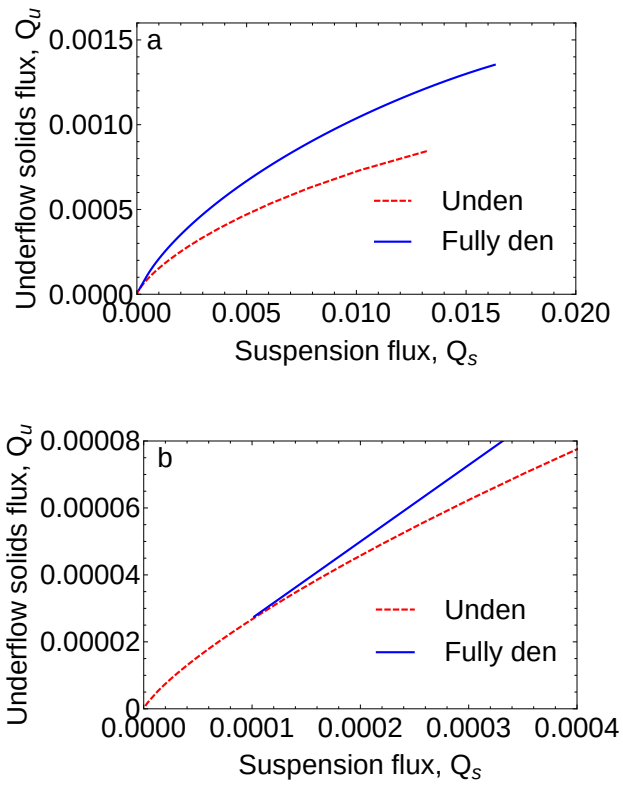

Figure 6.1: Relationships of the suspension flux, Q_s and the underflow solids flux, Q_u determined using Eq. (6.3.11) in the undensified state and the fully densified state, respectively. Note that each curve is plotted precisely over the domain where a local minimum point on the Q_u vs ϕ function *exists*; at higher Q_s values, that point might shift to the feed (Chancelier et al., 1997a). The sub-plot labelled 'b' is a zoomed picture of the sub-plot labelled 'a'.

flow solids volume fraction that is much larger than the solids volume fraction within the fully densified aggregates, $\phi_{agg,\infty}$ (Zhang et al., 2013b). The formula for $R_s(\phi, T_{res})$ coincides with that for $R_{s0}(\phi)$ in that limit (although neglect of the consolidated bed is also untenable in that limit) (Zhang et al., 2013b). This is the reason why the fully densified curve plotted in Fig. 6.1 coincides with the undensified counterpart as the dimensionless suspension flux, Q_s is sufficiently small.

Corresponding solids volume fraction

When controlling a steady state thickener, we define a so-called corresponding solids volume fraction, ϕ_{corres} to be a critical solids volume fraction that delivers a critical underflow solids flux (or equivalently the limiting solids flux). Once ϕ_{corres} is defined, ϕ_u can also be determined and turns out to be a factor $1 + |Q_{fs}(\phi_{corres})/Q'_{fs}(\phi_{corres})|$ larger

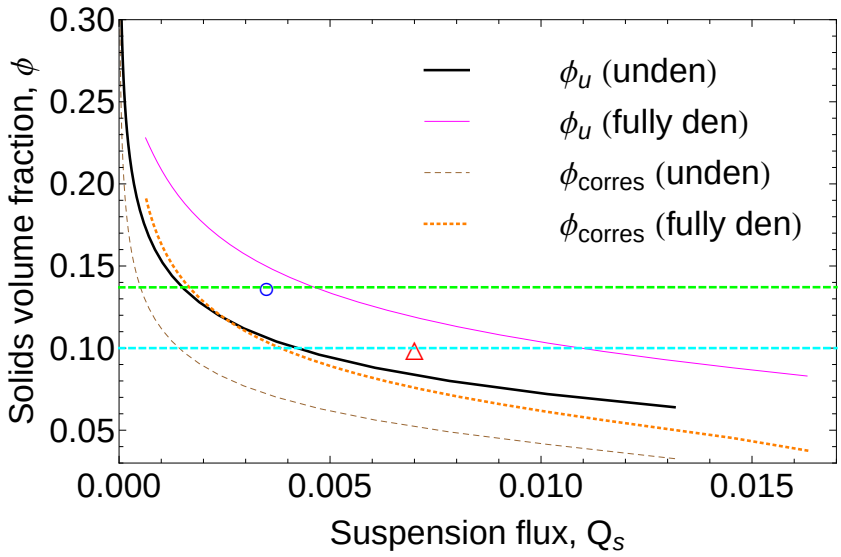

Figure 6.2: Determinations of the underflow solids volume fractions, ϕ_u for different specified dimensionless suspension flux, Q_s in both undensified and fully densified systems. Note that the relationships between the dimensionless suspension flux, Q_s and the corresponding solids volume fraction, ϕ_{corres} are also presented. The horizontal lines with '$\triangle$' and '$\circ$' represent the initially undensified gel point, $\phi_{g,0}$ and the fully densified gel point, $\phi_{g,\infty}$, respectively.

than ϕ_{corres}. The variable $Q'_{fs}(\phi_{corres})$ represents the derivative of $Q_{fs}(\phi)$ with respect to ϕ evaluated at ϕ_{corres}. Fig. 6.2 shows the maximum dimensionless suspension fluxes, $Q_{s,max}$ obtained using Eq. (6.4.2) in both undensified and fully densified systems for different specified underflow solids volume fractions, ϕ_u. We have however plotted Fig. 6.2 in the form of the solids volume fraction vs Q_s (rather than Q_s vs the solids volume fraction) so as to explain this in terms of the maximum available underflow solids volume fractions, $\phi_{u,max}$ that are achieved for different specified dimensionless suspension fluxes, Q_s. We can denote these underflow solids volume fractions by the symbol $\phi_{u,max}$ (as they deliver the maximum underflow solids flux at the given Q_s). The value of $\phi_{u,max}$ increases with the decrease of the dimensionless suspension flux, Q_s for both undensified systems and fully densified systems. As shown in Fig. 6.2, for a specified dimensionless suspension flux, Q_s, the value $\phi_{u,max}$ obtained in a fully densified system is larger than that obtained in an undensified system. Moreover, the dimensionless suspension flux, Q_s determined in an undensified system is smaller than that determined in a fully densified system for a given underflow solids volume fraction, ϕ_u.

Fig. 6.2 also shows the corresponding solids volume fractions, ϕ_{corres} determined for

specified suspension fluxes, Q_s. As shown in Fig. 6.2, the corresponding solids volume fraction, ϕ_{corres} increases with the decrease of the dimensionless suspension flux, Q_s for both undensified and fully densified systems. The curves determined in the fully densified system are above those determined in the undensified system, due to the decrease of the dimensionless hindered settling functions upon densification. Fig. 6.2 also shows that for a specified suspension flux, Q_s, the fully densified corresponding solids volume fractions, $\phi_{corres}^{full\ den}$ determined in the fully densified system tend to be larger than the fully densified gel point, $\phi_{g,\infty}$ if the undensified corresponding solids volume fraction, ϕ_{corres}^{unden} determined in the undensified system is larger than the undensified gel point, $\phi_{g,0}$ (although neglect of consolidation is then untenable). On the other hand, if $\phi_{corres}^{full\ den}$ is smaller than $\phi_{g,\infty}$, ϕ_{corres}^{unden} tends to be smaller than $\phi_{g,0}$ for a specified suspension flux, Q_s.

6.4.2 Outlook for thickeners with time-dependent densification

As discussed previously, maximum permitted underflow solids fluxes, $Q_{u,max}$ and the underflow solids volume fractions at these maxima, $\phi_{u,max}$ can be easily determined for specified suspension fluxes Q_s in both undensified and fully densified systems. If time-dependent densification occurs however, the determinations of maximum permitted underflow solids fluxes, $Q_{u,max}$ and the underflow solids volume fractions associated with these maxima, $\phi_{u,max}$ for specified suspension fluxes, Q_s are complicated, since the dimensionless densified hindered settling function, $R_s(\phi, T_{res})$ changes with both the local solids volume fraction, ϕ and the aggregate diameter ratio, D_{agg} which itself depends on the dimensionless solids residence time, T_{res}. Nevertheless, some upper bounds on the maximum permitted feed velocities, $Q_{0,max}$ (and/or the maximum permitted underflow solids fluxes, $Q_{u,max}$) and the underflow solids volume fractions associated with these maxima, $\phi_{u,max}$ for specified suspension fluxes, Q_s can be determined using the fully densified system (Grassia et al., 2014).

6.5 Analysis of the hindered settling region

In this section, we focus on the evolution of the solids volume fractions in the hindered settling region where the solids volume fraction is less than the gel point. The analysis of the solids behaviours in the hindered settling region is useful to design and control thickeners exhibiting time-dependent densification. We will also discuss the solids volume fraction profiles determined in the hindered settling regions of undensified thickeners, thickeners subject to time-dependent densification, and fully densified thickeners, respectively.

6.5.1 Undensified and fully densified thickeners with specified Q_s

At steady state, the solids flux formula (Eq. (6.3.11)) must be always valid in the hindered settling region. For a specified suspension flux, Q_s, the solids volume fraction profiles determined in the hindered settling regions of undensified and fully densified thickeners depend on the proposed feed velocity, Q_0 and/or the proposed underflow solids flux, Q_u. When a thickener is operated with a feed solids volume fraction, ϕ_f, a feed velocity, Q_0 and a proposed underflow solids flux, Q_u, it can happen that the solids volume fraction actually encountered in the hindered settling region can differ from ϕ_f. In particular when the thickener is *underloaded* it can happen that the solids volume fraction in the hindered settling region is even smaller than ϕ_f. This is believed to occur for waste water and/or biological sludges (Diehl, 2001), although the extent to which it happens when other suspensions and/or slurries are used is unknown. On the other hand for a *critically loaded* thickener, the hindered settling region selects a corresponding solids volume fraction, ϕ_{corres} (see e.g. Fig. 6.2), which is determined independently of the feed solids volume fraction (and may indeed be rather larger).

When the hindered settling region is analysed for a thickener that is (at least nominally) critically loaded, it can be divided into two cases depending upon the relationships between the corresponding solids volume fractions, ϕ_{corres} and the gel points, ϕ_g. If the corresponding solids volume fractions, ϕ_{corres}^{unden} determined in initially undensified thickeners and the corresponding solids volume fractions, $\phi_{corres}^{full\ den}$ determined in fully densified thickeners are smaller than the initially undensified gel points, $\phi_{g,0}$ and the fully den-

sified gel points, $\phi_{g,\infty}$, respectively, the solids flux formula (Eq. (6.3.11)) is satisfied. The solids volume fractions in the hindered settling regions are uniform and determined via Eq. (6.3.11) for undensified and fully densified thickeners, respectively (Bürger and Narváez, 2007). It should be noted that, in a state of critical loading, Eq. (6.3.11) may have *two* solutions: one that is smaller than the initial feed solids volume fraction, ϕ_f and the other that is larger than ϕ_f (Bürger and Narváez, 2007). A unique solution will be given by adding an entropy condition derived by Bürger and Narváez (2007), and this is the solution that we denote by ϕ_{corres} (usually $\phi_{corres} > \phi_f$ for critical loading). If ϕ_{corres}^{unden} and $\phi_{corres}^{full\ den}$ are larger than $\phi_{g,0}$ and $\phi_{g,\infty}$ determined in undensified and fully densified thickeners, respectively, consolidation must occur before ϕ_{corres} is ever attained and the proposed underflow solids flux must be below the underflow solid flux curve, due to the presence of the consolidated bed providing an upwards network force on solids. Under these circumstances in the hindered settling region, the thickener is actually underloaded (i.e. not critically loaded as first assumed) (Zhang et al., 2013a,b).

It is clear that knowing the values of ϕ_{corres} and ϕ_g is very useful for understanding the operation of undensified and fully densified thickeners. One of the objectives in what follows is to generalise the definitions of ϕ_{corres} and ϕ_g to the case of thickeners with time-dependent densification. Note that in the special case when $\phi_{corres} < \phi_g$, for undensified or fully densified thickeners, it is not necessary to define the heights and hence the solids residence times spent in the hindered settling regions (Fitch, 1966). Hence, engineers generally focus their design efforts on the determination of the required cross sectional area, B which can be calculated via using Eq. (6.2.15) (Fitch, 1966). In the case of time-dependent densification however, as we will see below, the predictions of heights and solids residence times need to be made even for $\phi_{corres} < \phi_g$.

6.5.2 Thickeners with time-dependent densification and specified Q_s

If time-dependent densification occurs for a specified suspension flux, Q_s, different proposed underflow solids fluxes, Q_u and the values of the corresponding solids volume fractions, ϕ_{corres} achieving the minimum of the underflow solids flux curves are what govern the solids volume fraction profiles in the hindered settling region. Given any

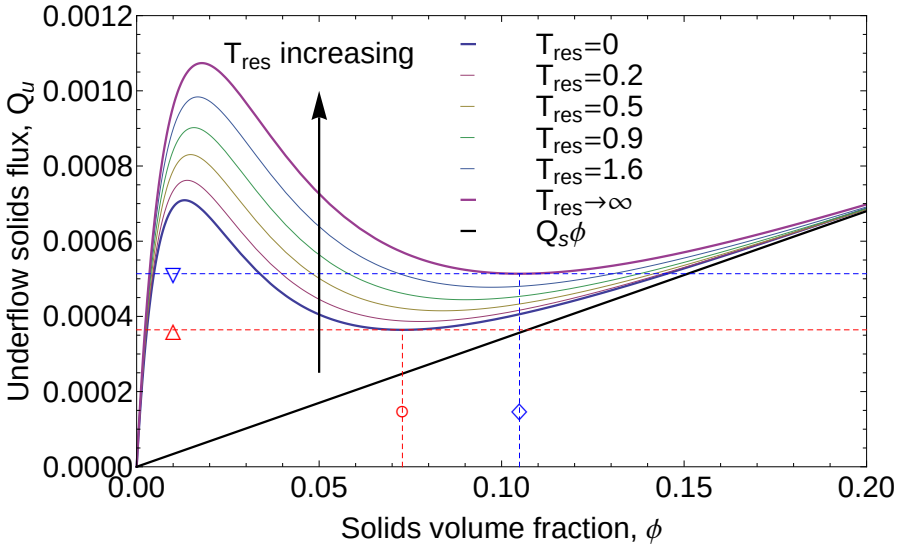

Figure 6.3: A general underflow solids flux vs. the local solids volume fraction curve. Note that this figure is plotted using the suspension flux, $Q_s = 0.0034$. $T_{res} = 0$ represents the initially undensified state and $T_{res} \to \infty$ represents the fully densified state. The horizontal lines with '$\triangle$' and '$\bigtriangledown$' represent the maximum permitted underflow solids fluxes determined in undensified and fully densified systems, respectively. The vertical lines with '$\circ$' and '$\diamond$' denote the corresponding solids volume fractions evaluated in undensified and fully densified systems, respectively.

dimensionless solids residence time, T_{res} for which aggregates have been subjected to densification at any point in the hindered settling region, and given a value of suspension flux, Q_s, we can plot an underflow solids flux, Q_u vs the solids volume fraction, ϕ curve (see e.g. Fig. 6.3): the corresponding solids volume fraction, ϕ_{corres} for time-dependent densification is defined as being the solids volume fraction giving the minimum of this curve for any particular T_{res}. In what follows, we think of T_{res} as determining the extent of densification that has occurred up to any point in the hindered settling region, and a parameter T_{corres} as determining the extent of densification that has occurred at the bottom of the hindered settling region (Grassia et al., 2014). The larger T_{corres} that is operated, the more densification that occurs in the hindered setting region, and this affects the value of ϕ_{corres} at the bottom of the hindered settling region, which we denote ϕ_{corres}^{crit}. There are two bounds of the corresponding solids volume fraction in a thickener with time-dependent densification: the lower bound that is ϕ_{corres}^{unden} and the upper bound that is $\phi_{corres}^{full\ den}$. These can be easily read off from the underflow solids flux curves such as those shown in Fig. 6.3. We analyse three situations depending upon different locations of the above two bounds.

The case $\phi_{corres}^{full\ den} < \phi_{g,\infty}$

For $\phi_{corres}^{full\ den} < \phi_{g,\infty}$, the critical corresponding solids volume fraction, ϕ_{corres}^{crit} determined using Eq. (6.3.11) with any hindered settling region corresponding solids residence time, T_{corres} is typically smaller than the so called critical densified gel point, $\phi_{g,c}$ defined as the gel point determined according to Eq. (6.3.3) and Eq. (6.3.9) using the same T_{corres}. The proposed corresponding solids residence time, T_{corres} will affect the evolution of the solids volume fractions in the hindered settling region for a specified suspension flux, Q_s. Note that the underflow solids volume fraction, ϕ_u can be larger than the critical densified gel point, $\phi_{g,c}$ at any given corresponding solids residence time, T_{corres}: it is only ϕ_{corres}^{crit} which we require to be less than $\phi_{g,c}$. When the corresponding solids residence time, T_{corres} and the suspension flux, Q_s are given, the underflow solids flux, Q_u is also determined which is the minimum value of Eq. (6.3.11) by setting T_{res} in Eq. (6.3.9) that equals T_{corres} (Grassia et al., 2014).

Our determination of the critical corresponding solids volume fraction, ϕ_{corres}^{crit} presupposes a critically loaded thickener at time T_{corres}. If on the other hand, the proposed underflow solids flux, Q_u is smaller than the maximum underflow solids flux determined in the *undensified* state, $Q_{u,max}^{unden}$, the thickener is invariably underloaded. The solids volume fraction in the hindered settling region which can be determined using Eq. (6.3.11) (or read off at each value of T_{res} from the point at which the underflow solids flux curve attains the target Q_u) decreases moving downwards the bottom of the hindered settling region (Grassia et al., 2014). Such a state is unstable and as a result the settling velocity need not be confined in the vertical but instead overturning could occur (with both horizontal and vertical velocity components) in an effort to redistribute higher solids volume fraction material below lower solids volume fraction material. A multidimensional solids flux theory might be needed in this case (Grassia et al., 2014). Nevertheless, for underloaded thickeners operated at very low suspension fluxes (and hence very low solids volume fractions in the hindered settling region), aggregate densification might not affect the solids volume fraction profiles in the hindered settling region, since the solids residence time spent in the hindered settling region will be typically very small. Little densification should take place there.

If the proposed underflow solids flux, Q_u is larger than the maximum underflow solids flux determined in the undensified state, $Q_{u,max}^{unden}$ but is smaller than that determined in the fully densified state, $Q_{u,max}^{full\ den}$, the solids volume fractions in the hindered settling region are not uniform but are determined via Eq. (6.3.11) (Grassia et al., 2014). This equation varies according to the amount of densification experienced at different points in the thickener. It is first necessary to determine a critical corresponding solids volume fraction, ϕ_{corres}^{crit} achieving the minimum value of the underflow solids flux curve plotted when setting $T_{res} = T_{corres}$. The maximum available solids volume fraction in the hindered settling region equals ϕ_{corres}^{crit} and the solids residence time spent in the hindered settling region equals T_{corres}. The maximum underflow solid flux, $Q_{u,max}$ is then evaluated at time T_{corres} and at the critical corresponding solids volume fraction, ϕ_{corres}^{crit}. The underflow solids flux must however be uniform over the entire hindered settling region. A solids volume fraction can then be obtained for each T_{res} ($0 \leq T_{res} \leq T_{corres}$) (Grassia et al., 2014). When calculating the solids volume fraction in the hindered settling region, the solution of Eq. (6.3.11) may not be unique, but the correct solution branch needs to satisfy that the solution must be larger than the initial feed solids volume fraction, ϕ_f but smaller than the critical corresponding solids volume fraction, ϕ_{corres}^{crit} (Bürger and Narváez, 2007; Grassia et al., 2014). The critical corresponding solids volume fraction, ϕ_{corres}^{crit} is most readily determined by specifying the corresponding solids residence time, T_{corres}. An alternative approach where we specify e.g. the height of the hindered settling region is much more computationally intensive (Grassia et al., 2014). The problem is that relating region heights to solids residence times relies on knowledge of the solids volume fraction and the underflow solids flux and these are only obtained directly in terms of T_{corres}, rather than in terms of region heights.

In summary, for the small underflow solids fluxes, Q_u which are equal to and/or smaller than $Q_{u,max}^{unden}$, the heights and the solids residence times required for the hindered settling region are not determined by theory. It is possible to determine a thickener's cross sectional area but not its height. However, for a larger proposed underflow solids flux, Q_u, the heights and the solids residence times associated with the hindered settling region can be determined (Grassia et al., 2014). In practice (for a given suspension flux, Q_s) it is

easiest to set the value of T_{corres} (which we interpret now as the *minimum* solids residence time permitted in the hindered settling region of the thickener to achieve our target underflow solids flux) and use this T_{corres} to fix Q_u. A minimum height in the hindered settling region (which is determined via Eq. (6.3.12)) can also be specified. Note that (in the case when $\phi_{corres}^{full\ den} < \phi_{g,\infty}$) we are free to choose any T_{corres} we like up to arbitrarily large values. The larger the T_{corres} value we choose, the closer the underflow solids flux delivered is pushed to $Q_{u,max}^{full\ den}$.

The case $\phi_{corres}^{full\ den} > \phi_{g,\infty}$ and $\phi_{corres}^{unden} < \phi_{g,0}$

In this situation, the configuration of a thickener with time-dependent densification is complicated. The problem is that if the material is considered to be in the hindered settling region, and to dewater under densification according to the hindered settling region theory just presented, eventually it may gel, i.e. the hindered settling region theory may cease to apply. Here, we assume that the proposed underflow solids flux, Q_u is larger than the maximum permitted underflow solids flux determined at the initially undensified state, $Q_{u,max}^{unden}$ but is smaller than that determined at the fully densified state, $Q_{u,max}^{full\ den}$. The critical corresponding solids volume fraction, ϕ_{corres}^{crit} determined via Eq. (6.3.11) by setting $T_{res} = T_{corres}$ could be either smaller or larger than the critical densified gel point, $\phi_{g,c}$ determined using Eq. (6.3.3) by setting $T_{res} = T_{corres}$, depending upon how much densification is assumed to occur in the hindered settling region.

If ϕ_{corres}^{crit} is smaller than $\phi_{g,c}$ for a given suspension flux, Q_s, the evolution of the solids volume fraction in the hindered settling region is the same as that analysed for cases where $\phi_{corres}^{full\ den} < \phi_{g,\infty}$. If ϕ_{corres}^{crit} is larger than $\phi_{g,c}$ for a specified suspension flux, Q_s however, this implies that the corresponding solids residence time, T_{corres} and the underflow solids flux, Q_u have been chosen too large. The theory presented in this work only exhibits physically sensible behaviour with a smaller T_{corres} value. We rationalise this behaviour as follows: physically we know that a suspension jumps from an ungelled hindered settling region to a gelled consolidated bed, but we do not know in advance where and when in the thickener that jump takes place. In fact T_{corres} is an *estimate* of time spent in the hindered settling region when that jump occurs. If the T_{corres} value we

initially select leads to ϕ_{corres}^{crit} larger than $\phi_{g,c}$, that is merely a sign that the jump to the gelled consolidated bed took place sooner than we estimated: less time is spent in the hindered settling region, and more time is spent in the bed.

The case $\phi_{corres}^{unden} > \phi_{g,0}$

For $\phi_{corres}^{unden} > \phi_{g,0}$, the critical corresponding solids volume fraction, ϕ_{corres}^{crit} determined via Eq. (6.3.11) with any T_{corres} tends to be larger than the critical densified gel point, $\phi_{g,c}$ determined at the same T_{corres}. We therefore consider that the system gels immediately into the consolidated bed without spending significant time in the hindered settling region. The solids volume fraction at the top of the bed is the undensified gel point, $\phi_{g,0}$ (Zhang et al., 2013a), and (owing to the presence of network stress) the underflow solids flux delivered can be any value up to the undensified maximum underflow solids flux, $Q_{u,max}^{unden}$.

In summary, there are various scenarios under which we can perform design calculations on the hindered settling region of critically-loaded thickeners subjected to time-dependent densification, but other scenarios in which such calculations are not possible. Depending on the relation between the corresponding solids volume fraction (that delivers the critically-loaded underflow solids flux) and the suspension gel point, it may be possible to perform these calculations for any solids residence time in the hindered settling region, or for short solids residence times (but not for longer time), or perhaps not at all. In cases when we can perform the hindered settling region calculations, the challenge now is to match the calculations onto the consolidated bed. This is addressed in the next section.

6.6 Analysis of the consolidation region

Consolidation is an important process in industrial plants since it is specifically in the consolidated bed region where the solids volume fraction can increase to a very large value. In this section, we analyse whether the consolidation region needs to be modelled during aggregate densification (for relatively modest underflow solids volume fractions, ϕ_u, the consolidated bed might be insignificant). Before describing a thickener with time-

dependent densification, it is necessary to analyse undensified and fully densified thickeners.

6.6.1 Undensified and fully densified thickeners with specified Q_s

For undensified and fully densified thickeners (where the suspension flux, Q_s and the underflow solids flux, Q_u are both specified), it is necessary to evaluate the underflow solids volume fraction, ϕ_u via Eq. (6.3.13) before further analysis of the configuration of thickeners. In an underloaded undensified thickener and/or an underloaded fully densified thickener, if ϕ_u is larger than either $\phi_{g,0}$ for an undensified thickener or $\phi_{g,\infty}$ for a fully densified thickener, it is easy to determine the bed heights, Z_b required for the consolidation region using either Eq. (6.3.14) for an undensified thickener or Eq. (6.3.16) for a fully densified thickener. The solids residence time, $T_{res,b}$ spent in the consolidation region is also easily determined via Eq. (6.3.12) once the solids volume fraction profiles in the consolidation region are obtained.

For a critically loaded undensified thickener and a critically loaded fully densified thickener, if the underflow solids volume fractions, ϕ_u are larger than $\phi_{g,0}$ for an undensified thickener and $\phi_{g,\infty}$ for a fully densified thickener, and in addition the corresponding solids volume fractions, ϕ_{corres}^{unden} and $\phi_{corres}^{full\ den}$ are smaller than $\phi_{g,0}$ and $\phi_{g,\infty}$, respectively, Eq. (6.3.14) and Eq. (6.3.16) are also used to determine bed heights needed for the consolidation regions of an undensified thickener and a fully densified thickener, respectively. The solids residence time is also predicted using Eq. (6.3.12). Note that now the proposed underflow solids fluxes can theoretically be equal to the limiting solids fluxes which are computed via Eq. (6.3.11) in both undensified and fully densified thickeners for suitably specified suspension fluxes, Q_s (a fact which follows because network forces only appear for solids volume fractions a finite amount above ϕ_{corres}^{unden} and/or $\phi_{corres}^{full\ den}$). As the suspension fluxes decrease, the corresponding solids volume fractions, ϕ_{corres}^{unden} and $\phi_{corres}^{full\ den}$ shift to larger values but calculations can still proceed provided these values are smaller than the gel points ($\phi_{g,0}$ and $\phi_{g,\infty}$, respectively).

On the other hand, if the underflow solids volume fractions, ϕ_u and the corresponding solids volume fractions ($\phi_{corrres}^{unden}$ and $\phi_{corres}^{full\ den}$) are all larger than the gel points $\phi_{g,0}$ for

a critically loaded undensified thickener and $\phi_{g,\infty}$ for a critically loaded fully densified thickener, the 'ungelled' underflow solids fluxes, Q_u determined using Eq. (6.3.11) for the specified suspension fluxes, Q_s cannot be achieved in undensified and fully densified thickeners, respectively, since the denominators of Eq. (6.3.14) and Eq. (6.3.16) become zero evaluated at the corresponding solids volume fractions. The beds then become arbitrarily tall (and may start to invade the clarification zone). There are two approaches for avoiding the above mentioned thickening failure: one that can decrease the proposed underflow solids fluxes, Q_u maintaining the same specified suspension fluxes, Q_s, and the other that can increase the suspension fluxes, Q_s maintaining the same underflow solids fluxes, Q_u. Both the above two approaches will decrease the available underflow solids volume fractions, ϕ_u. Eq. (6.3.14) and Eq. (6.3.16) are again used to determine bed heights for an undensified thickener and a fully densified thickener, respectively after adjusting the underflow solids fluxes and/or the suspension fluxes. In all these cases, the focus is upon computing the heights of (undensified or fully densified) consolidated beds. Indeed, the undensified and fully densified theories do not specify the heights of the hindered settling region, just the consolidated bed heights.

6.6.2 Thickeners with time-dependent densification and specified Q_s

In line with what was discussed above, the corresponding solids volume fractions in the *hindered* settling region turn out to be important parameters when analysing the solids behaviours and the configuration of a thickener with time-dependent densification. Thus, whether consolidation is even relevant in a thickener with time-dependent densification for a specified suspension flux, Q_s depends upon different values of the above mentioned corresponding solids volume fractions.

The case $\phi_{corres}^{full\ den} < \phi_{g,\infty}$

When the suspension flux, Q_s and the (hindered settling region) corresponding solids residence time, T_{corres} are given (with *any* value of T_{corres} now admitting a valid solution), the underflow solids flux, Q_u, the critical corresponding solids volume fraction, ϕ_{corres}^{crit}, and the underflow solids volume fraction, ϕ_u can all be determined. Whether

consolidation occurs or not depends upon the relationship between the underflow solids volume fraction, ϕ_u and the critical densified gel point, $\phi_{g,c}$ determined using Eq. (6.3.3) by setting $T_{res} = T_{corres}$. If $\phi_u < \phi_{g,c}$, consolidation will never occur in a thickener with time-dependent densification. Otherwise for $\phi_u > \phi_{g,c}$, consolidation will occur. The solids volume fraction at the top of the bed is equal to $\phi_{g,c}$, if consolidation occurs. The bed height, Z_b and hence the solids residence time, $T_{res,b}$ required for the consolidation region can be predicted using Eq. (6.3.15) and Eq. (6.3.12), respectively. Once the solids residence time required for the consolidation region is found, the total solids residence time, T_{res}^{total} required in a thickener with time-dependent densification which is the sum of T_{corres} and $T_{res,b}$ can also be determined. Note that the critical densified gel point, $\phi_{g,c}$ which is typically larger than ϕ_{corres}^{crit} could be any value ranging between the undensified gel point, $\phi_{g,0}$ and the fully densified gel point, $\phi_{g,\infty}$, depending on different proposed T_{corres}.

For ϕ_u which is larger than $\phi_{g,\infty}$, consolidation must invariably occur. Moreover if the solids residence time spent in the hindered settling region is sufficiently long, the consolidation region becomes fully densified and hence the solids volume fraction at the top of the bed is the fully densified gel point, $\phi_{g,\infty}$. Then Eq. (6.3.16) and Eq. (6.3.12) are used for the determinations of the bed height, Z_b and hence the solids residence time, $T_{res,b}$ required for the consolidation region, respectively.

The case $\phi_{corres}^{full\ den} > \phi_{g,\infty}$ and $\phi_{corres}^{unden} < \phi_{g,0}$

For this case, as a suspension flux, Q_s and a corresponding solids residence time, T_{corres} are given, the critical corresponding solids volume fraction, ϕ_{corres}^{crit} is either smaller than or larger than the critical gel point, $\phi_{g,c}$ determined at $T_{res} = T_{corres}$ depending upon how much densification is assumed to occur in the hindered settling region. We focus now on relatively small values of T_{corres} for which $\phi_{corres}^{crit} < \phi_{g,c}$. Both the proposed underflow solids flux, Q_u and the underflow solids volume fraction, ϕ_u can be determined when Q_s and T_{corres} are specified.

For $\phi_{corres}^{crit} < \phi_{g,c}$ and ϕ_u which is also smaller than $\phi_{g,c}$, there is no consolidated bed observed in a thickener with time-dependent densification. For $\phi_{corres}^{crit} < \phi_{g,c}$ but

ϕ_u which is larger than $\phi_{g,c}$ however, the consolidated bed should exist and the solids volume fraction at the top of the bed equals the critical densified gel point, $\phi_{g,c}$. Hence, the bed height, Z_b and the solids residence time, $T_{res,b}$ spent in the consolidation region are calculated using Eq. (6.3.15) and Eq. (6.3.12), respectively.

The case $\phi_{corres}^{unden} > \phi_{g,0}$

For cases where $\phi_{corres}^{unden} > \phi_{g,0}$, consolidation must occur in a thickener with time-dependent densification. We consider that the suspension gels immediately (the solids volume fraction being the undensified gel point, $\phi_{g,0}$ at the top of the bed) and therefore do not attempt to model the hindered settling region. We are free to set Q_s and Q_u independently, subject to the constraint that Q_u must not exceed $Q_{u,max}^{unden}$. When Q_u is chosen close to $Q_{u,max}^{unden}$, it is known that ϕ_u is strictly greater than ϕ_{corres}^{unden}, which in turn exceeds $\phi_{g,0}$ in this case. The consolidated bed might be determined using the theory presented in Zhang et al. (2013a).

6.7 Case studies

In this section, eight cases are illustrated. We choose two specified suspension fluxes, Q_s and two corresponding solids residence times, T_{corres} to analyse the solids behaviours in thickeners with time-dependent densification. Hence, four underflow solids fluxes, Q_u are evaluated. A large suspension flux, Q_s ($Q_s = 0.0034$) is given in Cases 1–4 whilst an intermediate suspension flux, Q_s ($Q_s = 0.0015$) is given in Cases 5–8. Two densification rate parameters, A which are chosen from previous studies ($A = 0.01\,\mathrm{s}^{-1}$ and $A = 0.001\,\mathrm{s}^{-1}$, respectively (Zhang et al., 2013a,b)) are considered in this work. Odd numbered cases have the smaller densification rate parameter, A ($A = 0.001\,\mathrm{s}^{-1}$). Even numbered cases operate the larger densification rate parameter, A ($A = 0.01\,\mathrm{s}^{-1}$). The solids volume fraction within the initially undensified aggregates, $\phi_{agg,0}$, the solids volume fraction within the fully densified aggregates, $\phi_{agg,\infty}$, and the fully densified gel point, $\phi_{g,\infty}$ are chosen to be 0.1667, 0.2286, and 0.1372, respectively, with the undensified gel point being $\phi_{g,0} = 0.1$ (Usher et al., 2009; Zhang et al., 2013a,b). The final aggregate diameter ratio, $D_{agg,\infty} = 0.9$ (Usher et al., 2009; Zhang et al., 2013a,b). The

density difference between the solids and the liquid is assumed to be $2200\,\mathrm{kg\,m^{-3}}$ (Usher et al., 2009; Zhang et al., 2013a). Rheological property values have been specified in Sections 6.2 and 6.3. In particular for the value $R_{Stokes,0}$ ($R_{Stokes,0} = 260469\,\mathrm{Pa\,s\,m^{-2}}$) given in Section 6.2, the Stokes settling velocity, $u_{Stokes,0} = 0.08277\,\mathrm{m\,s^{-1}}$. The fact that settling is hindered however gives typical velocities much smaller than $u_{Stokes,0}$.

Table 6.1 shows details of different operating parameters given in each case. In this work, for a specified suspension flux, Q_s, the *minimum* value on the underflow solids flux vs. the local solids volume fraction curve obtained at the fully densified state ($D_{agg} = D_{agg,\infty} = 0.9$) is always smaller than the *maximum* value on the underflow solids flux vs. the solids volume fraction curve determined at the undensified state ($D_{agg} = D_{agg,0} = 1$). In other words, pre-shearing of aggregates is not needed prior to the hindered settling region (a considerable simplification; see Grassia et al. (2014) for details). Table 6.1 also shows that the underflow solids volume fractions, ϕ_u obtained in Cases 1–8 are larger than the critical densified gel points, $\phi_{g,c}$. Thus, consolidation may occur in Cases 1–8. The critical corresponding solids volume fractions, ϕ^{crit}_{corres} calculated in Cases 1–8 are all smaller than $\phi_{g,c}$. Thus, the solids volume fraction at the top of the bed is equal to $\phi_{g,c}$ for those cases. The high suspension flux cases (e.g. Cases 1–4) actually exhibit that $\phi^{full\ den}_{corres}$ is smaller than $\phi_{g,\infty}$ meaning that solutions of Eq. (6.3.11) can be found for any T_{corres} (even though we only contemplate two given T_{corres} values in Table 6.1). The low suspension flux cases (e.g. Cases 5–8) have $\phi^{full\ den}_{corres}$ larger than $\phi_{g,\infty}$ but ϕ^{unden}_{corres} smaller than $\phi_{g,0}$. It turns out that (as we shall discuss later) solutions of Eq. (6.3.11) coupling the hindered settling region and the consolidated bed can only be obtained when the corresponding solids residence time, T_{corres} is less than a critical value ($T_{corres} \approx 0.378$) – although this is larger than the T_{corres} values contemplated in Table 6.1.

	Q_s	T_{corres}	Q_u	ϕ_u	ϕ^{crit}_{corres}	$\phi_{g,c}$
unden	0.0034	N/A	0.000364	0.1071	0.0728	0.1
Cases 1–2	0.0034	0.05	0.000370	0.1088	0.0741	0.1014
Cases 3–4	0.0034	0.3	0.000397	0.1166	0.0798	0.1082
Full den	0.0034	N/A	0.000513	0.1509	0.1049	0.1372
unden	0.0015	N/A	0.000205	0.1367	0.0982	0.1
Cases 5–6	0.0015	0.05	0.000208	0.1390	0.0999	0.1014
Cases 7–8	0.0015	0.3	0.000222	0.1483	0.1078	0.1082
Full den	0.0015	N/A	0.000285	0.19	0.1420	0.1372

Table 6.1: Operating parameters for Cases 1–8 and comparisons between undensified and fully densified cases (at critical loading for the given Q_s). The underflow solids flux, Q_u, and the underflow solids volume fraction, ϕ_u are determined using Eq. (6.3.11), and Eq. (6.3.13), respectively. Recall that the undensified gel point, $\phi_{g,0} = 0.1$ and the fully densified gel point, $\phi_{g,\infty} = 0.1372$.

6.8 Results and discussion

The simulation results presented below include the evolutions of the densified sludge rheological properties including the densified compressive yield stress, $p_y(\phi, T_{res})$ and the densified hindered settling function, $R_s(\phi, T_{res})$, the solids volume fraction profiles in both the hindered settling region and the consolidation region, bed heights, and solids residence times required for achieving the calculated underflow solids volume fractions, ϕ_u.

6.8.1 Evolution of sludge rheological properties

In the hindered settling region, the compressive yield stress, $p_y(\phi, T_{res})$ is nil, since aggregates settle separately in the hindered settling region (van Deventer, 2012). In the consolidation region however, the compressive yield stress, $p_y(\phi, T_{res})$ must be considered (Usher et al., 2009; van Deventer, 2012). Here, the evolutions of the above mentioned sludge rheological properties determined in both the hindered settling region and the consolidation region are presented.

Densified compressive yield stress, $p_y(\phi, T_{res})$

Figs 6.4–6.5 show the evolution of the compressive yield stress during aggregate densification for Cases 1–8. For a specified suspension flux, Q_s, and a specified aggregate densification rate parameter, A, the more densification that occurs in the hindered settling region, the smaller the compressive yield stress, $p_y(\phi, T_{res})$ that is obtained in the consolidation region for a given local solids volume fraction, since more densification occurring in the hindered settling region can lead to larger densified gel points at the top of the bed associated with smaller aggregate diameter ratios entering the consolidating bed. When the dimensionless suspension fluxes, Q_s, and the dimensionless corresponding solids residence times, T_{corres} are specified, the dimensionless compressive yield stresses determined using larger aggregate densification rate parameters are smaller than those obtained using smaller aggregate densification rate parameters when the local solids volume fractions are given, due to more rapid decreases in the aggregate diameter ratios in those cases where larger aggregate densification rate parameters are given. As shown in

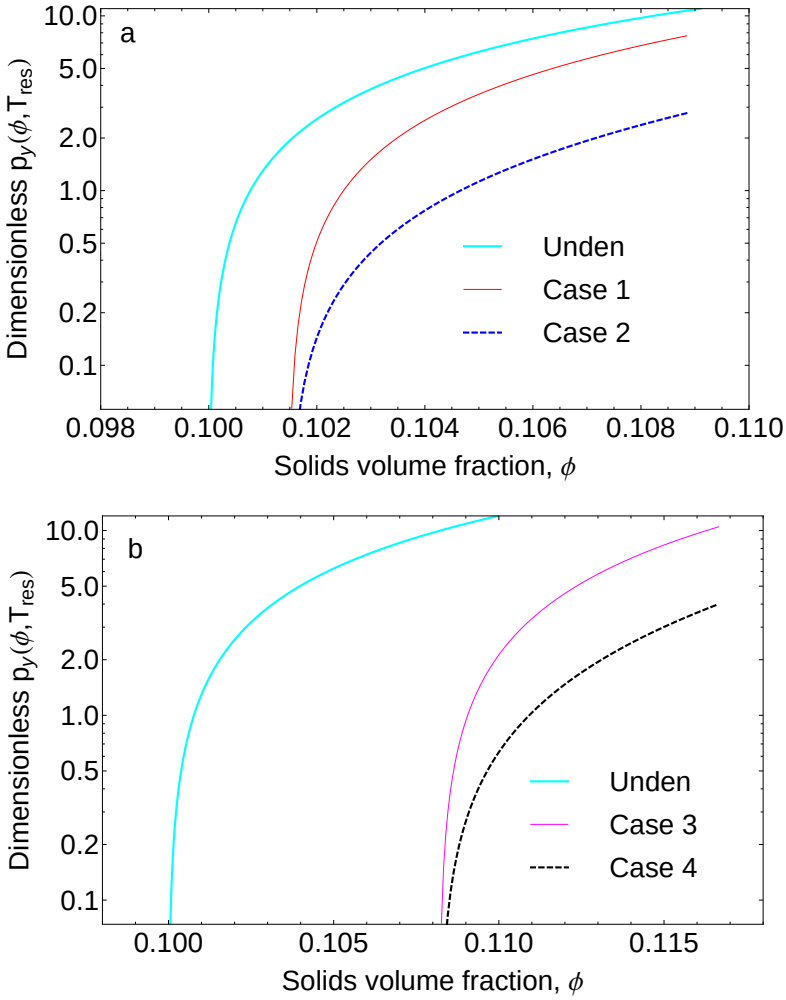

Figure 6.4: Evolutions of the dimensionless compressive yield stresses, $p_y(\phi, T_{res})$ for Cases 1–4. The fully densified compressive yield stresses are not shown here, since the system is not dewatered as far as the fully densified state gel point. Note that the curves for Cases 1–2 start from the same point which is the critical densified gel point. Again, the curves for Cases 3–4 start from the identical value which is also the critical densified gel point. Recall that the sub-plots labelled 'a' and 'b' are plotted using $T_{corres} = 0.05$ and $T_{corres} = 0.3$, respectively. In addition, the dimensionless suspension flux, Q_s given in Cases 1–4 is 0.0034.

Fig. 6.5, for larger solids volume fractions, the system is densified to the fully densified state when the larger aggregate densification rate parameter and the larger corresponding solids residence time are specified (e.g. Case 8).

Densified hindered settling function, $R_s(\phi, T_{res})$

The evolutions of the hindered settling function in the hindered settling region as well as in the consolidation region are presented here. Fig. 6.6 shows the evolutions of the hin-

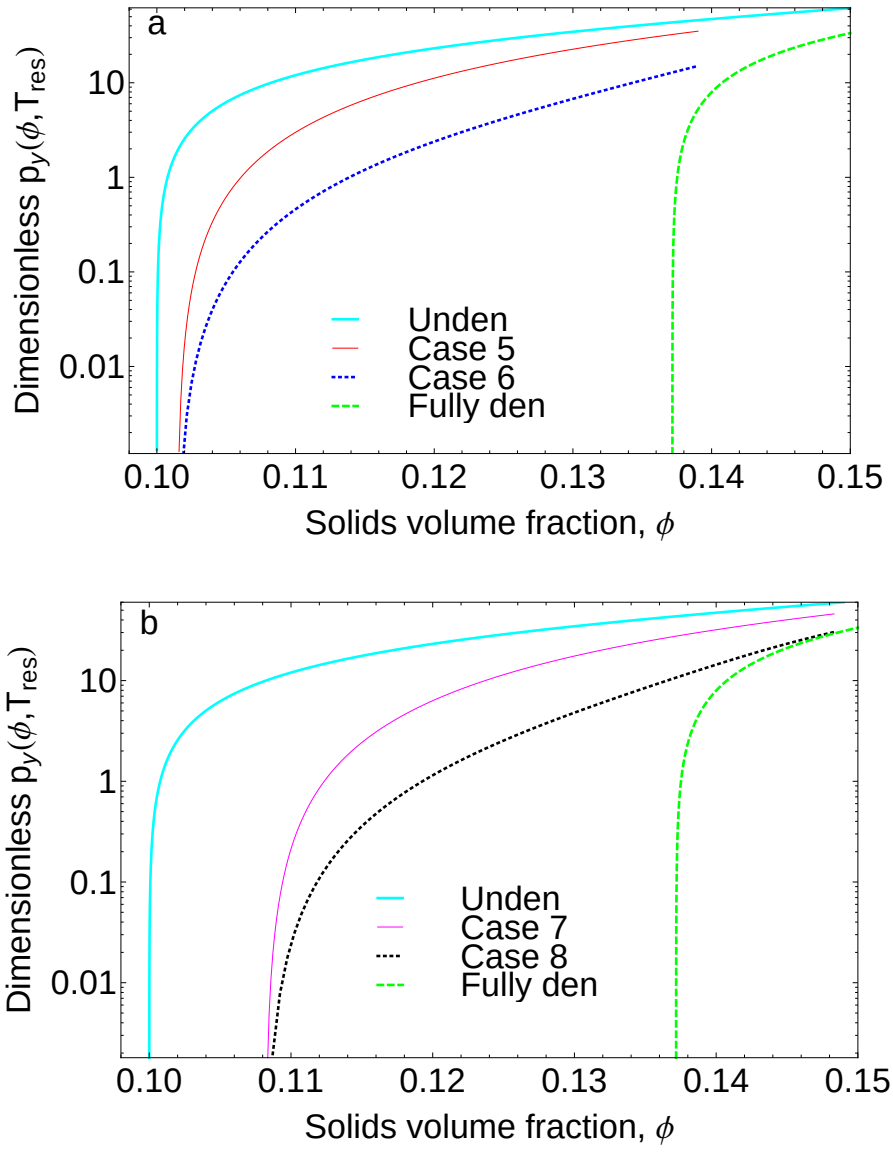

Figure 6.5: Evolutions of the dimensionless compressive yield stresses, $p_y(\phi, T_{res})$ for Cases 5–8. Recall that $T_{corres} = 0.05$ and $T_{corres} = 0.3$ are given in Cases 5–6 and Cases 7–8, respectively. The dimensionless suspension flux, $Q_s = 0.0015$ for Cases 5–8.

dered settling functions determined in the hindered settling region[2]. The dimensionless hindered settling functions, $R_s(\phi, T_{res})$ obtained in the hindered settling region increase with the increase of the local solids volume fractions from the feed point to the bottom of the hindered settling region for each case. As shown in Fig. 6.6, for a specified dimensionless suspension flux, Q_s, the dimensionless hindered settling function, $R_s(\phi, T_{res})$ determined in the hindered settling region becomes smaller for a given solids volume fraction

[2]Note that the effect of the densification rate parameter has been scaled out of the hindered settling region, therefore, the hindered settling functions determined in Cases 2, 4, 6, and 8 are identical for any given solids volume fraction to those determined in Cases 1, 3, 5, and 7.

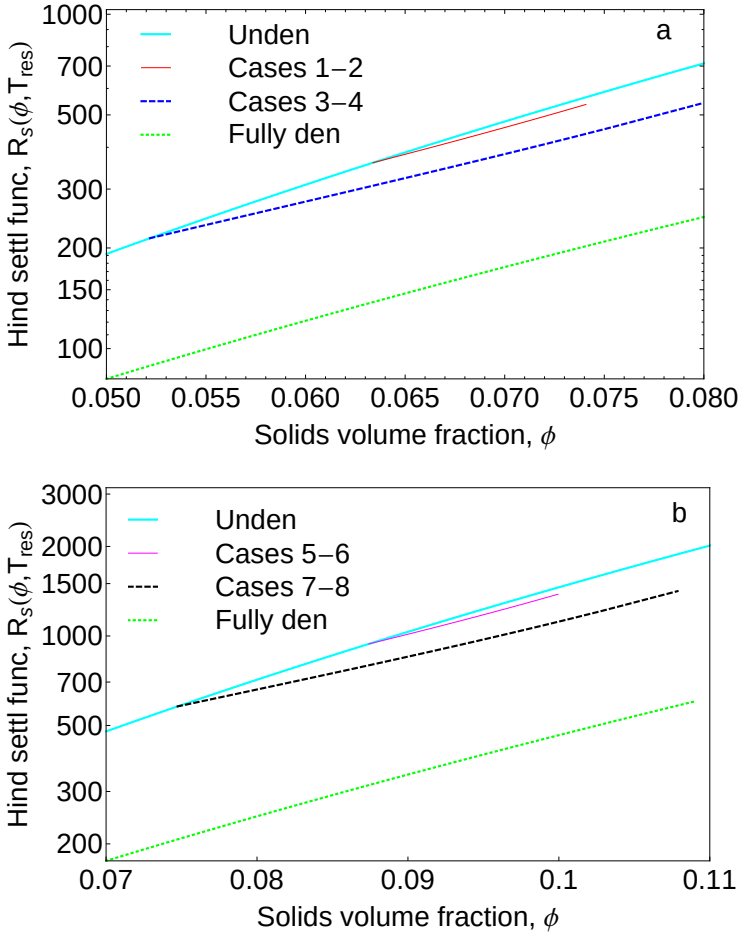

Figure 6.6: Evolutions of the dimensionless hindered settling functions, $R_s(\phi, T_{res})$ obtained in the hindered settling region for Cases 1–8. Recall that according to our chosen dimensionless scales, the *dimensionless* hindered settling functions determined in odd numbered cases are analogous to those determined in adjacent even numbered cases when the dimensionless suspension flux and the dimensionless corresponding solids residence time are specified. The sub-plots labelled 'a' and 'b' are plotted using a large suspension flux, $Q_s = 0.0034$ and an intermediate suspension flux, $Q_s = 0.0015$, respectively.

as more densification occurs in the hindered settling region, associated with aggregates attaining smaller diameters.

Figs. 6.7–6.9 show the determinations of the dimensionless hindered settling function, $R_s(\phi, T_{res})$ determined in the consolidation region. The dimensionless hindered settling functions, $R_s(\phi, T_{res})$ determined for Cases 1–4 in the consolidation region increase with the increase of the local solids volume fraction from the top of the bed to the bottom of the consolidation region. These are cases for which the gel point at the top of the bed, $\phi_{g,c}$ is quite some distance above ϕ^{crit}_{corres} (see Table 6.1), meaning that significant network stress gradients are required at the top of the bed to balance the resultant of gravity and

viscous drag (gravity and viscous drag only being in balance at ϕ_{corres}^{crit} not at $\phi_{g,c}$). To support these network stresses, the solids volume fraction must grow rapidly moving into the bed, and it is known that if the solids volume fraction grows more rapidly than the gel point itself, then $R_s(\phi, T_{res})$ must also grow (Zhang et al., 2013a). If the dimensionless suspension flux, Q_s, and the dimensionless corresponding solids residence time, T_{corres} are specified, the dimensionless hindered settling functions, $R_s(\phi, T_{res})$ determined in cases where larger aggregate densification rate parameters are given are smaller than those calculated in cases where smaller aggregate densification rate parameters are given for any specified local solids volume fractions. The reason for the above observations is due to a greater extent of densification happening in situ within the bed when larger aggregate densification rate parameters are given for a specified Q_s and a specified T_{corres}.

As shown in Fig. 6.8, for Cases 5–8, the dimensionless hindered settling functions, $R_s(\phi, T_{res})$ determined in the consolidation region decrease with the increase of the local solids volume fractions at early times and then increase with the increase of the local solids volume fractions later on. Zhang et al. (2013a,b) proposed an approximated functional form of the dimensionless hindered settling function, $\tilde{R}_s(\phi, T_{res})$ for suspension solids volume fraction significantly below the solids volume fraction within the aggregates themselves (see details in Zhang et al. (2013b))

$$\tilde{R}_s(\phi, T_{res}) \approx \frac{D_{agg}(1-\phi)^2 R_{s,0}(\phi_{g,0}\phi/\phi_g)}{(1-\phi_{g,0}\phi/\phi_g)^2} \tag{6.8.1}$$

where recall that $R_{s,0}(\phi_{g,0}\phi/\phi_g)$ represents the dimensionless undensified hindered settling function, which now is evaluated at a solids volume faction ϕ that times $\phi_{g,0}/\phi_g$. This solids volume fraction is smaller than the true solids volume fraction, ϕ.

At early times, shortly after entering the bed, the rate of change of the local solids volume fraction near the top of the bed roughly equals that of the densified gel point in the consolidation region for Cases 5–8 (Zhang et al., 2013a). This ultimately follows from the small difference between ϕ_{corres}^{crit} and $\phi_{g,c}$ reported in Table 6.1. Since gravity and viscous drag balance perfectly at ϕ_{corres}^{crit}, they are still in near balance upon entering the top of the bed at the solids volume fraction, $\phi_{g,c}$. The first two terms in the numerator

of Eq. (6.3.15) balance and the remaining terms in Eq. (6.3.15) then maintain $p_y(\phi, T_{res})$ roughly constant, which is achieved by keeping ϕ close to ϕ_g. Referring to Eq. (6.8.1), we see that the $R_{s,0}(\phi_{g,0}\phi/\phi_g)$ term remains roughly fixed (as its argument is fixed) and the denominator of Eq. (6.8.1) is likewise fixed. The remaining terms in the numerator of Eq. (6.8.1) then give a weak decrease in the dimensionless hindered settling function, $R_s(\phi, T_{res})$ as the local solids volume fraction, ϕ increases in line with the densified gel point, ϕ_g, and as the aggregate diameter ratio, D_{agg} shrinks due to densification (Zhang et al., 2013a). This situation persists until ϕ increases sufficiently that the balance of the first two terms in the numerator of Eq. (6.3.15) is lost. Then, the rate of change of the local solids volume fraction will exceed that of the densified gel point, the dimensionless hindered settling functions, $R_s(\phi, T_{res})$ increase again. Similar observations are also obtained in Zhang et al. (2013a). The hindered settling function curve for Case 8 approaches the fully densified hindered settling function curve, since Case 8 is densified nearly to the fully densified state at later times. Case 6 is also seen to migrate relatively close to the fully densified state, although to a lesser extent than Case 8.

6.8.2 Solids volume fraction profiles in a thickener subject to time-dependent densification

The solids volume fraction profiles determined in thickeners with time-dependent densification involve two parts: the solids volume fraction profiles obtained in the hindered settling region and the solids volume fraction profiles obtained in the consolidation region. Note that in addition to the profile in the hindered settling region and the profile in the consolidated bed, there is also a jump from the bottom of the hindered settling region (the critical solids volume fraction, ϕ_{corres}^{crit}) to the top of the consolidated bed (the critical densified gel point, $\phi_{g,c}$). We require $\phi_{corres}^{crit} < \phi_{g,c}$ here, but first we verify whether that expectation is borne out.

Comparison between ϕ_{corres}^{crit} and $\phi_{g,c}$

Figs. 6.10–6.11 show the evolution of the corresponding solids volume fractions with different specified dimensionless corresponding solids residence time for specified sus-

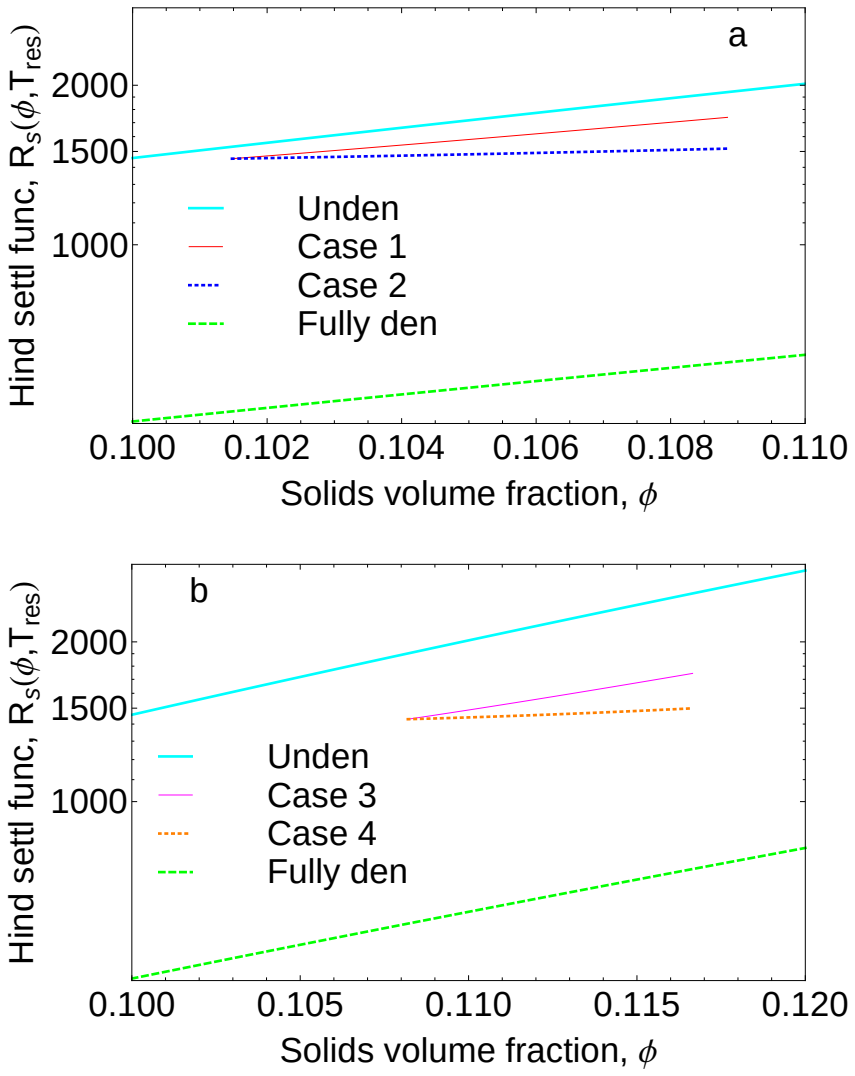

Figure 6.7: Evolutions of the dimensionless hindered settling functions, $R_s(\phi, T_{res})$ in the consolidation region for Cases 1–4. Note that the sub-plots labelled 'a' and 'b' are plotted using $T_{corres} = 0.05$ and $T_{corres} = 0.3$, respectively.

pension fluxes. In cases when the corresponding solids volume fraction curve shown in Fig. 6.10 is always underneath the gel point curve, it implies that the corresponding solids residence time, T_{corres} can be any value and the theory presented in this work can be applied (e.g. Cases 1–4). As shown in Fig. 6.11 however, in certain cases, the corresponding solids volume fraction curve intersects the gel point curve at some critical point ($T_{corres} \approx 0.378$). If the corresponding solids residence time, T_{corres} is larger than that intersection point, we interpret this to mean that T_{corres} has been chosen too large, and the system jumps into a consolidated bed sooner than we anticipated. We can however perform calculations with smaller T_{corres} values (e.g. Cases 5–8).

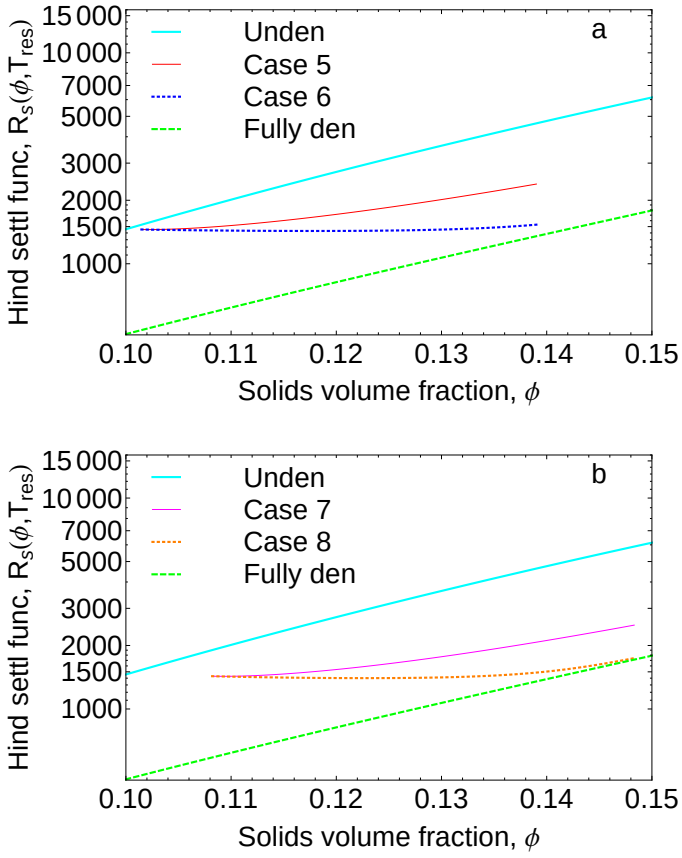

Figure 6.8: Evolutions of the dimensionless hindered settling functions, $R_s(\phi, T_{res})$ in the consolidation region for Cases 5–8. Recall that $T_{corres} = 0.05$ and $T_{corres} = 0.3$ are used to plot the sub-plots labelled 'a' and 'b', respectively.

Solids volume fraction profiles in the hindered settling region

Fig. 6.12 presents the evolution of the solids volume fractions in the hindered settling region for specified suspension fluxes and corresponding solids residence times. The maximum solids volume fraction achieved in the hindered settling region and the calculated underflow solids volume fraction obtained at the bottom of the thickener increase with the increase of the corresponding solids residence time for a specified suspension flux. In other words, for a specified suspension flux, more densification occurring in the hindered settling region leads to a larger solids volume fraction obtained at the bottom of the hindered settling region, and in addition a larger underflow solids volume fraction obtained at the bottom of the thickener. For a specified suspension flux and a specified corresponding solids residence time, although the heights required for the hindered settling region under our chosen dimensionless scales have exactly identical values for dif-

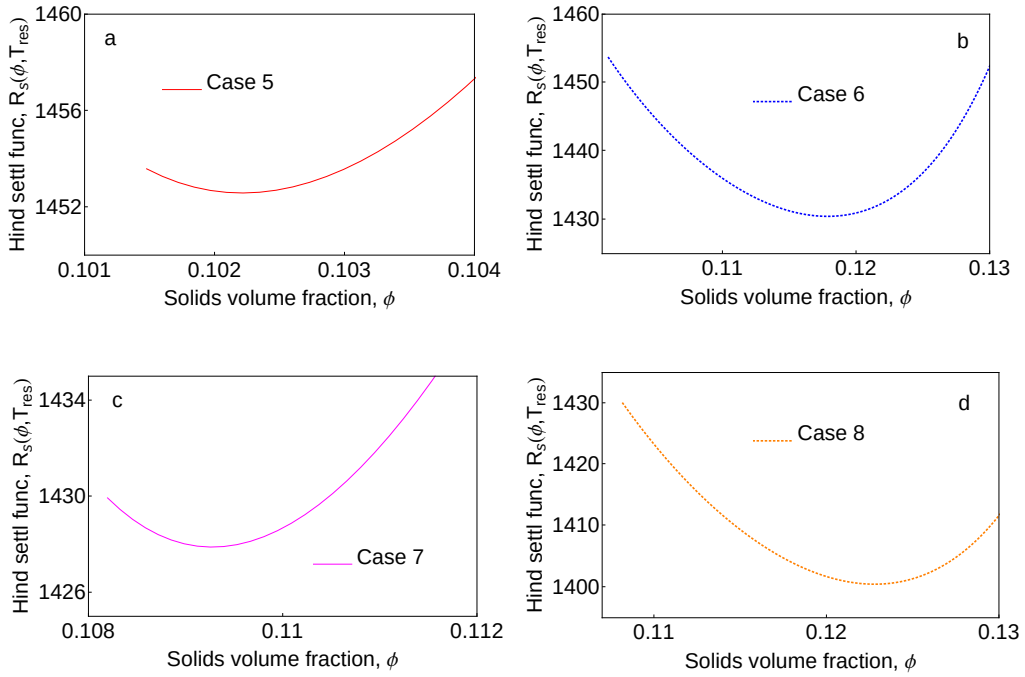

Figure 6.9: Zoomed hindered settling functions, $R_s(\phi, T_{res})$ determined in the consolidation region for Cases 5–8.

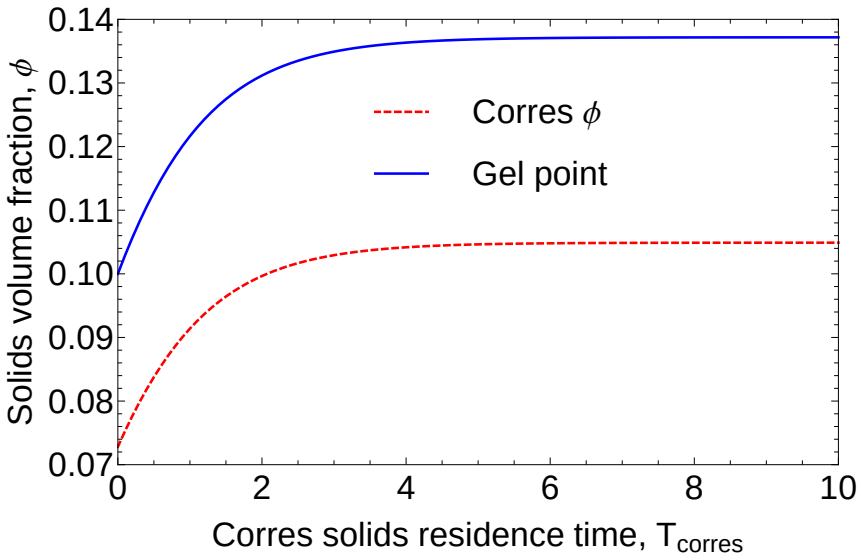

Figure 6.10: Evolution of the corresponding solids volume fraction, ϕ_{corres} with different corresponding solids residence time, T_{corres} – the large suspension flux, $Q_s = 0.0034$. Note that the gel point is determined via Eq. (6.3.3) with different T_{corres}.

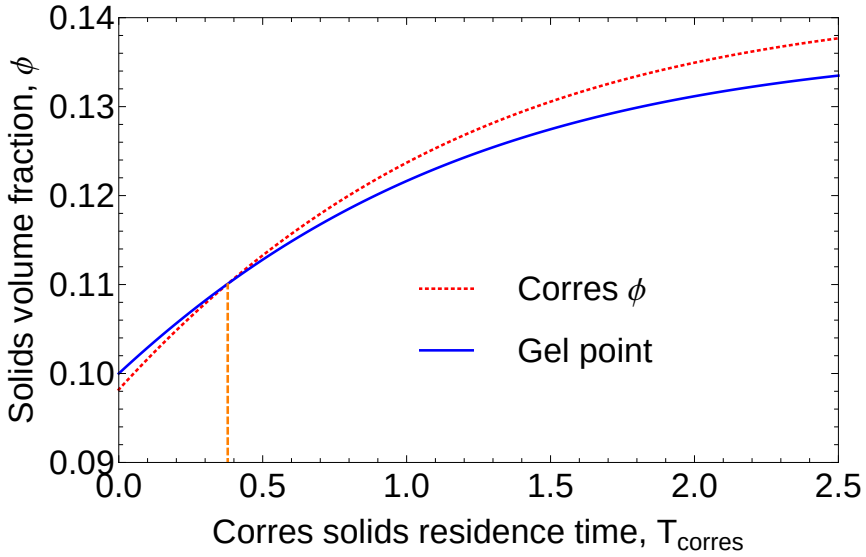

Figure 6.11: Evolution of the corresponding solids volume fraction, ϕ_{corres} with different corresponding solids residence time, T_{corres} – the intermediate suspension flux, $Q_s = 0.0015$. The vertical line represents the intersection point between the corresponding solids volume fraction curve and the gel point curve. The corresponding solids residence time at this intersection point is roughly 0.378. Again the gel point is evaluated using Eq. (6.3.3).

ferent aggregate densification rate parameters, shorter *dimensional* heights are required for the hindered settling region as a larger aggregate densification rate parameter, A is given, since densification occurs more rapidly in the hindered settling region for a larger aggregate densification rate parameter, A. Fig. 6.12 also shows that more densification of aggregates occurring in the hindered settling region leads to taller heights required for the hindered settling region, if the suspension flux is specified. Unsurprisingly more distance is covered in a longer corresponding solids residence time. However densification can also lead to slightly faster settling velocities averaged over the hindered settling region, meaning that the height of the hindered settling region can grow slightly faster than the growth in T_{corres}.

Solids volume fraction profiles in the consolidation region

Here, we present the solids volume fraction profiles in the consolidated bed, from which bed heights can be readily determined. It can be deduced from Table 6.1, consolidation will occur for all the Cases 1–8, since the underflow solids volume fractions, ϕ_u calculated for those cases are larger than the critical densified gel points, $\phi_{g,c}$. Figs. 6.13–

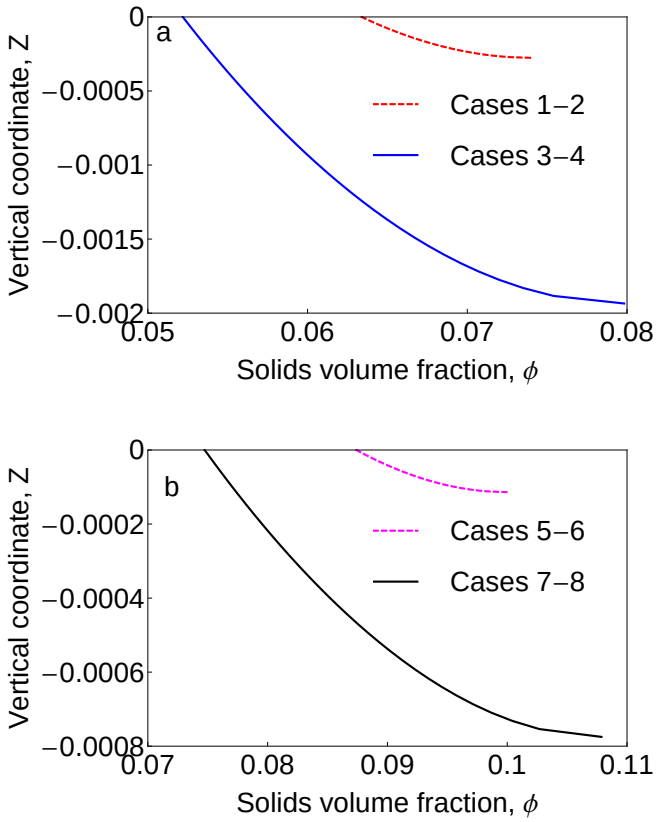

Figure 6.12: Evolutions of the solids volume fractions in the hindered settling region. Note that there is no difference between adjacent odd and even numbered cases, since they only differ in their value of the densification rate parameter, A. However the effect of this parameter has been scaled out of the hindered settling region. The sub-plots labelled 'a' and 'b' are plotted using a large suspension flux ($Q_s = 0.0034$) and an intermediate suspension flux, ($Q_s = 0.0015$), respectively. Recall that T_{corres} equals 0.05 for Cases 1–2 and Cases 5–6, and equals 0.3 for Cases 3–4 and Cases 7–8.

6.14 present the solids volume fraction profiles obtained in the consolidation region. For a specified suspension flux, Q_s and a specified aggregate densification rate parameter, A, the bed height required for the consolidation region increases with the increase of the dimensionless corresponding solids residence time, T_{corres} (compared Cases 1 vs 3, Cases 2 vs 4, Cases 5 vs 7, Cases 6 vs 8). In other words, more densification that occurs in the hindered settling region leads to a taller bed height required for the consolidation region when the suspension fluxes, and the aggregate densification rate parameters are specified. This is due to larger underflow solids volume fractions, associated with larger underflow solids fluxes. These larger underflow solids volume fractions need more bed heights to be attained despite the more densified aggregates entering the top of the bed. As shown in Figs. 6.13–6.14, the top of the beds are situated at the same coordinate location if the

solids volume fractions at the top of the bed are the same (e.g. Cases 1–2, 3–4, 5–6, and 7–8). This is a result of both the location of the top of the bed and the solids volume fraction there being set by the behaviour in the hindered settling region.

Fig. 6.14 shows that Cases 5–6 have the same slope near the top of the bed, since (owing to the fact that $\phi_{g,c}$ is only very slightly above ϕ_{corres}^{crit}) the solids volume fraction near the top of the bed needs to be at a level where gravity and viscous drag nearly match and the rate of change of the solids volume fraction is approximately identical to that of the densified gel point[3] near the top of the bed for Cases 5–6 (Zhang et al., 2013a). Similar observations are also found for Cases 7–8. Another interesting observation in Fig. 6.14 is the steep increase of the slope in Case 6 and Case 8 towards the bottom of the bed. These two cases end up fairly close to full densification. Near the bottom of the bed then, for Case 6 and Case 8, $\partial p_y(\phi, T_{res})/\partial T_{res}$ (the third term on the right hand side of Eq. (6.3.15)) vanishes. The middle term in the numerator of Eq. (6.3.15) always vanishes near the bottom of the bed (a manifestation of a no slip condition imposed between the solids and liquid there) (Martin, 2004; Zhang et al., 2013b; Grassia et al., 2014). Hence, we are left in Case 6 and Case 8 with a (gravity)-(fully densified network stress) balance at the bottom of the bed. The steepening of the slope $\mathrm{d}Z/\mathrm{d}\phi$ observed in Fig. 6.14 reflects a steep $\mathrm{d}p_y(\phi, T_{res})/\mathrm{d}\phi$ at the comparatively high solids volume fraction in the fully densified system (this also corresponds to the so called stress limit in Martin (2004)). Although conventionally we think of network stresses in densified systems as being less than their undensified counterparts, eventually (at the solids volume fraction within the aggregates, ϕ_{agg}) the densified and undensified network stresses must match, and this constraint then leads to an increase in the gradient $\mathrm{d}p_y(\phi, T_{res})/\mathrm{d}\phi$, and hence the large $\mathrm{d}Z/\mathrm{d}\phi$ observed in Fig. 6.14.

Finally we turn to the effect of varying the densification rate parameter, A (comparing the adjacent odd and even numbered cases). Although the *dimensionless* bed height calculated using a *small* aggregate densification rate parameter, A is *shorter* than that obtained using a *large* aggregate densification rate parameter, A, this is a result of our chosen dimensionless scale ($Z = z\Delta\rho g\alpha/a_0$). The *dimensional* bed height determined

[3]The result that ϕ changes at the same rate as ϕ_g follows from Eq. (6.3.15) under conditions when the first two terms in the numerator of Eq. (6.3.15) nearly cancel.

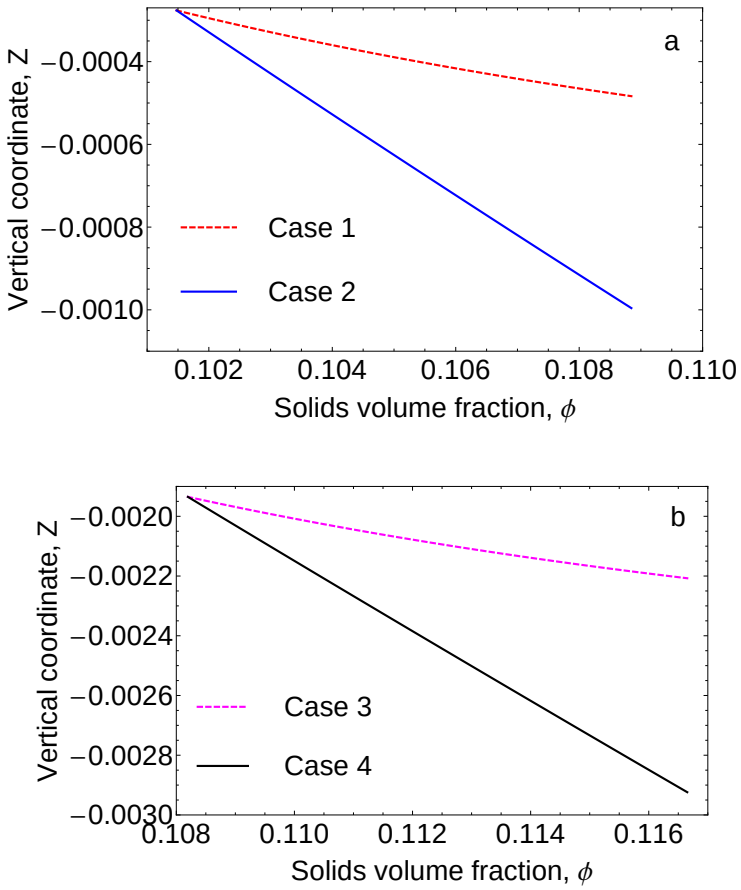

Figure 6.13: Solids volume fraction profiles determined in the consolidation region for the specified suspension flux, $Q_s = 0.0034$. Recall that the sub-plot labelled 'a' presents the results calculated using a small corresponding solids residence time ($T_{corres} = 0.05$) whilst the sub-plot labelled 'b' presents the profiles obtained using a large T_{corres} ($T_{corres} = 0.3$). The origin of the vertical coordinate, Z is placed at the top of the hindered settling region, and Z is measured upwards. Thus, the top of the consolidation region is already at a negative value of Z.

using a *large* aggregate densification rate parameter, A is *shorter* than that predicted using a *small* aggregate densification rate parameter, A, when the suspension flux and the corresponding solids residence time are both specified.

6.8.3 Total solids residence times and total thickener heights

The total solids residence time, T_{res}^{total} in dimensionless form, and the total thickener height, Z^{total}, are important parameters when controlling and designing a thickener. Table 6.2 shows that the dimensionless total solids residence times, T_{res}^{total} and the dimensionless total heights required for the thickener, $|Z^{total}|$ for each case. Consider first of all,

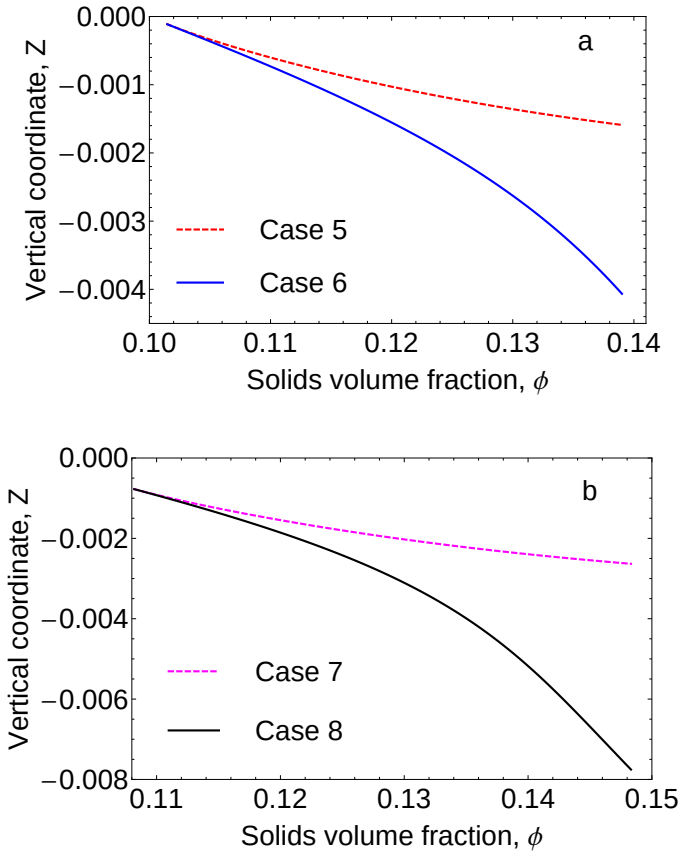

Figure 6.14: Solids volume fraction profiles determined in the consolidation region for the specified suspension flux, $Q_s = 0.0015$. Recall that the sub-plots labelled 'a' and 'b' are plotted using a small T_{corres} ($T_{corres} = 0.05$) and a large T_{corres} ($T_{corres} = 0.3$), respectively.

Cases 1 vs 2, 3 vs 4, 5 vs 6, 7 vs 8. For a specified suspension flux and a specified corresponding solids residence time, although the *dimensionless* solids residence time and the *dimensionless* height required in the hindered settling region are identical, regardless of the aggregate densification rate parameters, the *dimensional* solids residence time and the *dimensional* height required in the hindered settling region decrease in proportion with the increase in the aggregate densification rate parameters. The *dimensionless* solids residence time spent in the consolidated bed and the *dimensionless* consolidated bed heights *decrease* with the decrease in the aggregate densification rate parameters when the suspension flux and the corresponding solids residence time are both specified. However, the above *dimensional* results *increase* with the decrease in the aggregate densification rate parameters if the suspension flux and the corresponding solids residence time are both specified. Note that this can be inferred by rescaling the dimensionless heights and times

by the dimensionless parameter α (e.g. $T/\alpha = \Delta\rho g t u_{Stokes,0}/a_0$ and $Z/\alpha = z\Delta\rho g/a_0$). These rescalings come about quite naturally on the grounds that there is one set of scalings appropriate to collapse the data in the hindered settling region, but a different set of scalings that are more natural for the bed, especially when we are interested in varying the densification rate parameter as is the case here.

The total solids residence times and the total thickener heights can be obtained by summing the hindered settling region and the consolidation region contributions. As presented in Table 6.2 (Cases 1 vs 3, 2 vs 4, 5 vs 7, and 6 vs 8), increasing the corresponding solids residence time (in the hindered setting region) leads to an increasing amount of time spent in the bed. This is due to an increasing bed height required to attain an increasing underflow solids volume fraction (the underflow solids volume fractions are given in Table 6.1). Another way to achieve a high underflow solids volume fraction of course is to decrease the suspension flux, and the low suspension flux Cases 5–8 tend to have taller beds and significantly longer solids residence times spent in the consolidated bed than their high suspension flux counterparts (Cases 1–4). In all of Cases 5–8, the proportion of the solids residence time spent in the bed is far higher than the proportion spent in the hindered settling region.

When decreasing the suspension flux, the solids residence times spent in the consolidation region increase significantly, due both to smaller underflow solids fluxes and larger underflow solids volume fractions. As also shown in Table 6.2, if the suspension flux decreases, the proportion of the total height required for the consolidation region increases, due to larger underflow solids volume fractions.

It is worth recalling that to obtain the data of Table 6.2 we have (as in Grassia et al. (2014)) set the value of the corresponding solids residence time, T_{corres}, and then used this as a basis for computing hindered settling region heights, solids residence times spent in the consolidated bed, consolidated bed heights, overall solids residence times, and overall thickener heights. It is this procedure of setting T_{corres} which makes it remarkably easy to design the thickener and to couple the computations of the hindered settling region to those of the bed, since the densification state of the system and its solids volume fraction at the boundary between the hindered settling region and the consolidated bed regions

	T_{corres}	$T_{res,b}$	T_{res}^{total}
Case 1	0.05	0.0587	0.1087
Case 2	0.05	0.2044	0.2544
Case 3	0.3	0.0769	0.3769
Case 4	0.3	0.2802	0.5802
Case 5	0.05	0.8282	0.8782
Case 6	0.05	2.3423	2.3923
Case 7	0.3	1.0409	1.3409
Case 8	0.3	4.1924	4.4924

	$\lvert Z_h\rvert$	$\lvert Z_b\rvert$	$\lvert Z^{total}\rvert$
Case 1	0.000276	0.000207	0.000483
Case 2	0.000276	0.00072	0.000996
Case 3	0.00193	0.00028	0.00221
Case 4	0.00193	0.00099	0.00292
Case 5	0.000114	0.001476	0.00159
Case 6	0.000114	0.003946	0.00406
Case 7	0.000775	0.001855	0.00263
Case 8	0.000775	0.006975	0.00775

Table 6.2: Solids residence times spent in the consolidation region, $T_{res,b}$, total solids residence times, T_{res}^{total}, heights required for the hindered settling region, $|Z_h|$, bed heights, $|Z_b|$ and total thickener heights, $|Z^{total}|$ given for Cases 1–8. Here $T_{corrres}$ is the solids residence time in the hindered settling region (a parameter that we set). Note that the total solids residence time, T_{res}^{total} is equal to $T_{corres} + T_{res,b}$ and the total height required for the thickener, $|Z^{total}|$ equals $|Z_h| + |Z_b|$. Recall that the proposed (dimensionless) suspension flux, Q_s equals 0.0034 for Cases 1–4 and 0.0015 for Cases 5–8. Recall also that the (dimensional) densification rate parameters are $0.001\,\mathrm{s}^{-1}$ for odd numbered cases and $0.01\,\mathrm{s}^{-1}$ for even numbered cases. The dimensionless densification rate parameters, α are 2.125×10^{-6} and 2.125×10^{-5} for odd and even numbered cases, respectively.

are all well defined. Different T_{corres} values give different overall solids residence times and/or overall thickener heights. Attempting a design starting from a given total solids residence time or a given total thickener height is more laborious to compute however, as the boundary between the hindered settling region and the consolidated bed region is not known in advance.

6.9 Conclusions

If time-dependent densification occurs throughout a steady state thickener, the hindered settling region will affect the consolidation region via changing the densified gel point at the top of the bed and therefore changing the sludge rheological properties. For a specified dimensionless suspension flux in a thickener with time-dependent densification,

one approach for increasing the underflow solids volume fraction and hence the underflow solids flux is to operate more densification in the hindered settling region.

For a specified dimensionless suspension flux and a given aggregate densification rate parameter, more densification occurring in the hindered settling region may lead to taller beds and hence longer solids residence times, due to larger underflow solids volume fractions and smaller underflow solids fluxes. If an identical amount of densification of aggregates for a specified suspension flux is operated in the hindered settling region, shorter beds and shorter solids residence times are determined for the consolidation region when a larger aggregate densification rate parameter is given. The total heights and total solids residence times (the hindered settling region plus the consolidated bed) required for a thickener are also shorter under the above circumstances when a larger aggregate densification rate parameter is operated. When an identical amount of densification is given in the hindered settling region, the underflow solids volume fraction increases but the underflow solids flux decreases with the decrease of the suspension flux. However when the suspension flux becomes sufficiently small (such that the solids volume fraction computed in the hindered settling region might appear to exceed the suspension gel point), we interpret this to mean that the suspension actually spends a very limited amount of time in the hindered settling region, but instead jumps very quickly to the gelled state in the consolidated bed.

When the dimensionless suspension flux and the dimensionless corresponding solids residence time are specified, the solids volume fraction at the top of the bed is independent of the aggregate densification rate parameter. More densification occurring in the hindered settling region leads to an increase in the solids volume fraction at the top of the bed for a given suspension flux. For the identical amount of densification occurring in the hindered settling region and a specified suspension flux, the sludge rheological properties (i.e. $P_y(\phi, t_{res})$, and $R(\phi, t_{res})$ in dimensional form) decrease, at any given solids volume fraction, with the increase in the aggregate densification rate parameter. This implies that both the suspension permeability and compressibility are increased when a larger aggregate densification rate parameter is given.

Chapter 7

Conclusions and future work

This concluding chapter describes the main outcomes achieved from the simulations of batch settlers and continuous gravity thickeners subject to aggregate densification. Some future work related to dewatering of sludges subject to time-dependent aggregate densification is also illustrated in this chapter.

7.1 Conclusions

In this thesis, the pseudo-steady state model which neglects the hydrodynamic forces associated with both the solids flux and the solids motion is used to predict the solids behaviours in an initially networked batch settler subject to time-dependent densification. For such systems, different proposed initial suspension heights influence significantly the consolidated bed structures and the determinations of the consolidated bed heights due to the evolutions of the functional forms of the compressive yield stress for a specified initial feed solids volume fraction. The solids volume fractions obtained at the bottom of batch settlers after time-dependent aggregate densification, ϕ_{be} can be identical to values determined at the bottom of initially undensified equilibrium state batch settlers, $\phi_{be,0}$ for comparatively tall initial suspension heights, when the initial feed solids volume fraction is given. On the other hand, ϕ_{be} might be increased after time-dependent aggregate densification (compared to the undensified state) when a shorter initial suspension height is specified.

A shorter consolidated bed height is achieved at the equilibrium state after time-

dependent aggregate densification, compared to that obtained at the equilibrium state of the initially undensified batch settler for the initial feed solids volume fraction, ϕ_f smaller than the fully densified gel point, $\phi_{g,\infty}$. This is despite the fact that in the initial state some of the material is still contained in an unconsolidated column, whereas in the final state all of it is consolidated. For $\phi_f > \phi_{g,\infty}$ however, the consolidated bed height always increases with time until the fully densified equilibrium state is achieved. In other words, the consolidated bed height achieved at the fully densified equilibrium state is taller than that obtained at the initially undensified equilibrium state for $\phi_f > \phi_{g,\infty}$. This reflects a very significant amount of unconsolidated material in the undensified state when ϕ_f is high. Thus, correspondingly less mass is in the consolidated (but undensified) bed. For smaller initial feed solids volume fractions (e.g. $\phi_f < \phi_{g,\infty}$), the suspension height intersects the consolidated bed height at the critical time evaluated at $\phi_g = \phi_f$ in cases where time-dependent aggregate densification occurs. For larger ϕ_f (e.g. $\phi_f > \phi_{g,\infty}$) however, the above mentioned two heights will never intersect. In other words, the suspension height will always be taller than the consolidated bed height for $\phi_f > \phi_{g,\infty}$. Thus, a column of unconsolidated material persists even in the fully densified state.

There are differences in predicted behaviours according to whether the suspension is strongly or weakly gelled, terms which refer to the local functional form of the compressive yield stress in the neighbourhood of the gel point. If the initial feed solids volume fraction, ϕ_f is smaller than the fully densified gel point, $\phi_{g,\infty}$ but is larger than the initially undensified gel point, $\phi_{g,0}$, the consolidated bed heights predicted using the strongly gelled formula will always increase for the densification time smaller than the critical time evaluated at $\phi_g = \phi_f$ and then will decrease until the fully densified equilibrium state is reached. However, when using the weakly gelled formula for $\phi_f < \phi_{g,\infty}$ but $\phi_f > \phi_{g,0}$, the evolutions of the consolidated bed heights are subtle. The consolidated bed heights increase at early times and then commence to decrease already at some densification time that is smaller than the critical time determined at $\phi_g = \phi_f$. This is attributed to the inability of the uppermost part of the consolidated bed to bear virtually any weight at all in the weak gel case as ϕ_g approaches ϕ_f.

For a steady state continuous gravity thickener in situations where the hindered set-

tling region is neglected, larger maximum permitted underflow solids fluxes are achieved in both a thickener where time-dependent aggregate densification occurs, and a fully densified thickener, compared to those evaluated in an undensified thickener for smaller underflow solids volume fractions, ϕ_u. In addition, the maximum permitted underflow solids flux could be any arbitrary value in a thickener where time-dependent aggregate densification occurs for $\phi_u > \phi_{g,0}$ but $\phi_u < \phi_{g,\infty}$ (although this does require the capacity to preshear the suspension). On the other hand, the maximum permitted underflow solids fluxes determined in an undensified thickener, a thickener where time-dependent aggregate densification occurs, and a fully densified thickener are identical for a much larger underflow solids volume fraction, ϕ_u. When the proposed underflow solids volume fraction, ϕ_u is so large that the maximum permitted underflow solids flux cannot be increased, the improvement of thickener performance achieved after aggregate densification is insignificant.

In a steady state continuous gravity thickener where time-dependent aggregate densification occurs and the hindered settling region is neglected, a shorter consolidated bed height is achieved as small and/or intermediate underflow solids volume fractions and larger aggregate densification rate parameters are given. For a much larger underflow solids volume fraction, ϕ_u however, aggregate densification might affect insignificantly the predictions of consolidated bed heights. Away from this high ϕ_u regime, fully densified thickeners give lower consolidated bed heights than their undensified or only partly densified counterparts. After aggregate densification, the compressive yield stress and the hindered settling function are reduced when the underflow solids volume fraction and the underflow solids flux are given in a steady state continuous gravity thickener. The evolution of these sludge rheological properties is controlled by the aggregate densification rate parameter mentioned above. The larger the aggregate densification rate parameter that is given, the smaller the compressive yield stress and the hindered settling function that might be achieved for specified underflow solids volume fractions and underflow solids fluxes.

If a large underflow solids flux is operated for small and/or intermediate underflow solids volume fractions, pre-shearing of aggregates is required and hence the solids volume fraction determined at the top of the consolidated bed becomes a densified gel point

which is larger than the undensified gel point, $\phi_{g,0}$. The determination of this densified gel point is independent of the aggregate densification rate parameter but depends upon the proposed underflow solids flux, the proposed underflow solids volume fraction, and the aggregate diameter ratio determined at the top of the consolidated bed (Zhang et al., 2013a).

When considering a steady state continuous gravity thickener where time-dependent aggregate densification occurs but the hindered settling region cannot be ignored (but rather needs to be matched onto the consolidated bed), the hindered settling region might itself exhibit aggregate densification so as to increase the underflow solids volume fraction and the underflow solids flux for a specified suspension flux. The solids volume fraction determined at the top of the consolidated bed which is the densified gel point is affected by the presence of the hindered settling region during time-dependent aggregate densification. This densified gel point depends upon the proposed solids residence time in the hindered settling region, and hence the extent of densification that occurs in the hindered settling region. The hindered settling region can be neglected by giving a very small suspension flux. Giving more densification in the hindered settling region leads to *taller* consolidated bed heights if the suspension flux and the aggregate densification rate parameter are specified. This is due to an increase in the underflow solids volume fraction. When the suspension flux and the underflow solids flux are given, for a given amount of densification occurring in the hindered settling region, the consolidated bed tends to be shorter when a larger aggregate densification rate parameter is given.

7.2 Future work

Batch sedimentation considered in this thesis neglects the hydrodynamic forces associated with the solids motion during aggregate densification, an assumption which is only valid in the slow densification limit. However, ordinarily the hydrodynamic forces associated with the solids flux and the solids motion affect significantly the solids behaviours in a batch settler, especially for the initial feed solids volume fraction larger than the gel point (Buscall and White, 1987; Auzerais et al., 1988; Howells et al., 1990; van Deventer, 2012). Up to now, the numerical schemes in the literature can accurately predict the

solids behaviours in an initially unnetworked batch settler (including a settler exhibiting aggregate densification) where the initial feed solids volume fraction, ϕ_f is less than the gel point, ϕ_g (Auzerais et al., 1988; Bürger and Karlsen, 2001; Garrido et al., 2004; van Deventer et al., 2011; van Deventer, 2012). However, little attention is focused on the initially networked batch settler where $\phi_f > \phi_g$, when time-dependent aggregate densification occurs and the hydrodynamic drag forces associated with the solids fluxes are also considered. Hence, the numerical schemes for predicting the batch settling process consistent with time-dependent aggregate densification should be developed in the future.

This thesis only considers one dimensional solid mechanics. However, sedimentation and aggregate densification might be required to be described using the multidimensional solid mechanics (Lester et al., 2010). Using one dimensional solid mechanics might lead to failures for predicting the solids behaviours in a thickener subject to time-dependent aggregate densification particularly in cases where suspension overturning might occur, due e.g. to the high solids volume fraction material being placed above the lower solids volume fraction material (Grassia et al., 2014; Zhang et al., 2014). Hence, mathematical models should be established and/or extended using the multidimensional solid mechanics to describe the settling process and aggregate densification (Lester et al., 2010; Grassia et al., 2014; Zhang et al., 2014). This is one of the aims that will be addressed in the future.

In this thesis, only steady state thickeners where the underflow solids flux is uniform are considered. The transient continuous gravity thickeners where the solids flux is not spatially uniform and where the feed may vary with time have been predicted by many researchers (e.g. Martin (2004), Bürger et al. (2013) and Betancourt et al. (2014)). However, time-dependent aggregate densification was not considered when predicting the transient continuous gravity thickeners. It is of particular interest to consider aggregate densification in the transient continuous gravity thickeners in the future. The solids behaviours and the consolidated bed structures predicted in the transient continuous gravity thickeners subject to aggregate densification are also of particular interest in the future.

Experimental data have already been available for predicting the sludge rheological properties subjected to time-dependent aggregate densification in a low solids volume

fraction range (van Deventer et al., 2011; van Deventer, 2012). Our mathematical models presented in this thesis predict how the sludge rheological properties subjected to time-dependent aggregate densification evolve in the high solids volume fraction range which is larger than the gel point. However, experimental data of those sludge rheological properties subjected to time-dependent aggregate densification in the high solids volume fraction range should be obtained in the future. In addition, the performance of the thickener subjected to time-dependent aggregate densification has already been predicted using our mathematical models presented in this thesis. Experiments conducted by Gladman (2004) and Gladman et al. (2010) show partly the validation of our mathematical models: the underflow solids flux which can be increased after aggregate densification. However, when time-dependent aggregate densification occurs, experiments for determining the consolidated bed height and the solids residence time should be conducted in the future.

When time-dependent aggregate densification occurs, the value of the final steady state aggregate diameter ratio, $D_{agg,\infty}$ is an important parameter. In this thesis, $D_{agg,\infty}$ is chosen to be 0.9 which is generally used in the literature (Usher et al., 2009; van Deventer et al., 2011). Experiments have already been conducted for the determination of the value of $D_{agg,\infty}$ (van Deventer et al., 2011). Our mathematical models presented in this thesis are sensitive to the value of $D_{agg,\infty}$. Choosing different values of $D_{agg,\infty}$ may influence the results predicted using our mathematical models in this thesis. However, the objective of this thesis is to provide general mathematical models and/or widely used approaches predicting the performance of the thickener subjected to time-dependent aggregate densification. In the future, the simulation of a steady state thickener subjected to time-dependent aggregate densification using our mathematical models presented in this thesis may be required when specifying different values of $D_{agg,\infty}$.

Chapter 8

Appendix

This appendix presents all the fitting parameters and the values of those fitting parameters for the sludge rheological properties (including the hindered settling function and the compressive yield stress) used in the mathematical models presented in this thesis, as well as describes how one can obtain the values of those fitting parameters.

The fitting parameters used in the functional form of the initially undensified hindered settling function are r_g and r_n. The values of r_g and r_n are chosen to be 0.05 and 5, respectively (Usher et al., 2009; van Deventer et al., 2011). In Chapters 5–6, the fitting parameters used in the functional form of the initially undensified compressive yield stress are a_0, m, and n_0. The values of a_0, m, and n_0 are chosen as $3.7914\,\mathrm{Pa}$, 0.0363, and 10.8302, respectively (Zhang et al., 2013a). Two different functional forms of the initially undensified compressive yield stress (weak gel and strong gel, respectively) are chosen in Chapter 2. Table 8.1 presents all the fitting parameters as well as the values used in both the weakly and strongly gelled formulae in Chapter 2.

All the fitting parameters used in the functional forms of the hindered settling function, $R(\phi)$ and the compressive yield stress, $P_y(\phi)$ in this thesis are dependent on sludge

	b	$C_0/\,\mathrm{Pa}$	k_0	b_1	$c_0/\,\mathrm{Pa}$	k_3
Weak gel	0.002	3.1866	11	N/A	N/A	N/A
Strong gel	N/A	N/A	N/A	0.0363	3.7914	10.8302

Table 8.1: The values of fitting parameters used in the functional forms of the initially undensified compressive yield stress in Chapter 2. Note that all these values are chosen from Usher et al. (2009) and Zhang et al. (2013a).

materials and flocculation conditions (Usher, 2002; de Kretser et al., 2003). Using different sludge materials and different flocculation conditions can lead to different values of the fitting parameters for the functional forms of the hindered settling function, $R(\phi)$ and the compressive yield stress, $P_y(\phi)$ (Usher, 2002; de Kretser et al., 2003). In addition, one can develop different functional forms of the hindered settling function and the compressive yield stress once obtaining experimental data. However, it should be noted that the functional forms of the initially undensified hindered settling function and the compressive yield stress are required to be simple in order to obtain the densified counterparts.

As discussed in Chapter 1, the initially undensified gel point, $\phi_{g,0}$, the close packing solids volume fraction, ϕ_{cp}, and the sludge rheological properties (including the hindered settling function, $R(\phi)$ and the compressive yield stress, $P_y(\phi)$) can be determined via pressure filtration and centrifugation tests. A large amount of experiments have already been conducted for the determinations of the initially undensified hindered settling function and the compressive yield stress using different sludge materials in the past three decades (Buscall and White, 1987; Landman and White, 1992; Green et al., 1996; Green and Boger, 1997; Channell and Zukoski, 1997; Channell et al., 2000; de Kretser et al., 2001; Usher et al., 2001; Usher, 2002; Gladman, 2004; Gladman et al., 2005; Lester et al., 2005; Stickland et al., 2008; Usher et al., 2013).

Now, we turn to describe the general procedures obtaining the fitting parameters for initially undensified sludge rheological properties:

1. Choose a sludge sample and a proper technique (e.g. pressure filtration or centrifugation tests) determining the initially undensified hindered settling function and the compressive yield stress.

2. Choose the proper functional forms of the initially undensified hindered settling function and the compressive yield stress with several free unknown parameters.

3. Once obtaining experimental data, one can use the so called curve fitting technique obtaining the values of those free unknown parameters. This procedure is easy to implement using different software (e.g. Matlab, Mathematica, and Gnuplot).

References

F. M. Auzerais, R. Jackson, and W. B. Russel. The resolution of shocks and the effects of compressible sediments in transient settling. *J. Fluid Mech.*, 195:437–462, 1988.

S. Berres, R. Bürger, A. Coronel, and M. Sepúlveda. Numerical identification of parameters for a strongly degenerate convection-diffusion problem modelling centrifugation of flocculated suspensions. *Applied Numerical Mathematics*, 52:311–337, 2005a.

S. Berres, R. Bürger, A. Coronel, and M. Sepúlveda. Numerical identification of parameters for a flocculated suspension from concentration measurements during batch centrifugation. *Chemical Engineering Journal*, 111:91–103, 2005b.

F. Betancourt, R. Bürger, S. Diehl, and S. Farås. Modeling and controlling clarifier-thickeners fed by suspensions with time-dependent properties. *Minerals Engineering*, 62:91–101, 2014.

D. V. Boger. Rheology and the resource industries. *Chemical Engineering Science*, 64: 4525–4536, 2009.

B. Buratto, S. P. Usher, D. Parris, and P. J. Scales. Wall effects during settling in cylinders. *Colloids and Surfaces A: Physicochemical and Engineering Aspects*, 449:157–169, 2014.

R. Bürger and K. H. Karlsen. On some upwind difference schemes for the phenomenological sedimentation-consolidation model. *Journal of Engineering Mathematics*, 41: 145–166, 2001.

R. Bürger and A. Narváez. Steady-state, control, and capacity calculations for flocculated suspensions in clarifier–thickeners. *Int. J. Miner. Process.*, 84:274–298, 2007.

R. Bürger and W. L. Wendland. Sedimentation and suspension flows: Historical perspective and some recent developments. *Journal of Engineering Mathematics*, 41:101–116, 2001a.

R. Bürger, S. Evje, K. H. Karlsen, and K. A. Lie. Numerical methods for the simulation of the settling of flocculated suspensions. *Powder Technology*, 80:91–104, 2000.

R. Bürger, F. Concha, and K. H. Karlsen. Phenomenological model of filtration processes: 1. cake formation and expression. *Chemical Engineering Science*, 56:4537–4553, 2001b.

R. Bürger, K. H. Karlsen, and J. D. Towers. A model of continuous sedimentation of flocculated suspensions in clarifier–thickener units. *SIAM J. APPL. MATH.*, 65:882–940, 2005.

R. Bürger, S. Diehl, S. Farås, I. Nopens, and E. Torfs. A consistent modelling methodology for secondary settling tanks: a reliable numerical method. *Water Science & Technology*, 68:192–208, 2013.

R. Buscall and L. R. White. The consolidation of concentrated suspensions: Part 1. The theory of sedimentation. *J. Chem. Soc. – Faraday Trans.*, 83:873–891, 1987.

J. P. Chancelier, M. Cohen De Lara, C. Joannis, and F. Pacard. New insights in dynamic modeling of a secondary settler – 1. Flux theory and steady-states analysis. *Water Research*, 31:1847–1856, 1997a.

J. P. Chancelier, M. Cohen De Lara, C. Joannis, and F. Pacard. New insights in dynamic modeling of a secondary settler – 2. Dynamical analysis. *Water Research*, 31:1857–1866, 1997b.

G. M. Channell and C. F. Zukoski. Shear and compressive rheology of aggregated alumina suspensions. *AIChE Journal*, 43:1700–1708, 1997.

G. M. Channell, K. T. Miller, and C. F. Zukoski. Effects of microstructure on the compressive yield stress. *AIChE Journal*, 46:72–78, 2000.

H. S. Coe and G. H. Clevenger. Methods for determining the capacities of slime settling tanks. *Trans. Amer. Inst. Mining Engrs.*, 55:356–385, 1916.

K. E. Davis and W. B. Russel. An asymptotic description of transient settling and ultrafiltration of colloidal dispersions. *Phys. Fluids A*, 1:82–100, 1989.

R. G. de Kretser, S. P. Usher, P. J. Scales, D. V. Boger, and K. A. Landman. Rapid Filtration Measurement of Dewatering Design and Optimization Parameters. *AIChE Journal*, 47:1758–1769, 2001.

R. G. de Kretser, D. V. Boger, and P. J. Scales. Compressive rheology: An overview. *Rheology Reviews*, 1:125–165, 2003.

S. Diehl. Operating charts for continuous sedimentation 1: Control of steady states. *Journal of Engineering Mathematics*, 41:117–144, 2001.

S. Diehl. Operating charts for continuous sedimentation 2: Step responses. *Journal of Engineering Mathematics*, 53:139–185, 2005.

S. Diehl. Operating charts for continuous sedimentation 3: Control of step inputs. *Journal of Engineering Mathematics*, 54:225–259, 2006.

S. Diehl. Estimation of the batch–settling flux function for an ideal suspension from only two experiments. *Chemical Engineering Science*, 62:4589–4601, 2007.

S. Diehl. Operating charts for continuous sedimentation 4: Limitations for control of dynamic behaviour. *Journal of Engineering Mathematics*, 60:249–264, 2008a.

S. Diehl. The solids-flux theory–confirmation and extension by using partial differential equations. *Water Research*, 42:4976–4988, 2008b.

S. Diehl. Shock-Wave Behaviour of Sedimentation in Wastewater Treatment: A Rich Problem. In K. Åström, L.-E. Persson, and S. D. Silvestrov, editors, *Analysis for Science, Engineering and Beyond*, volume 6, pages 175–214, Berlin, 2012. Springer Proceedings in Mathematics.

B. Dobiáš. *Coagulation and flocculation: Theory and applications*. Marcel Dekker Inc., 1993.

J. B. Farrow, R. R. M. Johnston, K. Simic, and J. D. Swift. Consolidation and aggregate densification during gravity thickening. *Chemical Engineering Journal*, 80:141–148, 2000.

B. Fitch. Current theory and thickener design. *Industrial and Engineering Chemistry*, 58: 18–28, 1966.

B. Fitch. Kynch Theory and Compression Zones. *AIChE Journal*, 29:940–947, 1983.

B. Fitch. Thickening Theories–an Analysis. *AIChE Journal*, 39:27–36, 1993.

R. J. Flatt and P. Bowen. Yodel: A Yield Stress Model for Suspensions. *J. Am. Ceram. Soc.*, 89:1244–1256, 2006.

R. Font. Compression Zone Effect in Batch Sedimentation. *AIChE Journal*, 34:229–238, 1988.

R. Font. Analysis of the batch sedimentation test. *Chemical Engineering Science*, 46: 2473–2482, 1991.

R. Font and F. Ruiz. Simulation of batch and continuous thickeners. *Chemical Engineering Science*, 48:2039–2047, 1993.

G. V. Franks and Y. Zhou. Relationship between aggregate and sediment bed properties: Influence of inter-particle adhesion. *Advanced Powder Technology*, 21:362–373, 2010.

P. Garrido, R. Burgos, F. Concha, and R. Bürger. Settling velocities of particulate systems: 13. A simulator for batch and continuous sedimentation of flocculated suspensions. *Int. J. Miner. Process.*, 73:131–144, 2004.

B. Gladman, R. G. de Kretser, M. Rudman, and P. J. Scales. Effect of shear on particulate suspension dewatering. *Chemical Engineering Research and Design*, 83:933–936, 2005.

B. R. Gladman. *The effect of shear on dewatering of flocculated suspensionis*. PhD thesis, The University of Melbourne, Melbourne, Australia, 2004.

B. R. Gladman, M. Rudman, and P. J. Scales. The effect of shear on gravity thickening: Pilot scale modelling. *Chemical Engineering Science*, 65:4293–4301, 2010.

P. Grassia, S. P. Usher, and P. J. Scales. A simplified parameter extraction technique using batch settling data to estimate suspension material properties in dewatering applications. *Chemical Engineering Science*, 63:1971–1986, 2008.

P. Grassia, S. P. Usher, and P. J. Scales. Closed–form solutions for batch settling height from model settling flux functions. *Chemical Engineering Science*, 66:964–972, 2011.

P. Grassia, Y. Zhang, A. D. Martin, S. P. Usher, P. J. Scales, A. Crust, and R. Spehar. Effects of aggregate densification upon thickening of Kynchian suspensions. *Chemical Engineering Science*, 111:56–72, 2014.

M. D. Green and D. V. Boger. Yielding of Suspensions in Compression. *Ind. Eng. Chem. Res.*, 36:4984–4992, 1997.

M. D. Green, M. Eberl, and K. A. Landman. Compressive Yield Stress of Flocculated Suspensions: Determination via Experiment. *AIChE Journal*, 42:2308–2318, 1996.

R. Hogg. Flocculation and dewatering. *Int. J. Miner. Process.*, 58:223–236, 2000.

R. G. Holdich and G. Butt. Compression and channelling in gravity sedimenting systems. *Minerals Engineering*, 9:115–131, 1996.

I. Howells, K. A. Landman, A. Panjkov, C. Sirakoff, and L. R. White. Time-dependent batch settling of flocculated suspensions. *Appl. Math. Modelling*, 14:77–86, 1990.

H. Jones and D. V. Boger. Sustainability and Waste Management in the Resource Industries. *Ind. Eng. Chem. Res.*, 51:10057–10065, 2012.

T. M. Keinath. Operational dynamics and control of secondary clarifiers. *Journal WPCF*, 57:770–776, 1985.

G. J. Kynch. A theory of sedimentation. *Transactions of the Faraday Society*, 48:166–176, 1952.

K. A. Landman and L. R. White. Determination of the Hindered Settling Factor for Flocculated Suspensions. *AIChE Journal*, 38:184–192, 1992.

K. A. Landman and L. R. White. Solid/liquid separation of flocculated suspensions. *Advances in Colloid and Interface Science*, 51:175–246, 1994.

K. A. Landman, L. R. White, and R. Buscall. The continuous-flow gravity thickener: Steady state behavior. *AIChE Journal*, 34:239–252, 1988.

K. A. Landman, C. Sirakoff, and L. R. White. Dewatering of flocculated suspensions by pressure filtration. *Phys. Fluids A*, 3:1495–1509, 1991.

K. A. Landman, L. R. White, and M. Eberl. Pressure filtration of flocculated suspensions. *AIChE Journal*, 41:1687–1700, 1995.

K. A. Landman, J. M. Stankovich, and L. R. White. Measurement of the Filtration Diffusivity $D(\phi)$ of a Flocculated Suspension. *AIChE Journal*, 45:1875–1882, 1999.

V. D. Laquidara and T. M. Keinath. Mechanism of clarification failure. *Journal WPCF*, 55:54–57, 1983.

D. R. Lester, S. P. Usher, and P. J. Scales. Estimation of the Hindered Settling Function R(ϕ) from Batch–Settling Tests. *AIChE Journal*, 51:1158–1168, 2005.

D. R. Lester, M. Rudman, and P. J. Scales. Macroscopic dynamics of flocculated colloidal suspensions. *Chemical Engineering Science*, 65:6362–6378, 2010.

O. Lev, E. Rubin, and M. Sheintuch. Steady State Analysis of a Continuous Clarifier-Thickener System. *AIChE Journal*, 32:1516–1525, 1986.

A. Mahmoud, J. Olivier, J. Vaxelaire, and A. F. A. Hoadley. *Wastewater Reuse and Management*, chapter Advances in Mechanical Dewatering of Wastewater Sludge Treatment, pages 253–303. Springer, Berlin, 2013.

A. D. Martin. Optimisation of clarifier-thickeners processing stable suspensions for turn-up/turn-down. *Water Research*, 38:1568–1578, 2004.

A. D. Martin. Filtration of flocculated suspensions under declining pressure. *AIChE Journal*, 50:1418–1430, 2004a.

K. A. Northcott, I. Snape, P. J. Scales, and G. W. Stevens. Dewatering behaviour of water treatment sludges associated with contaminated site remediation in Antarctica. *Chemical Engineering Science*, 60:6835–6843, 2005.

W. H. Press, S. A. Teukolsky, W. T. Vetterling, and B. P. Flannery. *Numerical Recipes in C: The Art of Scientific Computing*. Cambridge University Press, Cambridge, 2nd edition, 1992.

M. Rudman, K. Simic, D. A. Paterson, P. Strode, A. Brent, and I. D. Šutalo. Raking in gravity thickeners. *Int. J. Miner. Processing*, 86:114–130, 2008.

A. Rushton, A. S. Ward, and R. G. Holdich. *Solid-Liquid Filtration and Separation Technology*. VCH, 1st edition, 1996.

C. Selomulya, G. Bushell, R. Amal, and T. D. Waite. Understanding the role of restructuring in flocculation: The application of a population balance model. *Chemical Engineering Science*, 58:327–338, 2003.

M. Shirato, H. Kato, K. Kobayashi, and H. Sakazaki. Analysis of settling of thick slurries due to consolidation. *Journal of Chemical Engineering of Japan*, 3:98–104, 1970.

A. D. Stickland. *Solid-Liquid Separation in the Water and Wastewater Industries*. PhD thesis, The University of Melbourne, Melbourne, Australia, 2005.

A. D. Stickland and R. Buscall. Whither compressional rheology? *J. Non-Newtonian Fluid Mech.*, 157:151–157, 2009.

A. D. Stickland, L. R. White, and P. J. Scales. Modelling of solid-bowl batch centrifugation of flocculated suspensions. *AIChE Journal*, 52:1351–1362, 2006.

A. D. Stickland, C. Burgess, D. R. Dixon, P. J. Harbour, P. J. Scales, L. J. Studer, and S. P. Usher. Fundamental dewatering properties of wastewater treatment sludges from filtration and sedimentation testing. *Chemical Engineering Science*, 63:5283–5290, 2008.

L. Svarovsky. *Solids–Liquid Separation*. Butterworth Heinemann, fourth edition, 2000.

W. P. Talmage and E. B. Fitch. Determining thickener unit areas. *Ind. Eng. Chem.*, 47: 38–41, 1955.

S. Tarleton and R. Wakeman. *Solids–Liquid Separation: Equipment Selection and Process Design*. Butterworth Heinemann, first edition, 2007.

G. Tchobanoglous and F. L. Burton. *Wastewater engineering: Treatment Disposal and Reuse*. Metcalf & Eddy Inc., third edition, 1991.

F. M. Tiller. Revision of Kynch Sedimentation Theory. *AIChE Journal*, 27:823–829, 1981.

S. P. Usher. *Suspension dewatering: Characterisation and optimisation*. PhD thesis, The University of Melbourne, Melbourne, Australia, 2002.

S. P. Usher and P. J. Scales. Steady state thickener modelling from the compressive yield stress and hindered settling function. *Chemical Engineering Journal*, 111:253–261, 2005.

S. P. Usher, R. G. de Kretser, and P. J. Scales. Validation of a New Filtration Technique for Dewaterability Characterization. *AIChE Journal*, 47:1561–1570, 2001.

S. P. Usher, P. J. Scales, and L. R. White. Prediction of Transient Bed Height in Batch Sedimentation at Large Times. *AIChE Journal*, 52:986–993, 2006.

S. P. Usher, R. Spehar, and P. J. Scales. Theoretical analysis of aggregate densification: Impact on thickener performance. *Chemical Engineering Journal*, 151:202–208, 2009.

S. P. Usher, L. J. Studer, R. C. Wall, and P. J. Scales. Characterisation of dewaterability from equilibrium and transient centrifugation test data. *Chemical Engineering Science*, 93:277–291, 2013.

B. B. G. van Deventer. *Aggregate Densification Behaviour in Sheared Supensions*. PhD thesis, The University of Melbourne, Melbourne, Australia, 2012.

B. B. G. van Deventer, S. P. Usher, A. Kumar, M. Rudman, and P. J. Scales. Aggregate densification and batch settling. *Chemical Engineering Journal*, 171:141–151, 2011.

J. Vaxelaire and J. Olivier. Compression Dewatering of Particulate Suspensions and Sludge: Effect of Shear. *Drying Technology*, 32:23–29, 2014.

D. I. Verrelli. *Drinking Water Treatment Sludge Production and Dewaterability*. PhD thesis, The University of Melbourne, Melbourne, Australia, 2008.

D. I. Verrelli, D. R. Dixon, and P. J. Scales. Effect of coagulation conditions on the dewatering properties of sludges produced in drinking water treatment. *Colloids and Surfaces A: Physicochemical and Engineering Aspects*, 348:14–23, 2009.

D. I. Verrelli, D. R. Dixon, and P. J. Scales. Assessing dewatering performance of drinking water treatment sludges. *Water Research*, 44:1542–1552, 2010.

P. A. Vesilind. *Treatment and Disposal of Wastewater Sludges*. Ann Arbor Science Publisher Inc, revised edition, 1979.

R. J. Wakeman. Separation technologies for sludge dewatering. *Journal of Hazardous Materials*, 144:614–619, 2007.

Y. Zhang, A. Martin, and P. Grassia. Mathematical modelling of time-dependent densified thickeners. *Chemical Engineering Science*, 99:103–112, 2013a.

Y. Zhang, A. Martin, and P. Grassia. Prediction of thickener performance with aggregate densification. *Chemical Engineering Science*, 101:346–358, 2013b.

Y. Zhang, P. Grassia, and A. Martin. Analysis and control of thickeners subject to aggregate densification. In Preparation, 2014.

Z. Zhou, M. J. Solomon, P. J. Scales, and D. V. Boger. The yield stress of concentrated flocculated suspensions of size distributed particles. *J. Rheol.*, 43:651–671, 1999.